

FORCED VIBRATIONS OF CIRCULAR FOUNDATIONS  
ON LAYERED MEDIA

by

EDUARDO ADOLFO MARTIN KAUSEL BOLT

Ingeniero Civil, Universidad de Chile (1967)

M.S., Massachusetts Institute of Technology (1972)

Submitted in partial fulfillment  
of the requirements for the degree of  
Doctor of Science

at the

Massachusetts Institute of Technology

January 1974

Signature of Author.....

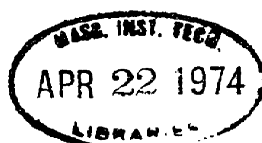
Department of Civil Engineering.....

Certified by.....

Thesis Supervisor

Accepted by.....

Chairman, Departmental Committee on Graduate  
Students of the Department of Civil Engineering



ABSTRACTFORCED VIBRATIONS OF CIRCULAR FOUNDATIONS  
ON LAYERED MEDIA

by

EDUARDO ADOLFO MARTIN KAUSEL BOLT

Submitted to the Department of Civil Engineering on January 1974 in partial fulfillment of the requirements for the degree of Doctor of Science.

The general three dimensional problem of an axisymmetric footing resting on (or embedded in) a semiinfinite viscoelastic layered stratum and subjected to arbitrary non-axisymmetric forced excitations is investigated by means of finite elements using a consistent energy absorbing boundary.

Comparisons are made with known analytical solutions for special cases involving parametric variations of the relative dimensions, properties and/or geometry. A general agreement with the theoretical halfspace solution is found, as well as with the results obtained from an approximate equivalent plane strain model.

## ACKNOWLEDGMENT

Gratitude is due to Prof. José M. Roësset and Prof. Günter Waas for their valuable suggestions and constructive criticism. Dr. A. Hsi, Mr. R. Skilton and Ms. H. Luongo contributed to the development and operation of the plotting subprograms, and Dr. D. Foster sacrificed hours of his free time to review the manuscript. The support of this study in the earlier stages by NSF Grant GI-35139 and later by Stone & Webster Eng. Co. is sincerely appreciated.

To Cecilia

## CONTENTS

I.	Title page.....	1
II.	Abstract.....	2
III.	Acknowledgment.....	3
IV.	Table of contents.....	4
V.	List of symbols.....	6
VI.	1. Introduction.....	8
	2. Soil properties: complex moduli representation..	11
	3. Theoretical background.....	21
	3.1 Displacements and loads.....	22
	3.2 Strain-displacement relations.....	25
	3.3 Stress-strain relations.....	28
	3.4 Wave equations.....	31
	3.5 Principle of virtual displacements.....	39
	3.6 Finite element formulation.....	45
	3.7 Energy absorbing boundary.....	49
	3.8 Base motion.....	87
	3.9 Summary of the procedure.....	105
	4. Parametric studies.....	106
	4.1 Effect of the size of the mesh.....	110
	a) Convergence.....	110
	b) Dynamic pressure bulb.....	116
	c) Location of the energy absorbing boundary.....	124



4.2	Influence of the stratum depth.....	127
a)	Static constants.....	127
b)	Stiffness coefficients.....	133
4.3	Influence of internal damping.....	145
4.4	Effect of Poisson's ratio.....	152
4.5	Effect of embedment.....	158
5.	Soil-structure interaction.....	172
6.	Summary and conclusions.....	231
VII.	References.....	234
VIII.	Author's biography.....	240

## List of Symbols

$\overline{\phantom{x}}$	Superscript bar: refers to Fourier expansion about the axis.
$\sim$	Tilde: refers to Fourier transform in time domain (harmonic variable).
	For the sake of notation simplicity, both the superscript bar and the tilde have been dropped after Sec. 3.5.
$\omega$	Horizontal natural frequency of stratum
$\omega_v$	Vertical natural frequency of stratum
$\lambda, \mu$	Lamé constants
$\nu$	Poisson's ratio
$G = \mu$	Shear modulus
$\beta$	Damping ratio
$\xi$	Attenuation ratio
$\alpha$	Participation factors
$k$	Wave number
$m$	Expansion order in finite elements
$l$	Number of discrete layers
$\mathbf{F} = \{f_1, f_2, f_3\}^T$	Displacement coefficients vector function (3*1)
$H_n$	Hankel function of second kind and $n^{\text{th}}$ order
$\mathbf{H}$	Hankel functions matrix defined by eq. 3-33 (3*3)
$\bar{\mathbf{H}}$	Diagonal matrix formed with $m+1$ submatrices $\mathbf{H}^T \mathbf{H}$ (3(m+1)*3(m+1))
$\mathbf{K}$	System stiffness matrix
$\mathbf{K}_d$	System dynamic stiffness matrix
$\mathbf{M}$	System mass matrix
$\mathbf{N} = \{q_j \mathbf{I}_j\}$	Expansion vector (eq. 3-66) for layer (3*3(m+1))
$\mathbf{P} = \{P_r, P_z, P_\theta\}^T$	Load vector (3*1)
$\mathbf{P}_i$	Load vector evaluated at $i^{\text{th}}$ interface (3*1)
$\mathbf{P}_o = \{\mathbf{P}_i \dots \mathbf{P}_{i+m}\}$	Layer load vector (3(m+1)*1)
$\mathbf{P}_k$	Layer load vector contributed by the $k^{\text{th}}$ propagation mode (3(m+1)*1)
$\mathbf{P}_{bk}$	Stratum load vector contributed by the $k^{\text{th}}$ propagation mode (3(m+1)*1)

- $P_b$  Stratum load vector at Waas-Lysmer boundary ( $3\ell \times 1$ )  
 $P$  System load vector  
 $R$  Waas-Lysmer boundary dynamic stiffness matrix ( $3\ell \times 3\ell$ )  
 $U = \{\bar{u}, \bar{w}, \bar{v}\}^T$  Displacement vector ( $3 \times 1$ )  
 $U_i$  Displacements at  $i^{\text{th}}$  interface ( $3 \times 1$ )  
 $U_o = \{U_i \dots U_{i+m}\}$  Displacement vector for 1 discrete layer ( $3(m+1) \times 1$ )  
 $U_b$  Stratum load vector at Waas-Lysmer boundary ( $3\ell \times 1$ )  
 $W$  Wave equation vector ( $3 \times 1$ )  
 $X_i = \{x_1, x_2, x_3\}^T$  F vector evaluated at  $i^{\text{th}}$  interface ( $3 \times 1$ )  
 $X = \{X_i \dots X_{i+m}\}$  Assembly of  $X_i$  vectors for 1 discrete layer ( $3(m+1) \times 1$ )  
 $X = \{X_i\}$  Stratum displacement coefficient vector: modal shapes obtained from quadratic eigenvalue problem ( $3\ell \times 1$ )  
 $\sigma_v$  Boundary stress vector ( $3 \times 1$ )  
 $\sigma_{vk}$  Boundary stress vector contributed by  $k^{\text{th}}$  mode ( $3 \times 1$ )

## 1.- Introduction:

In recent years, considerable effort has been made by researchers to obtain analytical or closed form solutions to the problem of the propagation of waves in soils, generated by forced vibrations of a circular plate welded to the free surface of a semi-infinite homogeneous elastic halfspace or to a stratum. The solution to this problem is of great interest for its application in geophysics and engineering, and particularly, for its importance in foundation and earthquake engineering.

Early analytical solutions were given by Lamb (17), and by Reissner (26), using greatly simplified boundary conditions. Further developments were contributed by Reissner & Sagoci (28), Marguerre (22), Bycroft (5), Awojobi & Grootenhuis (2), and others, and in recent years, full solutions to the general problem have been reported by Luco & Westmann (19), Veletsos & Wei (42), among other authors.

Despite their mathematical elegance, closed form solutions inherit a major drawback: they apply to ideally elastic, homogeneous, isotropic halfspaces, an abstraction that seldom approaches reality. Soils are usually non-homogeneous; their

properties vary with depth; they are stratified in layers; and underground water adds further complications to their physical nature. Thus, the analyst must rely on experimental or numerical techniques.

In the present dissertation, a numerical method is presented for the dynamic analysis of axisymmetric foundations resting on viscoelastic soil layers over rock of infinite horizontal extent. The solution constitutes a generalization of a technique developed recently by Waas & Lysmer (21), (44), and which is extended for the analysis of axisymmetric systems (e.g. Nuclear power plants) subjected to arbitrary non-axisymmetric loadings, using the Fourier expansion method developed by Wilson (51).

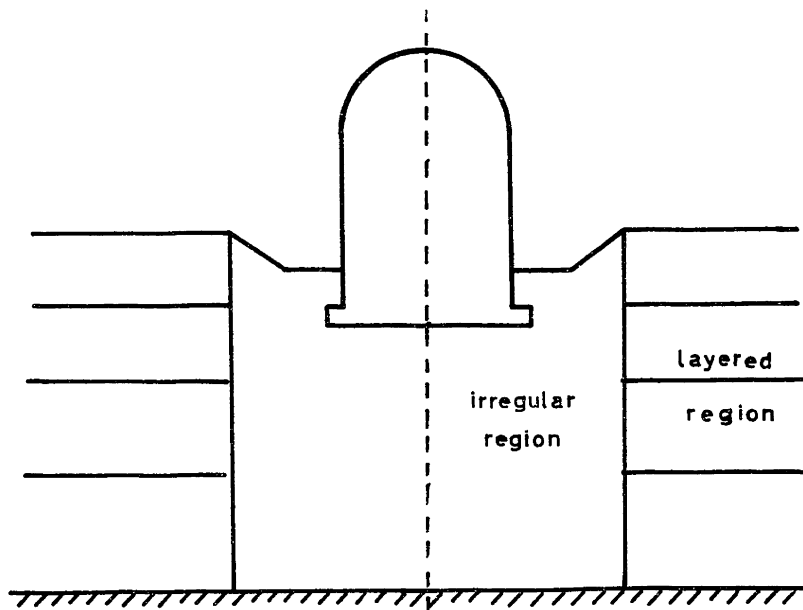


fig.1

The geometry is idealized by a finite irregular region joined to a semi-infinite far-field region as shown in Fig. 1 above. The irregular region is discretized by means of pseudotridentimensional toroidal finite elements of arbitrary expansion order, having three degrees of freedom per nodal ring. The far field is represented by a specially designed consistent energy absorbing boundary, whose dynamic stiffness matrix is expanded in Fourier series about the axis, as it is done for the forces and displacements in the finite element formulation. For the problems that will be considered in this dissertation, namely translation and rotation of a rigid circular footing, only the first two components in the Fourier series are of interest. The method can, however, be applied to cases where more than two terms in the series must be considered.

## 2.- Soil properties: complex moduli representation:

For a linearly elastic material, the stress field is related to the strain field by the generalized Hooke's law

$$\sigma_{ij} = E_{ijkl} \epsilon_{kl} \quad (2-1)$$

where  $E_{ijkl}$  is the constitutivity tensor. When a linear viscoelastic material is subjected to time-dependent variations of stress and strain, the above relation is no longer valid, but its mutual dependence is generally represented by linear partial differential equations of arbitrary order, or equivalently, through the convolution integral

$$\sigma_{ij} = \int G_{ijkl}(x, t-\tau) \frac{\partial \epsilon_{kl}}{\partial \tau} d\tau \quad (2-2)$$

where  $G_{ijkl}$  is referred to as the tensorial relaxation function. Symbolically, this is often written as

$$\sigma_{ij} = G_{ijkl} * \frac{\partial \epsilon_{kl}}{\partial \tau} \quad (2-3)$$

Detailed discussions are presented in many textbooks, and will not be repeated here. The foregoing relation between stress and strain can be visualized as being generated by an

equivalent network of springs and dashpots duplicating the mechanical behavior of the material under strain (36), (10).

If the applied stress is sufficiently small so that the relation between stress and strain is a function of time alone, and not of the stress magnitude, the principle of superposition holds, and the connection between convolution and Fourier transformation can be used:

$$\tilde{\sigma}_{ij} = i\Omega \tilde{G}_{ijkl} \tilde{\epsilon}_{kl} \quad (2-4)$$

where  $\tilde{G}_{ijkl}$  is the Fourier transform of the relaxation function, and  $\tilde{\sigma}_{ij}$ ,  $\tilde{\epsilon}_{ij}$  are the (complex) amplitudes of the frequency dependent stresses and strains. The superscript tilde refers to harmonic motion. It follows that alien frequencies will not be generated when the material is subjected to an applied load possessing one or more frequency components, as would be expected if the material were nonlinear.

If the material is isotropic, only two components  $G_1$ ,  $G_2$  are needed to define the relaxation function, and their Fourier transforms are  $\tilde{G}_1$  and  $\tilde{G}_2$ :



$$\tilde{G}_{ijkl} = \frac{1}{3} (\tilde{G}_2 - \tilde{G}_1) \delta_{ij} \delta_{kl} + \frac{1}{2} \tilde{G}_1 (\delta_{ik} \delta_{jl} + \delta_{il} \delta_{jk}) \quad (2-5)$$

For this case, the stress strain relation reduces to

$$\tilde{\sigma}_{ij} = \lambda \tilde{\epsilon}_{kk} \delta_{ij} + 2G \tilde{\epsilon}_{ij} \quad (2-6)$$

in which the (complex) Lamé constants are related to  $\tilde{G}_1$ ,  $\tilde{G}_2$  by

$$\left. \begin{aligned} \lambda &= \frac{1}{3} i \Omega (\tilde{G}_2 - \tilde{G}_1) \\ G &= \frac{1}{2} i \Omega \tilde{G}_1 \end{aligned} \right\} \quad (2-7)$$

Equation (2-6) is identical to that governing linear elasticity, except that the Lamé constants are substituted by complex moduli, which are in general functions of frequency. This equation is frequently written in matrix notation as

$$\tilde{\sigma} = D \tilde{\epsilon} \quad (2-8)$$

where  $D$  is the constitutivity matrix, and  $\tilde{\sigma}$ ,  $\tilde{\epsilon}$  are the stress and strain vectors.

solutions to the wave equation

$$G v_{i,jj} + (\lambda + G) v_{i,jj} = \gamma \ddot{u}_i \quad (2-9)$$

using complex moduli  $G, \lambda$  are of the form (10):

$$v_j = A n_j e^{i\Omega(t \pm \sqrt{\frac{\gamma}{\lambda+2G}} n_k x_k)} \quad (2-10)$$

$$v_j = C_j e^{i\Omega(t \pm \sqrt{\frac{\gamma}{G}} n_k x_k)} \quad (2-11)$$

where  $n_k$  are the director cosines of the direction of propagation of the wave,  $A$  is a complex constant, and  $C_j$  is a vector perpendicular to  $n_k$ .

The radicals in the exponent in (2-10) and 2-11) can be expressed as

$$\sqrt{\frac{\gamma}{\lambda + 2G}} = \frac{1}{v_p} = \frac{1}{c_p} (1 - i \xi_p) \quad (2-12)$$

$$\sqrt{\frac{\gamma}{G}} = \frac{1}{v_s} = \frac{1}{c_s} (1 - i \xi_s) \quad (2-13)$$

in which  $c_p, c_s$  can be interpreted as the dilatational and shear wave velocities, while the attenuation ratios  $\xi_p, \xi_s$ , can be related to the logarithmic decrements of these waves travelling in the damped continuum:

$$u_j = A n_j e^{-2\pi \xi_p \frac{n_A x_A}{l_p}} e^{i\Omega(t - \frac{n_A x_A}{c_p})} \quad (2-14)$$

and 
$$u_j = C_j e^{-2\pi \xi_s \frac{n_A x_A}{l_s}} e^{i\Omega(t - \frac{n_A x_A}{c_s})} \quad (2-15)$$

with 
$$l_p = \frac{2\pi}{\Omega} c_p, \quad l_s = \frac{2\pi}{\Omega} c_s$$

Snell's laws of refraction and reflection are valid in the damped medium only when both attenuation ratios are equal. For this particular case, the Lamé constants can be expressed as

$$\lambda = \lambda' \left( \frac{1 + i\xi}{1 + \xi^2} \right)^2 \quad (2-16)$$

$$G = G' \left( \frac{1 + i\xi}{1 + \xi^2} \right)^2 \quad (2-17)$$

where the undamped soil moduli  $\lambda', G'$  follow from

$$\lambda' = \rho (c_p^2 - 2c_s^2) \quad (2-18)$$

$$G' = \rho c_s^2 \quad (2-19)$$

Introducing the critical damping ratio  $\beta$ , equations (2-16), (2-17) can also be expressed as

$$\lambda = \lambda_0 (1 + 2i\beta) \quad (2-20)$$

$$G = G_0 (1 + 2i\beta) \quad (2-21)$$

in which  $\lambda_0, G_0, \beta$  are related to  $\lambda', G', \xi$  by

$$\lambda_0 = \lambda' \frac{(1 - \xi^2)}{(1 + \xi^2)^2}, \quad G_0 = G' \frac{(1 - \xi^2)}{(1 + \xi^2)^2}, \quad \beta = \frac{\xi}{1 - \xi^2} \quad (2-22)$$

For moderately dissipative soils, the attenuation ratio  $\xi$  and the critical damping ratio  $\beta$  are almost equal. Also,  $G_0 \approx G'$  and  $\lambda_0 \approx \lambda'$ .

In the following sections, the Lamé constants shall be interpreted in terms of equations (2-20) and (2-21).

For a Voigt-type solid, analogous to a spring-dashpot system in parallel, the real part of the Lamé constants is independent of frequency, whereas the imaginary part is directly proportional to it. For this particular case, the inverse Fourier transformation yields for the relaxation function

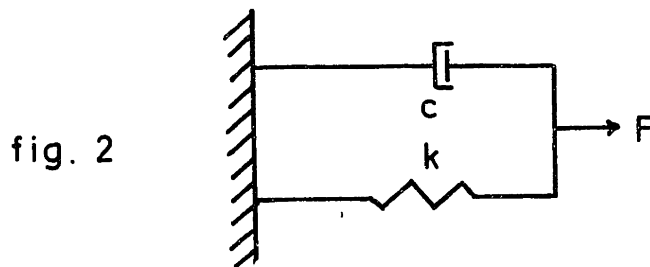
$$G_{ijke} = D_{ijke} u(t) + C_{ijke} \delta(t) \quad (2-23)$$

where  $u(t)$ ,  $\delta(t)$  are the unit step and Dirac delta functions. Substitution of (2-8) into (2-2) and integrating yields:

$$\sigma_{ij} = D_{ijkl} \epsilon_{kl} + C_{ijkl} \dot{\epsilon}_{kl} \quad (2-24)$$

This relation is formally analogous to the familiar expression

$$F = ku + c\dot{u} \quad (2-25)$$



of the Voigt model. This type of damping is usually referred to as of the viscous type.

If the imaginary part of the Lamé constants is also assumed independent of frequency, an assumption that corresponds to a linear hysteretic type of damping, a complex relaxation function is obtained, and no correspondence exists for the problem in the time domain; that is, hysteretic damping cannot be expressed in terms of linear differential equations, but must be derived instead from considerations about the average energy dissipation in a hysteresis loop over one

cycle of harmonic motion, which, in general, will also depend on the amplitude of the applied loads (displacements). This introduces the problem of the so-called "strain compatible moduli" of non-linear stress-strain relations.

It is generally accepted that the internal damping in soils is not of the viscous type. Experimental evidence seems to indicate for dry or relatively dry granular soils that this damping is of a hysteretic nature: the stress-strain curve for a cycle of steady state harmonic loading forms a closed loop. The damping behavior of cohesive soils and saturated sands is less clear and appears to be a superposition of both types of damping, as a result of relative motion between mineral skeleton and pore fluid on the one hand, and irreversible sliding between mineral particles on the other.

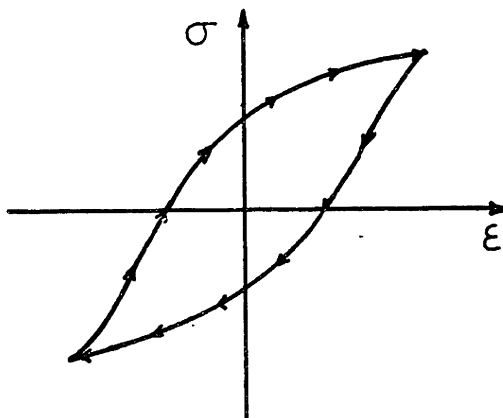


fig. 3

Best estimates for both types of soils are reported by Whitman (50) as ranging from 3 percent to 8 percent for relatively dry granular soils, and from 5 percent to

17 percent for clay. For the magnitudes of stress changes typically found under machine foundations, a damping ratio of 5 percent critical was suggested to account for internal friction in any soil.

Internal damping is less important for translational motions (swaying and vertical excitation) than for rotational motions (rocking, torsion). For the latter, the internal losses in the soil play a significant role in the response, especially at resonance. Investigators have shown that about  $2/3$  of all the energy lost in form of travelling waves (radiation damping) corresponds to surface waves. For this reason, the reflection of bodily waves at the base rock in a deep stratum will not significantly reduce the radiation damping, which accounts in the translational modes for most of the energy lost, and internal damping is of secondary importance. In the case of a shallow soil layer resting on a rigid base, however, the underlying rigid layer impedes the radiation away from the pressure bulb. This results in a decrease in the radiation damping, an effect which can be considerable for some cases. Furthermore, no waves at all can be propagated in a stratum below certain critical frequencies (which depend on the depth and physical properties of the stratum), and hence, no energy can be carried away from the source, thus eliminating the radiation damping effect. For

these cases, the proper choice of internal damping is of critical importance and significantly affects the results of the analysis.



### 3.- Theoretical background.

The finite element technique has been applied successfully in the stress analysis of many complex structures. Recently, the method was applied to the structural analysis of solids of revolution subjected to axisymmetric loads (53) and has been extended to the case of non-axisymmetric loads (51). In this approach, the problem is divided into a number of uncoupled two dimensional problems by representing the unsymmetric loading or displacement pattern by an equivalent Fourier series about the axis; but the three-dimensional nature of the problem is preserved, because of the three degrees of freedom associated with each node (nodal circle or ring). Due to the orthogonality of the Fourier series, each term in the loading series produces a displacement set in the same Fourier mode as the prescribed loading or displacement field. If the prescribed loads (displacements) do not vary too rapidly around the axis, a few terms in the series may be sufficient for an accurate representation. This pseudotridimensional analysis offers considerable savings in storage and computation time, as compared to a full tridimensional analysis.

In this study, only the first two modes in the series are needed, since they suffice to describe the general motion of a rigid circular plate (foundation) acting on the free surface of a soil stratum. These are  $n=0$  for vertical and torsional excitation (axisymmetric modes), and  $n=1$  for rocking and swaying (plane-symmetric modes).

### 3.1.- Displacements and loads:

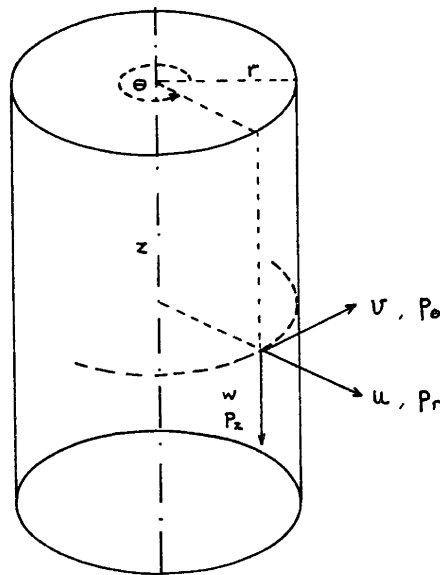


fig. 4

In the cylindrical coordinate system shown above, the displacements in the radial, vertical and tangential

directions are denoted by  $u$ ,  $w$ ,  $\theta$ , while the loads in these directions are denoted by  $p_r$ ,  $p_z$ ,  $p_\theta$ , respectively. They can always be expressed in Fourier series by:

$$\begin{aligned}
 u &= \sum_{n=0}^{\infty} (\bar{u}_s^n \cos n\theta + \bar{u}_a^n \sin n\theta) \quad , \quad p_r = \sum_{n=0}^{\infty} (\bar{p}_{rs}^n \cos n\theta + \bar{p}_{ra}^n \sin n\theta) \\
 w &= \sum_{n=0}^{\infty} (\bar{w}_s^n \cos n\theta + \bar{w}_a^n \sin n\theta) \quad p_z = \sum_{n=0}^{\infty} (\bar{p}_{zs}^n \cos n\theta + \bar{p}_{za}^n \sin n\theta) \\
 \theta &= \sum_{n=0}^{\infty} (-\bar{\theta}_s^n \sin n\theta + \bar{\theta}_a^n \cos n\theta) \quad p_\theta = \sum_{n=0}^{\infty} (-\bar{p}_{\theta s}^n \sin n\theta + \bar{p}_{\theta a}^n \cos n\theta)
 \end{aligned} \tag{3-1}$$

where the mode amplitudes with subscript  $s, a$  are referred to as the symmetric and antisymmetric displacement (load) components. For the sake of notation simplicity, the indices shall be dropped, writing simply

$$\begin{aligned}
 u &= \sum_n \bar{u} \begin{pmatrix} \cos n\theta \\ \sin n\theta \end{pmatrix} \\
 w &= \sum_n \bar{w} \begin{pmatrix} \cos n\theta \\ \sin n\theta \end{pmatrix} \\
 \theta &= \sum_n \bar{\theta} \begin{pmatrix} -\sin n\theta \\ \cos n\theta \end{pmatrix}
 \end{aligned} \tag{3-2}$$

with similar expressions for the loads. An alternate notation could be

$$\begin{aligned}
 u &= \sum_n \bar{u} e^{in\theta} \\
 w &= \sum_n \bar{w} e^{in\theta} \\
 v &= \sum_n i\bar{v} e^{in\theta}
 \end{aligned}
 \tag{3-3}$$

but since the modal amplitudes are complex for complex moduli, the latter notation is not advantageous.

The modal amplitudes (for harmonic loadings) are only functions of  $r, z$ , and do not depend on  $\theta$ . The minus sign introduced in the sine term for the tangential displacement (load) has the effect of yielding the same load-displacement equations (wave equations) for both the symmetric and antisymmetric components (same stiffness matrix in the finite element formulation).

It is convenient to partition the displacement vector into

$$\begin{aligned}
 \begin{Bmatrix} u \\ w \end{Bmatrix} &= \sum \begin{Bmatrix} \bar{u} \\ \bar{w} \end{Bmatrix} \begin{pmatrix} \cos n\theta \\ \sin n\theta \end{pmatrix} = \sum \bar{u}_1 \begin{pmatrix} \cos n\theta \\ \sin n\theta \end{pmatrix} \\
 \begin{Bmatrix} v \end{Bmatrix} &= \sum \begin{Bmatrix} \bar{v} \end{Bmatrix} \begin{pmatrix} -\sin n\theta \\ \cos n\theta \end{pmatrix} = \sum \bar{u}_2 \begin{pmatrix} -\sin n\theta \\ \cos n\theta \end{pmatrix}
 \end{aligned}
 \tag{3-4}$$

where

$$\begin{aligned}\bar{U}_1 &= \begin{Bmatrix} \bar{u} \\ \bar{w} \end{Bmatrix} \\ \bar{U}_2 &= \bar{v}\end{aligned}\quad (3-5)$$

The modal displacement vector is then:

$$\bar{U} = \begin{Bmatrix} \bar{U}_1 \\ \bar{U}_2 \end{Bmatrix} = \begin{Bmatrix} \bar{u} \\ \bar{w} \\ \bar{v} \end{Bmatrix} \quad (3-6)$$

### 3.2.- Strain-displacement relations:

The strain-displacement relations expressed in cylindrical coordinates are

$$\begin{aligned}\epsilon_{rr} &= \frac{\partial u}{\partial r} \\ \epsilon_{\theta\theta} &= \frac{u}{r} + \frac{1}{r} \frac{\partial v}{\partial \theta} \\ \epsilon_{zz} &= \frac{\partial w}{\partial z} \\ \gamma_{rz} &= \frac{\partial u}{\partial z} + \frac{\partial w}{\partial r} \\ \gamma_{r\theta} &= \frac{1}{r} \frac{\partial u}{\partial \theta} + \frac{\partial v}{\partial r} - \frac{v}{r} \\ \gamma_{\theta z} &= \frac{\partial v}{\partial z} + \frac{1}{r} \frac{\partial w}{\partial \theta}\end{aligned}\quad (3-7)$$

Introduction of the displacement expansions (3-2) into the expressions above yields (commas denote partial differentiation):

$$\begin{aligned}
 \xi_{rr} &= \sum_{n=0}^{\infty} \bar{\xi}_{rr} \begin{pmatrix} \cos n\theta \\ \sin n\theta \end{pmatrix}, & \bar{\xi}_{rr} &= \bar{u}_{,r} \\
 \xi_{\theta\theta} &= \sum_{n=0}^{\infty} \bar{\xi}_{\theta\theta} \begin{pmatrix} \cos n\theta \\ \sin n\theta \end{pmatrix}, & \bar{\xi}_{\theta\theta} &= \frac{1}{r} (\bar{u} - n\bar{v}) \\
 \xi_{zz} &= \sum_{n=0}^{\infty} \bar{\xi}_{zz} \begin{pmatrix} \cos n\theta \\ \sin n\theta \end{pmatrix}, & \bar{\xi}_{zz} &= \bar{w}_{,z} \\
 \gamma_{rz} &= \sum_{n=0}^{\infty} \bar{\gamma}_{rz} \begin{pmatrix} \cos n\theta \\ \sin n\theta \end{pmatrix}, & \bar{\gamma}_{rz} &= \bar{w}_{,r} + \bar{u}_{,z} \\
 \gamma_{r\theta} &= \sum_{n=0}^{\infty} \bar{\gamma}_{r\theta} \begin{pmatrix} -\sin n\theta \\ \cos n\theta \end{pmatrix}, & \bar{\gamma}_{r\theta} &= \frac{1}{r} (n\bar{u} - \bar{v} + r\bar{v}_{,r}) \\
 \gamma_{\theta z} &= \sum_{n=0}^{\infty} \bar{\gamma}_{\theta z} \begin{pmatrix} -\sin n\theta \\ \cos n\theta \end{pmatrix}, & \bar{\gamma}_{\theta z} &= \left( n \frac{\bar{w}}{r} + \bar{v}_{,z} \right)
 \end{aligned} \tag{3-8}$$

As in the case of the displacements, the modal strains  $\bar{\xi}_{rr}$ ,  $\bar{\xi}_{\theta\theta}$ ,  $\bar{\xi}_{zz}$  etc. are a function of only  $r$  and  $z$ . They can be written in compact forms as:

$$\bar{\xi} = A \bar{U} \tag{3-9}$$

where  $\bar{\xi} = \{ \bar{\xi}_{rr}, \bar{\xi}_{\theta\theta}, \bar{\xi}_{zz}, \bar{\gamma}_{rz}, \bar{\gamma}_{r\theta}, \bar{\gamma}_{\theta z} \}^T$  is the modal strain vector,  $\bar{U} = \{ \bar{u}, \bar{w}, \bar{v} \}^T$  is the modal displacement vector, and  $A$  is the partitioned matrix operator

$$A = \left\{ \begin{array}{cc|c} \frac{\partial}{\partial r} & 0 & 0 \\ \frac{1}{r} & 0 & -\frac{n}{r} \\ 0 & \frac{\partial}{\partial z} & 0 \\ \frac{\partial}{\partial z} & \frac{\partial}{\partial r} & 0 \\ \frac{n}{r} & 0 & r \frac{\partial}{\partial r} \left( \frac{1}{r} \right) \\ 0 & \frac{n}{r} & \frac{\partial}{\partial z} \end{array} \right\} \quad (3-10)$$

It is convenient to partition the strain vector into the in-plane and out-of-plane components,

$$\bar{\epsilon} = \begin{Bmatrix} \bar{\epsilon}_1 \\ \bar{\epsilon}_2 \end{Bmatrix} \quad (3-11)$$

where:

$$\bar{\epsilon}_1 = \begin{Bmatrix} \bar{\epsilon}_{rr} \\ \bar{\epsilon}_{\theta\theta} \\ \bar{\epsilon}_{zz} \\ \bar{\gamma}_{rz} \end{Bmatrix} \quad \bar{\epsilon}_2 = \begin{Bmatrix} \bar{\gamma}_{r\theta} \\ \bar{\gamma}_{z\theta} \end{Bmatrix} \quad (3-12)$$

With this notation, the true strains are:

$$\epsilon_1 = \sum \bar{\epsilon}_1 \begin{pmatrix} \cos n\theta \\ \sin n\theta \end{pmatrix} \quad (3-13)$$

$$\epsilon_2 = \sum \bar{\epsilon}_2 \begin{pmatrix} -\sin n\theta \\ \cos n\theta \end{pmatrix}$$

and the (modal) strain-displacement relations become:

$$\begin{aligned}\bar{\epsilon}_1 &= A_{11} \bar{U}_1 + n A_{12} \bar{U}_2 \\ \bar{\epsilon}_2 &= n A_{21} \bar{U}_1 + A_{22} \bar{U}_2\end{aligned}\quad (3-14)$$

where the operator matrix A was partitioned consistently into

$$A = \begin{Bmatrix} A_{11} & n A_{12} \\ n A_{21} & A_{22} \end{Bmatrix} \quad (3-15)$$

Here:

$$\begin{aligned}A_{11} &= \begin{Bmatrix} \frac{\partial}{\partial r} & 0 \\ \frac{1}{r} & 0 \\ 0 & \frac{\partial}{\partial z} \\ \frac{\partial}{\partial z} & \frac{\partial}{\partial r} \end{Bmatrix} & A_{12} &= \begin{Bmatrix} 0 \\ -\frac{1}{r} \\ 0 \\ 0 \end{Bmatrix} \\ A_{21} &= \begin{Bmatrix} \frac{1}{r} & 0 \\ 0 & \frac{1}{r} \end{Bmatrix} & A_{22} &= \begin{Bmatrix} r \frac{\partial}{\partial r} \left( \frac{1}{r} \right) \\ \frac{\partial}{\partial z} \end{Bmatrix}\end{aligned}$$

### 3.3.- Stress-Strain relations.

The stresses can be expanded in the same way as the strains, and the modal components are related by



$$\bar{\sigma} = D \bar{\epsilon} \quad (3-16)$$

where  $D$  is the constitutivity matrix containing the material properties. In general,  $D$  is a function of the point under consideration; in the present case,  $D$  is restricted to be a function of  $r$  and  $z$  only, that is, the material properties may not change with  $\theta$  (cross-anisotropy).

If, as in the case of the strains,  $\sigma$  is partitioned into

$$\bar{\sigma} = \begin{Bmatrix} \bar{\sigma}_1 \\ \bar{\sigma}_2 \end{Bmatrix} \quad \begin{aligned} \bar{\sigma}_1 &= \begin{Bmatrix} \bar{\sigma}_{rr} \\ \bar{\sigma}_{\theta\theta} \\ \bar{\sigma}_{zz} \\ \bar{\sigma}_{rz} \end{Bmatrix} \\ \bar{\sigma}_2 &= \begin{Bmatrix} \bar{\sigma}_{r\theta} \\ \bar{\sigma}_{z\theta} \end{Bmatrix} \end{aligned} \quad (3-17)$$

then the true stresses are given by:

$$\begin{aligned} \sigma_1 &= \sum_{n=0}^{\infty} \bar{\sigma}_1 \begin{pmatrix} \cos n\theta \\ \sin n\theta \end{pmatrix} \\ \sigma_2 &= \sum_{n=0}^{\infty} \bar{\sigma}_2 \begin{pmatrix} -\sin n\theta \\ \cos n\theta \end{pmatrix} \end{aligned} \quad (3-18)$$

For an isotropic material, the constitutivity matrix is given by:

$$D = \left\{ \begin{array}{ccc|cc} \lambda + 2\mu & \lambda & \lambda & & \\ \lambda & \lambda + 2\mu & \lambda & & \\ \lambda & \lambda & \lambda + 2\mu & & \\ \hline & & & u & \\ & & & \mu & \\ & & & & \mu \end{array} \right\} = \left\{ \begin{array}{c} D_1 \\ D_2 \end{array} \right\}$$

(3-19)

where  $\lambda$  and  $\mu$  are the (complex) Lamé constants. They are related to Young's modulus, Poisson's ratio and shear modulus through:

$$\lambda = E \frac{\nu}{(1+\nu)(1-2\nu)} = G \frac{2\nu}{1-2\nu}$$

$$\mu = G = E \frac{1}{2(1+\nu)} \quad (3-20)$$

The partitioning of this matrix into the submatrices  $D_1$ , and  $D_2$  (dashed lines) is consistent with that of the stresses and strains, and it follows that:

$$\bar{\sigma}_1 = D_1 \bar{\epsilon}_1$$

(3-21)

$$\bar{\sigma}_2 = D_2 \bar{\epsilon}_2$$

### 3.4.- Wave equation:

The general equations of wave propagation expressed in cylindrical coordinates are

$$\begin{aligned}\nabla^2 \ddot{u} &= (\lambda + 2G) \frac{\partial \Delta}{\partial r} - \frac{2G}{r} \frac{\partial \omega_z}{\partial \theta} + 2G \frac{\partial \omega_\theta}{\partial z} \\ \nabla^2 \ddot{w} &= (\lambda + 2G) \frac{\partial \Delta}{\partial z} - \frac{2G}{r} \frac{\partial}{\partial r} (r \omega_\theta) + \frac{2G}{r} \frac{\partial \omega_r}{\partial \theta} \\ \nabla^2 \ddot{v} &= (\lambda + 2G) \frac{1}{r} \frac{\partial \Delta}{\partial \theta} - 2G \frac{\partial \omega_r}{\partial z} + 2G \frac{\partial \omega_z}{\partial r}\end{aligned}\quad (3-22)$$

where

$$\begin{aligned}\Delta &= \epsilon_{rr} + \epsilon_{\theta\theta} + \epsilon_{zz} = \frac{1}{r} \frac{\partial (r v)}{\partial r} + \frac{1}{r} \frac{\partial v}{\partial \theta} + \frac{\partial w}{\partial z} \\ \omega_r &= \frac{1}{2} \left( \frac{\partial w}{r \partial \theta} - \frac{\partial v}{\partial z} \right) \\ \omega_\theta &= \frac{1}{2} \left( \frac{\partial u}{\partial z} - \frac{\partial w}{\partial r} \right) \\ \omega_z &= \frac{1}{2} \left( \frac{\partial (r v)}{\partial r} - \frac{\partial u}{\partial \theta} \right)\end{aligned}\quad (3-23)$$

Introducing the modal (Fourier) expansions into the expressions above, it is obtained for harmonic excitations (with frequency  $\Omega$ ):

$$\begin{aligned}
-\rho \Omega^2 \sum \bar{u} \begin{pmatrix} \cos n\theta \\ \sin n\theta \end{pmatrix} &= \sum \left[ (\lambda + 2G) \frac{\partial \bar{\Delta}}{\partial r} + 2G \frac{n \bar{\omega}_z}{r} + 2G \frac{\partial \bar{\omega}_\theta}{\partial z} \right] \begin{pmatrix} \cos n\theta \\ \sin n\theta \end{pmatrix} \\
-\rho \Omega^2 \sum \bar{w} \begin{pmatrix} \cos n\theta \\ \sin n\theta \end{pmatrix} &= \sum \left[ (\lambda + 2G) \frac{\partial \bar{\Delta}}{\partial z} - \frac{2G}{r} \frac{\partial r \bar{\omega}_\theta}{\partial r} - 2G \frac{n}{r} \bar{w}_r \right] \begin{pmatrix} \cos n\theta \\ \sin n\theta \end{pmatrix} \\
-\rho \Omega^2 \sum \bar{v} \begin{pmatrix} -\sin n\theta \\ \cos n\theta \end{pmatrix} &= \sum \left[ (\lambda + 2G) \frac{n \bar{\Delta}}{r} - 2G \frac{\partial \bar{\omega}_r}{\partial z} + 2G \frac{\partial \bar{\omega}_z}{\partial r} \right] \begin{pmatrix} -\sin n\theta \\ \cos n\theta \end{pmatrix}
\end{aligned}
\tag{3-24}$$

in which

$$\begin{aligned}
\bar{\Delta} &= \frac{\bar{u}}{r} + \frac{\partial \bar{u}}{\partial r} - n \frac{\bar{v}}{r} + \frac{\partial \bar{w}}{\partial z}, & \Delta &= \sum_n \bar{\Delta} \begin{pmatrix} \cos n\theta \\ \sin n\theta \end{pmatrix} \\
\bar{w}_r &= \frac{1}{2} \left( \frac{n}{r} \bar{w} - \frac{\partial \bar{v}}{\partial z} \right), & w_r &= \sum_n \bar{w}_r \begin{pmatrix} -\sin n\theta \\ \cos n\theta \end{pmatrix} \\
\bar{w}_\theta &= \frac{1}{2} \left( \frac{\partial \bar{u}}{\partial z} - \frac{\partial \bar{w}}{\partial r} \right), & w_\theta &= \sum_n \bar{w}_\theta \begin{pmatrix} \cos n\theta \\ \sin n\theta \end{pmatrix} \\
\bar{w}_z &= \frac{1}{2r} \left( \frac{\partial(r\bar{v})}{\partial r} - n \bar{u} \right), & w_z &= \sum_n \bar{w}_z \begin{pmatrix} -\sin n\theta \\ \cos n\theta \end{pmatrix}
\end{aligned}
\tag{3-25}$$

Since these equations must hold for any arbitrary angle  $\theta$ , and the modal displacements are independent of  $\theta$ , it follows that:

$$\begin{aligned}
-\rho \Omega^2 \bar{u} &= (\lambda + 2G) \frac{\partial \bar{\Delta}}{\partial r} + 2G \frac{n}{r} \bar{w}_z + 2G \frac{\partial \bar{w}_\theta}{\partial z} \\
-\rho \Omega^2 \bar{w} &= (\lambda + 2G) \frac{\partial \bar{\Delta}}{\partial z} - 2G \frac{\partial r \bar{w}_\theta}{\partial r} - 2G \frac{n \bar{w}_r}{r} \\
-\rho \Omega^2 \bar{v} &= (\lambda + 2G) \frac{n \bar{\Delta}}{r} - 2G \frac{\partial \bar{w}_r}{\partial z} + 2G \frac{\partial \bar{w}_z}{\partial r}
\end{aligned} \tag{3-26}$$

which shall be called the "modal wave equations". They are only a function of  $r$  and  $z$ , with the parameter  $n = 0, 1, 2, \dots$  dependent on the Fourier decomposition of the loadings or prescribed displacements.

The general solution to this system of partial differential equations is (34):

$$\begin{aligned}
\bar{u} &= \bar{u}_1 + \bar{u}_2 + \bar{u}_3 \\
\bar{w} &= \bar{w}_1 + \bar{w}_2 + \bar{w}_3 \\
\bar{v} &= \bar{v}_1 + \bar{v}_2 + \bar{v}_3
\end{aligned} \tag{3-27}$$

where the particular solutions  $\bar{u}_1, \bar{u}_2$ , etc. are given by

$$\begin{cases}
 \bar{u}_1 = k A \frac{\partial H_n^{(2)}(kr)}{\partial r} e^{-lz + i\omega t} \\
 \bar{w}_1 = -k l A H_n^{(2)}(kr) e^{-lz + i\omega t} \\
 \bar{v}_1 = k A \frac{n}{r} H_n^{(2)}(kr) e^{-lz + i\omega t}
 \end{cases}$$

$$\begin{cases}
 \bar{u}_2 = B \frac{n}{r} H_n^{(2)}(kr) e^{-mz + i\omega t} \\
 \bar{w}_2 = 0 \\
 \bar{v}_2 = B \frac{\partial}{\partial r} H_n^{(2)}(kr) e^{-mz + i\omega t}
 \end{cases}
 \tag{3-28}$$

$$\begin{cases}
 \bar{u}_3 = -C m \frac{\partial}{\partial r} H_n^{(2)}(kr) e^{-mz + i\omega t} \\
 \bar{w}_3 = C k^2 H_n^{(2)}(kr) e^{-mz + i\omega t} \\
 \bar{v}_3 = -C m \frac{n}{r} H_n^{(2)}(kr) e^{-mz + i\omega t}
 \end{cases}$$

in which  $H^{(2)}(kr)$  are second Hankel functions of order  $n$  (order of the Fourier component),  $A$ ,  $B$ ,  $C$  are integration constants,  $k$  is an arbitrary parameter (wave number), and:

$$l = \pm \sqrt{k^2 - \alpha^2} \quad \alpha = \frac{\Omega}{U_p} \quad (3-29)$$

$$m = \pm \sqrt{k^2 - \beta^2} \quad \beta = \frac{\Omega}{U_s}$$

$$\frac{1}{U_p} = \sqrt{\frac{P}{\lambda + 2G}} \quad \frac{1}{U_s} = \sqrt{\frac{P}{G}}$$

Actually, analogous expressions containing first Hankel functions  $H^{(1)}(kr)$  have been omitted in the particular solutions given by (3-28), since they correspond, in combination with the factor  $e^{i\Omega t}$ , to waves travelling from  $\infty$  towards the origin and thus must be disregarded in accordance with Sommerfeld's radiation principle. (Sources confined to the vicinity of the origin). For this reason, the index (2) and the argument  $(kr)$  in the Hankel functions, as well as the factor  $e^{i\Omega t}$ , will be dropped from now on, which shall be understood. Adding up the three particular solutions, and factoring out the Hankel functions, the general solution can be rewritten as:

$$\bar{u} = f_1(z) H_n' + f_3(z) \frac{n}{r} H_n$$

$$\bar{w} = f_2(z) k H_n \quad (3-30)$$

$$\bar{v} = f_1(z) \frac{n}{r} H_n + f_3(z) H_n'$$

where  $H_n' = \frac{\partial H_n^{(2)}(kr)}{\partial r}$

and

$$f_1(z) = k (A_1 e^{-lz} + A_2 e^{lz}) - m (C_1 e^{-mz} - C_2 e^{mz})$$

$$f_2(z) = -l (A_1 e^{-lz} - A_2 e^{lz}) + k (C_1 e^{-mz} + C_2 e^{mz}) \quad (3-31)$$

$$f_3(z) = B_1 e^{-mz} + B_2 e^{mz}$$

Equations (3-30) can be written in matrix notation as

$$\bar{U} = HF \quad (3-32)$$

where

$$H = \begin{pmatrix} H_n' & \frac{n}{r} H_n \\ k H_n & H_n' \\ \frac{n}{r} H_n & H_n' \end{pmatrix} \quad (3-33)$$



and

$$\mathbf{F} = \begin{Bmatrix} f_1(z) \\ f_2(z) \\ f_3(z) \end{Bmatrix} \quad (3-34)$$

Correspondingly, the modal wave equations can be expressed shortly as

$$\mathbf{W} = \mathbf{H}\mathbf{L} = \mathbf{0} \quad (3-35)$$

in which the components  $L_i$  of the  $\mathbf{L}$  vector are given by

$$(f_i' = \frac{\partial f_i}{\partial z}) :$$

$$L_1 = k(\lambda + 2G)(f_2' - k f_1) + G(f_1'' - k f_2') + \rho \Omega^2 f_1$$

$$L_2 = (\lambda + 2G)(f_2'' - k f_1') + G k(f_1' - k f_2) + \rho \Omega^2 f_2$$

$$L_3 = G(f_3'' - k^2 f_3) + \rho \Omega^2 f_3$$

(3-36)

Also, the expression of the strains and stresses in terms of the functions  $f_i$  will be needed later. Substituting (3-30) into (3-8) results in:

$$\bar{\epsilon}_{rr} = f_1 H_n'' + \frac{n}{r} f_3 \left( H_n' - \frac{H_n}{r} \right)$$

$$\bar{\epsilon}_{\theta\theta} = f_1 \left( \frac{H_n'}{r} - \frac{n^2}{r^2} H_n \right) - f_3 \frac{n}{r} \left( H_n' - \frac{H_n}{r} \right)$$

$$\bar{\epsilon}_{zz} = f_2' k H_n$$

(3-37)

$$\bar{\epsilon}_{rz} = f_1' H_n' + f_3' \frac{n}{r} H_n + k f_2 H_n'$$

$$\bar{\epsilon}_{r\theta} = 2 f_1 \frac{n}{r} \left( H_n' - \frac{H_n}{r} \right) + f_3 \left( H_n'' - \frac{1}{r} H_n' + \frac{n^2}{r^2} H_n \right)$$

$$\epsilon_{z\theta} = f_1' \frac{n}{r} H_n + f_3' H_n' + k f_2 \frac{n}{r} H_n$$

and with

$$\bar{\Delta} = (f_2' - k f_1) k H_n$$

(3-38)

the stresses follow

$$\bar{\sigma}_{rr} = 2G \bar{\epsilon}_{rr} + \lambda \bar{\Delta}$$

$$\bar{\sigma}_{\theta\theta} = 2G \bar{\epsilon}_{\theta\theta} + \lambda \bar{\Delta}$$

$$\bar{\sigma}_{zz} = 2G \bar{\epsilon}_{zz} + \lambda \bar{\Delta}$$

(3-39)

$$\bar{\sigma}_{rz} = G \bar{\epsilon}_{rz}$$

$$\bar{\sigma}_{r\theta} = G \bar{\epsilon}_{r\theta}$$

$$\bar{\sigma}_{z\theta} = G \bar{\epsilon}_{z\theta}$$

### 3.5.- Principle of virtual displacements:

In dynamics, the generalization of the principle of virtual displacements into a law of kinetics by use of D'Alembert's rule is referred to as Hamilton's principle. For non-conservative systems, the principle states that the work performed by the applied external loads and the inertial forces during an arbitrary virtual displacement field that is consistent with the constraints, is equal to the change in strain energy plus the energy dissipated by internal friction during that virtual displacement.

Hamilton's principle shall be specialized and adapted for the specific problem discussed in this dissertation in which the coordinate system is cylindrical, and the viscoelastic constants are complex. By applying two Fourier transformations, one in the time domain, and one in the  $\theta$  coordinate, the principle of virtual displacements for

axisymmetric systems subjected to a general harmonic excitation shall be developed.

A general form of Hamilton's principle in elasticity is

$$\int_{t_1}^{t_2} \left\{ \iiint_V \delta \epsilon_{ij} \sigma_{ij} dV - \iiint_V \delta u_i (b_i - \rho \ddot{u}_i) dV - \iint_{S_p} \delta u_i p_i dA \right\} dt = 0 \quad (3-40)$$

where  $\delta \epsilon_{ij}$  is the virtual strain field corresponding to the displacement field  $\delta u_i$  which is consistent with the constraints, and vanishes at the time  $t_1$  and  $t_2$ .  $S_p$  corresponds to that portion of the boundary where the forces are prescribed. The term  $\delta \epsilon_{ij} \sigma_{ij}$  represents the change in strain energy as well as the energy lost due to internal friction. Since the prescribed virtual displacements are arbitrary, a set of displacements can be chosen of the form:

$$\delta u_i(x, t) = \delta \tilde{u}_i(x) \cdot \delta(t) \quad x = (x_1, x_2, x_3) \quad (3-41)$$

$$\delta \epsilon_{ij}(x, t) = \delta \tilde{\epsilon}_{ij}(x) \cdot \delta(t) \quad t_1 \leq t \leq t_2$$

where  $x$  stands for the coordinate system, and  $\delta(t)$  is the Dirac delta function. Substitution in (3-40) and integration over the time domain yields

$$\iiint \delta \tilde{\epsilon}_{ij} \sigma_{ij} dV - \iiint \delta \tilde{u}_i (b_i - \rho \ddot{u}_i) dV - \iint_{S_p} \delta \tilde{u}_i p_i dA = 0$$

(3-42)

where  $\sigma_{ij}$  ,  $b_i$  ,  $\ddot{u}_i$  , and  $p_i$  are evaluated at the time  $t$ . Alternatively, it is possible to arrive at this result starting from the equilibrium equations (wave equations) and the boundary force equations, and conceiving the time variable to remain constant while the virtual displacements are applied, that is, the real motion is stopped while the virtual displacements are performed; however, the inertial forces must be assumed to persist. In other words, it is assumed that the performance of the virtual displacements consumes no time (18).

Applying a Fourier transformation (FT) to the equation above, and defining

$$\begin{aligned} \tilde{\sigma}_{ij}(\omega) &= \text{FT}(\sigma_{ij}(t)) \quad , \quad \tilde{b}_i(\omega) = \text{FT}(b_i(t)) \quad , \quad \tilde{p}_i(\omega) = \text{FT}(p_i(t)) \\ \tilde{u}_i(\omega) &= \text{FT}(u_i(t)) \quad , \quad -\omega^2 \tilde{u}_i(\omega) = \text{FT}(\ddot{u}_i(t)) \end{aligned} \quad (3-43)$$

yields

$$\iiint \delta \tilde{\epsilon}_{ij} \tilde{\sigma}_{ij} dV - \iiint \delta \tilde{u}_i (\tilde{b}_i + \rho \omega^2 \tilde{u}_i) dV - \iint_{S_p} \tilde{p}_i \delta \tilde{u}_i dA = 0 \quad (3-44)$$

where the transformed quantities are in general complex.

For a general viscoelastic material, the stresses  $\tilde{\sigma}_{ij}$  are related to the strains  $\tilde{\epsilon}_{ij}$  through the relaxation tensor  $\tilde{G}_{ijkl}$  (eq. 2-4)

$$\tilde{\sigma}_{ij} = i\Omega \tilde{G}_{ijkl} \tilde{\epsilon}_{kl} \quad (3-45)$$

which for an isotropic material has only two independent components  $G, \lambda$ . In vector notation, this was written as (eq. 2-8)

$$\tilde{\sigma} = D \tilde{\epsilon} \quad (3-46)$$

For real elastic moduli, the stresses will be real and in phase with the strains and displacements, whereas for complex moduli, they will be complex and there will be a phase lag between these two quantities.

An alternate form of equation (3-44) is obtained by integration by parts, resulting in

$$\iiint \delta \tilde{u}_i (\tilde{\sigma}_{ij,j} + \tilde{b}_i + \rho \Omega^2 \tilde{u}_i) dV + \iint_{S_F} \delta \tilde{u}_i (\tilde{p}_i - \alpha_{vj} \tilde{\sigma}_{ij}) dA = 0 \quad (3-47)$$

which for arbitrary variations of the virtual displacements  $\delta \tilde{u}_i$  yields the body and boundary equilibrium equations.

Using the stress strain relation (3-45), the term in parenthesis in the first integral becomes the wave equation, and

$$\iiint \delta \tilde{u}_i (\text{wave equation})_i dV + \iint_{S_p} \delta \tilde{u}_i (\tilde{p}_i - \alpha_{vj} \sigma_{ij}) dA = 0 \quad (3-48)$$

a form which shall be useful later on. Switching now from tensor to matrix notation, and dropping the superscript tilde, with the implicit understanding that the applied forces (displacements) are harmonic, equation (3-44) becomes then

$$\iiint \delta \mathbf{u}^T \boldsymbol{\sigma} dV - \iiint \delta \mathbf{u}^T (\mathbf{b} + \rho \omega^2 \mathbf{u}) dV - \iint_{S_p} \delta \mathbf{u}^T \mathbf{P} dA = 0 \quad (3-49)$$

The principle of virtual displacements, specialized for the modal components in the axisymmetric formulation, can be obtained now expanding the strains, stresses, forces and displacements as in sections 3.1 through 3.4 in Fourier series around the axis. For a cylindrically orthotropic (cross anisotropic) material ( $D_{12} = D_{21} = 0$ ), integration w/r to  $\theta$ , with  $dV = r dr d\theta dz$ , and using

$$\begin{aligned}
\int_0^{2\pi} \sin m\theta \sin n\theta d\theta &= (\delta_{mn} - \delta_{m0}\delta_{n0})\pi = \begin{cases} \pi & \text{for } m=n \neq 0 \\ 0 & \text{else} \end{cases} \\
\int_0^{2\pi} \cos m\theta \cos n\theta d\theta &= (\delta_{mn} + \delta_{m0}\delta_{n0})\pi = \begin{cases} \pi & \text{for } m=n \neq 0 \\ 2\pi & \text{" } m=n=0 \\ 0 & \text{else} \end{cases} \\
\int_0^{2\pi} \sin m\theta \cos n\theta d\theta &= 0
\end{aligned}$$

yields for the principle of virtual displacements

$$\begin{aligned}
\iint (\delta \bar{\mathbf{E}}_s^T \mathbf{D} \bar{\mathbf{E}}_s + \delta \bar{\mathbf{E}}_a^T \mathbf{D} \bar{\mathbf{E}}_a) r dr dz - \iint \rho \Omega^2 (\delta \bar{\mathbf{U}}_s^T \bar{\mathbf{U}}_s + \delta \bar{\mathbf{U}}_a^T \bar{\mathbf{U}}_a) r dr dz = \\
= \iint_{S_p} (\delta \bar{\mathbf{U}}_s^T \bar{\mathbf{P}}_s + \delta \bar{\mathbf{U}}_a^T \bar{\mathbf{P}}_a) r ds
\end{aligned}$$

or since  $(\delta \bar{\mathbf{E}}_s, \delta \bar{\mathbf{U}}_s)$  and  $(\delta \bar{\mathbf{E}}_a, \delta \bar{\mathbf{U}}_a)$  are independent and arbitrary

$$\iint \delta \bar{\mathbf{E}}^T \mathbf{D} \bar{\mathbf{E}} r dr dz - \iint \rho \Omega^2 \delta \bar{\mathbf{U}}^T \bar{\mathbf{U}} r dr dz = \int_{S_p} \delta \bar{\mathbf{U}}^T \mathbf{P} r ds \quad (3-50)$$

where the indices s, or a and the superscript bar referring to the Fourier modal amplitude have been dropped and are understood. Similarly,

$$\iint \delta \bar{\mathbf{U}}^T \mathbf{W} r dr dz + \int \delta \bar{\mathbf{U}}^T (\mathbf{P} - \boldsymbol{\sigma}_v) r ds = 0 \quad (3-51)$$

where  $\mathbf{W} = \mathbf{H}\mathbf{L}$  (eq. 3-35) are the modal wave equations, and  $\boldsymbol{\sigma}_v = \{\alpha_{vj} \sigma_{ij}\}$  are the projections of the modal stresses on



the unit outward boundary normal. Equation (3-51) will be of advantage over equation (3-50) or (3-49) when using the principle of virtual displacements to define the eigenvalue problem for the viscoelastic energy absorbing boundary, since it will not require a cumbersome integration of product of the Hankel functions over the coordinate  $r$ .

### 3.6.- Finite element formulation:

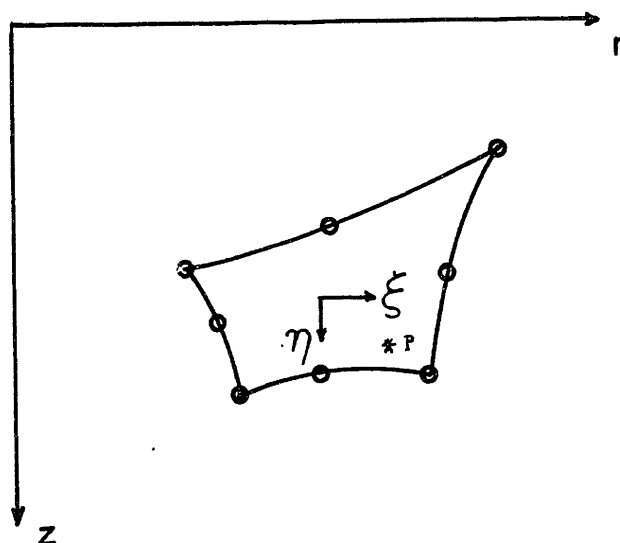


fig. 5

In the isoparametric formulation, the displacements are expanded in the same way as the coordinates. Let  $\emptyset$  denote the expansion vector; the coordinates of a point  $P$  can be then expressed as:

$$r = \phi^T R_o \quad R_o = \{ r_i \} \quad (3-52)$$

$$z = \phi^T Z_o \quad Z_o = \{ z_i \}$$

and using the same expansions for the displacements,

$$u = \Phi^T u_o \quad u = \begin{Bmatrix} \bar{u} \\ \bar{w} \\ \bar{v} \end{Bmatrix} \quad u_o = \begin{Bmatrix} \{ \bar{u}_i \} \\ \{ \bar{w}_i \} \\ \{ \bar{v}_i \} \end{Bmatrix} \quad (3-53)$$

where

$$\Phi = \begin{Bmatrix} \phi & & \\ & \phi & \\ & & \phi \end{Bmatrix} \quad (3-54)$$

is the expansion matrix.

On the other hand, the strains are given in terms of the displacements:

$$\epsilon = A u$$

$$\therefore \epsilon = A \Phi u_o$$

or by defining

$$B = A \Phi^T = \begin{Bmatrix} b_{11} & n b_{12} \\ n b_{21} & b_{22} \end{Bmatrix} \quad (3-55)$$

it follows that

$$\boldsymbol{\varepsilon} = \mathbf{B} \mathbf{u}_e \quad (3-56)$$

Substitution into equation (3-50) gives

$$\sum_{\text{Elements}} \delta \mathbf{u}_e^T \left\{ \iint (\mathbf{B}^T \mathbf{D} \mathbf{B} - \rho \Omega^2 \boldsymbol{\Phi} \boldsymbol{\Phi}^T) \mathbf{u}_e r dr dz - \int \boldsymbol{\Phi} \mathbf{P} r ds \right\} = 0 \quad (3-57)$$

and from the arbitrariness of the virtual displacements,

$$(-\rho \Omega^2 \mathbf{m} + \mathbf{K}) \mathbf{u} = \mathbf{P} \quad (3-58)$$

where  $\mathbf{u}$ ,  $\mathbf{P}$  stand now for the total nodal displacement and load vectors. The total stiffness and mass matrices  $\mathbf{K}$ ,  $\mathbf{m}$  and the load vector  $\mathbf{P}$  are assembled from the element matrices:

$$\begin{aligned} \mathbf{M}_k &= \iint \rho \boldsymbol{\Phi} \boldsymbol{\Phi}^T r dr dz \\ \mathbf{K}_k &= \iint \mathbf{B}^T \mathbf{D} \mathbf{B} r dr dz \\ \mathbf{P}_k &= \int \boldsymbol{\Phi} \mathbf{P} r ds \end{aligned} \quad (3-59)$$

where the index  $k$  refers to the  $k^{\text{th}}$  element. Substitution of

$$D = \begin{Bmatrix} D_1 & \\ & D_2 \end{Bmatrix} \quad B = \begin{Bmatrix} b_{11} & n & b_{12} \\ n & b_{21} & b_{22} \end{Bmatrix} \quad \Phi = \begin{Bmatrix} \phi & & \\ & \phi & \\ & & \phi \end{Bmatrix}$$

gives

$$K_k = \begin{Bmatrix} K_1 + n^2 K_2 & n K_3 \\ n K_3^T & K_4 + n^2 K_5 \end{Bmatrix} \quad (3-60)$$

$$M = \begin{Bmatrix} m & & \\ & m & \\ & & m \end{Bmatrix}$$

where

$$K_1 = \iint b_{11}^T D_1 b_{11} r dr dz$$

$$K_2 = \iint b_{21}^T D_2 b_{21} r dr dz$$

$$K_3 = \iint (b_{11}^T D_1 b_{12} + b_{21}^T D_2 b_{22}) r dr dz \quad (3-61)$$

$$K_4 = \iint b_{22}^T D_2 b_{22} r dr dz$$

$$K_5 = \iint b_{12}^T D_1 b_{12} r dr dz$$

and

$$m = \iiint_V \phi \phi^T r dr dz$$

The integration in each element is carried out by means of Gaussian quadrature with the dimensionless coordinates  $\xi, \eta$ . The details of the isoparametric formulation will be omitted, since they are well known and need not be repeated here. Since in the Gaussian quadrature scheme (3x3 points used) there are no points on the boundary of the elements, no problems are encountered with the singularity of the integrand at the symmetry axis ( $r=0$ ) for those elements adjacent to it.

### 3.7.- Energy absorbing boundary:

As has been mentioned earlier, the far field region is to be substituted in the finite element formulation by the dynamic stiffness matrix of a consistent energy absorbing boundary. The idea behind this boundary is as follows:

If the core region is removed and substituted by equivalent distributed forces corresponding to the actual internal stresses as given by the continuum theory, then the equilibrium as well as the dynamic behavior of the far field

region is preserved. Since there are no other prescribed forces acting on this region, the displacements at the boundary (and in any other point in the far field as well) are uniquely defined in terms of these fictitious boundary stresses. Therefore, if these stresses could be related to the corresponding displacements by means of a dynamic stiffness function, then the entire far-field could be substituted by this stiffness function as to the effect of the far-field on the displacement of the core region. On the other hand, it is always possible to express the displacements in the far-field region, and particularly at the boundary, in terms of eigenfunctions corresponding to the natural modes of wave propagation in the stratum. The general solution to the wave propagation problem is given by equations (3-28), which depend on the integration constants  $A$ ,  $B$ ,  $C$ , etc. and on an undetermined parameter  $k$ , the wave number. In an unbounded medium, any value of  $k$ , and hence, any wave length is admissible; for a layered stratum, however, only a discrete spectrum of wave numbers and propagation modes can be found that satisfy the given boundary conditions. Therefore, at any given driving frequency  $\Omega$ , there exists an infinite but discrete number of such propagation modes with associated wave numbers  $k$ , which can be found from a transcendental eigenvalue problem resulting from establishing the continuity of the stresses

and displacements across the layer interfaces, and the use of the boundary conditions at the base rock and free surface. For each of these eigenfunctions, the distribution of the stresses can be determined in terms of the modal displacements at the boundary up to a multiplicative constant, the participation factor of the mode. Combining these modal stresses as to match the actual (unknown) distribution of stresses at the boundary, the modal participation factors can be computed in terms of the boundary displacements, and from here, the stiffness function relating boundary stresses to displacements.

The solution of the transcendental eigenvalue problem for the continuum solution is extremely difficult, and can in general be found only by search procedures. However, by substituting the actual dependence of the displacements on the  $z$  coordinate, as given by equations (3-31), by a discrete expansion consistent with that used for the finite elements joining the boundary, it is possible to reduce the transcendental eigenvalue problem to an algebraic one with finite number of modes, for which numerical solution methods are readily available. Operating with this discrete solution, the dynamic stiffness matrix (in place of the stiffness functions) relating nodal forces to nodal displacements can be determined and then added to the total

dynamic stiffness matrix of the core region to form the dynamic stiffness matrix of the system.

Consider a toroidal section of the far-field limited by two cylindrical surfaces of arbitrary coordinates  $r$  and  $r+l$ , as shown in the figure below:

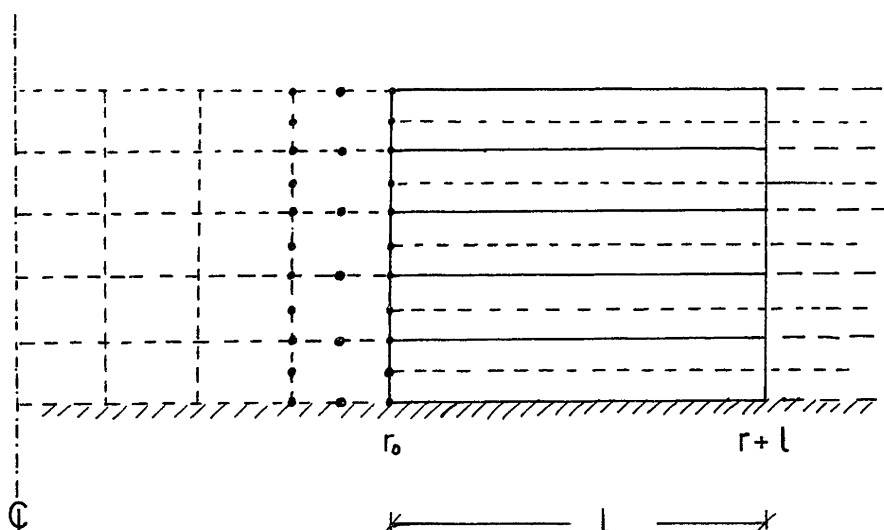


fig. 6

The stratum, as shown above, is discretized in horizontal layers, the interfaces of which match the nodal joints (circles) of the finite element mesh in the core region. The displacements for free harmonic waves in any layer in the far-field region are given by (equations (3-32)):



$$U = HF, \quad F = \begin{Bmatrix} f_1 \\ f_2 \\ f_3 \end{Bmatrix} \quad (3-62)$$

where  $F$  contains functions of  $z$  only (equations (3-31)). Let the values of these functions at the interfaces be defined by

$$X_i = \begin{Bmatrix} x_1 \\ x_2 \\ x_3 \end{Bmatrix}_i \quad (3-63)$$

where the index  $i$  refers to the interface. Consider also any particular discrete layer:

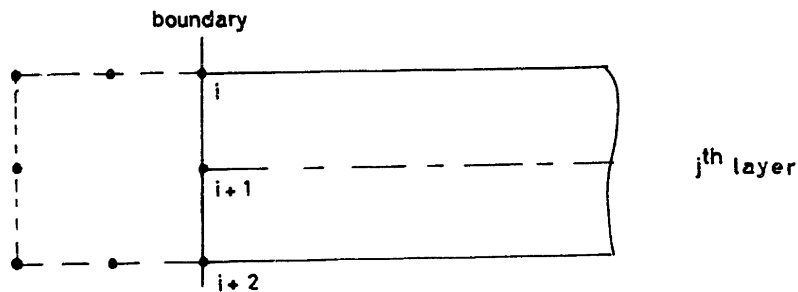


fig. 7

The layer vector  $X_j$ , assembled with the elements of the  $X_i$  vectors associated with that layer is now defined as follows:

$$X = \begin{Bmatrix} X_i \\ \vdots \\ X_{i+m} \end{Bmatrix} = \begin{Bmatrix} \begin{pmatrix} X_1 \\ X_2 \\ X_3 \end{pmatrix}_i \\ \vdots \\ \begin{pmatrix} X_1 \\ X_2 \\ X_3 \end{pmatrix}_{i+m} \end{Bmatrix} \quad (3-64)$$

where  $m$  is the order of the finite element expansion joining the far-field boundary. Rather than using the exact expressions for the  $F$  functions which contain the unknown integration constants and the eigenvalue  $k$ , these functions are expanded in terms of the nodal values  $X_i$ , using the same expansions as for the coordinates and displacements in the finite element region:

$$F = NX \quad (3-65)$$

where

$$N = \{ g_1 I, g_2 I, \dots, g_{m+1} I \}, \quad I = \begin{Bmatrix} 1 & & \\ & 1 & \\ & & 1 \end{Bmatrix} \quad (3-66)$$

$$= \{ g_j I_j \}$$

contains the expansion coefficients  $g_j$ .

For linear expansion ( $m=1$ ), the coefficients are  $g_1 = 1-\eta$ ,  $g_2 = \eta$ , and the expansion matrix is

$$N = \begin{Bmatrix} 1-\eta & & 1+\eta \\ & 1-\eta & & 1+\eta \\ & & 1-\eta & & 1+\eta \end{Bmatrix}, \quad -1 \leq \eta \leq 1 \quad (3-67)$$

For quadratic expansion ( $m=2$ ), the coefficients are  $g_1 = \frac{1}{2} \eta (\eta-1)$ ,  $g_2 = 1-\eta^2$ ,  $g_3 = \frac{1}{2} \eta (\eta+1)$ , and the expansion matrix is

$$N = \begin{Bmatrix} \frac{1}{2} \eta (\eta-1) & & 1-\eta^2 & & \frac{1}{2} \eta (\eta+1) \\ & \frac{1}{2} \eta (\eta-1) & & 1-\eta^2 & & \frac{1}{2} \eta (\eta+1) \\ & & \frac{1}{2} \eta (\eta-1) & & 1-\eta^2 & & \frac{1}{2} \eta (\eta+1) \end{Bmatrix}$$

$$, \quad -1 \leq \eta \leq 1 \quad (3-68)$$

From here, it follows that the displacements across the layer are given by

$$U = HNX \quad (3-69)$$

In particular,

$$U_i = HX_i = \begin{Bmatrix} \bar{u}_i \\ \bar{w}_i \\ \bar{v}_i \end{Bmatrix} \quad (3-70)$$

are the nodal displacements, so that

$$U = NU_0, \quad U_0 = \begin{pmatrix} U_1 \\ \vdots \\ U_{i,m} \end{pmatrix} \quad (3-71)$$

The variation in the vertical direction of the displacements at the finite element - far field boundary, as given by equation (3-71), is consistent with that of the finite elements, since the same expansion is used in both cases.

The purpose now is to determine admissible solutions to the free wave propagation problem using the approximate displacement expansions (3-71). The exact expression (3-62) satisfies the principle of virtual displacements, equation (3-50) or (3-51) identically, since it is a solution to the wave equation. In the approximate solution, defined in an energy sense, equation (3-69) is substituted into equation (3-51) (although equation (3-50) is equivalent to (3-51), the latter is preferable, since it avoids a cumbersome integration over  $r$ ), integrated over the region (see Fig. 8 below), and required to vanish for arbitrary virtual displacements  $\delta U$ . Further, one requires that equilibrium be preserved on the average at any arbitrary vertical section by applying consistent nodal boundary forces  $P_0$ ,  $P'_0$ , at  $r=r_0$  and  $r=r_0+1$  as predicted by the displacement expansion.

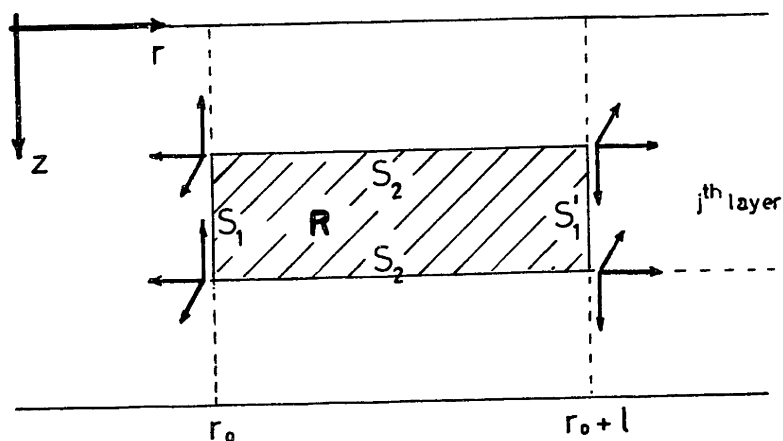


fig. 8

Defining by  $S_1$ ,  $S_1'$  the vertical boundaries, and by  $S_2$  the (discrete) layer interfaces, equation 3-51 can be written as

$$\sum_{\text{layers}} \left\{ \iint \delta \mathbf{u}^T \mathbf{W} r dr dz + \int_{S_1} \delta \mathbf{u}^T (\mathbf{P} - \boldsymbol{\sigma}_v) r ds + \int_{S_1'} \delta \mathbf{u}^T (\mathbf{P} - \boldsymbol{\sigma}_v) r ds + \int_{S_2} \delta \mathbf{u}^T (\mathbf{P} - \boldsymbol{\sigma}_v) r ds \right\} = 0 \quad (3-72)$$

Consistent nodal forces  $\mathbf{P}_0$ ,  $\mathbf{P}_0'$  are applied at each of the boundaries  $r_0$ ,  $r_0 + l$ , such that the integrals over  $S_1$ ,  $S_1'$  vanish, obtaining

$$\sum_{\text{layers}} \left\{ \delta \mathbf{u}^T \mathbf{P}_0 = \int_{S_1} \delta \mathbf{u}^T \mathbf{P} r ds = \int_{S_1} \delta \mathbf{u}^T \boldsymbol{\sigma}_v r ds \right\} \quad (3-73)$$

and a similar expression, which is not needed, for  $S_1'$ .

On the other hand, there are no external prescribed forces acting at the layer interfaces, so that

$$\sum_{\text{layers}} \left\{ \iint \delta u^T w r dr dz - \int_{S_2} \delta u \sigma_v r ds \right\} = 0 \quad (3-74)$$

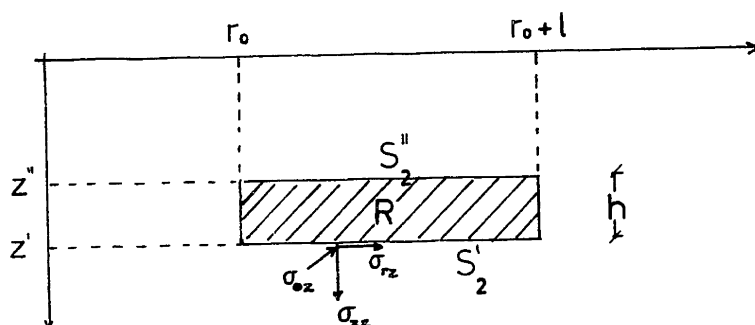


fig.9

Now, for the layer interfaces  $S_2$ ,  $\sigma_v$  is given by

$$\sigma_v = \begin{matrix} + \\ (-) \end{matrix} \begin{Bmatrix} \sigma_{rz} \\ \sigma_{zz} \\ \sigma_{\theta z} \end{Bmatrix} \quad (3-75)$$

where the positive sign corresponds to the face  $z=z'$  ( $S_2'$ ), while the negative sign to the face  $z=z''$  ( $S_2''$ ). Defining  $\sigma_v$  to be the vector with the positive sign, equation (3-74) can be modified to

$$\sum_{\text{layers}} \left\{ \iint \delta u^T w r dr dz - \int_0^h \delta u^T \sigma_v \Big|_0^h r dr \right\} = 0 \quad (3-76)$$

Now, it is always possible to make the transformation

$$\begin{aligned} \int \delta u^T \sigma_y r dr &= \iint \frac{\partial}{\partial z} (\delta u^T \sigma_y) r dr dz \\ &= \iint \delta u^T \frac{\partial \sigma_y}{\partial z} r dr dz + \iint \delta \left( \frac{\partial u^T}{\partial z} \right) \sigma_y r dr dz \quad (3-77) \end{aligned}$$

and substituting into (3-76)

$$\sum_{\text{layers}} \left\{ \iint \delta u^T \left( W - \frac{\partial \sigma_y}{\partial z} \right) r dr dz - \iint \delta \left( \frac{\partial u^T}{\partial z} \right) \sigma_y r dr dz \right\} = 0$$

or

$$\sum_{\text{layers}} \int \left\{ \int \delta u^T \left( W - \frac{\partial \sigma_y}{\partial z} \right) dz - \int \delta \left( \frac{\partial u^T}{\partial z} \right) \sigma_y dz \right\} r dr = 0 \quad (3-78)$$

On the other hand, from (3-37) and (3-39)

$$\sigma_y = \begin{pmatrix} G \left[ (f_1' + k f_2) H_n' + \frac{n}{r} H_n f_3' \right] \\ \left[ (\lambda + 2G) f_2' - \lambda k f_1 \right] k H_n \\ G \left[ (f_1' + k f_2) \frac{n}{r} H_n + f_3' H_n' \right] \end{pmatrix}$$

or

$$\sigma_y = H \begin{Bmatrix} G (f_1' + k f_2) \\ (\lambda + 2G) f_2' - \lambda k f_1 \\ G f_3' \end{Bmatrix} \quad (3-79)$$

where the matrix  $H$  is the same as the one given by equation (3-33). The wave equations (3-35), and the boundary stresses  $\sigma_y$  can be expressed as

$$W = HL = H \mathcal{L} F$$

$$\sigma_y = H S F \quad (3-80)$$

where the operator matrices  $\mathcal{L}$  and  $S$  are given by

$$\mathcal{L} = \begin{Bmatrix} \rho \Omega^2 - k^2 (\lambda + 2G) + G \frac{\partial^2}{\partial z^2} & k (\lambda + 2G) \frac{\partial}{\partial z} & 0 \\ -k (\lambda + 2G) \frac{\partial}{\partial z} & \rho \Omega^2 - k^2 G + (\lambda + 2G) \frac{\partial^2}{\partial z^2} & 0 \\ 0 & 0 & \rho \Omega^2 - k^2 G + G \frac{\partial^2}{\partial z^2} \end{Bmatrix}$$

(3-81)



$$\mathbf{S} = \begin{pmatrix} G \frac{\partial}{\partial z} & G k \\ -\lambda k & (\lambda + 2G) \frac{\partial}{\partial z} \\ & & G \frac{\partial}{\partial z} \end{pmatrix}$$

It follows then, with  $\delta \mathbf{u} = \mathbf{H} \mathbf{N} \delta \mathbf{X}$  and  $\mathbf{F} = \mathbf{N} \mathbf{X}$

$$\sum_{\text{Layers}} \int_r \left\{ \int_z \delta \mathbf{X}^T \mathbf{N}^T \mathbf{H}^T (\mathcal{L} - \frac{\partial}{\partial z} \mathbf{S}) \mathbf{N} \mathbf{X} dz - \int_z \delta \mathbf{X}^T \frac{\partial \mathbf{N}}{\partial z} \mathbf{H}^T \mathbf{H} \mathbf{S} \mathbf{N} \mathbf{X} dz \right\} r dr = 0$$

(3-82)

But,

$$\mathbf{N} = \{ g_j \mathbf{I}_j \}$$

$$\mathbf{N}^T \mathbf{N} = \{ g_i g_j \mathbf{I}_{ij} \}$$

(3-83)

$$\frac{\partial \mathbf{N}}{\partial z} = \{ g'_j \mathbf{I}_j \} = \mathbf{N}'$$

$$\mathbf{I}_j = \begin{pmatrix} 1 & & \\ & 1 & \\ & & 1 \end{pmatrix}$$

$$\mathbf{I}_{ij} = \mathbf{I}_i \mathbf{I}_j$$

Also,

$$\frac{\partial}{\partial z} \mathcal{S} = \mathcal{S}' = \left\{ \begin{array}{cc} G \frac{\partial^2}{\partial z^2} & G k \frac{\partial}{\partial z} \\ -\lambda k \frac{\partial}{\partial z} & (\lambda + 2G) \frac{\partial^2}{\partial z^2} \\ & & G \frac{\partial^2}{\partial z^2} \end{array} \right\} \quad (3-84)$$

$$\mathcal{L} - \mathcal{S}' = \rho \mathcal{L}^2 \left\{ \begin{array}{ccc} 1 & & \\ & 1 & \\ & & 1 \end{array} \right\} - k^2 \left\{ \begin{array}{cc} \lambda + 2G & \\ & G \\ & & G \end{array} \right\} - k \left\{ \begin{array}{cc} 0 & -\lambda \\ G & 0 \\ & & 0 \end{array} \right\} \frac{\partial}{\partial z}$$

It is possible now to make the following transformation:

$$N^T H^T (\mathcal{L} - \mathcal{S}) N = \bar{H} N^T (\mathcal{L} - \mathcal{S}) N \quad (3-85)$$

$$N^T H^T \mathcal{S} N = \bar{H} N^T \mathcal{S} N$$

where the matrix  $\bar{H}$  is given by

$$\bar{H} = \left\{ \begin{array}{ccc} H^T H & & \\ & H^T H & \\ & & \ddots \\ & & & H^T H \end{array} \right\} \quad (3-86)$$

and is formed with  $m+1$  ( $m$ =order of F.E. expansion)  $3 \times 3$  submatrices  $H^T H$ . Since  $\bar{H}$  is independent of  $z$ , substitution of (3-85) into (3-82) yields

$$\sum_{\text{layers}} \delta X^T \left\{ \int_r \bar{H} r dr \right\} \left\{ \int_z N(\mathcal{L}-S)N dz - \int_z N^T S N dz \right\} X = 0 \quad (3-87)$$

or defining

$$\int_{r_0}^{r_0+\ell} \bar{H} r dr = \mathcal{H} \quad (3-88)$$

gives

$$\sum_{\text{layers}} \delta X^T \mathcal{H} \left\{ \int_0^h N^T(\mathcal{L}-S)N dz - \int_0^h N^T S N dz \right\} X = 0 \quad (3-89)$$

Since the non-singular matrix  $\mathcal{H}$  is the same for all layers, requiring equation (3-89) to vanish for any arbitrary virtual  $\delta X$  leads to the biquadratic eigenvalue problem

$$(A k^2 + B k + G - \Omega^2 M) X = 0 \quad (3-90)$$

or briefly, with  $C = G - \Omega^2 M$  (3-91)

$$(A k^2 + B k + C) X = 0 \quad (3-92)$$

where the matrices A, B, G, M, are assembled from the layer submatrices  $A_j$ ,  $B_j$ ,  $G_j$ ,  $M_j$ , overlapping the corresponding nodal elements:

$$A = \left\{ \begin{array}{ccc} & A_1 & \\ & & A_j \\ & & & A_l \end{array} \right\} \quad \begin{array}{l} l = \text{number of layers} \\ \text{this portion not used, since } U_{\text{rock}} = 0 \end{array} \quad (3-93)$$

The modal shapes  $X$  in equation (3-91) above refer now to the whole stratum:

$$X = \{X_i\} = \left\{ \begin{array}{c} \left( \begin{array}{c} X_1 \\ X_2 \\ X_3 \end{array} \right)_1 \\ \vdots \\ \left( \begin{array}{c} X_1 \\ X_2 \\ X_3 \end{array} \right)_l \end{array} \right\} \quad (3-94)$$

The submatrices  $A_j$ ,  $B_j$ , etc. involve integration of terms of the form  $\int N^T N dz$ ,  $\int N'^T N dz$ ,  $\int N'^T N' dz$ , and therefore, the integrals of  $\{g_i g_j\}$ ,  $\{g_i' g_j\}$ ,  $\{g_i g_j'\}$ ,  $\{g_i' g_j'\}$

are needed.

a) Linear expansion: using (3-67),

$$\int_0^h \{g_i g_j\} dz = \frac{h}{6} \begin{pmatrix} 2 & 1 \\ 1 & 2 \end{pmatrix}$$

$$\int_0^h \{g_i g'_j\} dz = \frac{1}{2} \begin{pmatrix} -1 & 1 \\ -1 & 1 \end{pmatrix}$$

(3-95)

$$\int_0^h \{g'_i g_j\} dz = \frac{1}{2} \begin{pmatrix} -1 & -1 \\ 1 & 1 \end{pmatrix}$$

$$\int_0^h \{g'_i g'_j\} dz = \frac{1}{h} \begin{pmatrix} 1 & -1 \\ -1 & 1 \end{pmatrix}$$

and the layer matrices are

$$\mathbf{A}_j = \frac{h}{6} \begin{pmatrix} 2(\lambda+2G) & & & \lambda+2G & & \\ & 2G & & & G & \\ & & 2G & & & G \\ \lambda+2G & & & 2(\lambda+2G) & & \\ & G & & & 2G & \\ & & G & & & 2G \end{pmatrix}$$

$$\mathbf{B}_j = \frac{1}{2} \left\{ \begin{array}{cccccc} 0 & \lambda - G & 0 & 0 & -(\lambda + G) & 0 \\ \lambda - G & 0 & 0 & \lambda + G & 0 & 0 \\ 0 & 0 & 0 & 0 & 0 & 0 \\ 0 & \lambda + G & 0 & 0 & (\lambda - G) & 0 \\ -(\lambda + G) & 0 & 0 & -(\lambda - G) & 0 & 0 \\ 0 & 0 & 0 & 0 & 0 & 0 \end{array} \right\}$$

$$\mathbf{G}_j = \frac{1}{h} \left\{ \begin{array}{cccccc} G & & & -G & & \\ & \lambda + 2G & & & -(\lambda + 2G) & \\ & & G & & & -G \\ -G & & & G & & \\ & -(\lambda + 2G) & & & \lambda + 2G & \\ & & -G & & & G \end{array} \right\} \quad (3-96)$$

$$\mathbf{M}_j = \frac{\rho h}{6} \left\{ \begin{array}{cccccc} 2 & & & 1 & & \\ & 2 & & & 1 & \\ & & 2 & & & 1 \\ 1 & & & 2 & & \\ & 1 & & & 2 & \\ & & 1 & & & 2 \end{array} \right\}$$

b) Quadratic expansion: using (3-68) ,

$$\int_0^h \left\{ g_i g_j \right\} dz = \frac{h}{30} \begin{pmatrix} 4 & 2 & -1 \\ 2 & 16 & 2 \\ -1 & 2 & 4 \end{pmatrix}$$

$$\int_0^h \left\{ g_i g_j' \right\} dz = \frac{1}{6} \begin{pmatrix} -3 & 4 & -1 \\ -4 & 0 & 4 \\ 1 & -4 & 3 \end{pmatrix}$$

(3-97)

$$\int_0^h \left\{ g_i' g_j \right\} dz = \frac{1}{6} \begin{pmatrix} -3 & -4 & 1 \\ 4 & 0 & -4 \\ -1 & 4 & 3 \end{pmatrix}$$

$$\int_0^h \left\{ g_i' g_j' \right\} dz = \frac{1}{3h} \begin{pmatrix} 7 & -8 & 1 \\ -8 & 16 & -8 \\ 1 & -8 & 7 \end{pmatrix}$$

and the layer matrices are

$$A_j = \frac{R}{30} \left\{ \begin{array}{ccccccc} 4(\lambda+2G) & 4G & 2(\lambda+2G) & 2G & -(\lambda+2G) & -G & -G \\ 2(\lambda+2G) & 2G & 16(\lambda+2G) & 16G & 2(\lambda+2G) & 2G & 2G \\ -(\lambda+2G) & -G & 2(\lambda+2G) & 2G & 4(\lambda+2G) & 4G & 4G \end{array} \right\} \quad (3-98)$$

$$B_j = \frac{1}{6} \left\{ \begin{array}{cccccccc} 0 & 3(\lambda - G) & 0 & 0 & 0 & -4(\lambda + G) & 0 & (\lambda + G) \\ 3(\lambda - G) & 0 & 0 & 4(\lambda + G) & 0 & 0 & 0 & 0 \\ 0 & 0 & 0 & 0 & 0 & 0 & 0 & 0 \\ 0 & 4(\lambda + G) & 0 & 0 & 0 & 0 & 0 & -4(\lambda + G) \\ -4(\lambda + G) & 0 & 0 & 0 & 0 & 4(\lambda + G) & 0 & 0 \\ 0 & 0 & 0 & 0 & 0 & 0 & 0 & 0 \\ 0 & -(\lambda + G) & 0 & 4(\lambda + G) & 0 & 0 & 0 & -3(\lambda - G) \\ (\lambda + G) & 0 & 0 & -4(\lambda + G) & 0 & 0 & -3(\lambda - G) & 0 \\ 0 & 0 & 0 & 0 & 0 & 0 & 0 & 0 \end{array} \right\}$$



$$\begin{aligned}
\mathbf{G}_j &= \frac{1}{3h} \begin{pmatrix} 7G & -8G & 7G(\lambda+2G) & -8G & -8(\lambda+2G) & 6 & (\lambda+2G) & 6 \\ -8G & 16G & 7G & 16G & -8(\lambda+2G) & -8G & -8G & 6 \\ -8(\lambda+2G) & -8G & -8G & -8G & (\lambda+2G) & 6 & -8(\lambda+2G) & -8G \\ 6 & -8G & -8G & -8G & -8(\lambda+2G) & -8G & -8(\lambda+2G) & -8G \\ -8G & 6 & -8G & 6 & 6 & -8G & 6 & -8G \\ -8(\lambda+2G) & -8G & -8G & -8G & -8G & -8G & -8G & -8G \\ 6 & -8G & -8G & -8G & -8G & -8G & -8G & -8G \\ -8G & -8G & -8G & -8G & -8G & -8G & -8G & -8G \end{pmatrix} \\
\mathbf{M}_j &= \frac{9h}{30} \begin{pmatrix} 4 & 2 & 4 & 2 & 4 & 2 & 4 & 2 \\ 2 & 4 & 2 & 4 & 2 & 4 & 2 & 4 \\ 4 & 2 & 4 & 2 & 4 & 2 & 4 & 2 \\ 2 & 4 & 2 & 4 & 2 & 4 & 2 & 4 \\ 4 & 2 & 4 & 2 & 4 & 2 & 4 & 2 \\ 2 & 4 & 2 & 4 & 2 & 4 & 2 & 4 \\ 4 & 2 & 4 & 2 & 4 & 2 & 4 & 2 \\ 2 & 4 & 2 & 4 & 2 & 4 & 2 & 4 \end{pmatrix}
\end{aligned}$$

Examination of the matrices (3-96) or (3-98) shows that they define two uncoupled eigenvalue problems for  $k$ : a quadratic

one, involving the  $x_1$ ,  $x_2$  variables (nodal  $f_1$ ,  $f_2$ ), and a linear one in  $k^2$  for the  $x_3$  (nodal  $f_3$ ) variable, since the corresponding terms in the B matrix are zero. These are called the generalized Rayleigh and Love eigenvalue problems respectively. The reason for this denomination transpires from (3-30), where it is seen that  $f_1$ ,  $f_2$  define (for  $n=0$ ) a vertically polarized (Rayleigh) wave, while  $f_3$  defines a horizontally polarized (Love) wave. Since the eigenvalue problems for the natural modes of wave propagation are independent of  $n$ , the Fourier expansion number for the  $\theta$  coordinate, it follows that any arbitrary 3-dimensional displacement field in a layered stratum can be expressed as superposition of Rayleigh and Love waves with wave numbers as given by the 2-dimensional plane-strain theory, and weighted with the appropriate participation factors,  $\cos n\theta$  ( $\sin n\theta$ ) factor, and Hankel functions. A further discussion on the properties of these eigenvalue problems can be found in the original work by Waas (44).

Consider now equation (3-73). For the sake of notation simplicity, the summation over the layers sign will be dropped, writing simply

$$\delta U_P = \int_{S_1} \delta \mathbf{U}^T \boldsymbol{\sigma}_y \mathbf{r} \, ds \quad (3-99)$$

or since  $\delta \mathbf{U}^T = \delta \mathbf{U}_o^T \mathbf{N}^T$ ,  $ds = dz$ ,  $r = r_o$

$$\delta \mathbf{U}_o^T \mathbf{P}_o = \delta \mathbf{U}_o^T \int_z \mathbf{N}^T \sigma_y r_o dz = \delta \mathbf{U}_o^T r_o \int \mathbf{N}^T \sigma_y dz \quad (3-100)$$

and for arbitrary variations of the nodal displacements

$$\mathbf{P}_o = r_o \int_0^h \mathbf{N}^T \sigma_y dz \quad (3-101)$$

On the other hand, for each propagation mode with wave number  $k$  and participation factor  $\alpha_k$ , the stresses at the vertical boundary are  $\sigma_y = \alpha_k \sigma_{yk}$  and the corresponding nodal forces are

$$\mathbf{P}_k = r_o \alpha_k \int_0^h \mathbf{N}^T \sigma_{yk} dz \quad (3-102)$$

The modal boundary stress vector  $\sigma_{yk}$  is given by

$$\sigma_{yk} = - \begin{Bmatrix} \sigma_{rr} \\ \sigma_{rz} \\ \sigma_{r\theta} \end{Bmatrix}_{k^{th} \text{ mode}} \quad (3-103)$$

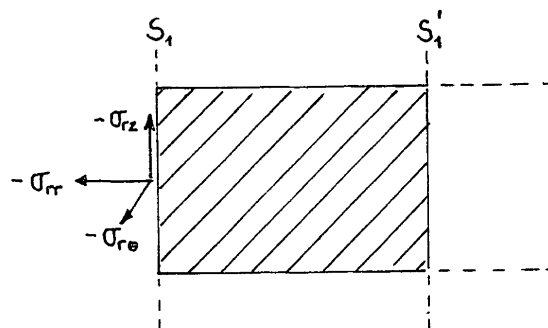


fig.10

Also, from (3-37 and (3-39),

$$\sigma_{\nu k} = - \begin{pmatrix} 2G H_n'' - \lambda k^2 H_n & \lambda & 2G \frac{n}{r_0} (H_n' - \frac{H_n}{r_0}) \\ G H_n' \frac{\partial}{\partial z} & G k H_n' & G \frac{n}{r_0} H_n \frac{\partial}{\partial z} \\ 2G \frac{n}{r_0} (H_n' - \frac{H_n}{r_0}) & 0 & (H_n'' - \frac{1}{r_0} H_n' + (\frac{n}{r_0})^2 H_n) G \end{pmatrix} \begin{pmatrix} f_1 \\ f_2 \\ f_3 \end{pmatrix}$$

(3-104)

or briefly

$$\sigma_{\nu k} = S F + T F' \quad (3-105)$$

where

$$S = - \begin{pmatrix} 2G H_n'' - \lambda k^2 H_n & 2G \frac{n}{r_0} (H_n' - \frac{1}{r_0} H_n) \\ & G k H_n' \\ 2G \frac{n}{r_0} (H_n' - \frac{1}{r_0} H_n) & G (H_n'' - \frac{1}{r_0} H_n' + (\frac{n}{r_0})^2 H) \end{pmatrix}$$

$$T = - \begin{pmatrix} 0 & \lambda k H_n & \\ G H_n' & 0 & G \frac{n}{r_0} H_n \\ & & 0 \end{pmatrix} \quad (3-106)$$

Now,  $F = NX$ ,  $F' = N'X$  and

$$\sigma_{y_k} = (SN + TN')X \quad (3-107)$$

Also  $N^T \sigma_{y_k} = N^T (SN + TN')X$

$$= (N^T S N + N^T T N')X$$

$$= (N^T N \bar{S} + N N'^T \bar{T})X \quad (3-108)$$

where the modified  $\bar{S}$  and  $\bar{T}$  matrices are defined as

$$\bar{S} = \left\{ \begin{array}{c} S \\ \vdots \\ S \end{array} \right\}, \quad \bar{T} = \left\{ \begin{array}{c} T \\ \vdots \\ T \end{array} \right\} \quad (3-109)$$

and are assembled with  $m+1$  submatrices  $S$ ,  $T$ .

Therefore

$$P_k = \alpha_k r_0 \left\{ \left[ \int N^T N dz \right] \bar{S} + \left[ \int N^T N' dz \right] \bar{T} \right\} X \quad (3-110)$$

The values of the integrals  $\int N^T N dz$  etc. are assembled with (3-95) or (3-97) for the linear and quadratic expansions.

On the other hand, the Hankel functions satisfy Bessel's equation, and hence

$$H_n'' = -\frac{1}{r} H_n' - \left(k^2 - \left(\frac{n}{r}\right)^2\right) H_n \quad (3-111)$$

From here,

$$2G H_n'' - \lambda k^2 H_n = -\left(2G + \lambda\right) k^2 H_n - \frac{1}{r} 2G \left(H_n' - \frac{n^2}{r} H_n\right) \quad (3-112)$$

and

$$G \left(H_n'' - \frac{1}{r} H_n' + \left(\frac{n}{r}\right)^2 H_n\right) = -\frac{2G}{r} \left(H_n' - \frac{n^2}{r} H_n\right) - G k^2 H_n \quad (3-113)$$

Using the recurrence relations for the first derivative:

$$H_n' = k H_{n-1} - \frac{n}{r} H_n \quad (H_{-1} = -H_1) \quad (3-114)$$

it follows that

$$2G H_n'' - \lambda k^2 H_n = -(\lambda + 2G) k^2 H_n - \frac{2G}{r} \left( k H_{n-1} - \frac{n(n+1)}{r} H_n \right) \quad (3-115)$$

$$G \left( H_n'' - \frac{1}{r} H_n' + \left( \frac{n}{r} \right)^2 H_n \right) = -\frac{2}{r} \left( k H_{n-1} - \frac{n(n+1)}{r} H_n \right) - k^2 H_n$$

Also,

$$2G \frac{n}{r} \left( H_n' - \frac{H_n}{r} \right) = -2G \frac{n}{r} \left( \frac{n+1}{r} H_n - k H_{n-1} \right) \quad (3-116)$$

With these relations, the matrices S, T can be separated into

$$\begin{aligned} \mathbf{S} &= k^2 \mathbf{S}_1 + k \mathbf{S}_2 + \mathbf{S}_3 \\ \mathbf{T} &= k \mathbf{T}_1 + \mathbf{T}_2 \end{aligned} \quad (3-117)$$

in which

$$\mathbf{S}_1 = \begin{pmatrix} 2G + \lambda & & \\ & G & \\ & & G \end{pmatrix} \begin{pmatrix} H_n \\ -H_{n-1} \\ H_n \end{pmatrix}$$

$$\mathbf{S}_2 = -\frac{2G}{r_0} \begin{pmatrix} 1 & & \\ & 0 & \\ & & 1 \end{pmatrix} \begin{pmatrix} -H_{n-1} \\ H_n \\ -H_{n-1} \end{pmatrix} + \frac{Gn}{r_0} \begin{pmatrix} & 2 & \\ & 1 & \\ 2 & & \end{pmatrix} \begin{pmatrix} -H_{n-1} \\ H_n \\ -H_{n-1} \end{pmatrix}$$

$$\mathbf{S}_3 = -\frac{2n(n+1)}{r_0^2} G \begin{pmatrix} 1 & & -1 \\ & 0 & \\ -1 & & 1 \end{pmatrix} \begin{pmatrix} H_n \\ -H_{n-1} \\ H_n \end{pmatrix} \quad (3-118)$$

$$T_1 = \begin{Bmatrix} 0 & -\lambda & \\ G & 0 & \\ & & 0 \end{Bmatrix} \begin{Bmatrix} -H_{n-1} \\ H_n \\ -H_{n-1} \end{Bmatrix}$$

$$T_2 = -\frac{Gn}{r_0} \begin{Bmatrix} 0 & & \\ -1 & 0 & 1 \\ & & 0 \end{Bmatrix} \begin{Bmatrix} H_n \\ -H_{n-1} \\ H_n \end{Bmatrix}$$

Defining the modified modal shapes  $\psi_k, \phi_k$  and the boundary load vector  $P_{bk}$ :

$$\psi_{ik} = \begin{Bmatrix} H_n \\ -H_{n-1} \\ H_n \end{Bmatrix} \begin{Bmatrix} x_1 \\ x_2 \\ x_3 \end{Bmatrix}_i, \quad \psi_k = \{\psi_{ik}\} \quad (3-119)$$

$$\phi_{ik} = \begin{Bmatrix} -H_{n-1} \\ H_n \\ -H_{n-1} \end{Bmatrix} \begin{Bmatrix} x_1 \\ x_2 \\ x_3 \end{Bmatrix}_i, \quad \phi_k = \{\phi_{ik}\}$$

$P_{bk} = \left\{ \begin{array}{l} \text{overlapping corresponding elements in the } P_k \text{'s of each} \\ \text{discrete layer} \end{array} \right\}$

and expressing  $\bar{S}, \bar{T}$ , in terms of  $S_1, S_2, S_3, T_1, T_2$ , and integrating (3-110), gives for  $P_{bk}$ :



$$P_{bk} = \alpha_k r_0 \left\{ A \psi_k k^2 + (D - E + nN) \phi_k k - \left( \frac{n(n+1)}{2} L + nQ \right) \psi_k \right\} \quad (3-120)$$

where the matrices  $A$ ,  $D$ ,  $E$ ,  $N$ ,  $L$ , and  $Q$  are formed with the layer matrices  $A_j$ ,  $D_j$ , etc. in a similar fashion as in the eigenvalue problem.

For linear expansion, they are given by:

$$A_j = \frac{h}{6} \left\{ \begin{array}{ccccc} 2(2G + \lambda) & & & & \\ & 2G & & & \\ & & 2G & & \\ \lambda + 2G & & & 2(\lambda + 2G) & \\ & G & & & 2G \\ & & G & & & 2G \end{array} \right\}$$

$$E_j = \frac{Gh}{3r_0} \left\{ \begin{array}{ccccc} 2 & & & & 1 \\ & 0 & & & 0 \\ & & 2 & & 1 \\ 1 & & & 2 & \\ & 0 & & & 0 \\ & & 1 & & & 2 \end{array} \right\}$$

$$D_j = \frac{1}{2} \begin{pmatrix} 0 & \lambda & & -\lambda & 0 \\ -G & 0 & & G & \\ & & 0 & & \\ & \lambda & & 0 & -\lambda \\ -G & & & G & 0 \\ 0 & & & & 0 \end{pmatrix}$$

$$N_j = \frac{Gh}{6r_0} \begin{pmatrix} & & 4 & & 2 \\ & 2 & & & 1 \\ 4 & & & 2 & \\ & & 2 & & 4 \\ & 1 & & & 2 \\ 2 & & & 4 & \end{pmatrix}$$

$$L_j = \frac{2}{3} \frac{Gh}{r_0^2} \begin{pmatrix} 2 & & -2 & 1 & & -1 \\ & 0 & & & 0 & \\ -2 & & 2 & -1 & & 1 \\ 1 & & -1 & 2 & & -2 \\ & 0 & & & 0 & \\ -1 & & 1 & -2 & & 2 \end{pmatrix}$$

$$Q_j = \frac{G}{2r_0} \begin{pmatrix} 0 & & & & & 0 \\ 1 & 0 & -1 & -1 & 0 & 1 \\ & & 0 & 0 & & \\ & & 0 & 0 & & \\ 1 & 0 & -1 & -1 & 0 & 1 \\ c & & & & & 0 \end{pmatrix}$$

while for quadratic expansion, they are given by

$$\begin{aligned}
 \mathbf{A}_j &= \frac{\hbar}{30} \left\{ \begin{array}{cccccc} 4(\lambda+2G) & 4G & 2(\lambda+2G) & 2G & -(\lambda+2G) & -G \\ & 4G & 16(\lambda+2G) & 16G & 2(\lambda+2G) & -G \\ & & 2(\lambda+2G) & 2G & 4(\lambda+2G) & 2G \\ & & & -G & 2G & 4G \end{array} \right\} \\
 \mathbf{E}_j &= \frac{G\hbar}{15r_0} \left\{ \begin{array}{cccccc} 4 & 0 & 2 & 0 & -1 & 0 \\ & 0 & 4 & 2 & 0 & 0 \\ & & 16 & 0 & 4 & 0 \\ & & & 2 & 2 & 0 \\ & & & & -1 & 2 \\ & & & & & -1 \end{array} \right\}
 \end{aligned}$$

$D_j$

$$= \frac{1}{6} \begin{pmatrix} 0 & 3\lambda & -4\lambda & -6 & \lambda & 0 \\ -3G & 0 & 4G & 0 & 0 & -4\lambda \\ -4G & 0 & 0 & 0 & -3\lambda & 0 \\ 0 & 0 & -4G & 0 & 0 & 0 \end{pmatrix} \begin{pmatrix} 0 \\ 0 \\ 0 \\ 0 \end{pmatrix}$$

$$= \frac{GR}{30r_0} \begin{pmatrix} 8 & 4 & -2 \\ 4 & -2 & 4 \\ -2 & 4 & 8 \end{pmatrix} \begin{pmatrix} -2 \\ -1 \\ 8 \end{pmatrix}$$



The A matrix is the same as the one used in the eigenvalue problem, while D has the property that

$$B = D + D^T \quad (3-123)$$

where  $B$ , is also one of the matrices used in the eigenvalue problem.

Adding up the contributions of each mode gives for the nodal displacement vector:

$$\begin{aligned} P_b &= \sum_{b_k} P_{b_k} \\ &= \sum \alpha_k r_o \left\{ A \psi_k^2 + (D - E + n N) \phi_k k + n \left( \frac{n+1}{2} L + Q \right) \psi_k \right\} \\ &= r_o \left\{ A \Psi K^2 + (D - E + n N) \Phi K + n \left( \frac{n+1}{2} L + Q \right) \Psi \right\} \Gamma \end{aligned} \quad (3-124)$$

where  $K = \{k\}$  and  $\Gamma = \{\alpha\}$  are a diagonal matrix and a vector containing the wave numbers and the modal participation factors. The modified modal shape matrices  $\Psi, \Phi$  are formed as

$$\Psi = \{ \psi_k \} = \{ \psi_1 \dots \psi_{3l} \} \quad l = \text{number of layers}$$

(3-125)

$$\Phi = \{ \phi_k \} = \{ \phi_1 \dots \phi_{3l} \}$$

Now, at any particular node  $i$ , the displacement vector is given by (3-70), weighted with the participation factor. From here,

$$u_i = \sum \alpha_k H X_i, \quad X_i = X_i(k) \quad (3-126)$$

and the boundary displacement vector is ( $u_b = \{u_i\}$ )

$$u_b = w \Gamma \quad (3-128)$$

where the  $(3 \times 3)$  matrix  $w = \{w_i\}$  is assembled with the  $(3 \times 3)$  nodal matrices  $w_i$ . The latter is given, for any particular node  $i$  by:

$$w_i = \begin{pmatrix} H_n'(k, r_o) x_{1,1} & \dots & H_n'(k_{2\ell} r_o) x_{1,2\ell}; \frac{n}{r} H_n(k_{2\ell+1} r_o) x_{3,2\ell+1} & \dots & \frac{n}{r} H_n(k_{3\ell} r_o) x_{3,3\ell} \\ k_1 H_n(k, r_o) x_{3,1} & \dots & k_{2\ell} H_n(k_{2\ell} r_o) x_{3,2\ell} & 0 & \dots & 0 \\ \frac{n}{r} H_n(k, r_o) x_{1,1} & \dots & \frac{n}{r} H_n(k_{2\ell} r_o) x_{1,2\ell}, H_n'(k_{2\ell+1} r_o) x_{3,2\ell+1} & \dots & H_n'(k_{3\ell} r_o) x_{3,3\ell} \end{pmatrix}$$

(3-128)

In the expression above, the  $x_{i,k}$  are obtained from the modal matrix defining the quadratic eigenvalue problem (equation (3-94)). The row with zeroes follows from the fact that the Rayleigh and Love wave eigenvalue problems are uncoupled.

From here, it follows that

$$\Gamma = W^{-1} U_b \quad (3-129)$$

Also, if  $\mathcal{R}$  is the dynamic stiffness matrix of the energy absorbing boundary, then

$$P_b = \mathcal{R} U_b \quad (3-130)$$



Substitution of (3-129) and (3-130) into (3-124) results in

$$\mathcal{R} u_b = r_0 \left\{ A \Psi K^2 + (D - E + \eta N) \Phi K + \eta \left( \frac{n+1}{2} L + Q \right) \Psi \right\} W^{-1} u_b$$

and since it must hold for arbitrary  $u_b$ , it follows finally

$$\mathcal{R} = r_0 \left\{ A \Psi K^2 + (D - E + \eta N) \Phi K + \eta \left( \frac{n+1}{2} L + Q \right) \Psi \right\} W^{-1} \quad (3-131)$$

This matrix is symmetric, as the principle of reciprocity requires, and it relates the nodal forces at the boundary with the corresponding nodal displacements.

The proof that the matrix is symmetric when  $n \neq 0$  is cumbersome, and will not be attempted here. The corresponding proof for the particular case  $n=0$  can be found in the original work by Waas (44), where use is made of a special orthogonality condition of the quadratic eigenvalue problem. In any case, the symmetry was checked in many tests done with the computer program, and it was found an agreement of at least 7 significant figures (working in double precision).

Equation (3-130) represents the forces applied at the energy absorbing boundary when the finite element region is removed.

The reaction forces acting on the finite element region follow then from equilibrium considerations:

$$P_b = -R U_b \quad (3-132)$$

Increasing the size of (3-132) with as many zeroes as necessary to match the dimensions of the finite element system equation (3-58), and adding it to the right-hand-side of the latter equation results in

$$(-\rho \Omega^2 M + K) U = P - R U$$

$$(-\rho \Omega^2 M + K + R) U = P \quad (3-133)$$

or, defining the dynamic stiffness matrix

$$K_d = -\rho \Omega^2 M + K + R \quad (3-134)$$

yields finally

$$K_d U = P \quad (3-135)$$

which can be solved by the conventional numerical techniques. For arbitrary dynamic loadings, it must be solved in the frequency domain, as the dynamic stiffness matrix is a

function of the driving frequency. Time histories are then obtained using the well known Fourier transformation procedures.

### 3.8.- Base Motion:

There exist in structural dynamics well established methods to determine the response of a multidegree of freedom structure to a given support motion, and in particular, to an earthquake motion. For this analysis to be possible the loading history must be known. Due to the random nature of an earthquake, this motion cannot be established in advance, but it is possible in some cases to obtain useful results employing records of both historic and artificially generated earthquakes. These records can be specified directly as support motions for structures founded on firm ground (rock) only when it is reasonable to assume that the system behaves in cascade, that is, when the response and feedback of the structure to the ground has a negligible effect on the primary input. Many structures, however, are founded on softer soil deposits or stratum over rock, a condition which substantially alters at the founding level the power spectrum of the design earthquake assumed to occur at bedrock (which is usually an earthquake recorded in a geologically similar area at the outcrop of rock) as a result of soil

amplification and filtering. In addition, the flexibility of the soil at the building site must be taken into account in many cases in order to properly evaluate the response of the structure, which in turn modifies the primary motion of the soil in the neighborhood of it.

In the present section, the theory will be extended, and the possibility to determine the response of an axisymmetric system subjected to a given bedrock (base) motion will be investigated. This extension will include the effect of the amplification, filtering, feedback, radiation and flexibility of the soil layer on which the structure is founded.

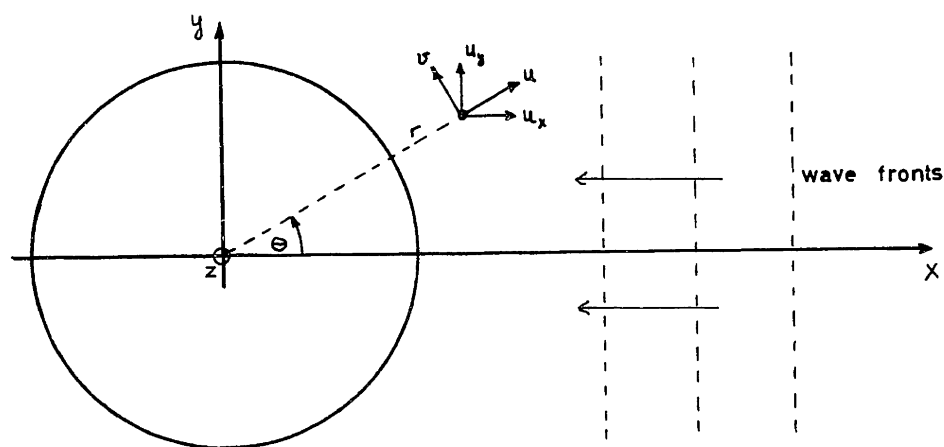


fig. 11

If the epicenter of the earthquake (source of the motion) is sufficiently far away from the building site, it is reasonable to assume that the arriving wave fronts are cylindric, that is, independent of the  $y$  coordinate, and

propagate toward the structure in the form of Rayleigh, Love or other type of plane waves.

A single component of the motion can be represented by

$$\begin{aligned} u_x &= \tilde{u}_x e^{i(kx + \Omega t)} \\ u_y &= \tilde{u}_y e^{i(kx + \Omega t)} \\ u_z &= \tilde{u}_z e^{i(kx + \Omega t)} \end{aligned} \quad (3-135)$$

in which  $\Omega$  is the frequency, and  $k$  the wavenumber of the wave under consideration. The amplitudes  $\tilde{u}_x$ ,  $\tilde{u}_y$ ,  $\tilde{u}_z$ , are generally complex, to account for possible phase differences, and are also functions of the depth  $z$ .

A transformation of variables to the cylindrical system gives for the radial, tangential, and vertical displacements at a point with coordinates  $r, \theta, z$ :

$$\begin{aligned} u &= u_x \cos \theta + u_y \sin \theta \\ v &= -u_x \sin \theta + u_y \cos \theta \\ w &= u_z \end{aligned} \quad (3-136)$$

or substituting (3-135)

$$\begin{aligned}
 u &= (\tilde{u}_x \cos \theta + \tilde{u}_y \sin \theta) e^{i(kx + \Omega t)} \\
 v &= (-\tilde{u}_x \sin \theta + \tilde{u}_y \cos \theta) e^{i(kx + \Omega t)} \\
 w &= \tilde{u}_z e^{i(kx + \Omega t)}
 \end{aligned}
 \tag{3-137}$$

Expansion in Fourier series around the axis gives

$$\begin{aligned}
 u &= \sum_{n=0}^{\infty} (\bar{u}_{ns} \cos n\theta + \bar{u}_{na} \sin n\theta) \\
 v &= \sum_{n=0}^{\infty} (-\bar{u}_{ns} \sin n\theta + \bar{u}_{na} \cos n\theta) \\
 w &= \sum_{n=0}^{\infty} (\bar{w}_{ns} \cos n\theta + \bar{w}_{na} \sin n\theta)
 \end{aligned}
 \tag{3-138}$$

Multiplication by  $\cos m\theta$ ,  $\sin m\theta$ , and integration over 1 period yields (with  $kx = krcos \theta$ , omitting the factor  $e^{i\Omega t}$ , and  $C_n = 1$  for  $n \neq 0$ ,  $C_n = 1/2$  for  $n = 0$ ):

$$\bar{u}_{n3} = \frac{C_n}{\pi} \int_0^{2\pi} \cos n\theta (\tilde{u}_x \cos \theta + \tilde{u}_y \sin \theta) e^{ikr \cos \theta} d\theta$$

$$\bar{u}_{n2} = \frac{C_n}{\pi} \int_0^{2\pi} \sin n\theta (\tilde{u}_x \cos \theta + \tilde{u}_y \sin \theta) e^{ikr \cos \theta} d\theta$$

$$\bar{v}_{n3} = -\frac{C_n}{\pi} \int_0^{2\pi} \sin n\theta (-\tilde{u}_x \sin \theta + \tilde{u}_y \cos \theta) e^{ikr \cos \theta} d\theta$$

$$\bar{v}_{n2} = \frac{C_n}{\pi} \int_0^{2\pi} \cos n\theta (-\tilde{u}_x \sin \theta + \tilde{u}_y \cos \theta) e^{ikr \cos \theta} d\theta$$

(3-139)

$$\bar{w}_{n3} = \frac{C_n}{\pi} \int_0^{2\pi} \cos n\theta (\tilde{u}_z) e^{ikr \cos \theta} d\theta$$

$$\bar{w}_{n2} = \frac{C_n}{\pi} \int_0^{2\pi} \sin n\theta (\tilde{u}_z) e^{ikr \cos \theta} d\theta$$

Transforming these expressions with the aid of the relations

$$\cos n\theta \cos \theta = \frac{1}{2} (\cos (n+1)\theta + \cos (n-1)\theta)$$

$$\sin n\theta \sin \theta = \frac{1}{2} (\cos (n-1)\theta - \cos (n+1)\theta)$$

(3-140)

$$\sin n\theta \cos \theta = \frac{1}{2} (\sin (n-1)\theta + \sin (n+1)\theta)$$

$$\cos n\theta \sin \theta = \frac{1}{2} (\sin (n+1)\theta - \sin (n-1)\theta)$$

and using the integrals (12)

$$\frac{1}{2\pi} \int_0^{2\pi} \cos m\theta e^{iz \cos \theta} d\theta = i^m J_m(z) \quad (3-141)$$

$$\frac{1}{2\pi} \int_0^{2\pi} \sin m\theta e^{iz \cos \theta} d\theta = 0$$

$$i = \sqrt{-1} \quad , \quad z = \text{complex} \quad , \quad J_m(z) = \text{Bessel function}$$

gives for the displacement components:

$$\bar{u}_{n3} = C_n i^{n-1} (J_{n-1}(kr) - J_{n+1}(kr)) \tilde{u}_x \quad , \quad C_n = \begin{cases} 1 & n \neq 0 \\ \frac{1}{2} & n = 0 \end{cases}$$

$$\bar{u}_{n2} = C_n i^{n-1} (J_{n-1}(kr) + J_{n+1}(kr)) \tilde{u}_y$$

$$\bar{v}_{n3} = C_n i^{n-1} (J_{n-1}(kr) + J_{n+1}(kr)) \tilde{u}_x$$

$$\bar{v}_{n2} = C_n i^{n-1} (J_{n-1}(kr) - J_{n+1}(kr)) \tilde{u}_y \quad (3-142)$$

$$\bar{w}_{n3} = C_n 2 i^n$$

$$\bar{w}_{n2} = 0$$



or alternatively, using the recurrence relations for the Bessel functions, and omitting the argument  $kr$ :

$$\begin{aligned}\bar{u}_{ns} &= 2C_n \tilde{u}_x \frac{i^{n-1}}{kr} \left( \frac{dJ_n}{dr} \right), \quad C_n = \begin{cases} 1 & n \neq 0 \\ \frac{1}{2} & n = 0 \end{cases} \\ \bar{u}_{na} &= 2C_n \tilde{u}_y \frac{ni^{n-1}}{kr} J_n \\ \bar{v}_{ns} &= 2C_n \tilde{u}_x \frac{ni^{n-1}}{kr} J_n \\ \bar{v}_{na} &= 2C_n \tilde{u}_y \frac{i^{n-1}}{kr} \left( \frac{dJ_n}{dr} \right) \\ \bar{w}_{ns} &= 2C_n \tilde{u}_z i^n J_n \\ \bar{w}_{na} &= 0\end{aligned} \tag{3-143}$$

Equations (3-142) and (3-143) describe the motion of a particle of coordinates  $r, \theta, z$ , in terms of the modal components and the wave amplitudes  $\tilde{u}_x, \tilde{u}_y, \tilde{u}_z$  for the homogeneous case in which no structure is present on top of the stratum in the neighborhood of the origin. Let  $Y^*$  be the nodal displacement vector defined be either the symmetric or antisymmetric components (which yield uncoupled problems) in equations (3-142) at the nodes of the boundary joining the

layered region with the finite element region. Further, let  $P^*$  be the consistent nodal forces necessary to preserve equilibrium at the boundary when the layered region is removed. From the knowledge of the displacement pattern, it is possible to relate these nodal forces to the displacements by means of the matrix equation:

$$P^* = \mathfrak{D} Y^* \quad (3-144)$$

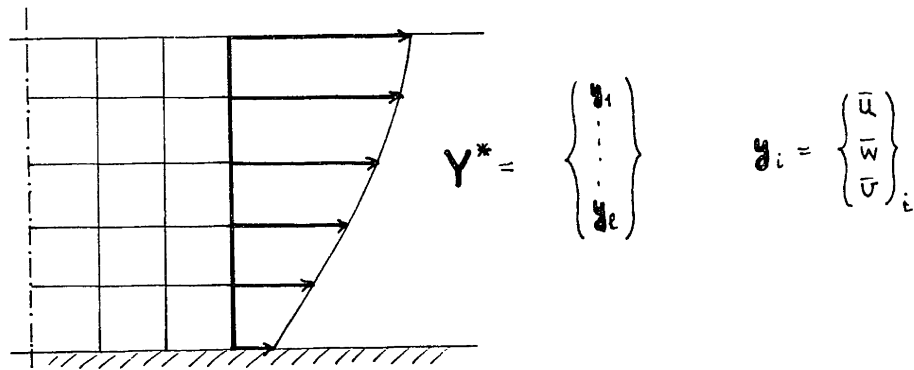


fig. 12

The exact form of the dynamic stiffness matrix  $\mathfrak{D}$  depends on the displacement pattern of the (homogeneous) wave propagation problem.

Using the relation (3-144), the incident wave can be replaced in the dynamic equation of the finite element system by the equivalent set of prescribed forces  $P^*$  applied at the nodes of the energy absorbing boundary. The application of the

specified displacements at the base of the system with the structure, and the forces  $P^*$  at the lateral boundary causes the system to vibrate, generating the presence of the structure a secondary set of waves which radiate outwards. The nodal forces necessary to balance these secondary waves at the FE boundary when the latter is removed are

$$\Delta P = -R(Y - Y^*) = -RY + RY^*$$

where  $Y - Y^*$  represents the deviation of the displacements produced by the secondary wave train, and  $R$  is the stiffness matrix of the far-field as defined in the previous section. Increasing the size of  $Y^*, R$ , etc, with as many zeroes as necessary to match the dimensions of  $m, K$ ,

$$(-\Omega^2 m + K)Y = DY^* - RY + RY^* + P \quad (3-145)$$

$$(-\Omega^2 m + K + R)Y = (D + R)Y^* + P \quad (3-146)$$

and

$$K_d Y = (D + R)Y^* + P \quad (3-147)$$

The system dynamic stiffness matrix  $\mathbf{K}_d$  is identical to the one defined in the preceeding section, except that now it has to be modified for the specified support (displacement) conditions at the base of the core region. Since no corrective term was allowed for secondary waves travelling past the base, the radiation damping will entirely be due to dissipation at the energy absorbing boundary (layer waves). The underlying assumption is that the base rock is much stiffer than the soil stratum; this is consistent with the theory developed in the preceeding sections, where the base rock was assumed infinitely rigid.

Since the shear wave velocity in the basal rock is about 1 order of magnitude higher than that of a typical stratum, the phase velocity of the incoming waves will be rather large, and the wave number  $k$  relatively small, even in the case when the wave fronts have grazing incidence. For larger incidence angles, the wave number decreases further, and for normal incidence, it becomes zero.

The particular case of normal incidence will be analyzed, since it is the easiest to evaluate, and the most widely used in soil amplification studies. Theoretically, it is possible also to examine other cases, and eventually include in the analysis only the first few modes (low  $n$ ), as the Bessel

coefficients decay rapidly with increasing order. In fact, perhaps the first two fundamental modes ( $n = 0$  and  $n = 1$ ) might be sufficient, since they are the only ones that involve rigid body translations (rotations) of the foundation and are therefore able to transmit the motion to the structure; the higher modes require a deformation of the (usually rigid) foundation mat, and hence will be filtered out to a high degree. Larger responses in the fundamental modes for non-normal incidence could be expected, as it involves simultaneous motion components in the horizontal and vertical directions in each fundamental mode. However, the main difficulties will be in the determination of the free field (no structure) wave pattern and the corresponding determination of the  $Y^*$  vector and  $\mathbf{D}$  matrix. For this reason, only the case of an infinitely large phase velocity will be considered here. For this case,  $k = 0$ , and equations (3-142) reduce, in view of

$$J_n(0) = \delta_{0n} = \begin{cases} 1 & \text{for } n=0 \\ 0 & \text{else} \end{cases}$$

to :

$$n = 0$$

$$\bar{u}_{n5} = \bar{u}_{na} = \bar{v}_{n5} = \bar{v}_{na} = 0 \quad \text{for any } r$$

$$\bar{w}_{n5} = \tilde{u}_z \quad (3-148)$$

$$n = 1$$

$$\bar{u}_{n5} = \tilde{u}_x \quad \bar{v}_{n5} = \tilde{u}_x$$

$$\bar{u}_{na} = \tilde{u}_y \quad \bar{v}_{na} = \tilde{u}_y$$

$$\bar{w}_{n5} = 0 \quad \bar{w}_{na} = 0$$

(3-149)

that is, for  $n = 0$  the base motion is a homogeneous vertical excitation of amplitude  $\tilde{u}_z$ , and for  $n = 1$ , it corresponds to a uniform horizontal shaking of amplitude  $\sqrt{\tilde{u}_x^2 + \tilde{u}_y^2}$ . Since there are no preferred directions for these cases,  $\tilde{u}_y = 0$  can be assumed.

The expressions for  $y^*, \theta$  will be determined now for these two particular cases.

a) vertical excitation ( $n = 0$ ):

The only non-zero wave equation is

$$-\Omega^2 \rho w = (\lambda + 2G) \frac{\partial^2 w}{\partial z^2} \quad (3-150)$$

where  $w$  is the absolute vertical displacement. Using the (modified) principle of virtual displacements, equations (3-76), (3-101), the (reduced) expansion vector  $N = \{g_j\}$  and the boundary stresses

$$\begin{aligned} \sigma_z &= (\lambda + 2G) w' \\ \sigma_r &= \sigma_\theta = \lambda w' \end{aligned} \quad (3-151)$$

yields

$$\sum_{\text{layers}} \left\{ \int \delta w \left[ (\lambda + 2G) \frac{\partial^2 w}{\partial z^2} + \Omega^2 \rho w \right] r dz - \int \frac{\partial}{\partial z} \left( \delta w (\lambda + 2G) w' \right) r dz \right\} = 0 \quad (3-152)$$

or with  $w = \mathbf{N} \mathbf{Y}_j^*$ ,  $\mathbf{Y}_j^* = \begin{Bmatrix} y_i \\ \vdots \\ y_{i+m} \end{Bmatrix}$ ,  $m = \text{order of expansion}$

$$\sum_{\text{layers}} \int \delta \mathbf{Y}_j^{*T} \left\{ \rho \Omega^2 \mathbf{N}^T \mathbf{N} - (\lambda + 2G) \mathbf{N}^{iT} \mathbf{N}' \right\} \mathbf{Y}_j^* dz = 0 \quad (3-153)$$

which leads to the matrix equation (dimension  $(l + 1)(l + 1)$ ,  $l = \text{number of layers}$ )

$$(\mathbf{G} - \Omega^2 \mathbf{M}) \mathbf{Y}^* = 0 \quad (3-154)$$

where

$$\begin{aligned} \mathbf{M} &= \{\mathbf{M}_j\} & \mathbf{M}_j &= \gamma \Omega^2 \int_0^R \{g_i g_j\} dz \\ \mathbf{G} &= \{\mathbf{G}_j\} & \mathbf{G}_j &= (\lambda + 2G) \int_0^R \{g_i' g_j'\} dz \end{aligned} \quad (3-155)$$

The layer submatrices,  $\mathbf{M}_j$ ,  $\mathbf{G}_j$  are given for linear and quadratic expansion directly by (3-95), (3-97), except for the  $\gamma \Omega^2$  and  $\lambda + 2G$  factors. Equation (3-154) is solved introducing the support condition at the base  $y_{L+1} = w_{\text{rock}}$  and eliminating the last row and column of  $\mathbf{M}$  and  $\mathbf{G}$ , thus reducing them to  $1 \times 1$  matrices (condensation)

On the other hand,  $U_j = \sigma_{rr} = \lambda w'$ , obtaining for  $\mathbf{P}_j^*$  (contribution of  $j^{\text{th}}$  layer) =  $\begin{Bmatrix} p_i \\ \vdots \\ p_{i+m} \end{Bmatrix}^*$

$$\mathbf{P}_j^* = r_0 \int \mathbf{N}^T \lambda w' dz = r_0 \lambda \left\{ \int \mathbf{N}^T \mathbf{N}' dz \right\} \mathbf{Y}_j^* = \mathfrak{D}_j \mathbf{Y} \quad (3-156)$$

$$\mathfrak{D}_j = r_0 \lambda \int \{g_i g_j'\} dz \quad (3-157)$$



which yields for linear and quadratic expansions:

$$\mathcal{D}_j = \frac{\lambda r_0}{2} \begin{pmatrix} -1 & 1 \\ -1 & 1 \end{pmatrix} \quad (\text{linear}) \quad (3-158)$$

$$\mathcal{D}_j = \frac{\lambda r_0}{6} \begin{pmatrix} -3 & 4 & -1 \\ -4 & 0 & 4 \\ 1 & -4 & 3 \end{pmatrix} \quad (\text{quadratic}) \quad (3-159)$$

The (unidimensional) displacement vector  $Y^*$  and load vector  $P^*$  are now increased threefold in size, adding the zeroes corresponding to the  $r$  and  $\theta$  components:

$$Y_o^* = \left\{ \begin{array}{c} \begin{pmatrix} 0 \\ y_1 \\ 0 \end{pmatrix} \\ \vdots \\ \begin{pmatrix} 0 \\ y_l \\ 0 \end{pmatrix} \end{array} \right\} \quad P_o^* = \left\{ \begin{array}{c} \begin{pmatrix} 0 \\ p_1 \\ 0 \end{pmatrix} \\ \vdots \\ \begin{pmatrix} 0 \\ p_l \\ 0 \end{pmatrix} \end{array} \right\} \quad (3-160)$$

and the  $\mathfrak{D}_j$  matrix can be modified to

$$\mathfrak{D}_j = -\frac{1}{2} \left\{ \begin{array}{cccccc} 0 & \lambda & 0 & 0 & -\lambda & 0 \\ -G & 0 & 0 & G & 0 & 0 \\ 0 & 0 & 0 & 0 & 0 & 0 \\ 0 & \lambda & 0 & 0 & -\lambda & 0 \\ -G & 0 & 0 & G & 0 & 0 \\ 0 & 0 & 0 & 0 & 0 & 0 \end{array} \right\} \quad (3-161) \quad (\text{linear exp.})$$

The addition of the  $G$  terms is irrelevant, since the corresponding force and displacement terms are zero. Comparison of (3-161) with (3-121) shows that, except for the (-) sign, the  $\mathfrak{D}$  and  $D$  matrices are identical.

b) Horizontal excitation ( $n = 1$ ):

For this case,  $u = v, w = 0$

Wave equations:

$$\begin{aligned} -\Omega^2 \rho u &= G \frac{\partial^2 u}{\partial r^2} \\ -\Omega^2 \rho v &= G \frac{\partial^2 v}{\partial r^2} \end{aligned} \quad (3-162)$$

Boundary stresses:

$$\sigma_{rz} = G \frac{\partial u}{\partial z} \quad (3-163)$$

$$\sigma_{\theta z} = G \frac{\partial v}{\partial z}$$

Following an entirely analogous procedure as in the case a), we obtain for  $Y^* = \{y_i\}$  ( $y_i$  stands for either  $u_i$  or  $v_i$ )

$$(G - \Omega^2 M) Y^* = 0 \quad (3-164)$$

where the  $G$  matrix differs from (3-155) in that the factor  $\lambda + 2G$  is replaced by  $G$ :

$$G_{ij} = G \int_0^h \{g_i' g_j'\} dz \quad (3-165)$$

The load displacement relation is for this case

$$P_1^* = \mathfrak{D}_1 Y_1^* \quad Y_1^* = \left\{ \begin{array}{c} \left\{ \begin{array}{c} y_1 \\ 0 \\ y_1 \end{array} \right\} \\ \vdots \\ \left\{ \begin{array}{c} y_l \\ 0 \\ y_l \end{array} \right\} \end{array} \right\} = \left\{ \begin{array}{c} y_1 \left\{ \begin{array}{c} 1 \\ 0 \\ 1 \end{array} \right\} \\ \vdots \\ y_l \left\{ \begin{array}{c} 1 \\ 0 \\ 1 \end{array} \right\} \end{array} \right\} \quad (3-166)$$

in which the  $\mathfrak{D}$  is this time identical to  $D$ , also in sign. The results for horizontal and vertical excitation can then be summarized by

$$P_n^* = -(-1)^n D Y_n^* \quad n = 0, 1 \quad (3-167)$$

Since equations (3-154) and (3-164) are linear in the prescribed displacement, it is convenient to compute  $Y^*(\Omega)$  and the system response  $U(\Omega)$  for unit base motion, and weight later the response with the appropriate displacement factor.  $U(\Omega)$  would represent in this case the transfer function of the system for unit base motion. The true time history can be obtained by means of the well known inverse Fourier transformation

$$u(t) = \text{IFT} (U(\Omega) \cdot F(\Omega))$$

where  $F(\Omega)$  is the Fourier transform of the earthquake record.

### 3.9.- Summary of the procedure:

- a) Generate finite element mass and stiffness matrices, and load vector.
- b) Generate layer matrices.
- c) Form and solve eigenvalue problems for Love and Rayleigh waves.
- d) Form boundary matrix , and together with the matrices of the F.E. region, form the dynamic stiffness matrix of the system.
- e) Modify for support conditions
- g) Solve in the frequency domain
- h) Obtain desired effects (moments, forces, displacements, etc)
- i) Obtain time history (if desired) with inverse Fourier transformation.

#### 4.- Parametric Studies:

The influence of the geometry and material properties of a viscoelastic stratum on the response of a rigid circular plate welded to the stratum and subjected to forced harmonic excitations will be studied in this section. The main objectives are: to check the applicability and accuracy of the computer program based on the theory presented in this dissertation; to present results for cases for which no known analytical solutions exist; to assess the usefulness of the halfspace theory in the case of a stratum on top of a rigid rock base; and to derive simple rules to extrapolate the values of the soil spring constants for a stratum from the theoretical values of the halfspace.

Only the planesymmetric displacement modes (rocking and swaying) will be discussed in this section, as the other two, namely vertical and torsional motion (axisymmetric modes) have already been presented and discussed in Waas' doctoral dissertation. The computer program, however, is capable of handling all four cases. The rigid circular plate was idealized by a row of (massless) finite elements of very high rigidity ( $10^6$  times higher than that of the stratum).

Consider a massless rigid circular plate welded to a homogeneous stratum of depth  $H$ :

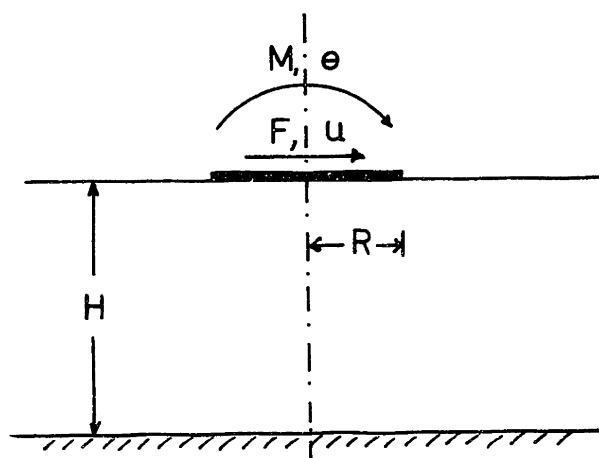


fig. 13

$$\begin{aligned} C_s &= 1. \\ \zeta &= 1. \\ R &= 1. \\ \nu &= 1/3 \\ \beta &= 0.05 \end{aligned}$$

The plate is subjected to a prescribed harmonic displacement (rotation) of unit amplitude at the plate-soil interface, and the force (moment) necessary to preserve equilibrium is computed with the aid of the program. This resultant is numerically equal to the dynamic (complex) stiffness function of the soil at that particular driving frequency:

$$F = K_s u, \quad \text{for } u = 1 \implies F = K_s$$

$$M = K_\varphi \theta, \quad \text{for } \theta = 1 \implies M = K_\varphi$$

The forced horizontal displacement case will be referred to as swaying (sliding), while the forced rotation about a horizontal axis will be referred to as rocking. The rotation in the former case and the horizontal translation in the

latter case were not restrained in order to avoid the additional complication of cross stiffness terms in the subgrade stiffness matrix.

It is always possible to write the stiffness functions as

$$K_s = K_{s0} (k_1 + i a_0 c_1) (1 + 2i \beta_{h1}) \quad (4-1)$$

$$K_q = K_{q0} (k_2 + i a_0 c_2) (1 + 2i \beta_{h2})$$

where  $K_{s0}$ ,  $K_{q0}$  are the real parts of the stiffness functions in the static case (static "spring constants"),  $a_0 = \frac{\Omega R}{C_s}$  is the dimensionless frequency, and  $k_1$ ,  $k_2$ ,  $c_1$ ,  $c_2$  are the stiffness and (viscous) damping coefficients (functions of  $a_0$ ). If the internal damping coefficient  $\beta$  is constant throughout the (homogeneous) stratum, then the hysteretic damping coefficient  $\beta_h$  is identical to it. Unless stated otherwise, the internal damping in the soil was assumed to be 5 percent critical ( $G = G_0 \cdot (1 + 2 \cdot 0.05 i)$ ), in order to eliminate the narrow peaks in the response of the undamped system due to resonance and reflections at the interfaces and bedrock.

The functions  $k$ ,  $c$  were found with the aid of the program, and determined as follows:



$$K_0 = \operatorname{Re} [K(\Omega=0)]$$

$$\beta_R = \frac{1}{2} \operatorname{Im} \left[ \frac{K(\Omega=0)}{K_0} \right] \quad (4-2)$$

$$R = \operatorname{Re} \left[ \frac{K}{K(\Omega=0)} \right], \quad C = \frac{1}{a_0} \operatorname{Im} \left[ \frac{K}{K(\Omega=0)} \right]$$

$$K(\Omega=0) = K_0 (1 + 2i\beta_R)$$

Dimensionless analysis was used throughout, and the results were plotted against the non-dimensional frequencies:

$$f_0 = \frac{f R}{C_s} \quad a_0 = \frac{\Omega R}{C_s} \quad (4-3)$$

that is,  $a_0 = 2\pi f_0$  (4-4)

The halfspace solutions for the static spring constants are

$$K_{s0} = \frac{8 G R}{2 - \nu} \quad \text{swaying} \quad (4-5)$$

$$K_{r0} = \frac{8 G R^3}{3(1-\nu)} \quad \text{rocking}$$

where  $G = \rho C_s^2$  is the shear modulus of elasticity of the soil, and  $\nu$  its Poisson's ratio;  $R$  is the radius of the

plate. Unless stated otherwise, a Poisson's ratio  $\nu = 1/3$  was used in the analysis.

#### 4.1.- Effect of the size of the mesh:

Earlier studies on the finite element method applied to dynamic problems indicate that the size of the largest element in a system should be smaller than a certain fraction, usually  $1/8$  to  $1/10$ , of the shortest wavelength that is expected to be reasonably reproduced. In the case of a layered stratum, and particularly for a deep one, it is often economically unfeasible to cover the whole depth with a fine mesh, and it becomes necessary to investigate the possibility of using narrower (longer) elements with increasing depth, away from a hypothetical dynamic pressure bulb. At the same time, it is of interest to check the rate of convergence towards the continuum solution as the mesh is refined.

##### a) Convergence:

To evaluate the convergence of the F.E. solution with decreasing element size, three meshes with a depth ratio  $H/R=2$  were considered: coarse, regular and fine:

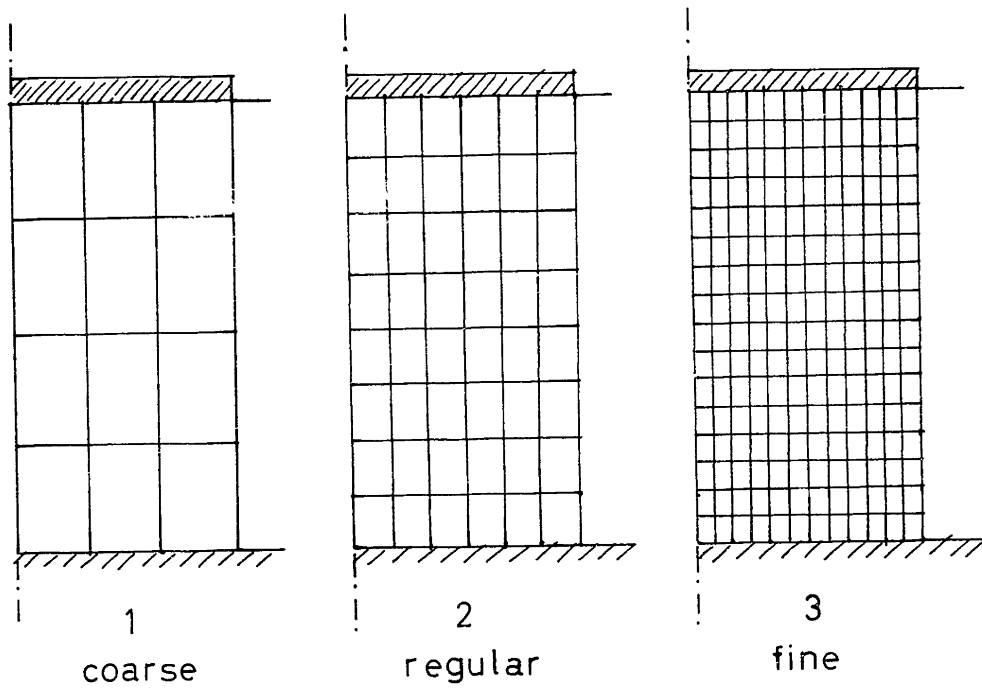


fig. 14

The results for the three meshes shown above are presented for swaying in Fig. 16 as a function of the dimensionless frequency  $f_0$ . Also, the static values  $K_{s_0}$ ,  $K_{\varphi_0}$  are plotted in fig. 15 below against the reciprocal of the number of sublayers (size of the element). The approximate execution times in the IBM 370-155 computer were 1 sec, 10 sec and 100 sec per frequency, respectively.

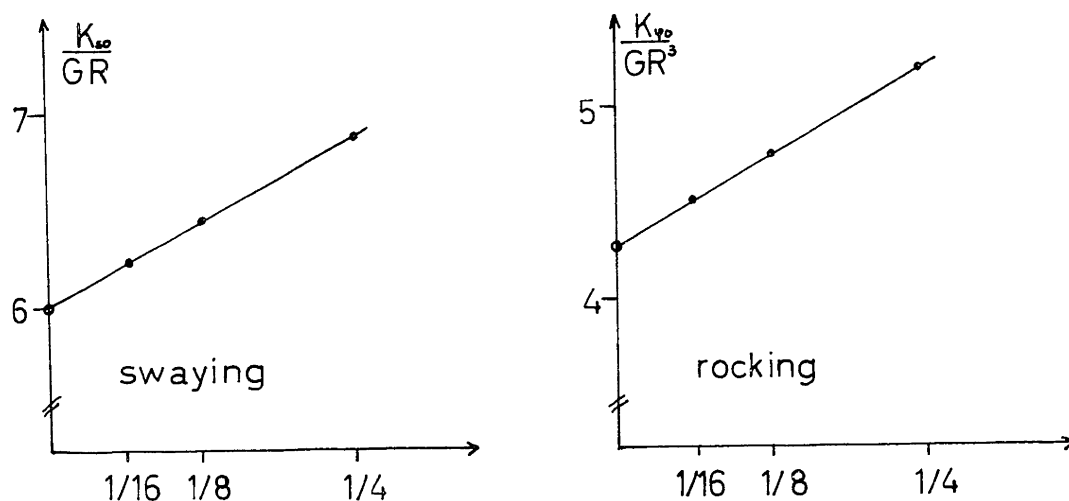


fig 15

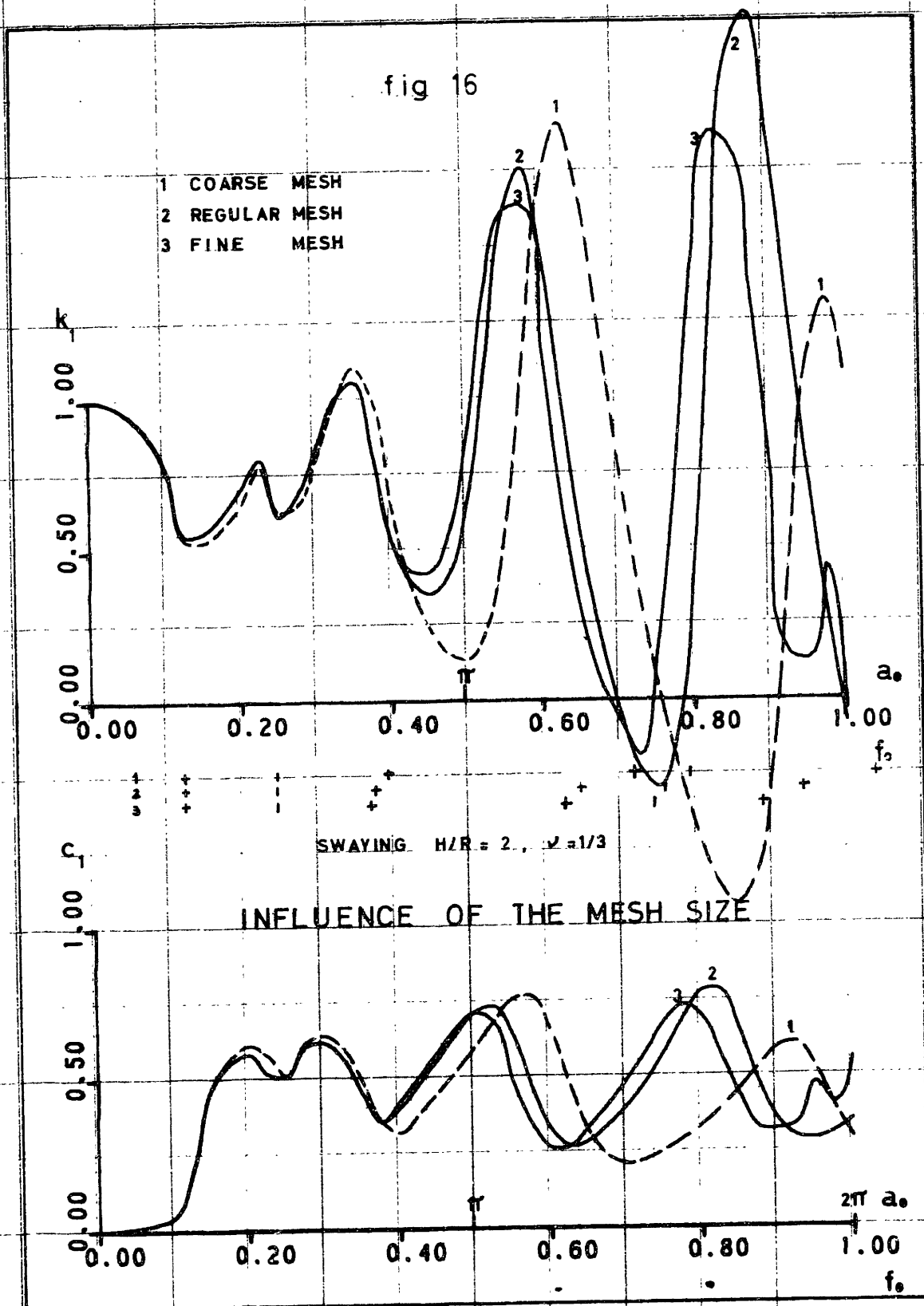
It is interesting to notice that the three static solutions for both rocking and swaying seem to lie in a straight line. This suggests that the continuum solution could be extrapolated by the intersection of this line with the vertical axis. Since a linear expansion was used for the finite element mesh, the relative error in the displacements should be proportional to the square of the typical element size. Stresses and forces are given with less degree of accuracy: as they depend on the partial derivatives of the displacements the error for them should be approximately linear. The spring constants are determined as reaction forces, and therefore, should converge at an approximate linear rate towards the continuum solution as the mesh is refined. The results above are consistent with this

expectation, and therefore suggest a useful procedure to determine static continuum solutions with the aid of a coarse and a regular mesh. This extrapolation procedure is to be used later in other cases to be studied.

The function  $k_1$  shows good agreement for all three meshes up to a frequency of  $f_0 = 0.40$  ( $\alpha_0 = 2.5$ ), at which the coarser mesh starts to diverge substantially from the other two meshes. This frequency represents a dimensionless shear wavelength  $\lambda_0 = \frac{\lambda}{R} = \frac{1}{f_0} = \frac{1}{0.40} = 2.50$  which is about five times the length of the longest element size in the coarse mesh. A similar result is observed for meshes 2 and 3, which begin to diverge significantly at a frequency  $f_0 = 0.70 \rightarrow \lambda_0 = 1.43$  that is, about six times the length of an element in the regular mesh. The deviation of the coarser meshes with respect to the more refined solutions consists mainly of two effects:

- first, a frequency shift is observed, which is partially due to the shift in the natural frequencies of the stratum as computed from the associated classical one dimensional discrete (consistent mass) eigenvalue problem. (The natural frequencies of the stratum are represented in Fig. 16 by (+) for horizontal motion, and (•) for vertical motion)

fig 16



- second, the amplitudes later start to diverge, and the functions cease to have significance at higher frequencies for the more crude meshes, as could be expected.

In addition, the absolute amplitudes of the stiffness functions are larger for the coarser (stiffer) meshes, as their static values are higher. This can be corrected by the extrapolation method mentioned earlier.

It appears, therefore, that the longest element size in the region of relevance (high strain gradients) should be smaller than  $1/6$  of the shortest shear wavelength expected, a result which agrees with previous studies on this subject. The frequency dependent functions  $k$ ,  $c$ , of this "regular" mesh can then be combined with an extrapolated static spring value for the continuum solution. This correction is necessary, since it reduces the stiffness function in its entire frequency range by about 15 percent, while the deviations in the frequency dependence of the stiffness coefficients (at high frequencies) when a relatively coarse mesh is used are essentially local.

b) Dynamic pressure bulb

The idea of a dynamic pressure bulb is a generalization of the concept of pressure bulb as defined in statics in the study of pressure distributions under footings. It represents the zone of influence under the plate (footing) which commands its dynamic response, and beyond which coarser finite elements may be employed without significantly affecting the dynamic behavior of the system. It is desirable, in order to ensure the efficiency and economy of the F. E. solution, to use larger elements away from the zone of influence, provided that such a zone exists.

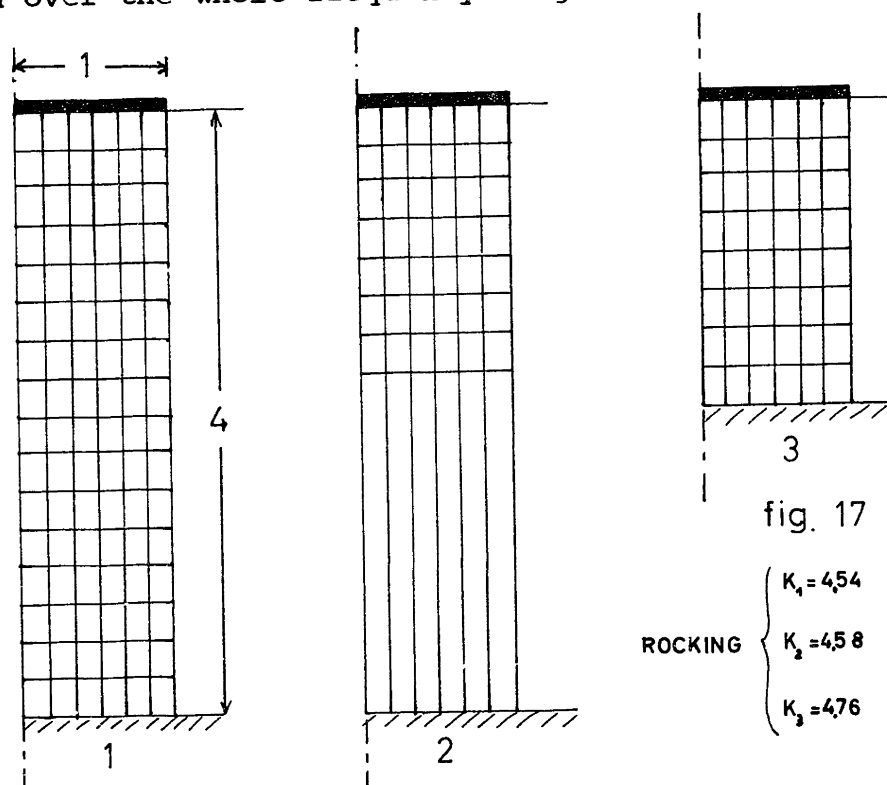
A series of test runs were made to assess the size of the influence region for both rocking and swaying. The results are shown in Figs. 19 through 21.

It must be conceded that the coarse meshes used employing narrow bottom elements (Figs. 17 and 18) constitute an extreme case, for the slenderness of the bottom elements, although in most cases it is convenient to use such narrow elements in very deep strata.

In the case of rocking (figs. 19 and 20), only negligible differences are noticed throughout the frequency range



studied (aspect ratio  $H/R = 4$ ), which indicates that the dynamic pressure bulb is smaller than the diameter of the plate. However, it should not be concluded from this that it is permissible to suppress completely the lower (long element) portion, as this results in an increased value for the static constant, which in turn affects the values of the stiffness function over the whole frequency range.

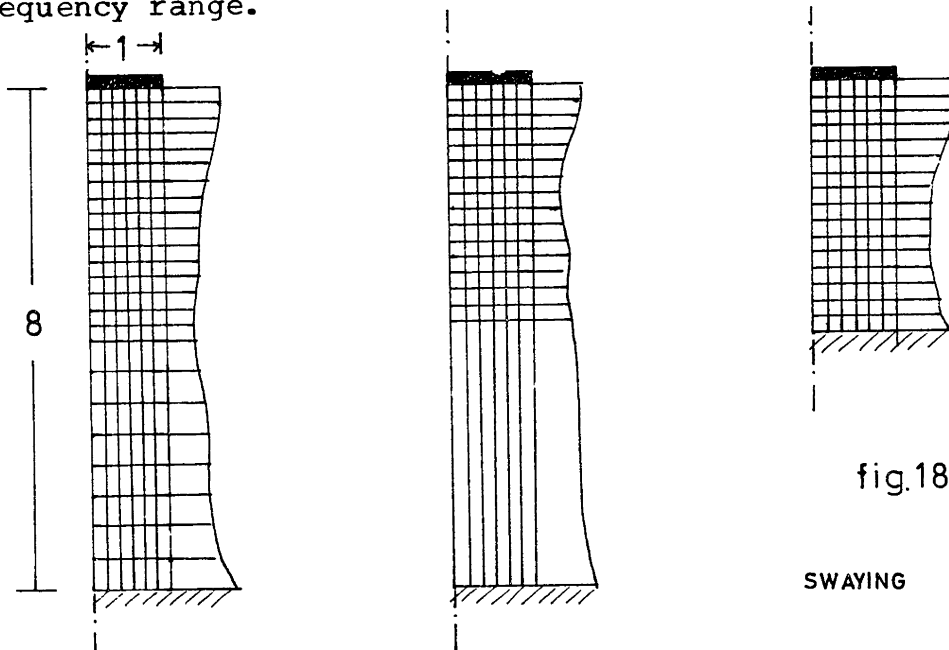


For instance, the static spring constants obtained for  $H/R = 4$ ,  $\nu = 1/3$  with the fine and economic meshes are 4.54 and 4.58 respectively, while the corresponding value for  $H/R = 2$  (that is, eliminating the long element) is 4.76, and the absolute error is 5 times larger. Similar conclusions

apply also for a Poisson's ratio  $\nu = 0.45$ , which was also tested.

On the other hand, swaying does not behave as nicely as rocking, as inspection of fig. 21 reveals. The dynamic pressure bulb for this case, if it exists at all, is much larger than twice the diameter of the plate ( $4R$ ). The stiffness coefficient function starts to diverge markedly from the refined solution at a shear wave length of some 3 to 4 times the length of the long elements; that is, at a dimensionless frequency of  $f_0 = \frac{R}{\lambda} = \frac{1}{\lambda_0} = \frac{R}{3l}$  ( $l$ =length of long element). It is concluded then that the finite element mesh for swaying should have elements that in the regions of high strain gradients (near the plate) are smaller than  $1/6$  to  $1/8$  the shortest shear wave length of interest, and smaller than  $1/3$  to  $1/4$  the shortest shear wave length throughout the finite element region. Possibly, the dynamic pressure bulb for swaying is some 3 to 4 times the diameter of the plate, but since the behavior of strata deeper than four diameters rapidly approaches that of the halfspace (see sec. 4.2), and the refined mesh for  $H/R = 8$  (4D) is already expensive in terms of computer execution time, it seems unnecessary to further pursue the determination of the zone of influence for strata deeper than  $H/R = 8$ , for which the halfspace solution may be used. The dimensions of the pressure bulb will

certainly be affected by the presence of internal damping, which decreases the influence of regions away from the plate by attenuation of the waves generated at the source of the motion (plate). On the other hand, the static values of the swaying spring constant are barely affected by the long elements (which shows that the static pressure bulb is much smaller than the dynamic one), but again, these long elements contribute significantly to the total flexibility (stiffness) of the system, as well as to the dynamic behavior in the low frequency range.



$$K = 5,352$$

$$f_1 = 0,03125$$

$$f_2 = 0,0940$$

$$\vdots$$

$$K = 5.369$$

$$f_1 = 0,03141$$

$$f_2 = 0,1095$$

$$\vdots$$

$$K = 5,696$$

$$f_1 = 0,06253$$

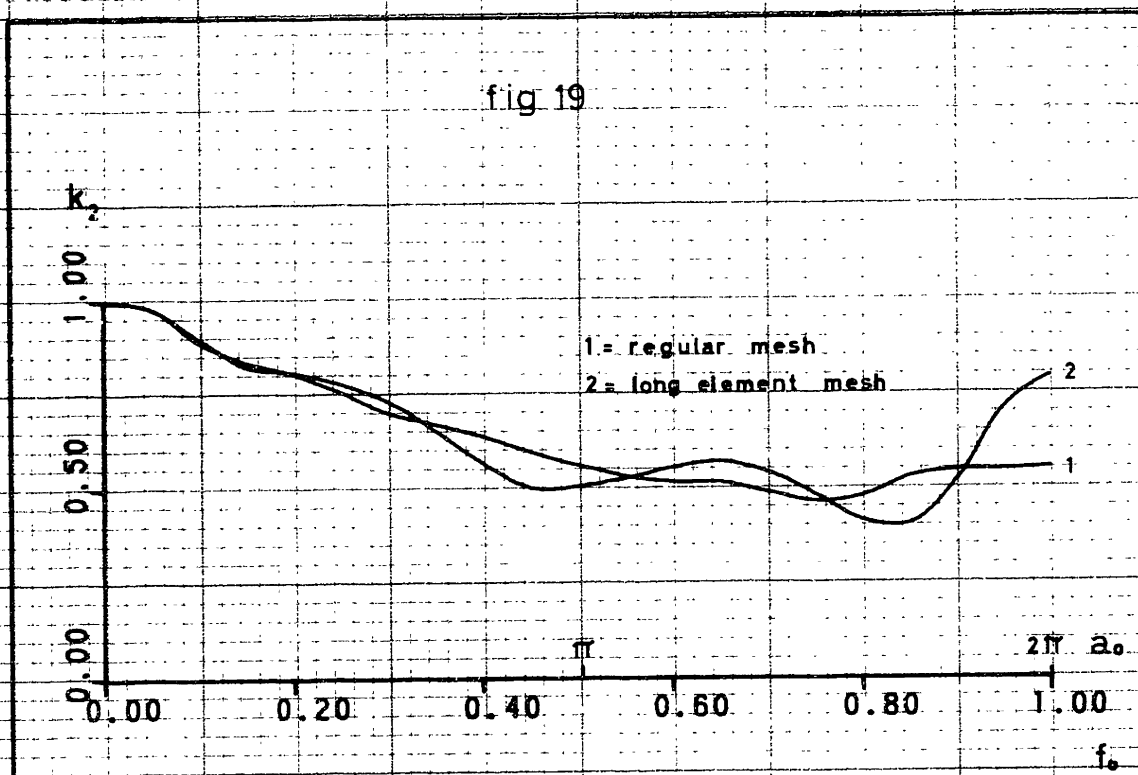
$$f_2 = 0,1882$$

$$\vdots$$

fig.18

SWAYING

fig 19



TEST PRESSURE BULB

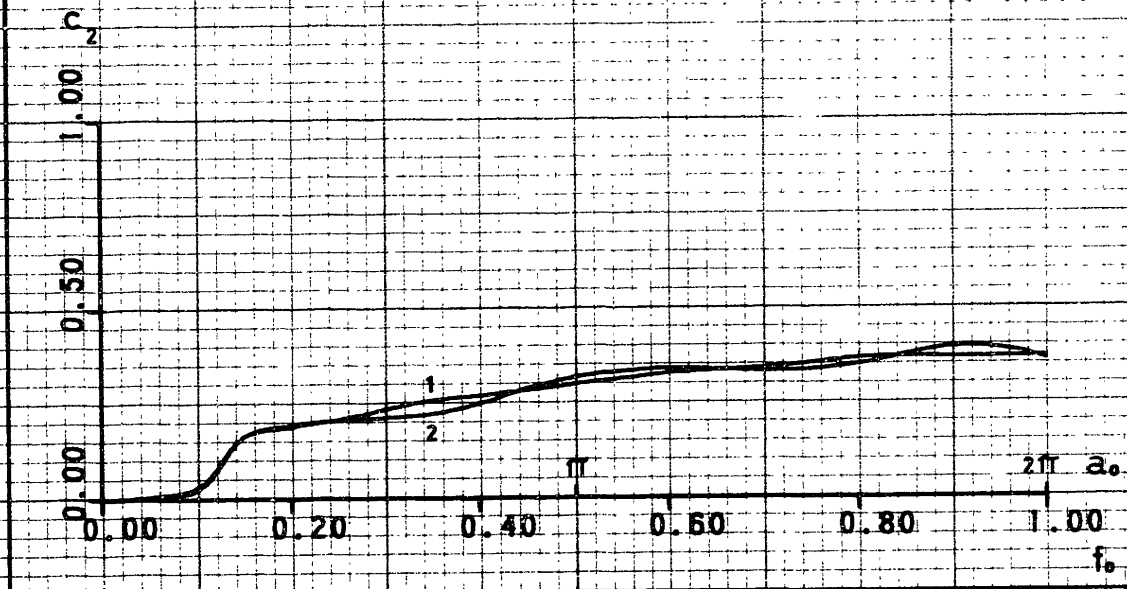
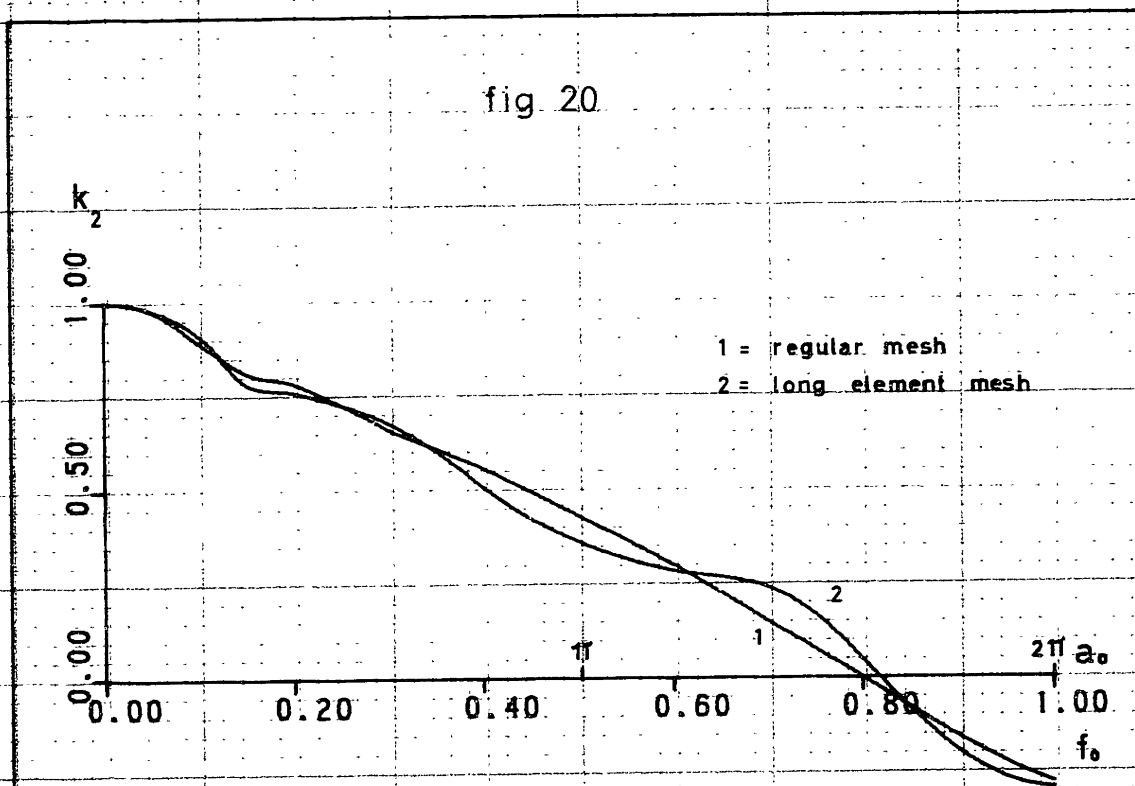
rocking,  $H/R = 4$ ,  $\nu = 1/3$ 

fig 20



## TEST PRESSURE BULB

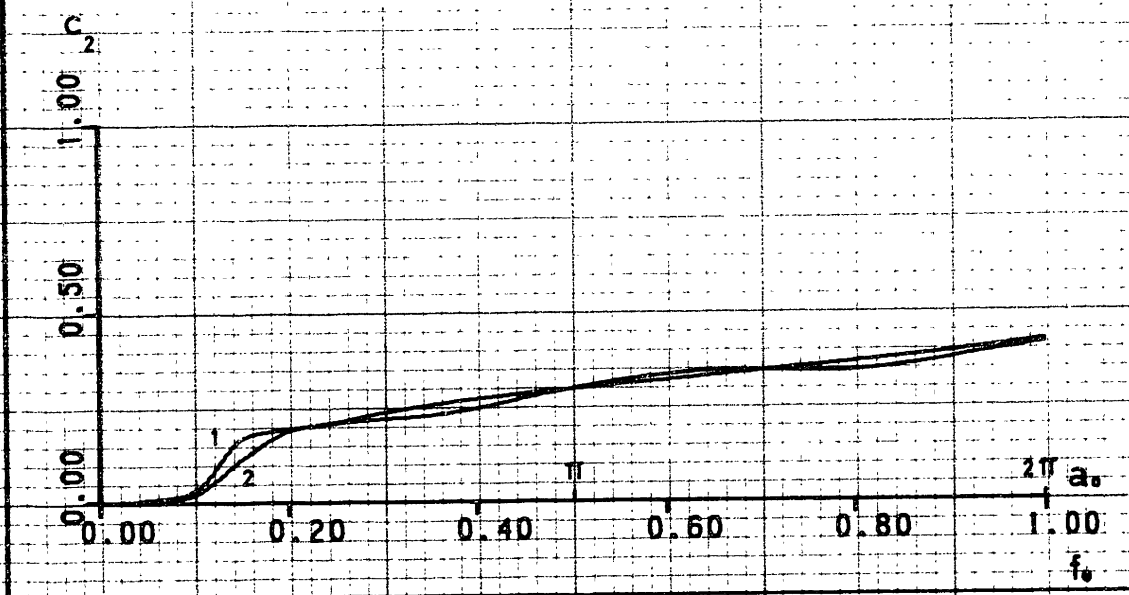
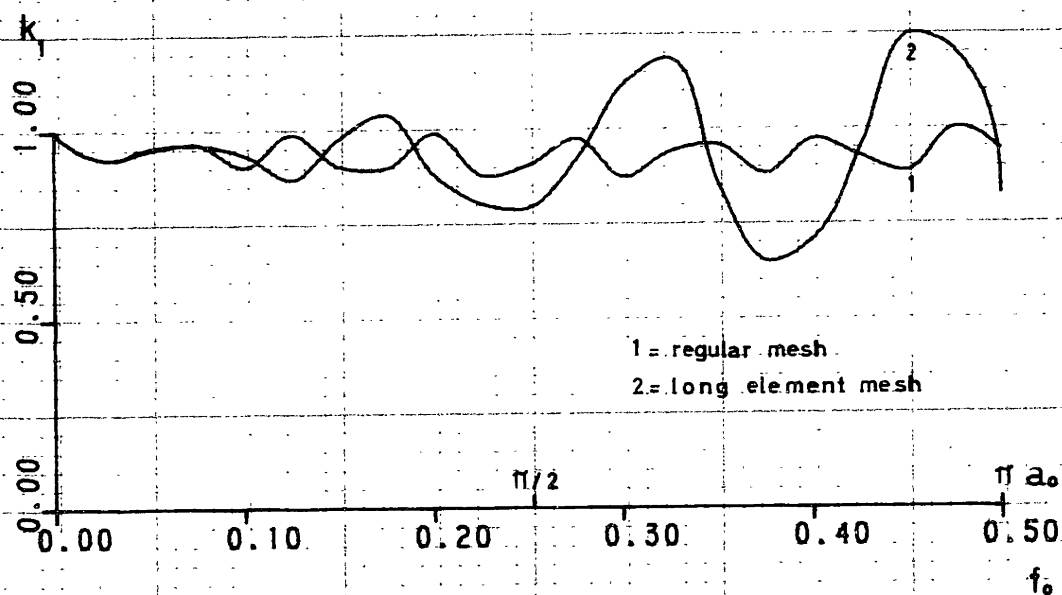
rocking ,  $H/R = 4$  ,  $\nu = 0.45$ 

fig 21 a



## TEST PRESSURE BULB

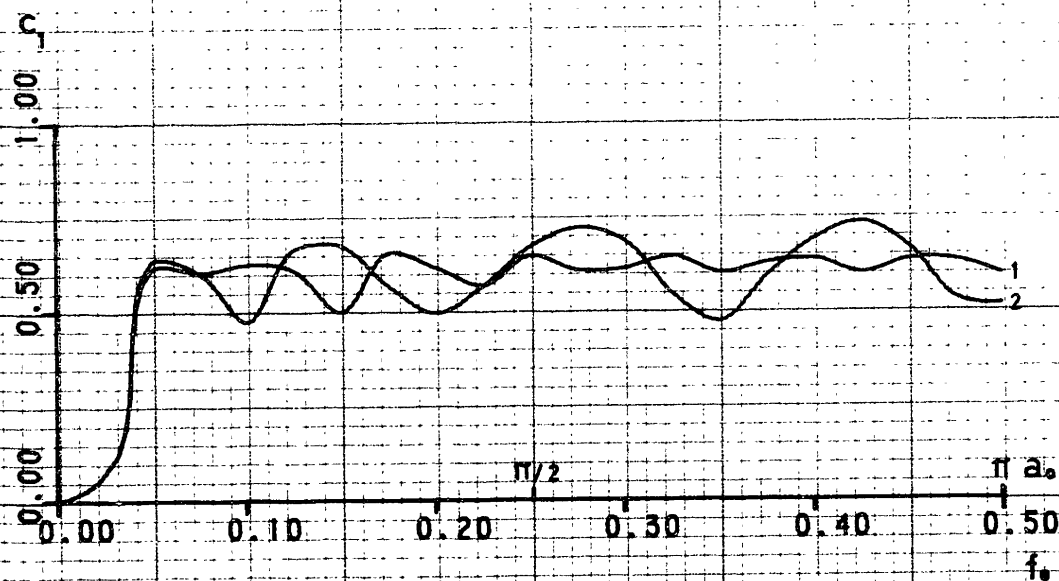
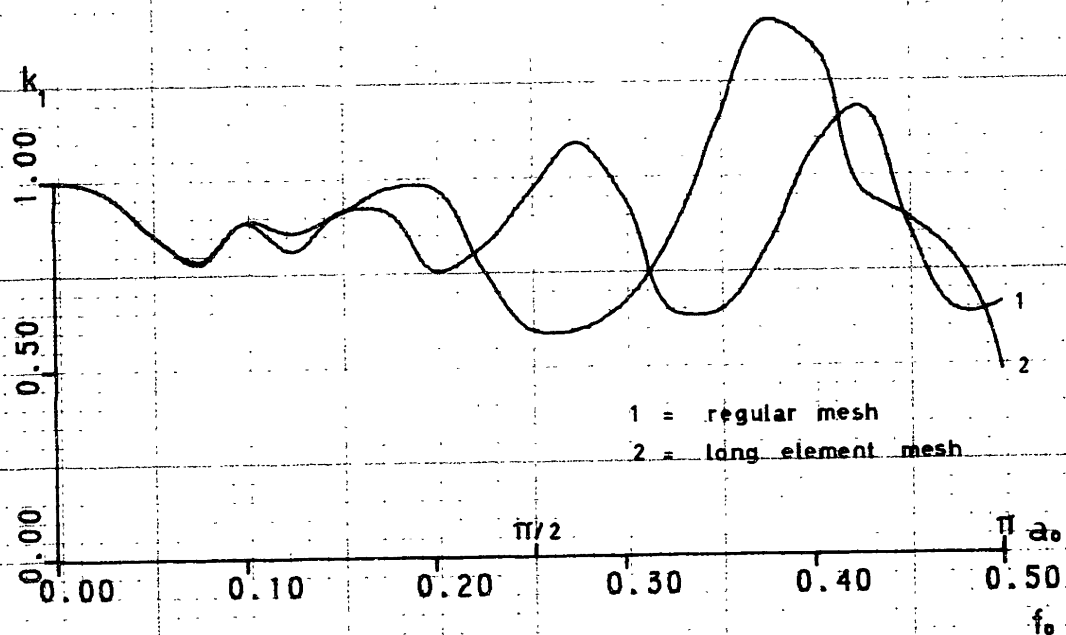
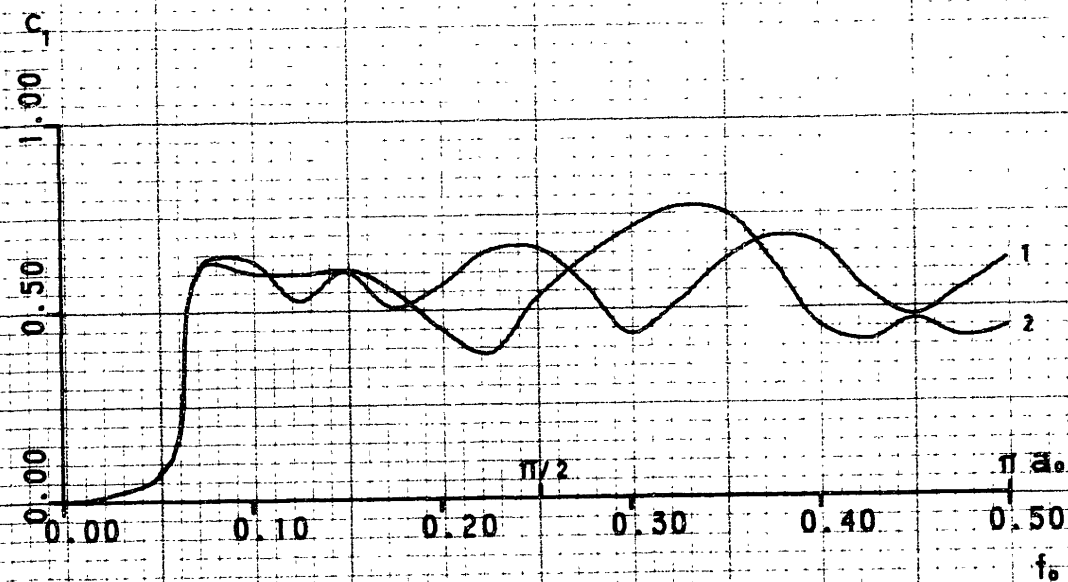
swaying,  $H/R = 8$ ,  $V = 1/3$ 

fig 21 b



## TEST PRESSURE BULB

swaying,  $H/R=4$ ,  $\nu=1/3$ 

The first two natural frequencies of the stratum, as computed with the corresponding discrete (consistent) one dimensional problem for the three meshes in Fig. 18 show good agreement between the refined and the economic meshes, while the half-depth mesh differs in its eigenvalues by a factor of 2, emphasizing the convenience of including the long element in the finite element mesh.

On the other hand, the stiffness coefficient functions tend at higher frequencies (except for a frequency shift) to the results of the shallower (half-depth) stratum, that is, with the long element replaced by rock (see for comparison Fig. 29 in next section).

c. Location of the energy absorbing boundary:

In general, one will place the energy absorbing boundary as close as possible to the core region in order to avoid unnecessary finite element columns and realize a saving in computation time. Nevertheless, it is of interest to investigate the effect of adding more element columns to the finite element mesh, and compare the results with those obtained without the additional elements. For this purpose, the following meshes were considered:



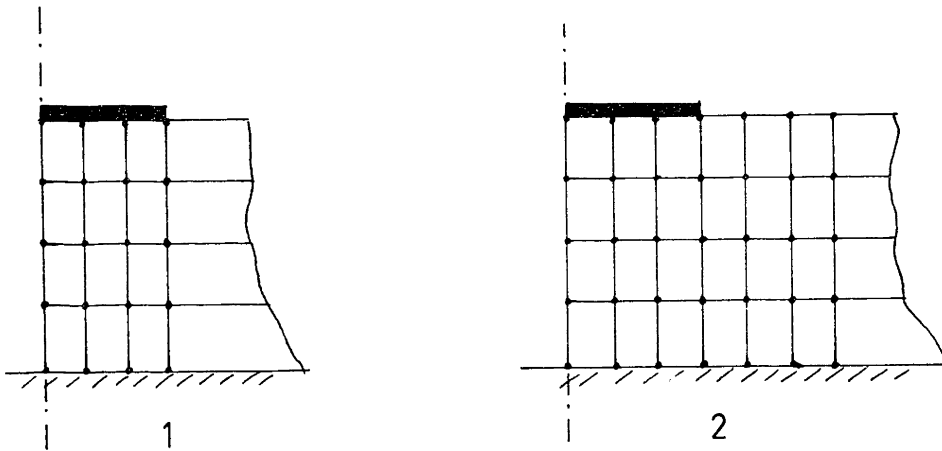


fig. 22

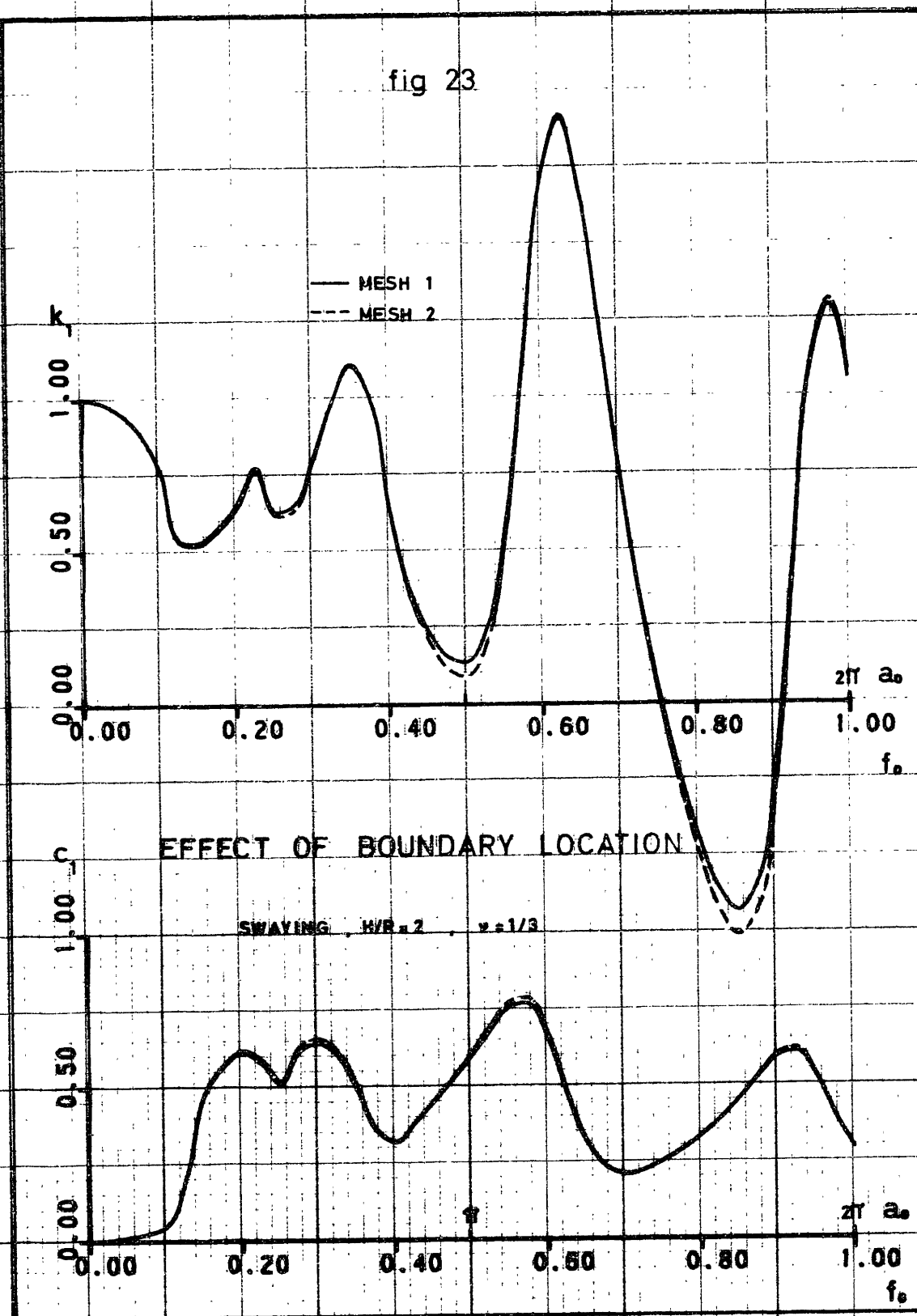
Both cases were analyzed for a unit prescribed horizontal displacement, and the static reaction forces were found to be

$$K_1 = 6.85$$

$$K_2 = 7.00$$

that is, the second mesh is somewhat stiffer than the first one. The reason for this can be found in the fact that the energy absorbing boundary uses the consistent expansion in the vertical direction, but the exact expansion in the radial direction and is thus more flexible. The frequency dependence, however, was negligibly affected, and both meshes showed substantially the same response (dashed curve in Fig. 23).

fig 23



This example demonstrates the convenience of locating the boundary as close as possible, both for computational efficiency and for accuracy of the results.

#### 4.2.- Influence of the stratum depth:

The depth of the layer, for a given plate dimension, influences the results for the stiffness function in two ways:

- first, it determines the value of the static constant, and therefore, the absolute value of the stiffness function over the whole frequency range, and
- second, it affects the shape of the stiffness function, since the dynamic response of the plate is significantly influenced by the natural modes of vibration of the stratum, as well as by reflections at the rock-soil interface.

##### a) Static constant:

Consider, as in sec. 4.1, three typical meshes in which the element sizes follow a converging sequence (fig. 24). Use of the program yields table 1 of static values.

Employing the method suggested in 4.1 to obtain the extrapolated values for the continuum solution, the values in

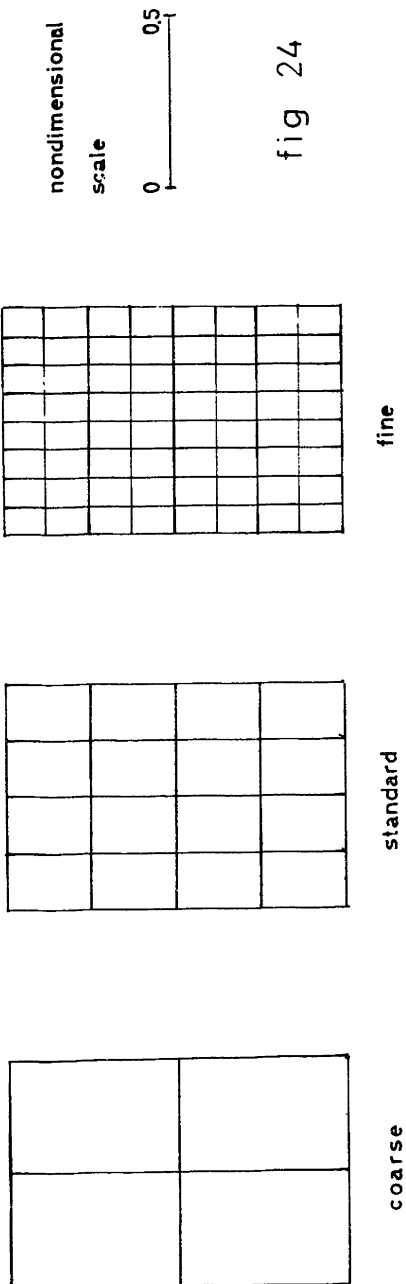
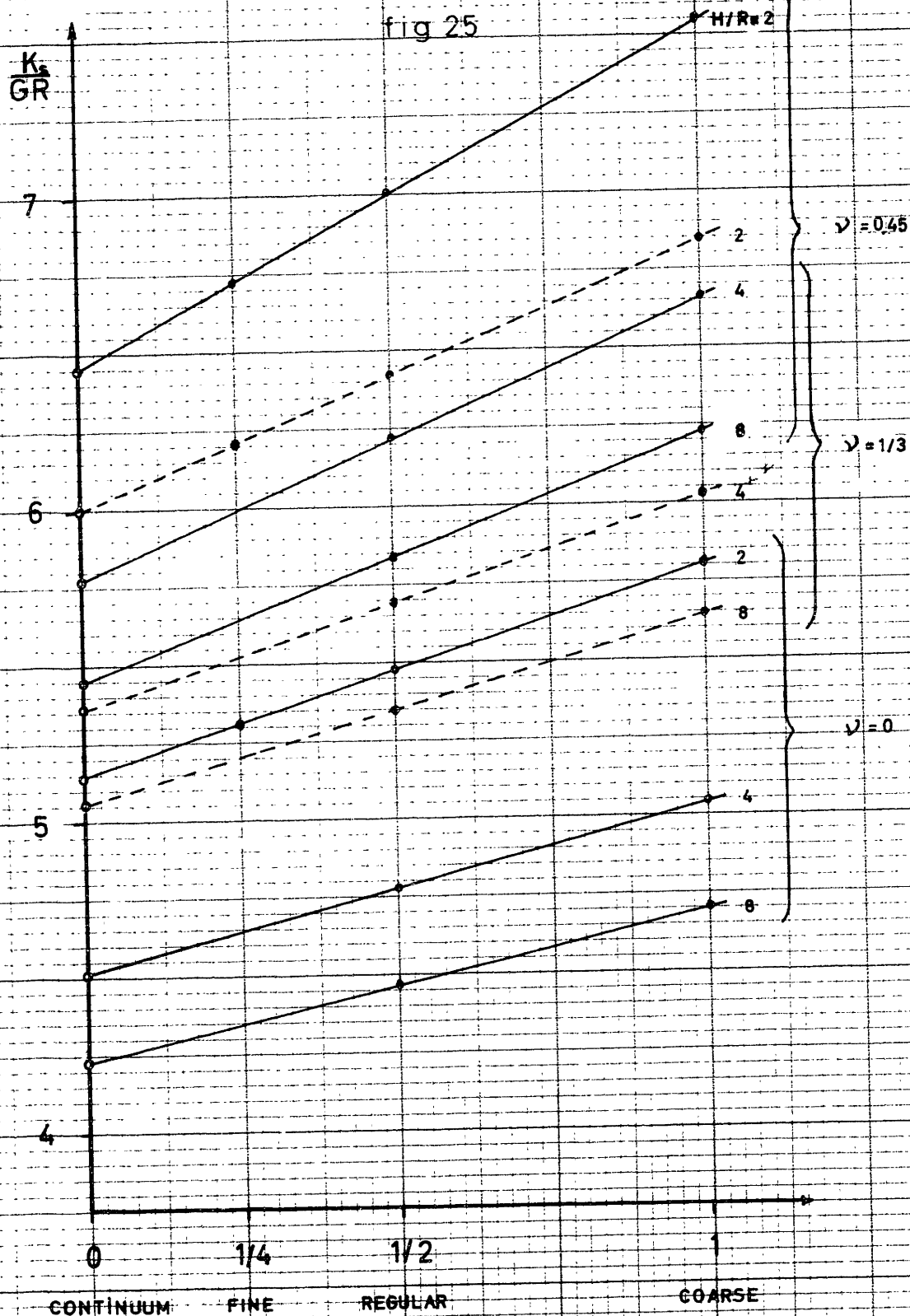


fig 24

Table 1

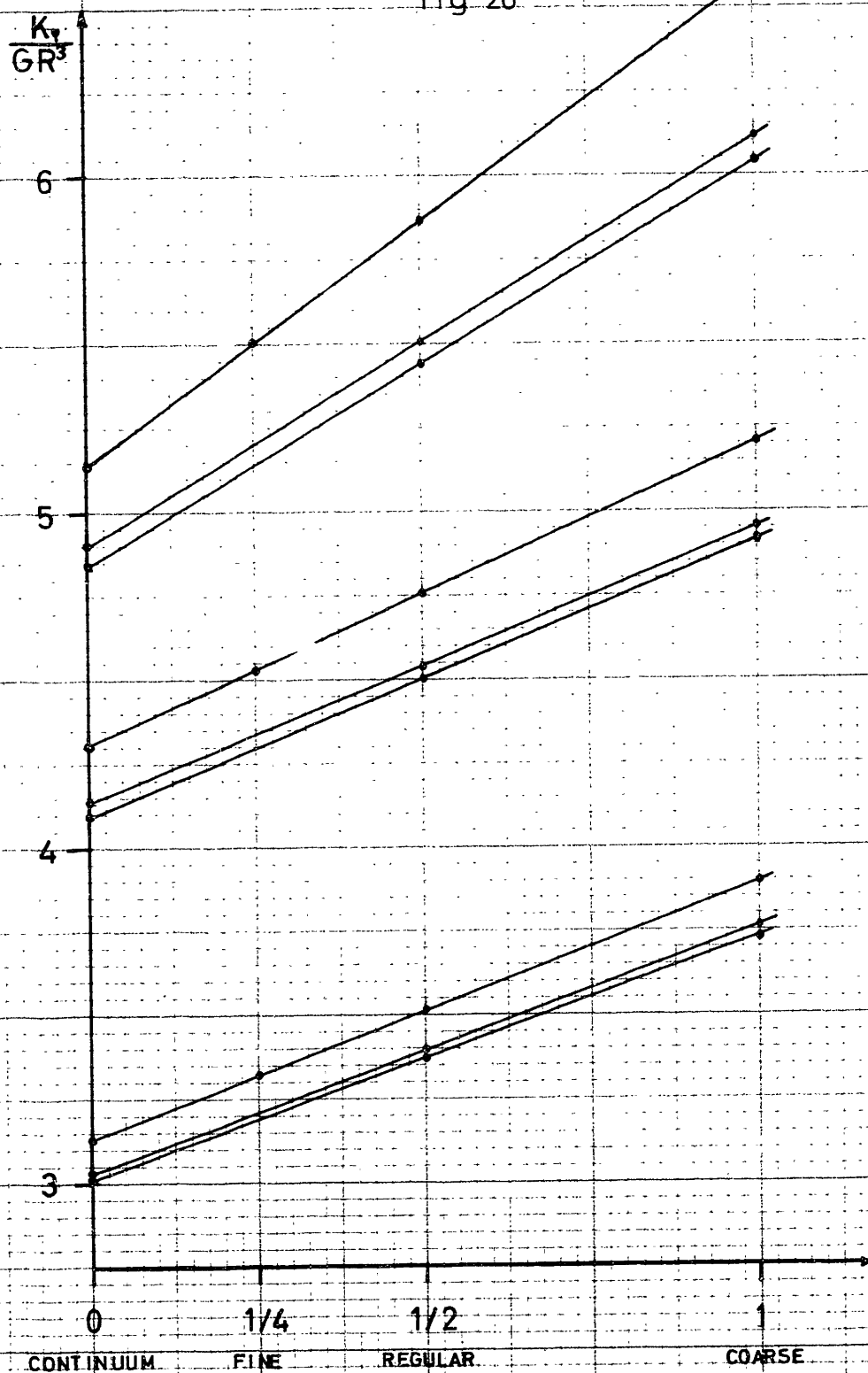
	H/R	$\nu = 0$				$\nu = 1/3$				$\nu = 0.45$			
		cont	fine	stand	coarse	cont	fine	stand	coarse	cont	fine	stand	coarse
S w a y i n g	2	5.15	5.320	5.485	5.817	6.00	6.207	6.437	6.851	6.46	6.724	7.008	7.553
	4	4.52		4.789	5.052	5.38		5.696	6.032	5.79		6.217	6.667
	8	4.23		4.473	4.705	5.06		5.352	5.650	5.45		5.845	6.244
	$\infty$	4.00	—	—	—	4.80	—	—	—	5.17	—	—	—
R o c k i n g	2	3.13	3.326	3.519	3.900	4.31	4.533	4.757	5.208	5.13	5.506	5.865	6.596
	4	3.03		3.397	3.758	4.15		4.540	4.953	4.90		5.503	6.117
	8	3.01		3.378	3.734	4.10		4.506	4.912	4.84		5.448	6.048
	$\infty$	2.67	—	—	—	4.00	—	—	—	4.85	—	—	—

fig 25



EXTRAPOLATION SWAYING SPRINGS

fig 26

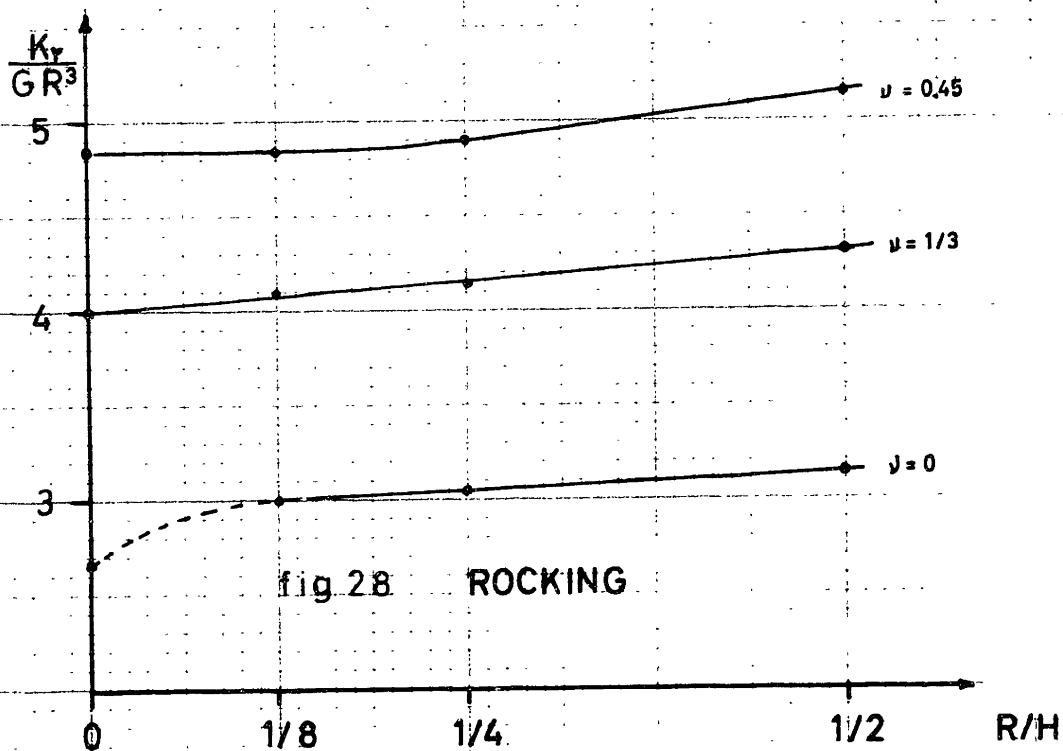
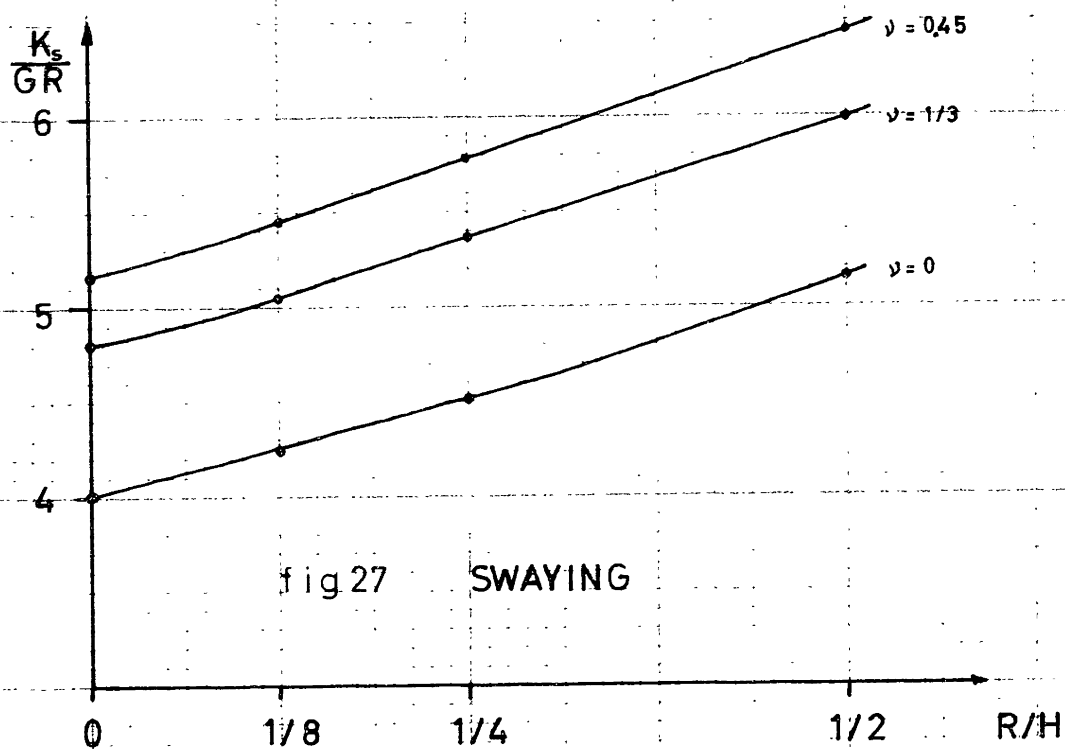


EXTRAPOLATION ROCKING SPRINGS

the table are plotted in Figs. 25 and 26 as a function of the relative element size, arbitrarily assigning the value 1 to the coarse mesh. Full dots represent table values, while (o) are the extrapolated values for the continuum solution.

These extrapolated continuum values are then plotted in Figs. 27 and 28 as a function of the the stratum depth ratio  $R/H$  using the theoretical halfspace values for  $R/H=0$ .

For swaying, the points can very closely be approximately by straight lines. That these straight lines are nearly parallel implies independence of Poissons's ratio and provides an easy way of computing the static spring constant of a stratum from that of the halfspace. For rocking, however, the curves are not exact straight lines, and show also some dependence on Poisson's ratio. It is not clear why the curve for  $\nu = 0$  should have the sudden drop (dashed line) at  $R/H = 1/8$ . Previously, it was shown that rocking has a small pressure bulb and therefore no dramatic changes can be expected by increasing the depth beyond four diameters. Probably the reason for the deviation is that for a low Poissons ratio, the soil is softer and a stronger bending environment exists near the plate which cannot be adequately reproduced by elements with linear expansion. Nevertheless, both the relative error and the increase in the





rocking stiffness with  $R/H$  are small, and this stiffness can, for all practical purposes, be approximated by a straight line with some average slope, say that for  $\nu = 1/3$ , which is a probable value to be used for dynamic loadings.

It follows then that the stratum constants can be obtained from the approximate empiric relations

$$K_{s_0} = \bar{K}_{s_0} \left( 1 + \frac{1}{2} \frac{R}{H} \right) = \frac{8GR}{2-\nu} \left( 1 + \frac{1}{2} \frac{R}{H} \right) \quad (4-6)$$

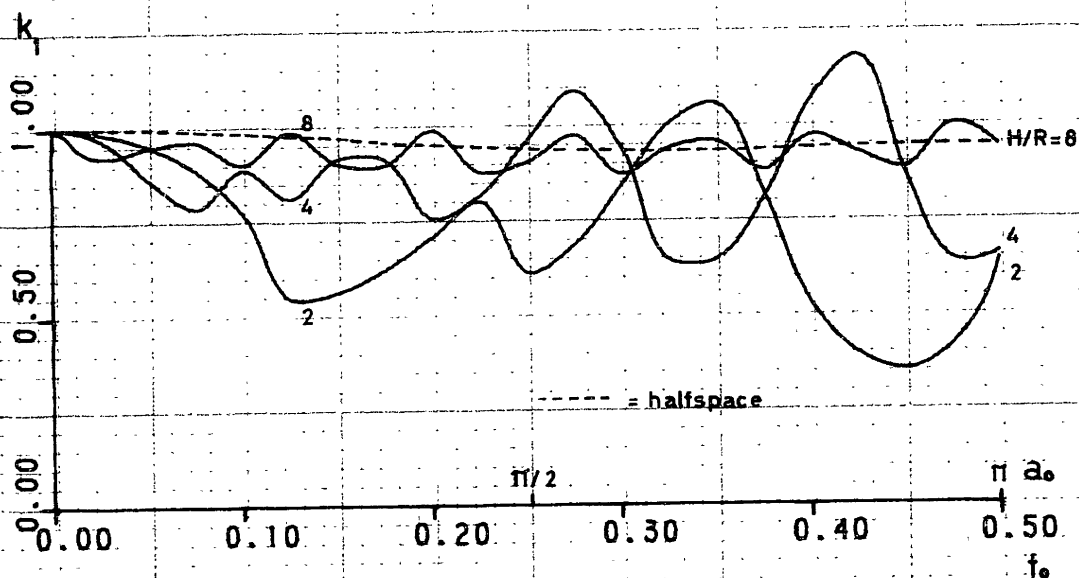
$$K_{\varphi_0} = \bar{K}_{\varphi_0} \left( 1 + \frac{1}{6} \frac{R}{H} \right) = \frac{8GR^3}{3(1-\nu)} \left( 1 + \frac{1}{6} \frac{R}{H} \right) \quad (4-7)$$

where  $\bar{K}_{s_0}$ ,  $\bar{K}_{\varphi_0}$  are the halfspace static stiffnesses. It is believed that for strata shallower than 1 plate diameter, the flexibility of the base rock has to be included in the analysis, and (4-6), (4-7) will overestimate the static spring constants.

b) Stiffness coefficients:

Examination of Figs. 29 and 30 shows several interesting features in the frequency dependence of the stiffness functions. The real part of the stiffness coefficients behave markedly different for rocking and swaying.

fig 29



## EFFECT OF LAYER DEPTH

swaying,  $\nu = 1/3$

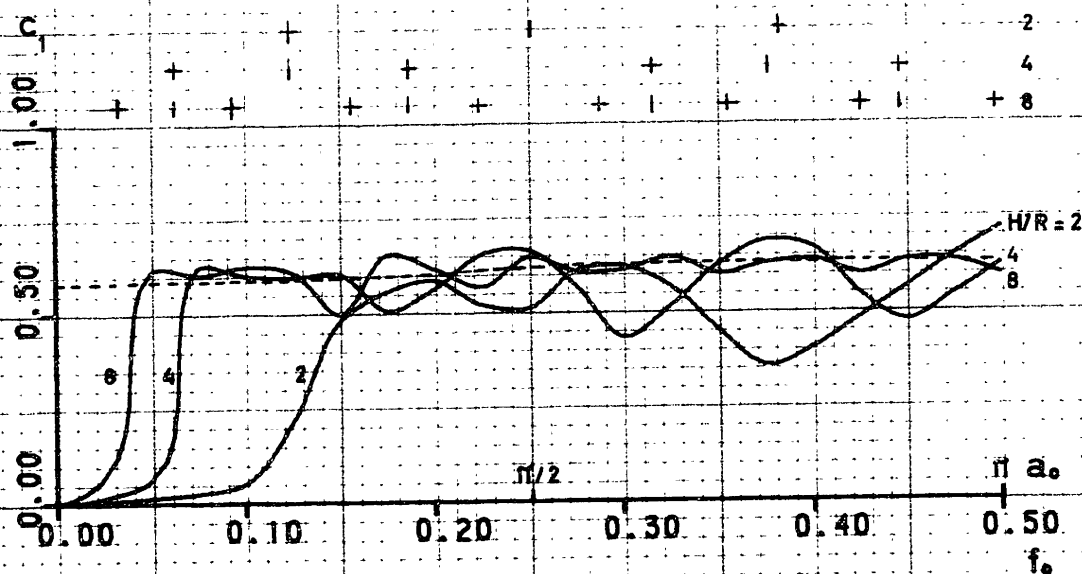
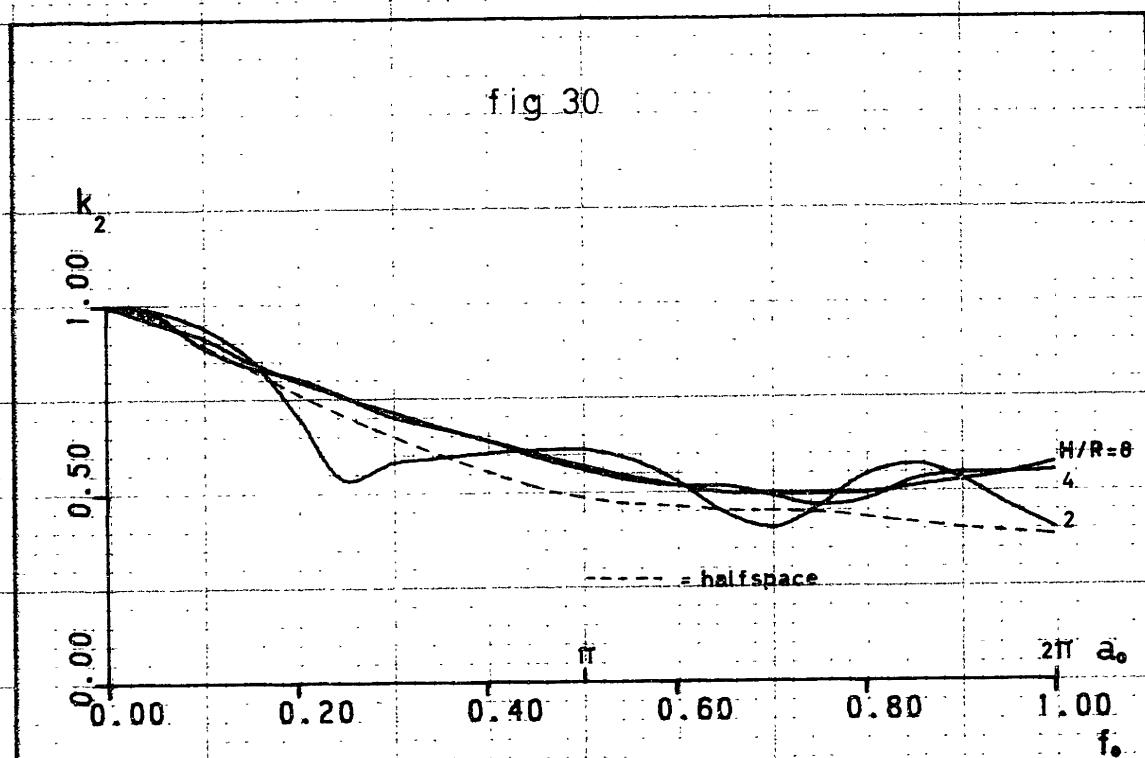
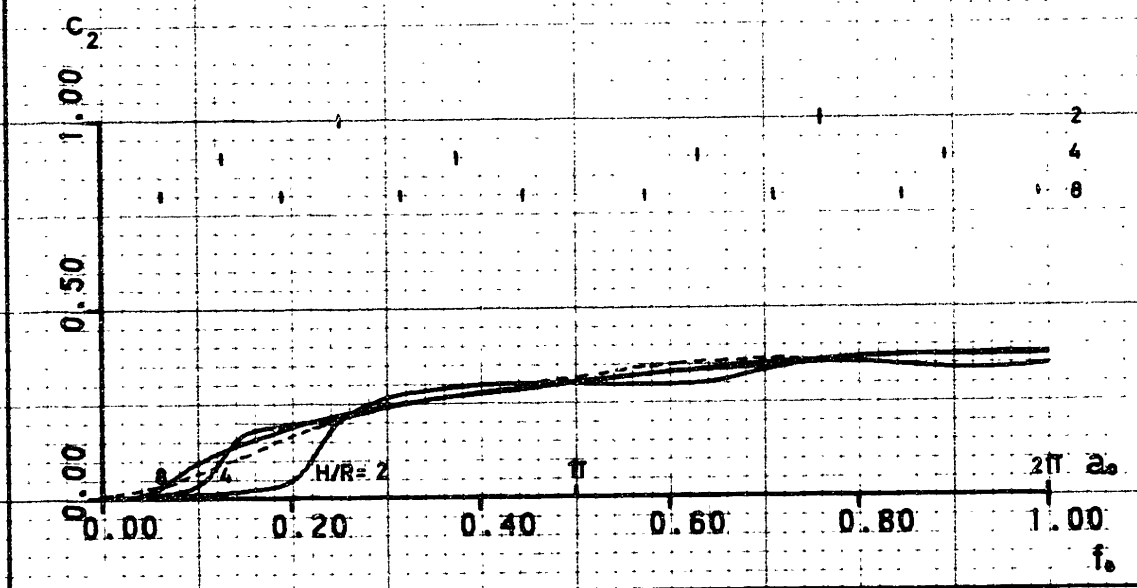


fig 30



## EFFECT OF LAYER DEPTH

rocking,  $\nu = 1/3$ 

The former is a relatively smooth curve, for which the depth of the layer exercises little influence and approaches remarkably the analytical halfspace solution after Veletsos & Wei (42) throughout most of the frequency range studied. Swaying, however, displays a wavy pattern in which the valleys occur close to the natural vibration frequencies of the soil, an effect that becomes pronounced for shallow strata. Nevertheless, as the depth of the layer is increased, the amplitudes of the peaks and valleys decrease rapidly, and for  $H/R=8$  (4 diameters) it already approaches Veletsos and Wei's halfspace solution. Had the internal damping been chosen equal to zero, then the stiffness function would have vanished at each horizontal natural frequency of the layer, since it would have required no energy to sustain the stratum oscillating at its natural translational mode of vibration. No such compatible mode of vibration of the stratum with the plate exists for rocking, although for the shallowest geometry shown (1 plate diameter) the rocking stiffness function has slight critical points at the vertical natural frequency of the soil. In the following, the horizontal and vertical natural frequencies of the stratum shall be abbreviated with HNFS and VNFS respectively. They are given for a homogeneous stratum by:

$$\text{HNFS} = \frac{c_s}{4H} (1 + 2k) \quad , \quad k=0,1,2,3,\dots \quad (4-8)$$

$$\text{VNFS} = \sqrt{\frac{2(1-\nu)}{1-2\nu}} \text{HNFS} \quad (4-9)$$

On the other hand, the imaginary part of the stiffness functions, which represents an equivalent viscous damping due to radiation of energy away from the plate, shows only negligible differences w/r to the halfspace solution for rocking, and except for the wavy nature in shallow strata, is remarkably close to it for swaying. There is one important difference, however, between the strata and the halfspace solutions: the former has no radiation damping in the low frequency range, and then rises abruptly at certain critical frequencies. These critical frequencies correspond to the first HNFS (swaying) and VNFS (rocking) below which no Love or Rayleigh waves can be propagated. Therefore, within this low frequency range, the only damping that limits the motion of a mass (machine or building) on top of the layer is provided by the internal energy dissipation. This effect, which was already pointed out by Arnold et al (1), is particularly important for large mass ratios over shallow strata (tall buildings, heavy equipment), for which the fundamental coupled rocking-swaying frequency is smaller than the natural vibration frequencies of the soil. To estimate

approximately when this will happen, assume that the swaying frequency is given by

$$f_s = \frac{1}{2\pi} \sqrt{\frac{k}{M}}$$

where  $k = \frac{8GR}{2-\nu}$  is the halfspace spring constant, and  $M$  is the mass of the building.

With  $G = \frac{1}{2} c_s^2$ ,  $M = \frac{1}{2} R^3 b$ ,  $HNFS = f_h = \frac{c_s}{4H}$ , ( $b$  = mass ratio) it follows then

$$\frac{f_s}{f_h} = \frac{4}{\pi} \frac{H}{R} \sqrt{\frac{2}{(2-\nu)b}}$$

Taking  $\nu = 0.4$  and  $\pi^2 \approx 10$ , this reduces to

$$\frac{f_s}{f_h} = \frac{H}{R} \sqrt{\frac{2}{b}}$$

which is smaller than 1 for

$$b \geq 2 \left( \frac{H}{R} \right)^2 \quad (4-10)$$

For instance, if  $H/R = 2$ , a mass ratio  $b > 8$  will produce swaying frequencies smaller than the VNFS of the soil, and thus, a large response could be expected, depending on the frequency contents of the excitation. Similar results can be

obtained for rocking, but taking as a reference frequency the vertical natural mode of vibration  $f_v = \text{VNFS}$ :

$$f_v = \frac{C_s}{4H} \sqrt{\frac{\lambda + 2G}{G}} = \frac{C_s}{4H} \sqrt{\frac{2(1-\nu)}{1-2\nu}}$$

For this case

$$k_r = \frac{8 G R^3}{3(1-\nu)} = \frac{8 \rho C_s^2 R^3}{3(1-\nu)}$$

$$f_r = \frac{1}{2\pi} \sqrt{\frac{k_r}{I}}$$

For a uniform solid cylinder of mass  $M$ , height  $h$  and radius  $R$ , the moment of inertia  $I$  can be written as

$$I = \frac{\rho b R^5}{4} \left( 1 + \frac{4}{3} \xi^2 \right), \quad \xi = \frac{h}{R} \quad (\text{aspect ratio})$$

so that

$$\frac{f_r}{f_v} = \frac{8H}{\pi R} \sqrt{\frac{1-2\nu}{3(1-\nu)^2 \left( 1 + \frac{4}{3} \xi^2 \right) b}}$$

which for  $\nu = 0.4$  can be approximated by

$$\frac{f_r}{f_v} = 1.1 \frac{H}{R} \sqrt{\frac{1}{\left( 1 + \frac{4}{3} \xi^2 \right) b}}$$

This ratio is less than 1 if

$$b > \frac{1.2 \left(\frac{H}{R}\right)^2}{1 + \frac{4}{3} \xi^2} \quad (4-11)$$

Since  $M = \rho_s \pi R^2 h = \rho R^3 b$  it follows that

$$b = \pi \frac{\rho_s}{\rho} \frac{h}{R} = \pi \delta \xi, \quad \delta = \frac{\rho_s}{\rho} \quad (4-12)$$

where  $\delta$  is the density ratio. Assuming  $\rho_s = \frac{1}{5} \cdot 0.15 = 0.03 \text{ K/cf}$ ,  
 $\rho = 0.12 \text{ K/cf}$  we obtain for  $\delta$

$$\delta = \frac{0.03}{0.12} = 0.25$$

hence

$$b = 0.25 \pi \xi, \quad \xi = 4 \frac{b}{\pi}$$

The condition  $\frac{f_c}{f_r} \leq 1$  is then

$$b > \frac{1.2 \left(\frac{H}{R}\right)^2}{1 + \frac{4}{3} \left(4 \frac{b}{\pi}\right)^2} = \frac{1.2 \left(\frac{H}{R}\right)^2}{1 + \frac{64}{3\pi^2} b^2} \quad (4-13)$$

For a stratum depth  $H/R=2$ , the above expression can be solved by trial and error, obtaining  $b \geq 1.19$ , which in turn implies



$\xi > 1.5$  , that is ,  $h > 1.5R$ , or  $h > .75D$  , a case frequently encountered in practice.

If the subsoil is saturated with water, it has a high Poisson's ratio, and it is likely that the rocking frequency of the soil-structure system will be smaller than the VNFS, and therefore, the motion of the mass will be highly undamped. Experimental data given by Arnold et al (1) for the rocking mode show that for shallow strata ( $H/R=0.84$ ), the motions are four to six times greater than for the halfspace.

An additional effect which can contribute to large responses in shallow strata, is related to the natural frequencies of the stratum with a mass. To illustrate this point, consider the equation which gives the (non-dimensional) swaying frequency for a mass  $M$  on top of a stratum:

$$f_s = \frac{1}{2\pi} \frac{R}{C_s} \sqrt{\frac{K_s}{M}} = \frac{1}{2\pi} \frac{R}{C_s} \sqrt{\frac{K_{so} R_i}{M}}$$

Since (eq. 4-6)

$$K_{so} = \frac{8GR}{2-\nu} \left( 1 + \frac{1}{2} \frac{R}{H} \right)$$

it follows that

$$f_s = \frac{1}{\pi} \sqrt{\frac{2 \left(1 + \frac{1}{2} \frac{H}{R}\right) k_1}{b(2-\nu)}}$$

and solving for the stiffness coefficient  $k_1$

$$k_1 = \frac{2-\nu}{2} \frac{\pi^2 b f_s^2}{\left(1 + \frac{1}{2} \frac{R}{H}\right)} \quad (4-14)$$

For  $\nu = 1/3$  ,  $R/H = 1/2$  this reduces to

$$k_1 = 6.58 b f_s^2 \quad (4-15)$$

At the same time ,  $k_1$  must also be a point in the graph giving the variation of the stiffness coefficient with the frequency. This provides a graphical method to determine the swaying frequency of a structure with mass ratio  $b$  . Using the results for the stratum  $H/R=2$  ,  $\nu = 1/3$  ,  $\beta = 0.05$ , the (non-dimensional) swaying frequencies for this particular case can be determined as the intersections of equation (4-15) with the graph of the stiffness function obtained with the aid of the program:

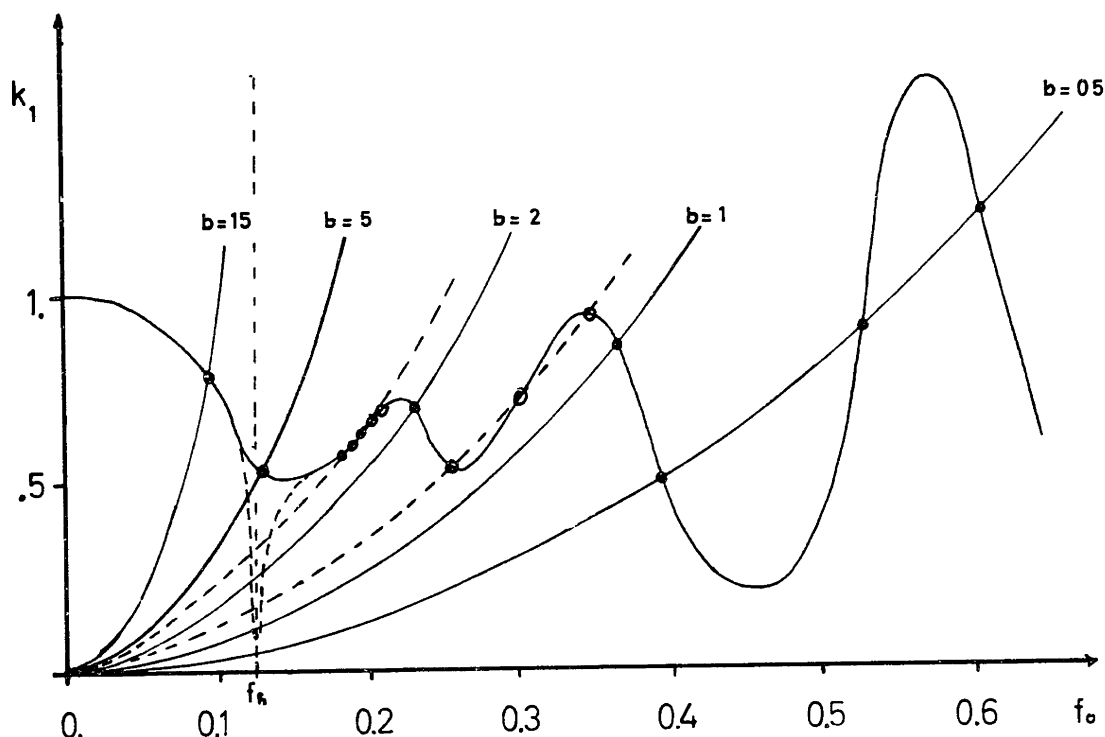


fig 31

Several properties of the solution are worth noting:

- Mass ratios larger than 5 imply swaying frequencies less than the HNFS. This is consistent with the results found before using the approximate calculation.

- For mass ratios slightly larger than 2, and slightly larger than 1, (dashed lines in Fig. 31) equation 4-15 yields a parabola which nearly coincides with the stiffness coefficient curve in the frequency ranges 0.175-0.225 and 0.250 -0.350, respectively. This implies that any frequency

in these ranges is nearly a solution, and therefore, a natural swaying frequency. From here, it follows that for these particular mass ratios and within these frequency intervals the dynamic response will show wide resonant bands. This is a consequence of the wavy nature of the swaying stiffness function, an effect that will not show up in the rocking mode. It is this nature of the swaying problem which will increase considerably the uncertainty in the determination of the swaying frequency when using the static spring constant approach. This is particularly important in v.gr. machine foundation design when one has to estimate the resonant frequencies and ensure that the operating frequency differs from the resonant by a certain specified factor (at least 1.5)

- The stiffness function shown in Fig. 31 was computed with an internal damping ratio of 0.05. For smaller damping ratios (see also next section), there will be a sharp and narrow valley for the stiffness function at the HNFS (as suggested by the dashed line), and therefore, there will be a solution for the swaying mode at this frequency for mass ratios in the range 1-5, approximately. That is, the natural frequency of the soil is also a natural swaying frequency, a result which will considerably increase the response of the system when subjected to motions with components at this

frequency. However, this is only true for unrealistically small internal damping ratios, which are not generally encountered in practice.

#### 4.3.- Influence of internal damping:

Internal friction in soils is always present to a certain degree, and as was shown in sec. 2, can be accounted for in the theory by means of complex elastic moduli. The energy dissipation produced by this internal friction avoids the build-up of resonant peaks in the flexibility functions (valleys in the stiffness functions) and therefore softens the frequency dependence of the functions, erasing the sharp peaks and valleys.

Two possible ways of defining the stiffness functions when internal damping is included in the analysis are:

$$K = K_0 (k + i a_0 c) (1 + 2i\beta) \quad (4-16a)$$

$$\text{and} \quad K = K_0 (\bar{k} + i(a_0 \bar{c} + 2\beta)) \quad (4-16b)$$

Both expressions give a valid definition for the stiffness and damping coefficients, and yield nearly identical results ( $k \approx \bar{k}$ ,  $c \approx \bar{c}$ ) when the damping ratio  $\beta$  is small, say less

than 0.05. If the principle of correspondence were strictly valid, then the first expression should give stiffness coefficients  $k, c$  which were independent of the damping ratio  $\beta$ . However, this is not the case. Because of the inertial effects, the results are strongly dependent on the assumed damping ratio. For this reason, neither of the two representations provide a better definition. For a comparison between both representations, see Figs. 32 through 35.

To interpret the term  $a_o c$ , consider the vibration of a mass  $M$  supported by the rigid plate foundation. The static spring constant is  $K_o$ , and the equivalent viscous dashpot is  $C$ .

Then,

$$K_o a_o c_1 = \Omega C \quad , \quad \frac{K_o}{M} a_o c_1 = \frac{\Omega C}{M}$$

$$= 2 \beta_v \omega \Omega$$

where  $\beta_v$  is the viscous damping ratio defined w/r to the (resonant) frequency  $\omega = \sqrt{\frac{K_o}{M}}$ . From here, it follows that

$$a_o c_1 = 2 \beta_v \frac{\Omega}{\omega} = 2 \beta_v \frac{a_o}{a_{no}}$$

$$a_{no} = \frac{\omega R}{C_s}$$

hence 
$$K = K_o \left( \bar{k} + 2i \frac{a_o}{a_{no}} \beta_r \right) (1 + 2i \beta_h) \quad (4-17a)$$

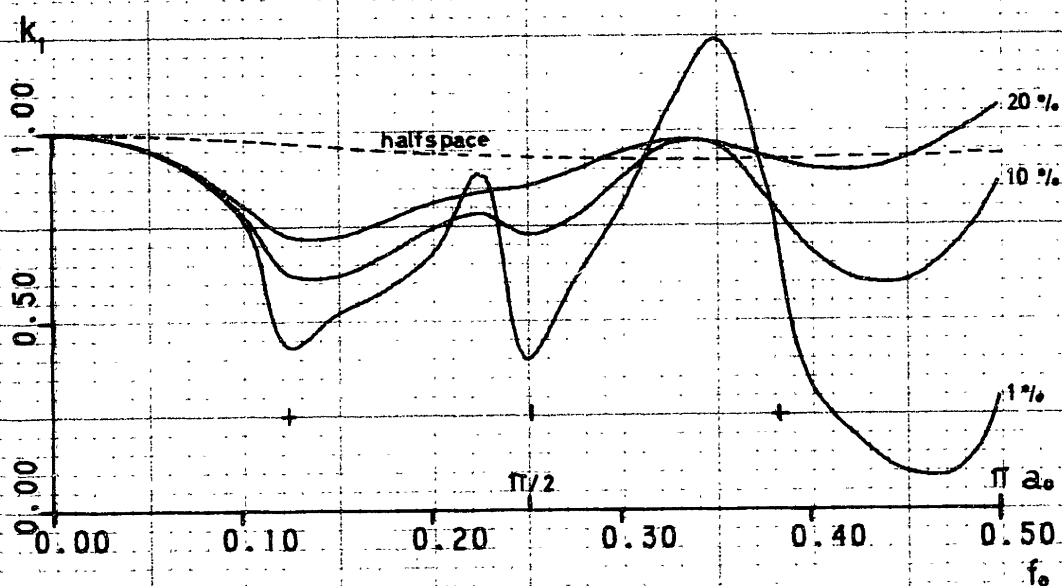
or

$$K = K_o \left( \bar{k} + 2i \left( \frac{a_o}{a_{no}} \bar{\beta}_r + \beta_h \right) \right) \quad (4-17b)$$

and the analogy to a spring dashpot system is obvious; however,  $\beta_r$  is in general a function of the frequency  $\Omega$ . The second expression can be interpreted as the addition of a "viscous" and a "hysteretic" dashpot in parallel. However, since the first representation gives a better approximation to the halfspace solution, it was preferred throughout this study.

The stiffness and damping coefficient functions are plotted in Figs. 32 through 35 for the two loading cases, with  $H/R = 2$ ,  $\nu = 1/3$ . Figs. 32 and 33 correspond to the first representation, while Figs. 34 and 35 depict the second one. The results are highly dependent on the attenuation ratio  $\beta_h$  selected, an effect which seems more important for swaying than for rocking. The influence of the internal damping ratio on the imaginary part of the rocking stiffness function (damping coefficient) is negligible, and moderate for swaying, except when very low damping ratios are considered.

fig 32



## EFFECT OF INTERNAL DAMPING

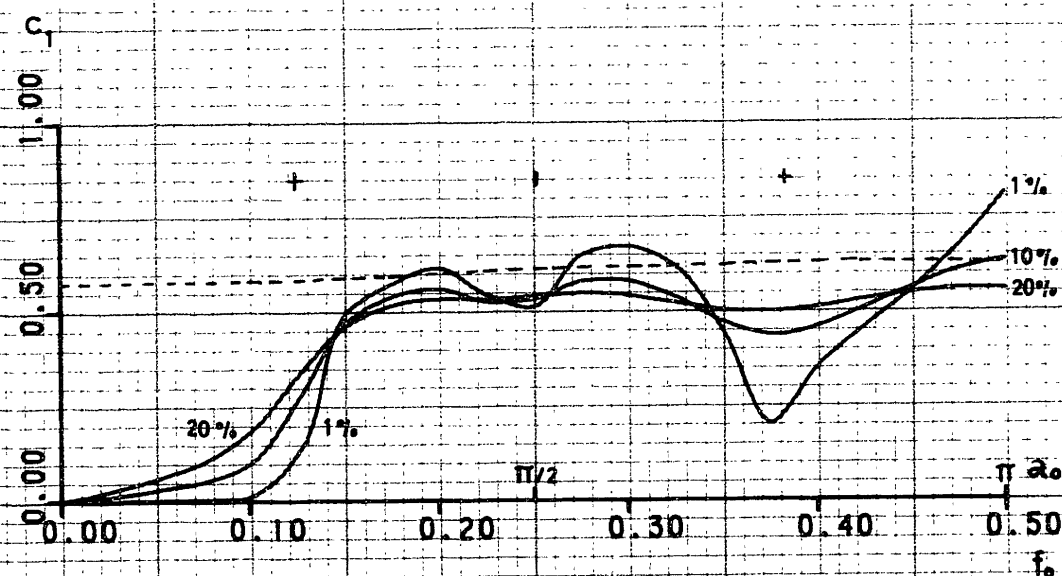
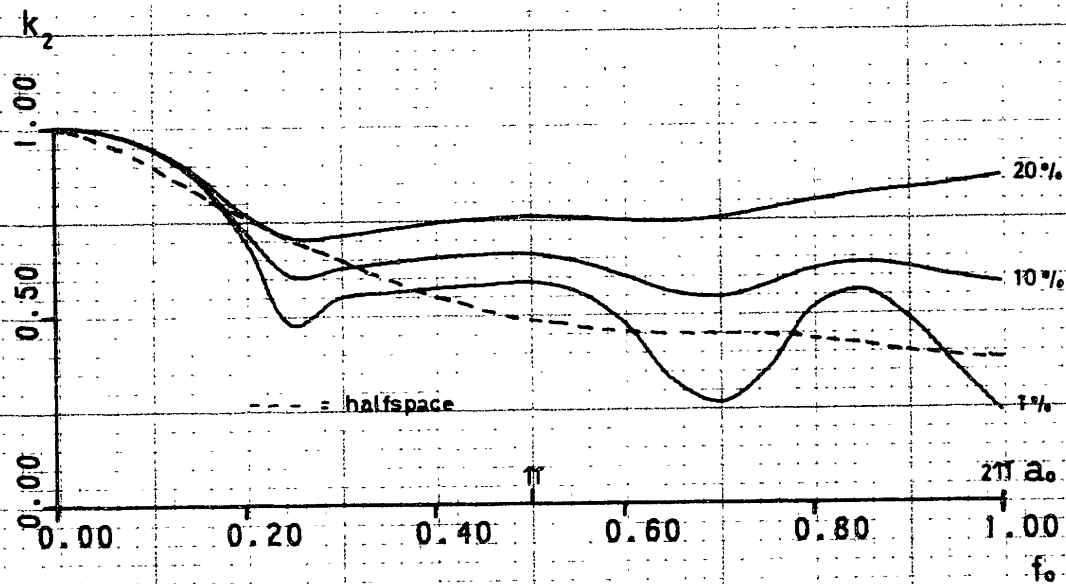
swaying,  $H/R=2$ ,  $\nu=1/3$ 



fig 33



## EFFECT OF INTERNAL DAMPING

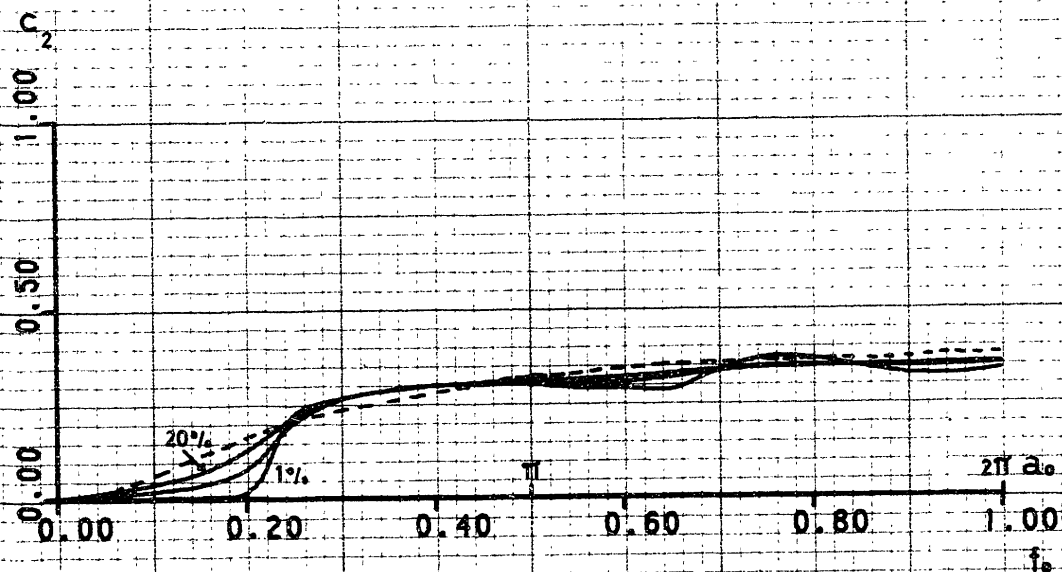
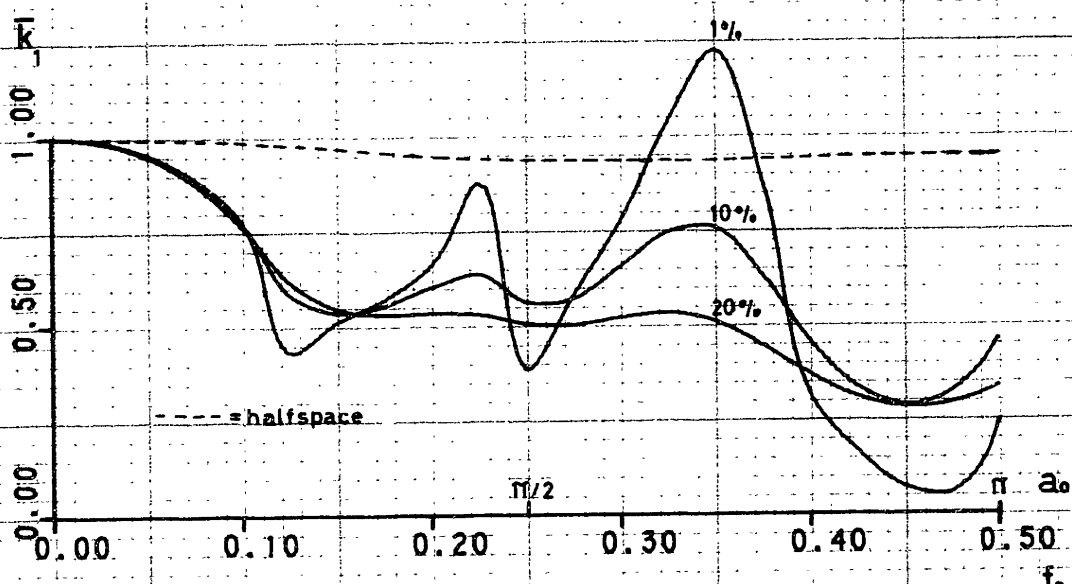
rocking,  $H/R=2$   $\nu=1/3$ 

fig 34



## EFFECT OF INTERNAL DAMPING

ALTERNATE DEFINITION

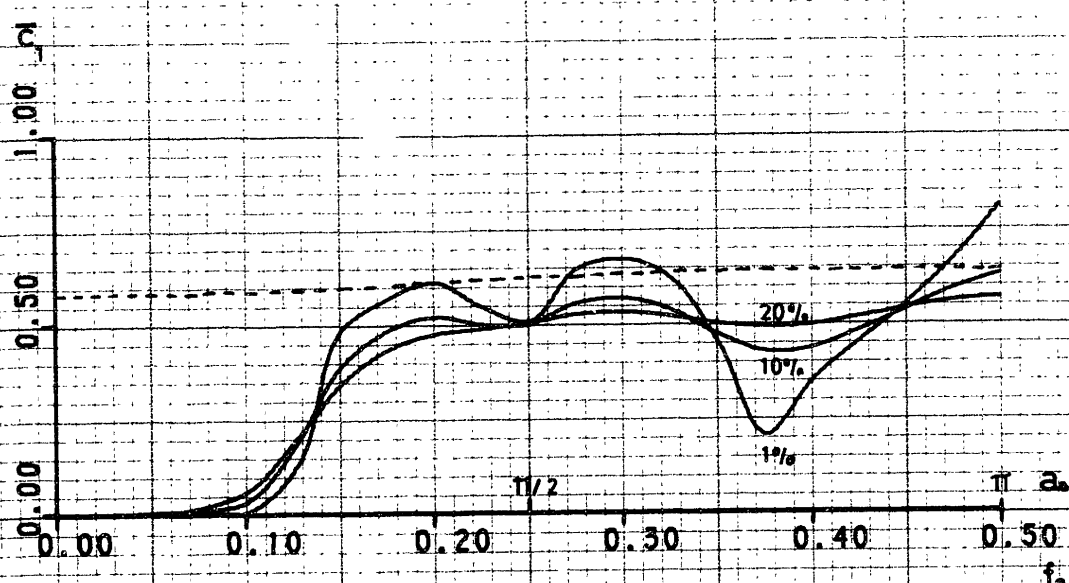
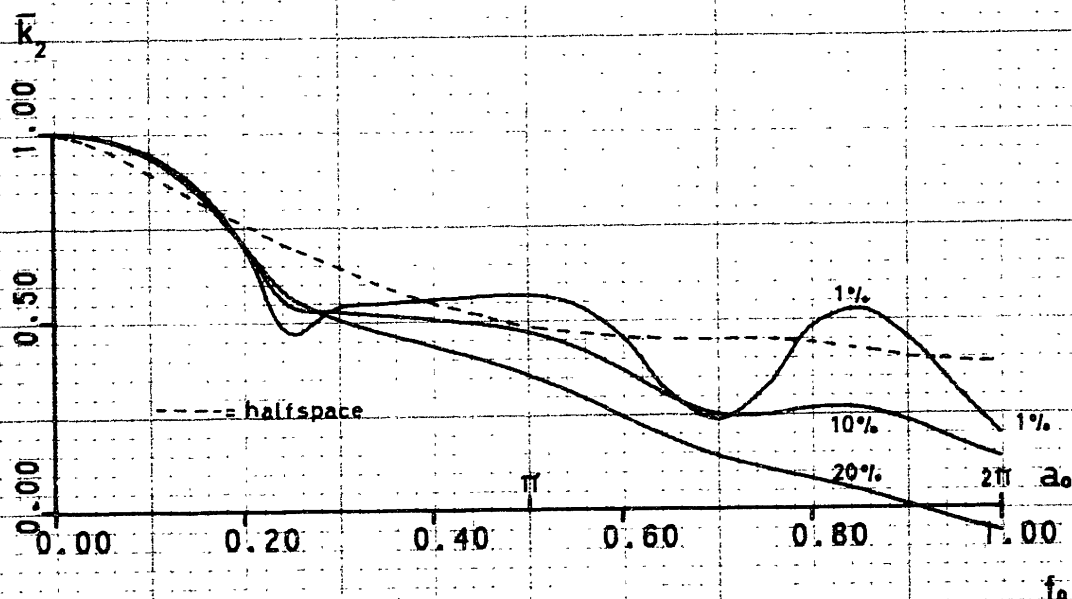
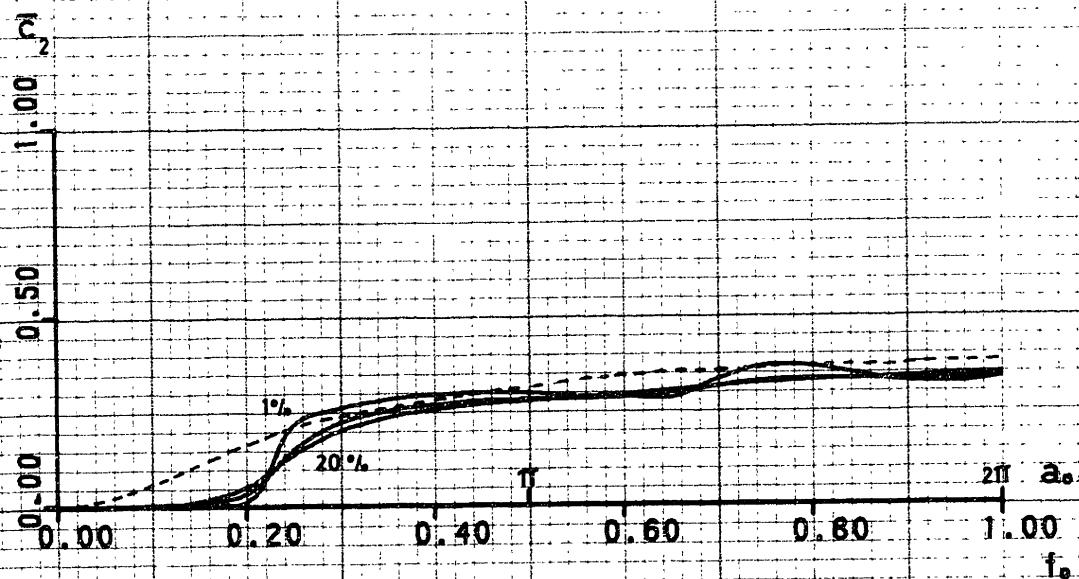
swaying,  $H/R = 2$ ,  $\nu = 1/3$ 

fig 35



## EFFECT OF INTERNAL DAMPING

ALTERNATE DEFINITION

rocking,  $H/R = 2$ ,  $\nu = 1/3$ 

For very high damping ratios, the frequency response for either the rocking or swaying function is flat and the stiffnesses are essentially constant ( 1st representation).

The fact that the obtained stiffness curves are so sensitive to the assumed internal damping ratio discredits to a large extent the possibility of deriving "damped" halfspace theory curves by merely multiplying the theoretical undamped stiffness functions by the factor  $1 + 2i\beta_k$ . Useful results could be obtained if only low damping ratios, say less than 5 percent, are considered, but then the radiation damping completely overshadows the internal damping, except in the low frequency range, and in particular, below the natural frequencies of vibration of the soil if a stratum is being considered.

#### 4.4.- Effect of Poisson's ratio:

The dependence of the static stiffnesses in a stratum upon Poisson's ratio was found in sec. 4.2.-a) to be the same as that of the halfspace for both rocking and swaying, eqs. (4-6), (4-7):

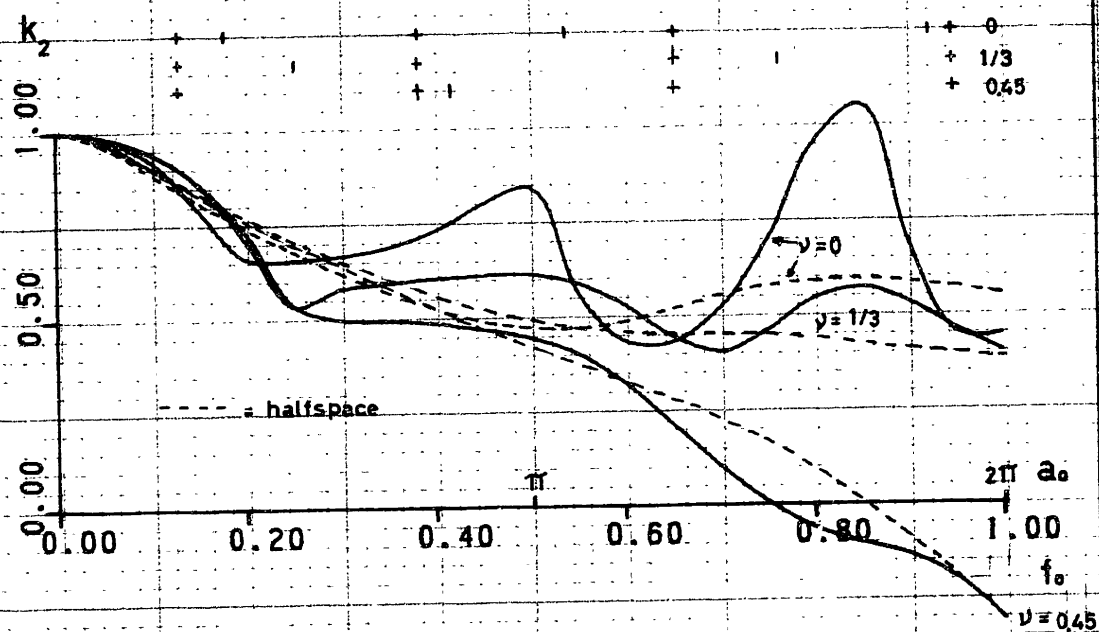
$$K_{so} = \frac{8GR}{2-\nu} \left( 1 + \frac{1}{2} \frac{R}{H} \right)$$

$$K_{yo} = \frac{8GR^3}{3(1-\nu)} \left( 1 + \frac{1}{6} \frac{R}{H} \right)$$

As in the case of the halfspace, the dynamic stiffness functions are very sensitive to changes in this parameter. This sensitivity is increased further in the case of a stratum by the dependence of the vertical natural frequency of the stratum (VNFS) upon Poisson's ratio, which in turn affects the location of the peaks and valleys in the stiffness curves. Furthermore, the influence is stronger for the rocking case than for the swaying case, since the former generates mainly pressure waves, while the latter produces mainly shear waves independent of Poisson's ratio.

Referring to Figs. 36 and 37, it can be seen that the general nature of the variation of the rocking stiffness coefficient for the depth ratio  $H/R=2$  is remarkably close to Veletson & Wei's (42) halfspace solution for the three ratios studied. For  $H/R=4$ , the agreement improves significantly. This fact confirms the accuracy of both the numerical method used, as well as that of the halfspace solution, based on relaxed boundary conditions.

fig 36



## EFFECT OF POISSON'S RATIO

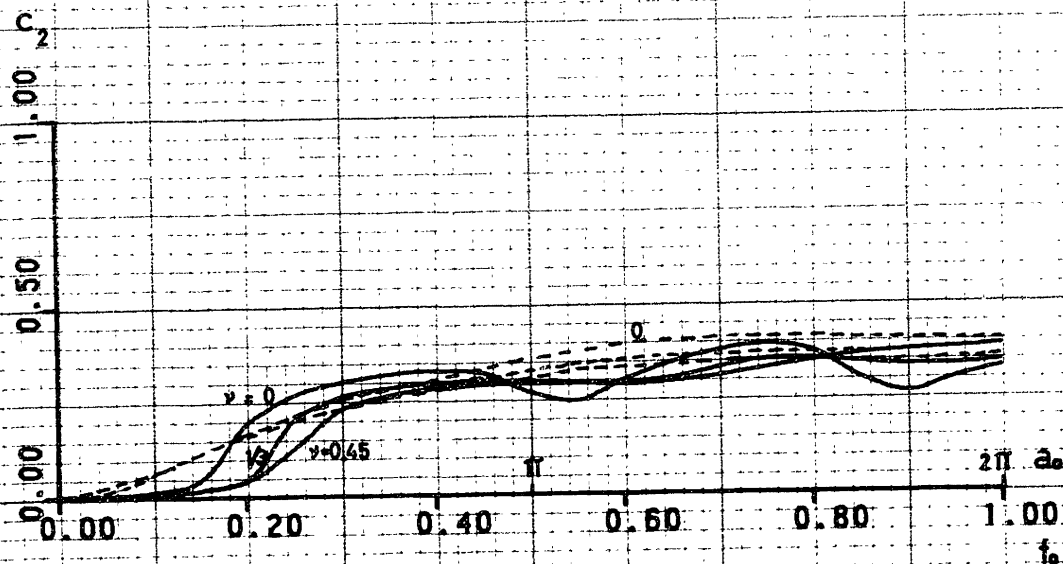
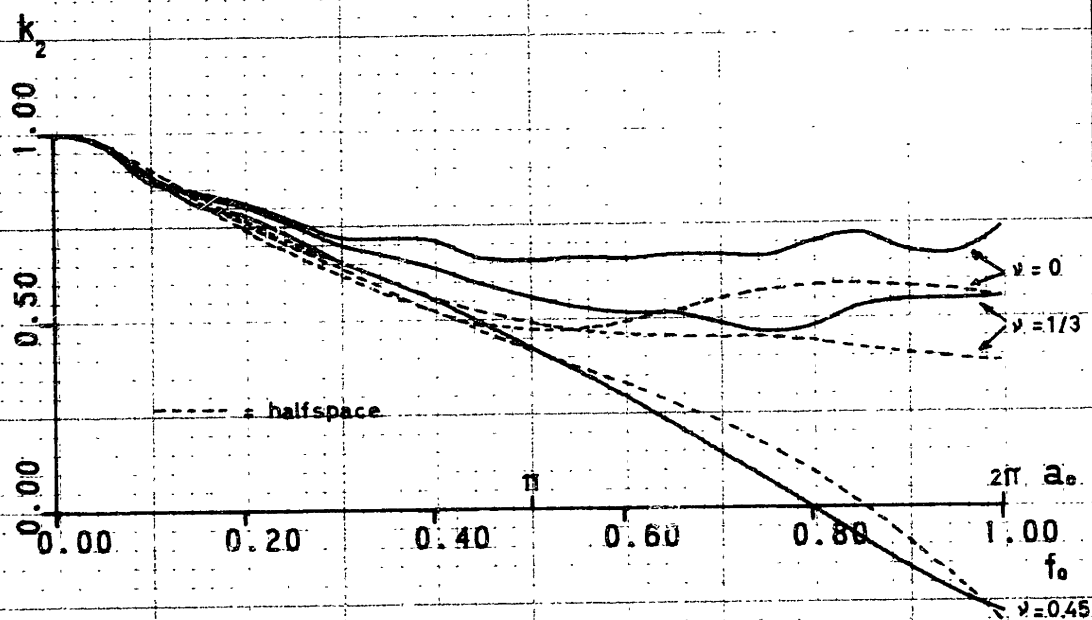
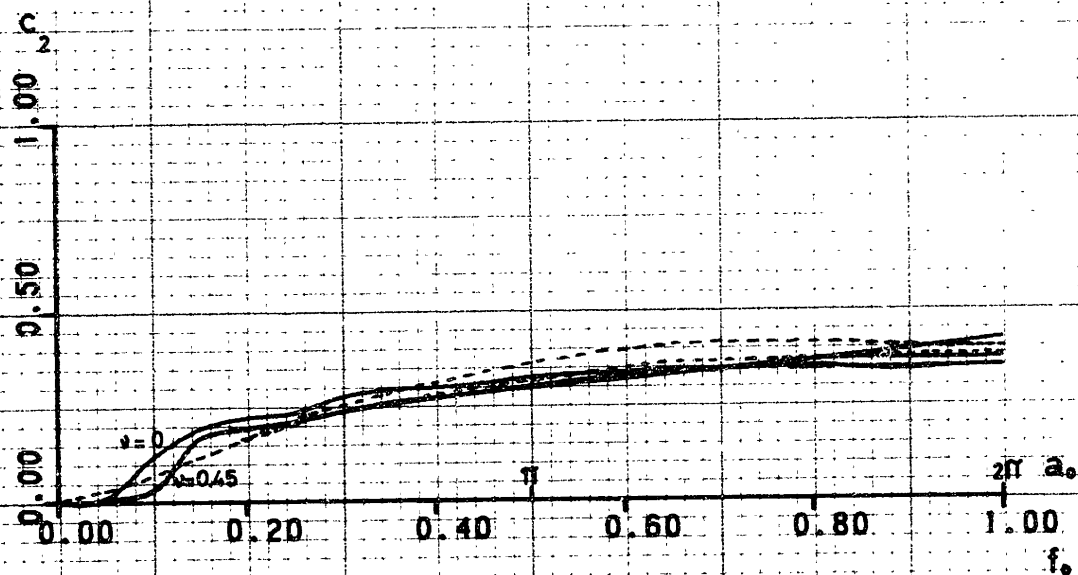
rocking,  $H/R = 2$ 

fig 37



## EFFECT OF POISSON'S RATIO

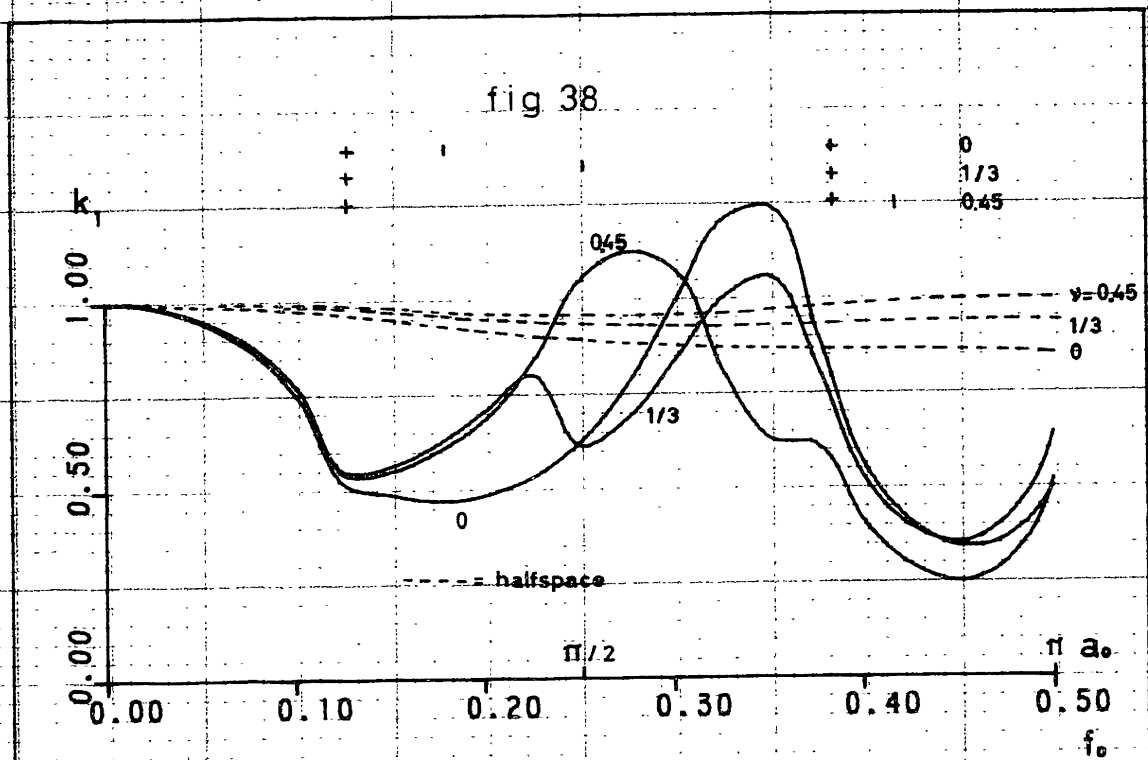
rocking,  $H/R = 4$ 

To understand better the behavior of the swaying curves, the (mesh consistent) natural frequencies of vibration have been indicated in Fig. 38 for the three Poisson's ratios studied. The discrepancies between these curves arise mainly at the VNFS. For  $\nu = 1/3$ , the 1st VNFS is located midway between the first and second HNFS.

The agreement between halfspace and stratum solution is not as close for swaying as it is for rocking. For deeper strata, and particularly with a slightly larger damping ratio, say 10 percent, it is expected that the swaying curves will approach the halfspace solution as was the case for the ratio  $\nu = 1/3$  studied in sec. 4.2. (Fig. 29)

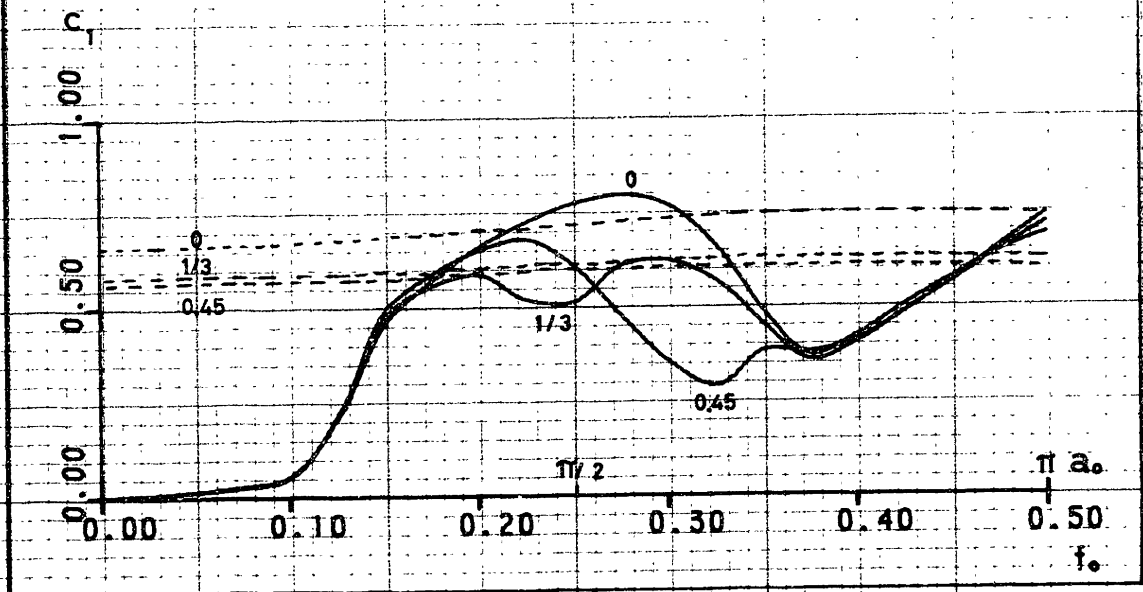
Usually, the swaying degree of freedom is unimportant in soil-structure-interaction problems, except for exceptionally heavy structures. For this reason, it is believed that the halfspace solution can be used with good results in many practical cases, provided that the static stiffnesses are modified adequately, say, according to the empiric equations (4-6) and (4-7).





# EFFECT OF POISSON'S RATIO

swaying,  $H/R = 2$



#### 4.5.- Effect of embedment:

Only in very few instances are structures founded directly on top of the soil. Usually, they are embedded to a certain degree, and it becomes necessary to investigate the effect of this embedment on the dynamic response of a structure having the rigid plate as foundation mat. The exact analytical solution for this problem is exceedingly difficult, if possible at all, due to the complicated boundary conditions.

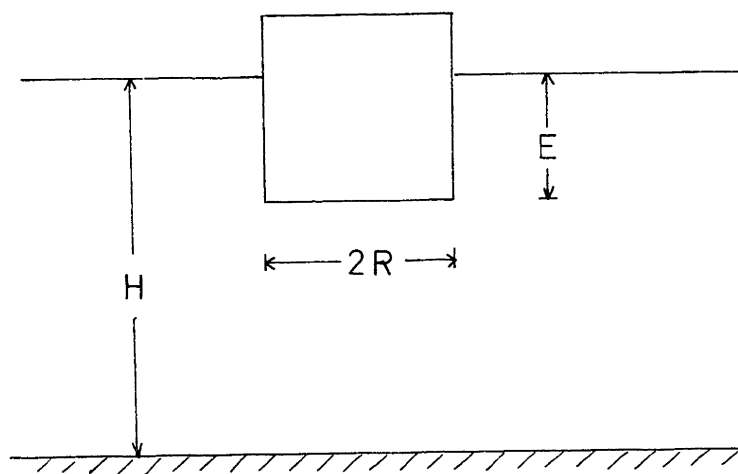
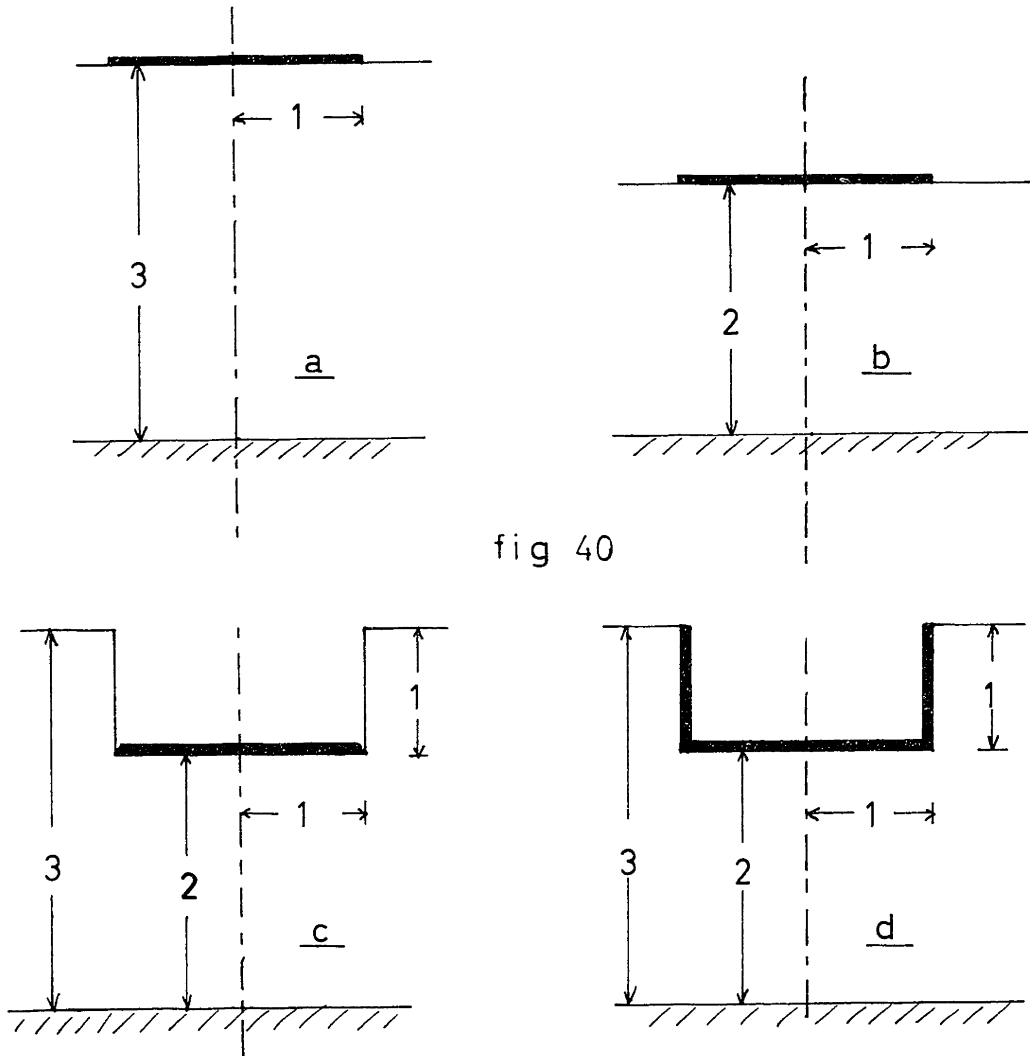


fig 39

It is generally believed that the embedment increases the stiffness of the foundation, and hence, that it increases the natural vibration frequencies of a mass (structure)

interacting with the foundation soil. This assumption is confirmed by experimental evidence; by approximate calculations (23), (24); and by numerical solutions (16), (44). However, most of the results published so far have dealt mainly with the response of an embedded mass (structure) rather than a massless plate subjected to a harmonic dynamic loading. This is unfortunate in the sense that most of the effects and details of the embedment are filtered out of the solution, except for the shift in the resonant peak due to the increased static stiffness, and therefore, a comparison with the halfspace/stratum solution is obscured. In addition, the results given usually are for soil-structure systems having a relatively low non-dimensional resonant frequency, in the range where it is permissible to neglect the frequency dependence of the stiffness functions. For this reason, it appears desirable to investigate the frequency dependence of the stiffness functions for some particular case, and assess the effect of embedment.

Consider the following cases of rigid plate foundation with  
 $\nu = 1/3$  ,  $\beta = 5\%$  :



The particular embedment ratio  $E/R = 1$  was chosen because it represents a case often encountered in the design of nuclear power-plants.

The subgrade stiffness matrix relates the external applied forces to the plate displacements. For the two degrees of freedom under consideration, this symmetric matrix is:

$$\mathbf{K} = \begin{Bmatrix} K_{xx} & K_{x\varphi} \\ K_{\varphi x} & K_{\varphi\varphi} \end{Bmatrix} = \begin{Bmatrix} K_{xx0} (k_{11} + i a_0 c_{11}) & K_{xx0} (k_{12} + i a_0 c_{12}) \\ K_{xx0} (k_{21} + i a_0 c_{21}) & K_{\varphi\varphi0} (k_{22} + i a_0 c_{22}) \end{Bmatrix}$$

It is always possible in the static case to define a point at a height  $h$  above the plate, which can be denoted by center of stiffness, for which the stiffness matrix has zero cross-coupling terms. The displacements of this point are

$$\bar{u} = u + h \varphi$$

$$\bar{\varphi} = \varphi$$

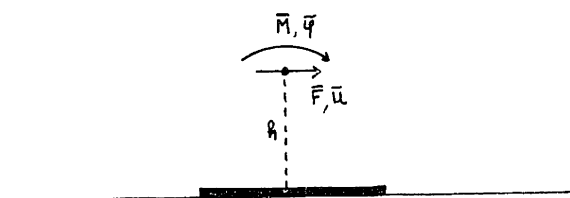
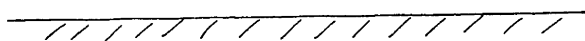


fig 41



Also, the forces are

$$\begin{aligned}\bar{F} &= F \\ \bar{M} &= M - Fh\end{aligned}\quad \text{and} \quad \begin{pmatrix} \bar{F} \\ \bar{M} \end{pmatrix} = \bar{\mathbf{K}} \begin{pmatrix} \bar{u} \\ \bar{\varphi} \end{pmatrix}$$

From here it follows that

$$\bar{\mathbf{K}} = \begin{pmatrix} K_{xx} & \\ & K_{\varphi\varphi} - \frac{K_{x\varphi}^2}{K_{xx}} \end{pmatrix} = \begin{pmatrix} K_{xx} & \\ & K_{\varphi} \end{pmatrix} \quad (4-18)$$

$$\text{also, } h = K_{\varphi x} / K_{xx} \quad (4-19)$$

For surface foundations, the height  $h$  is small, and  $K_{\varphi} = K_{\varphi\varphi} - K_{x\varphi} \cdot h \approx K_{\varphi\varphi}$ , that is, the cross coupling term is small and can usually be neglected.

For dynamic loadings, the ratio  $h = K_{\varphi x} / K_{xx}$  becomes complex, although its absolute value remains small, and the interpretation of the "height"  $h$  becomes more difficult. If, as has been done in the previous sections, the rotation (translation) of the plate is relaxed for the swaying (rocking) motion, then the following approximate stiffnesses are obtained:

$$K_s = K_{xx} - K_{xy}^2 / K_{yy} = K_{s0} (k_1 + i a_0 c_1) \quad (4-20a)$$

$$K_y = K_{yy} - K_{xy}^2 / K_{xx} = K_{y0} (k_2 + i a_0 c_2) \quad (4-20b)$$

which for the rocking term gives the same result as (4-18) above. For the four cases shown in Fig. 40, the static stiffnesses, uncorrected for mesh size, are:

	$\frac{K_{xx0}}{GR}$	$\frac{K_{xy0}}{GR^2}$	$\frac{K_{yy0}}{GR^3}$	$\frac{K_{x0}}{GR}$	$\frac{K_{y0}}{GR^3}$	$\frac{h}{E}$
a) H/R=3	5.96	-0.33	4.61	5.94	4.59	-0.056
b) H/R=2	6.45	-0.26	4.77	6.44	4.76	-0.070
c) No sidewall	9.27	-0.85	6.48	9.16	6.40	-0.092
d) with sidewall	13.84	4.51	16.65	12.61	15.18	0.326

Except for the last case, the height of the center of stiffness is small, and the differences in the stiffnesses  $K_{xx}$ ,  $K_s$  and  $K_{yy}$ ,  $K_y$  are negligible for all practical purposes. Even when sidewalls are presents, the modifications in the stiffnesses are relatively moderate. For this case, however, the effect of the coupling terms (measured by the height  $h$ ) can no longer be neglected, unless the height of the center of stiffness is small in comparison to the height of the center of gravity of the structure above the foundation mat.

From the table above, it becomes apparent that the embedment increases substantially the static stiffnesses, specially when rigid sidewalls are part of the foundation system. However, great care should be observed in extrapolating these results to practical foundation design, since they are based on three unrealistic assumptions, namely:

1. The sidewalls are completely rigid (although, this is not too bad an assumption for cylindrical walls)
2. The walls are perfectly welded to the soil, being therefore capable of transmitting both pressures and tensions. Because of the dead weight of the structure, the "tensile" stresses below the mat are usually the result of decreased compression stresses. Except for the active pressure of the soil, no such precompression exists for the backfill which can justify the assumption of perfect weldment of the sidewalls to the backfill.
3. The lateral soil (backfill) has the same strength and properties of the foundation soil below the mat (a very weak assumption, indeed).

As a result of these effects, the static stiffnesses of case d), and particularly the rocking stiffness, can be

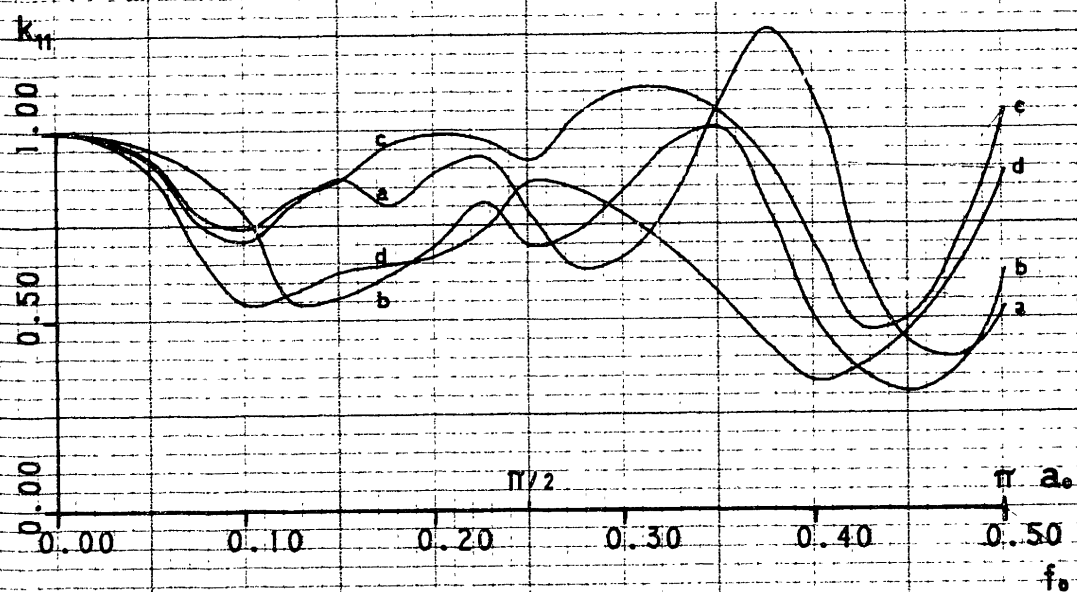


substantially decreased. In the limit, when no sidewall action is present as in case c, the rocking static stiffness is reduced from a value of 16.65 to 6.48, which is only slightly higher than the static stiffness for the case  $H/R=2$ . The swaying constant is not decreased in the same proportion (from 13.84 to 9.27, compared to 6.45 for  $H/R=2$ ).

Figs. 42 through 45 show the frequency dependence of the various stiffness and damping coefficients defined. A comparison of the functions  $k_{11}$  with  $k_1$ , and  $k_{22}$  with  $k_2$  shows that they differ only slightly, even for the case with sidewalls.

For the swaying motion, the curves for the four cases have a similar variation pattern; in the low frequency range, the stiffness curves for embedded foundation follow more closely the behavior of the surface foundation with  $H/R=3$  (total depth of the stratum) rather than that of  $H/R=2$  (that is, removing the lateral soil). A similar statement can be made of the damping coefficients, except that they yield substantially higher damping values for case d) with sidewalls. The fact that the damping increases relatively as well as absolutely, because of the higher static constant, indicates that for an embedded foundation the complex stiffness is very high; since the swaying mode plays

fig 42



## EFFECT OF EMBEDMENT

## swaying

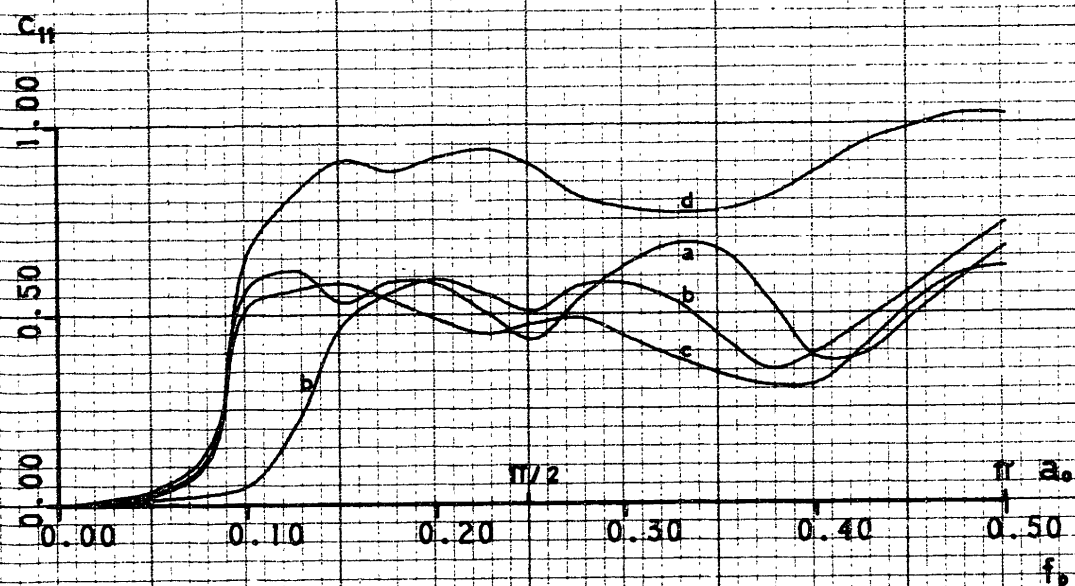
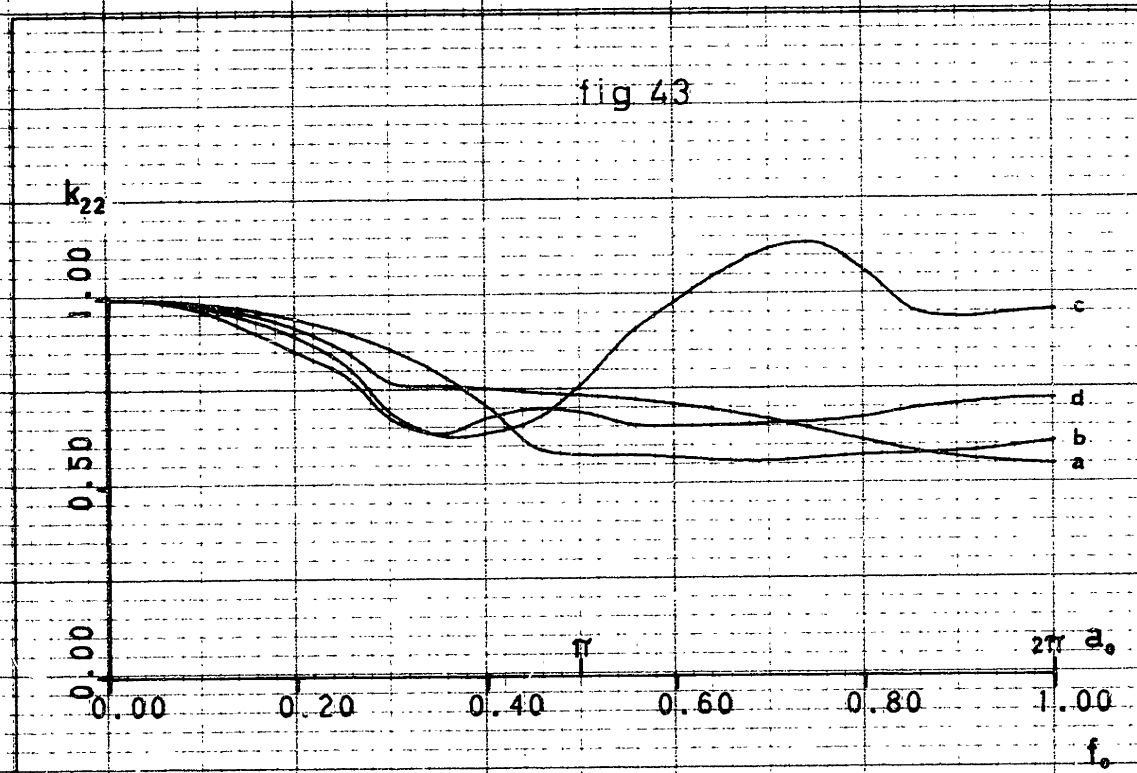


fig 43



## EFFECT OF EMBEDMENT

rocking

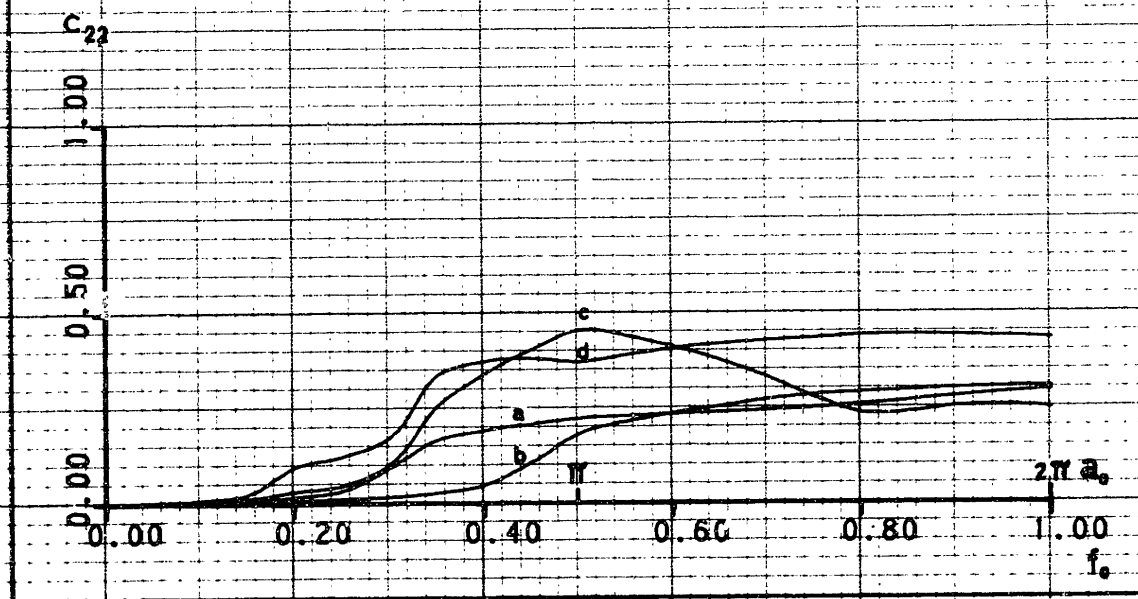
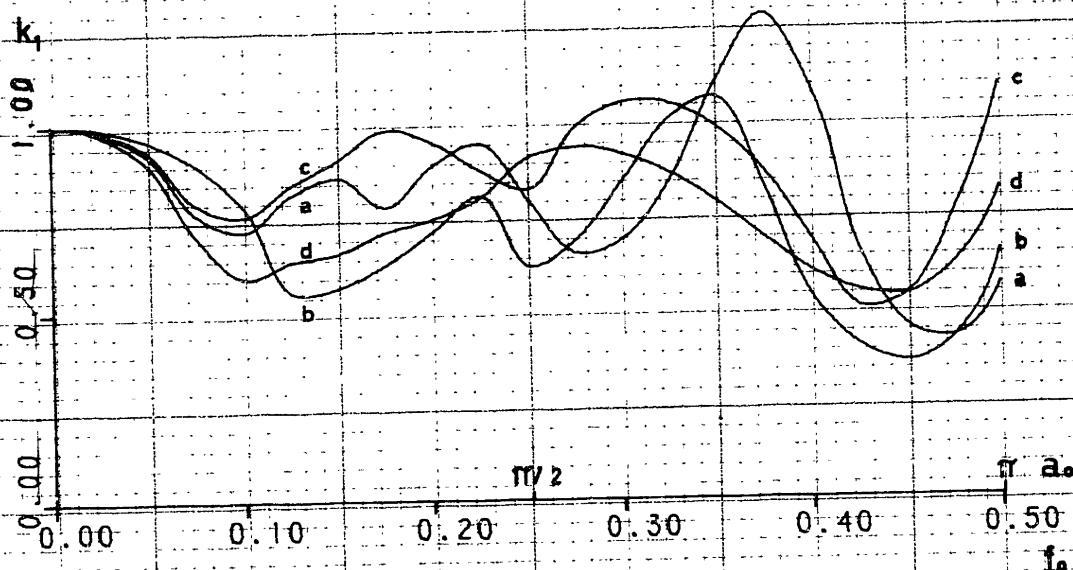


fig 44



## EFFECT OF EMBEDMENT

SWAYING, RELAXED STIFFNESS COEFFICIENTS

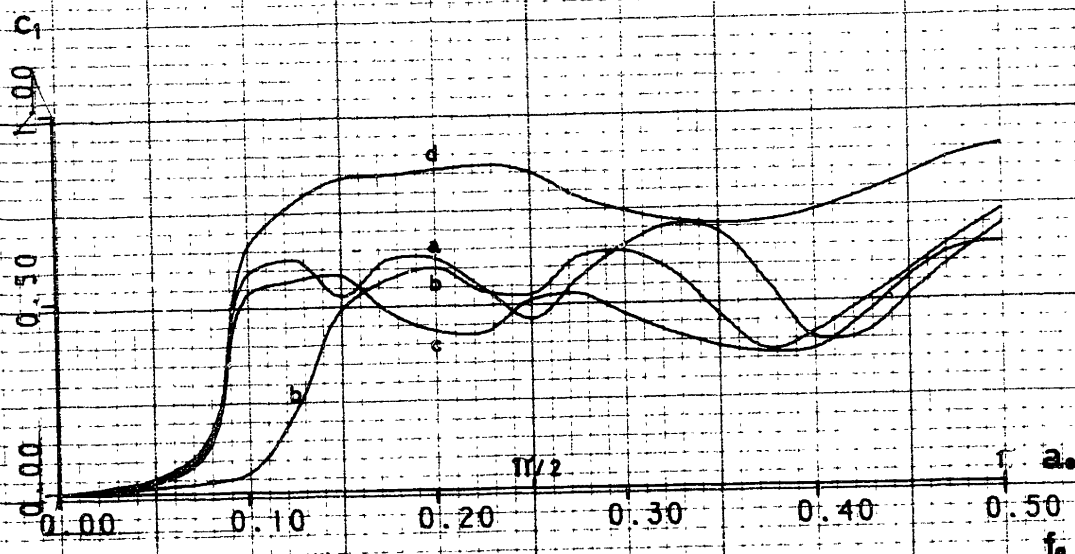
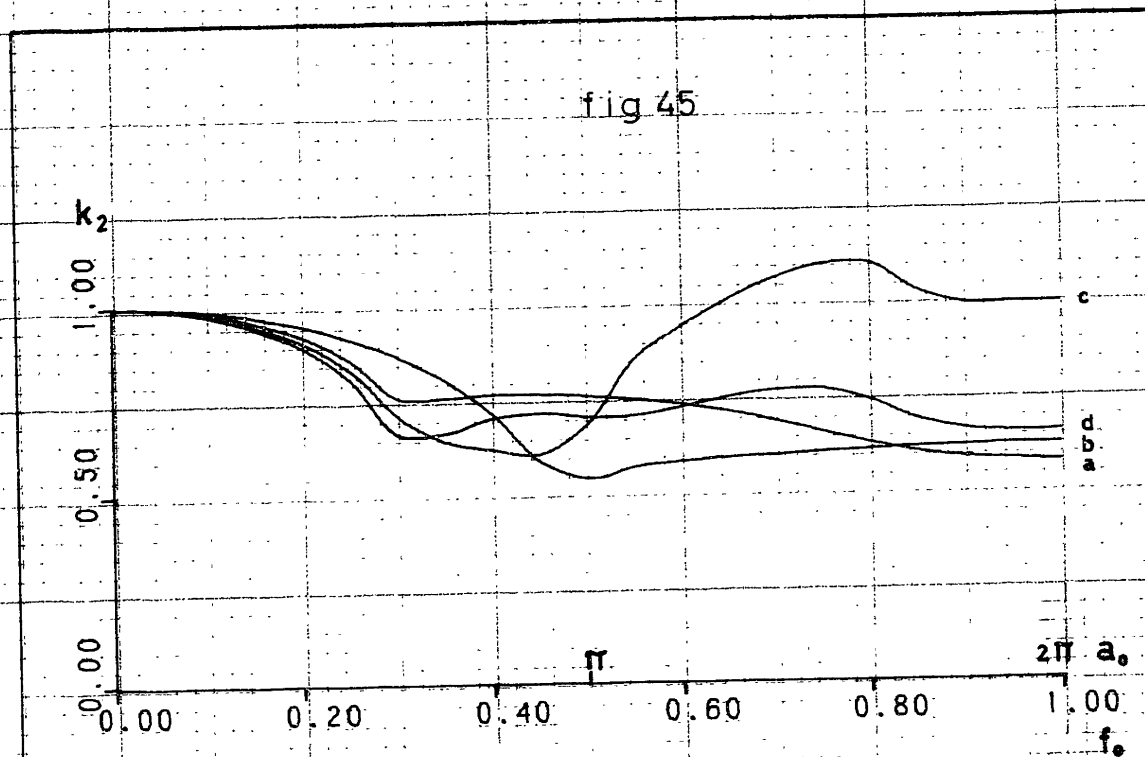
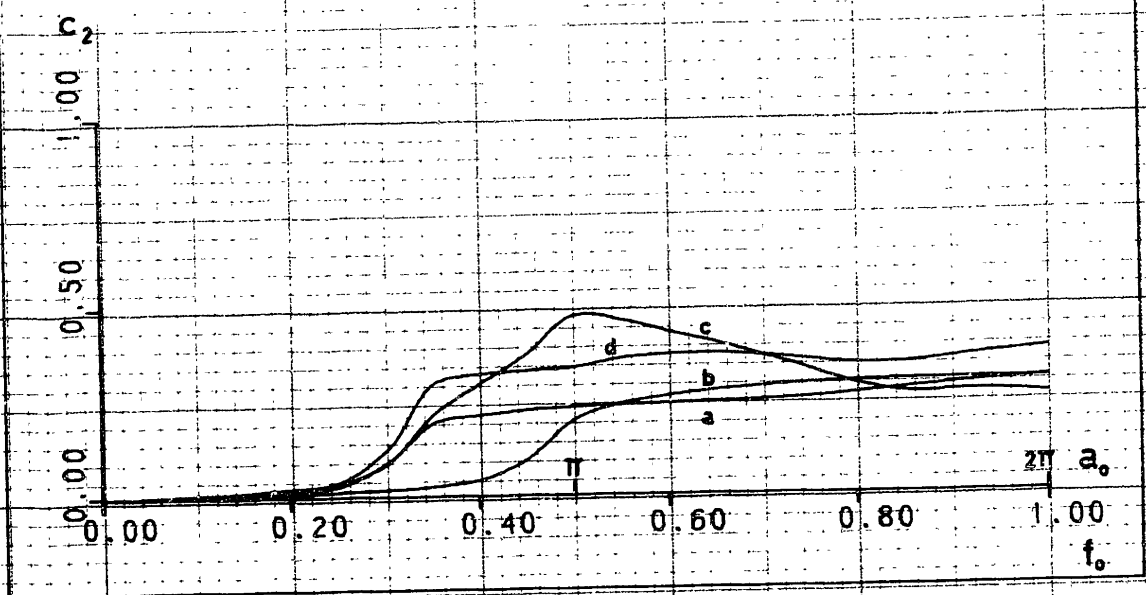


fig 45



## EFFECT OF EMBEDMENT

ROCKING, RELAXED STIFFNESS COEFFICIENTS



generally a minor role in soil-structure interaction problems (48) , it is expected that this influence will be reduced further for embedded foundations. This suggests that in most practical cases, the swaying degree of freedom can be suppressed, except for very heavy masses on soft soil.

The rocking stiffness and damping coefficients  $k_{22}$  ,  $k_2$  ,  $c_{22}$  ,  $c_2$  agree remarkably well for cases a) , b) and d) . These results were obtained for a shallow stratum, and it is therefore expected that the agreement should improve further for deeper strata. As in the swaying case, the embedment increases significantly the radiation damping. For the case with no sidewalls, the rocking stiffness coefficient increases substantially after the 2nd HNFS, but this gain is offset by a sharp decrease in the damping coefficient.

On the other hand, the rocking stiffness coefficients agree well with the halfspace solution. Also, for the particular embedment ratio studied, the height of the center of stiffness remained essentially constant at about  $h \approx 1/3 E$  , as can be observed in Fig. 46 below. Hence, for practical purposes, it appears that the halfspace solution could be used changing the static stiffness by some appropriate method, and making provision for the cross coupling terms by assuming a certain height  $h$  of the center of stiffness above

the rigid foundation. If an infinitely horizontal spring is assumed, this point has to be taken as center of rotation.

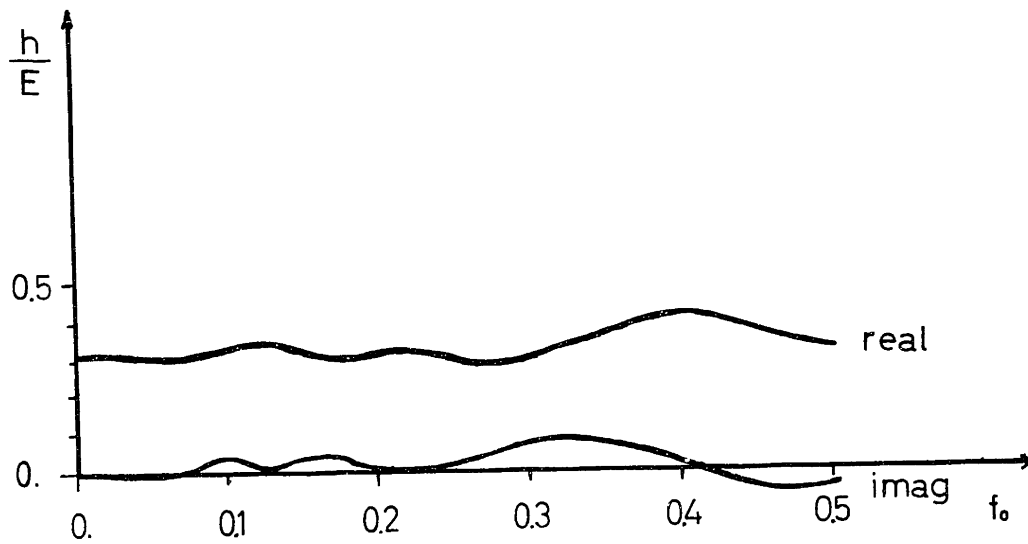


fig 46

## 5. - Soil-structure interaction:

Growing attention has been given recently to the problems of soil-structure interaction and soil amplification as connected with the design of nuclear power plants, tall buildings, or vibration sensitive equipment such as radar structures. At the same time, disagreement and controversy have increased correspondingly among the experts as to how these effects should be included and considered in analysis and design.

Currently, there appear to be three basic methods to deal with the problem of soil-structure interaction, and they are based on:

- a) Constant, lumped soil springs and dashpots as given by a static halfspace analysis, with weighted modal damping coefficients (33). The analysis is done in the time domain.
- b) Frequency dependent stiffness (compliance) functions as given by the halfspace theory for surface foundations (19), (42) or approximate theories for embedded foundations (23). The analysis must be done in the frequency domain.



c) Numerical methods, as the one developed in this dissertation.

The first method seems attractive to the engineer for its simplicity; it has received wide application, particularly in preliminary design and approximate calculations. On the other hand, the numerical methods such as the finite element method described in this dissertation are ideally suited for the analysis of complex problems in which the geometry and material properties are a function of space and time. Nevertheless, this advantage is gained at the expense of considerable increases in the cost of computation, which in many cases will inhibit the analyst to cover a wide range of design parameters to ensure adequate protection against the uncertainties inherent to the nature of soils.

Since the execution time for a given finite element problem increases rapidly with the number of degrees of freedom, it becomes attractive to compare the results of a full 3-dimensional analysis obtained with the method presented herein with the more economic "equivalent" 2-dimensional plane strain model as described by Waas (44). The sense of the implied equivalence between the two models has to be carefully defined, as there is, strictly speaking, no such thing as an equivalent plane model. In the following

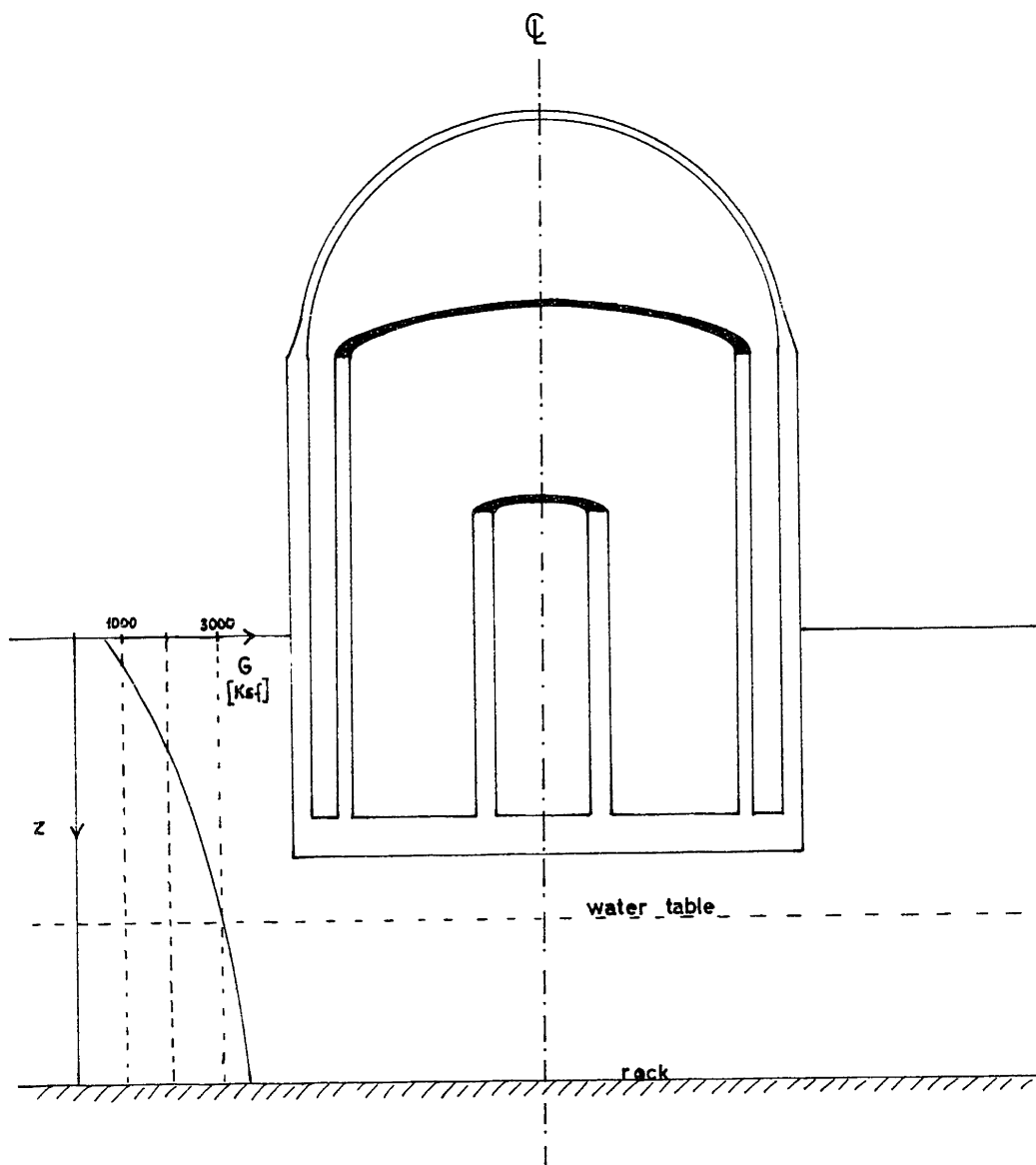
section, the results obtained by the two methods shall be analyzed and discussed for a particular problem. The plane strain program PLAXLY written by G. Waas (44) was used for the 2-D problem.

Both the two and the three dimensional models are based on a finite element region and a layered region resting on rigid rock, that is, they are based on the results for an elastic stratum. For earthquake loadings, this introduces the controversial question as to where the control motion should be specified. The simple assumption of 1-dimensional amplification offers the disadvantage of unrealistically high resonant peaks at the natural frequencies of the stratum when the motion is specified at the basal rock, or dubious deamplification to the foundation level when it is specified at the free surface. It was shown in Sec. 3.8 that it is possible to use in the analysis 2-dimensional wave propagation, but this not only increases the difficulties of the model, but it also raises further questions regarding the wave types and pattern, incidence angles, etc. In the present discussion, that controversy shall be avoided, arbitrarily specifying the motion at the free surface. It should not be implied from here that the author advocates this alternative as a sound basis for design. The aim is merely to compare two approaches to the problem, and in

particular, to justify or discredit the claim of exactness attributed to the equivalent plane model. The comparison shall be made for a typical containment structure of a nuclear power plant with the geometry shown in Fig. 47 and soil properties indicated in Table 2.

TABLE 2

layer	layer thickness	specific weight	shear modulus	Poisson's ratio	shear wave velocity	depth below grade
	ft	Kcf	Ksf		ft/sec	ft
1	5	.12	682	0.3	428	2.50
2	5	.12	978	0.3	512	7.50
3	5	.12	1298	0.3	590	12.50
4	5	.12	1550	0.3	645	17.50
5	5	.12	1781	0.3	691	22.50
6	7.5	.12	2033	0.3	738	28.75
7	7.5	.12	2254	0.3	777	36.25
8	7.5	.12	2435	0.3	808	43.75
9	7.5	.12	2682	0.3	848	51.25
10	7.5	.12	2888	0.3	877	58.75
11	7.5	.12	2979	0.3	894	66.25
12	10.	.15	3132	0.48	880	75.00
13	10.	.15	3299	0.48	903	85.00
14	12.5	.15	3467	0.48	926	96.25
15	12.5	.15	3522	0.48	934	108.75



STRUCTURAL IDEALIZATION

fig 47

8% linear hysteretic damping was used throughout the soil stratum.

For the structure, the following properties were assumed:

$$G = 200\ 000\ \text{Ksf}$$

$$\nu = 0.15$$

$$\zeta = 0.15\ \text{Kcf}$$

The structure being fairly rigid, the response at the foundation level is quite insensitive to slight inaccuracies in the parameters  $G$  and  $\nu$  above. The total mass of the structure is about 3500 Kslug.

The soil and the structure were discretized in layers and finite elements (using linear expansion order), and the mesh is shown in Fig. 48. The execution time for the 3-D model was about 20 sec per frequency in an IBM 370-155 computer.

In the 2-D model, the structure was represented by 2 coaxial columns of lumped masses and springs attached to a massless rigid foundation with flexible (massless) retaining walls (Fig. 49). Masses and stiffnesses were normalized w/r to an equivalent width  $b$  obtained equating the areas of a rectangular foundation to that of the circular foundation:

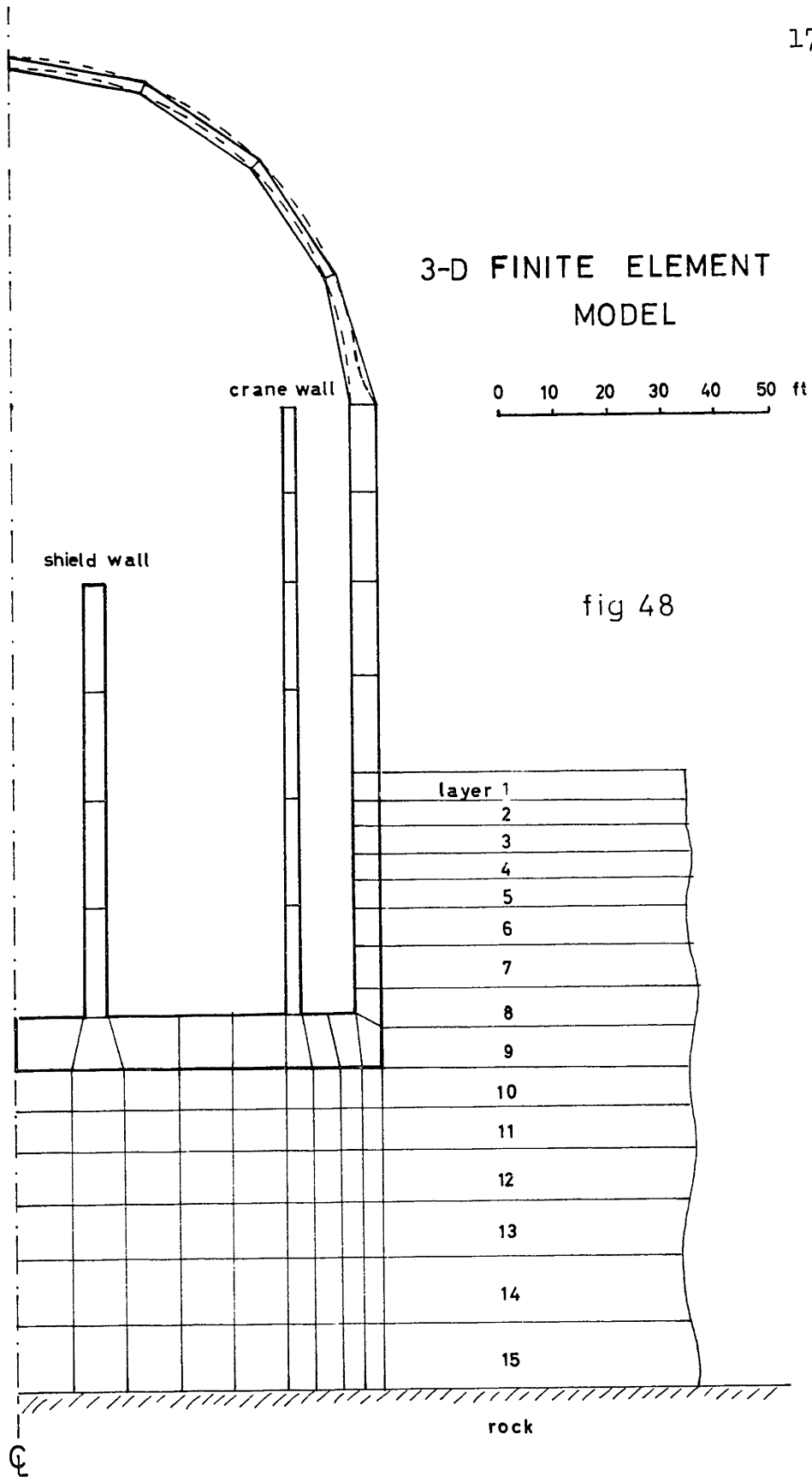
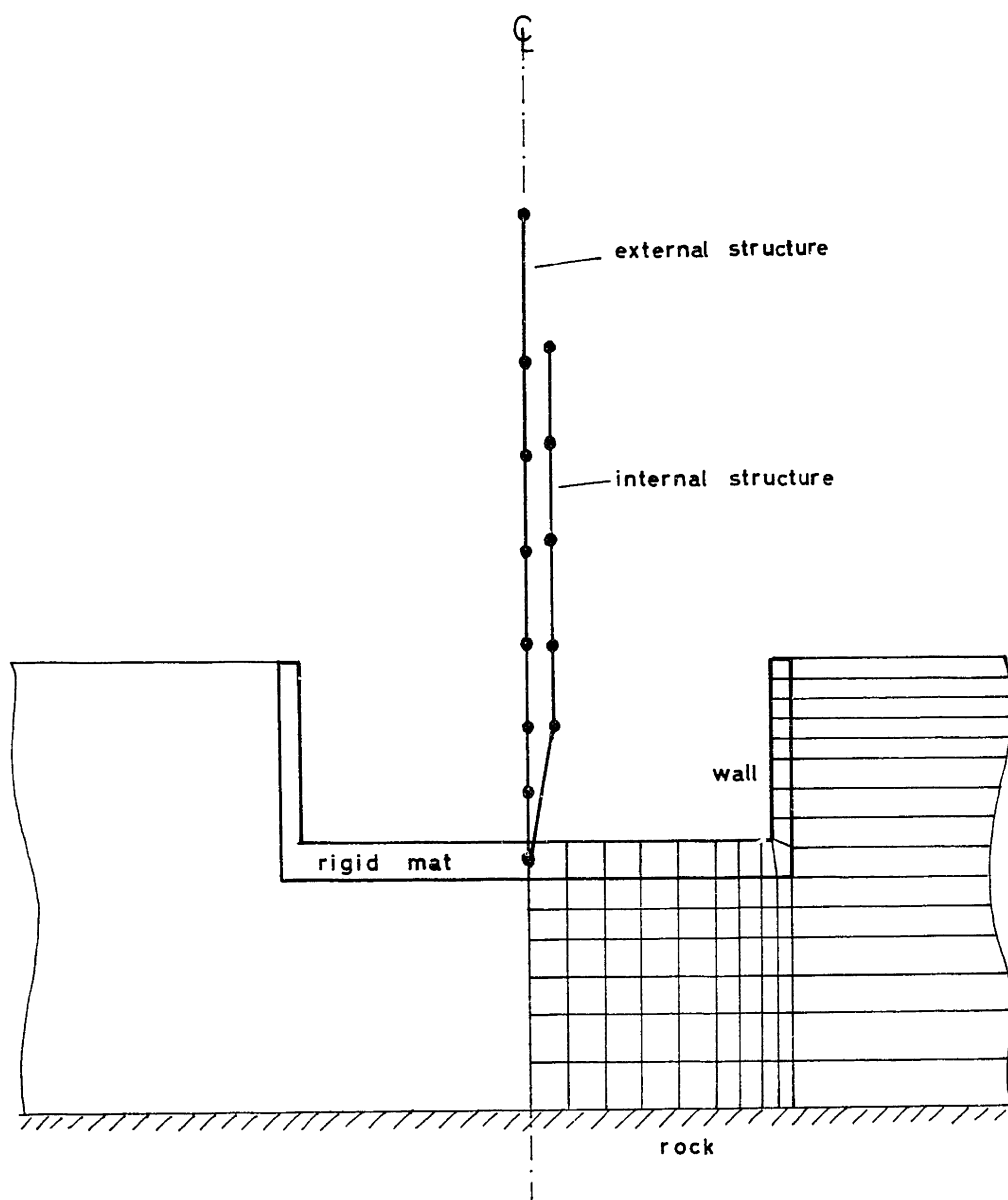


fig 48



2-D MODEL

fig 49

$$2 R b = \pi R^2 \quad b = \pi R/2$$

Also, use is made of symmetry, working with the right half of the model, and dividing the masses and stiffnesses in the structural columns by 2.

The retaining walls in the 2-D model correspond to the embedded portion of the cylindric containment wall. They are included to properly reproduce the embedment effect. The actual containment wall, however, deforms mainly due to shear, while the corresponding 2-D retaining walls will deform mainly due to bending. This requires the selection of a fictitious stiffness for these walls in order to achieve a performance comparable to that of the real 3-D case. For this purpose, the shear modulus of the wall was adjusted to give under bending the same displacement at grade as the cylindric wall under shear for a uniform lateral load.

In order to estimate the natural rocking-swaying frequencies of the system, the static subgrade stiffnesses were determined. For the 3-D model, they are:



$$\left. \begin{aligned}
 K_s &= 2.8 \cdot 10^6 \text{ Kip/ft} \\
 K_{sy} &= 35 \cdot 10^6 \text{ Kip/rad} \\
 K_y &= 11 \cdot 10^9 \text{ Kip-ft/rad}
 \end{aligned} \right\} \begin{aligned}
 \bar{K}_s &= K_s - \frac{K_{sy}^2}{K_y} = 2.69 \cdot 10^6 \text{ Kip/ft} \\
 \bar{K}_y &= K_y - \frac{K_{sy}^2}{K_s} = 10.6 \cdot 10^9 \text{ Kip-ft/rad}
 \end{aligned}$$

Notice that for an embedment ratio  $E/R=0.83$ , the height of the center of stiffness is  $h=35 \cdot 10^6 / 2.8 \cdot 10^6 = 12.5$  ft, and  $h/E=12.5/55 = 0.23$ . This ratio is significantly smaller than that for the homogeneous case studied in Sec. 4.5; this confirms that the weak backfill soil decreases the embedment effect substantially.

Use of  $M=3500$  Kslug,  $R=67.5$  ft,  $H=170$  ft ( $H$ =total height of the structure), and the approximate value for the moment of inertia

$$I = M \left( \frac{R^2}{4} + \frac{H^2}{3} \right)$$

gives for the uncoupled frequencies:

$$\begin{array}{ll}
 f_r = 3.3 \text{ cps} & \text{rocking} \\
 f_s = 4.5 \text{ cps} & \text{swaying}
 \end{array}$$

and for the coupled rocking-swaying frequencies, after solving the 2nd order linear eigenvalue problem,

$$f_I = 2.6 \text{ cps}$$

$$f_{II} = 8 \text{ cps}$$

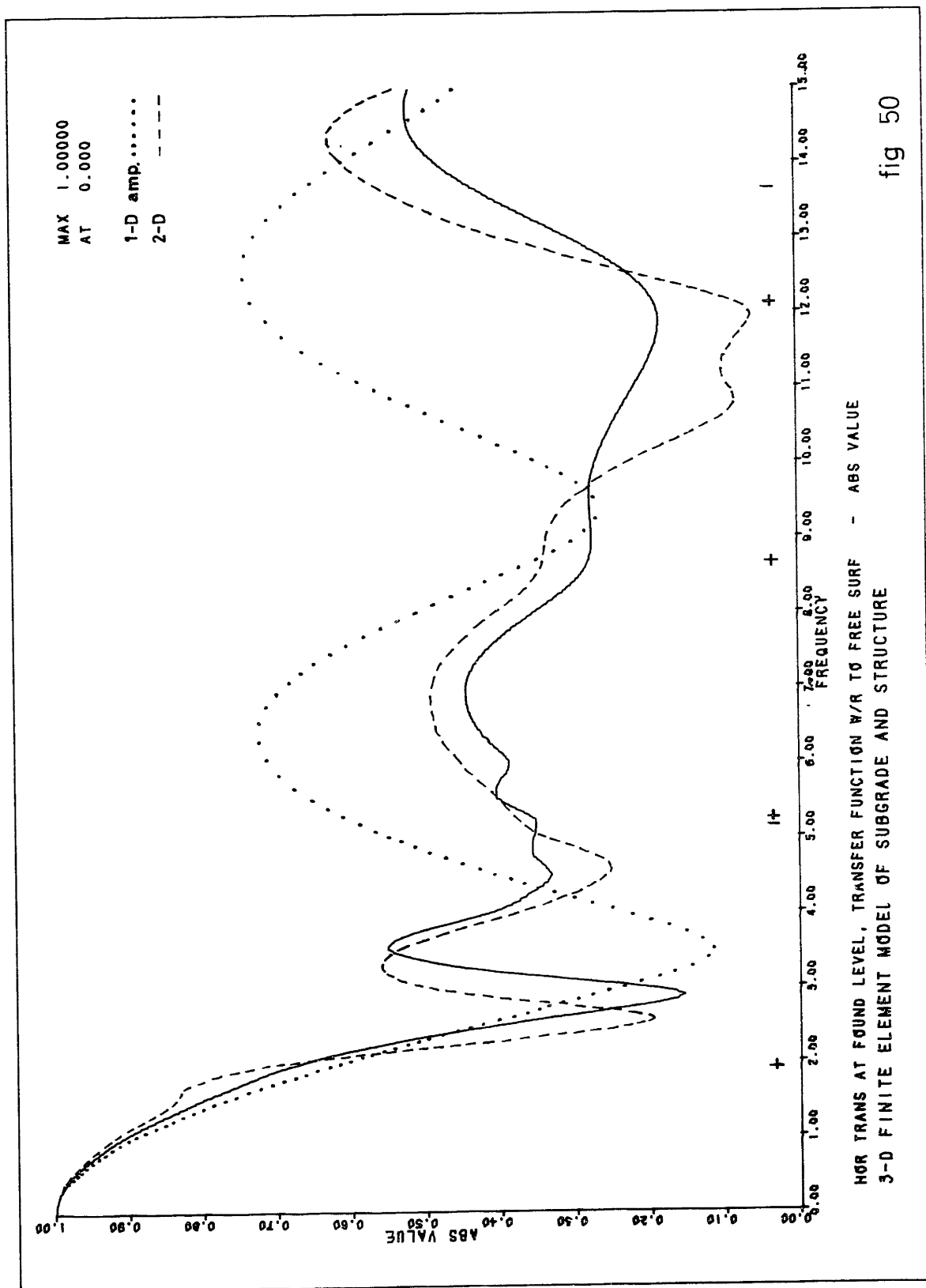
These values are approximate, because of the frequency dependence of the stiffness functions, the flexibility of the foundation, and the approximate expressions and values used.

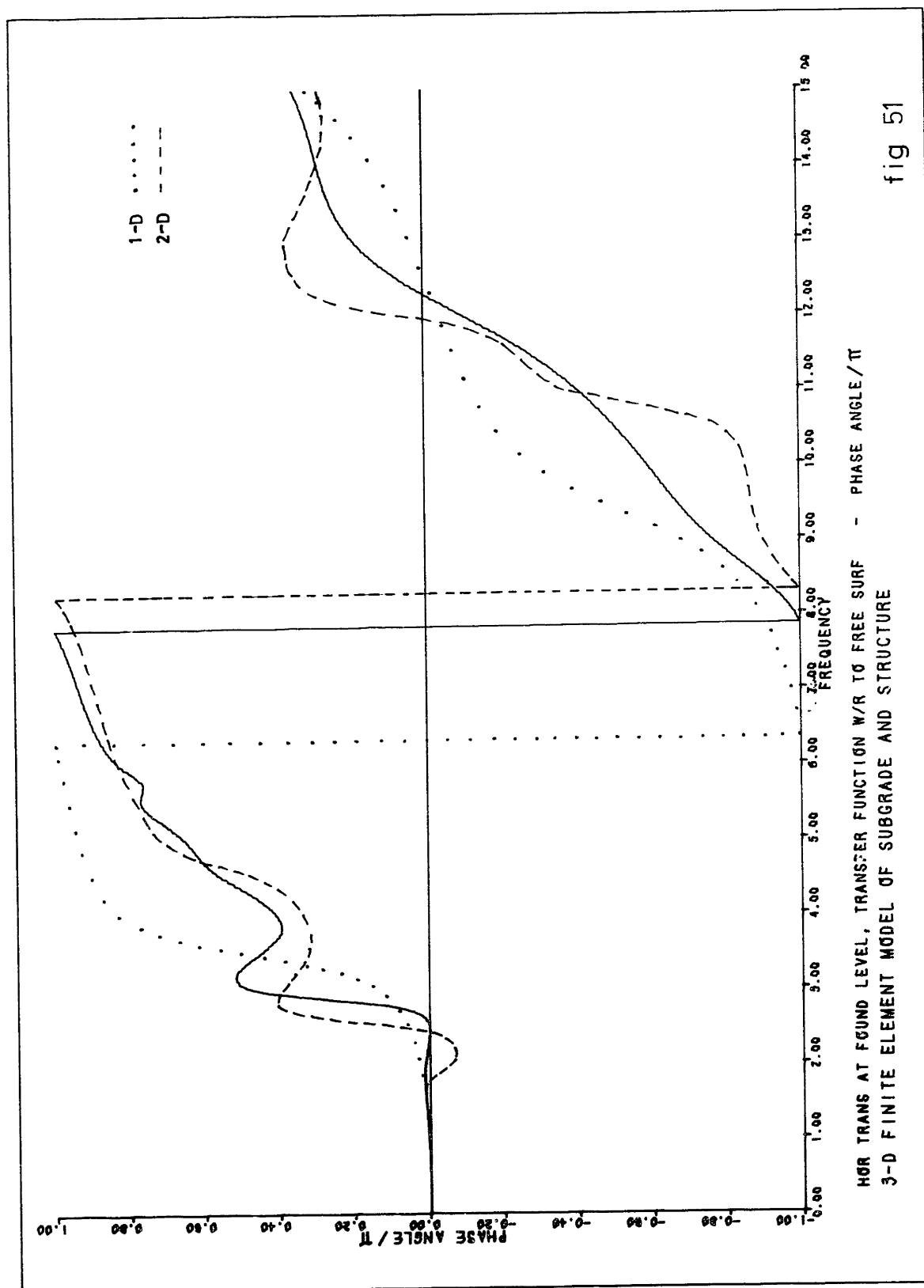
For both the plane and the 3-D problems, the response at the foundation level was determined for a unit prescribed acceleration at the free surface. The translation (acceleration) at the base of the structure was taken as that of the point at the axis; since the foundation mat acts as a rigid diaphragm, the displacements (accelerations) at the other points at the mat-soil interface are essentially identical. The plate rotation was taken in a first approximation to be equal to the vertical displacement at the edge of the mat divided by the foundation radius; for the 3-D case in which the actual rigidity of the mat was used, this will provide a reasonable estimate of the foundation rotation only in the lower frequency range. For higher frequencies, an important bending distortion of the mat takes place, as will be shown.

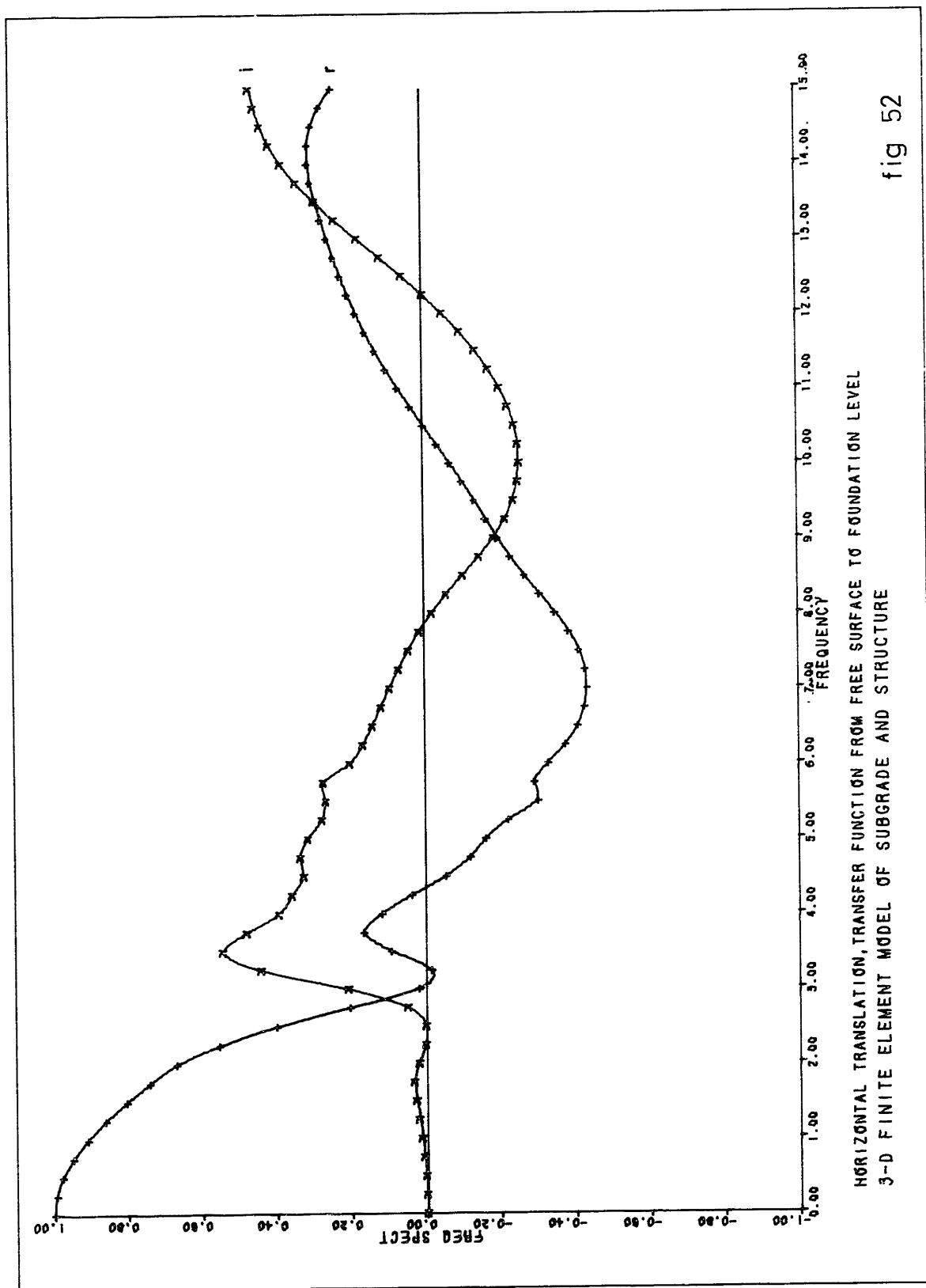
Figs. 50 through 55 show the transfer functions for the two effects studied. Figs. 56 through 61 depict the same effects, but computed with a massless structure. For the translational modes, the unidimensional amplification (deamplification w/r to the surface) is also shown. The natural frequencies of the stratum are indicated by (+) and (i) for the horizontal and vertical modes.

The agreement between the two models is good for both translation and rotation, and probably good enough for practical purposes, if economies in computation costs are a decisive factor. However, the fact that the translational response is not very different for the cases with and without structural mass shows that the soil-structure interaction effect, at least in what the horizontal displacement is concerned, is not large. For cases with more interaction effect, the discrepancies between the two models could become large.

For the massless foundation, the absolute value of the transfer function for the horizontal displacement decays rapidly with frequency up to the first natural horizontal frequency of the stratum ( $f=1.97$ ), and then oscillates about the deamplified value, influenced by the higher resonant frequencies of the stratum and the embedment effect. The

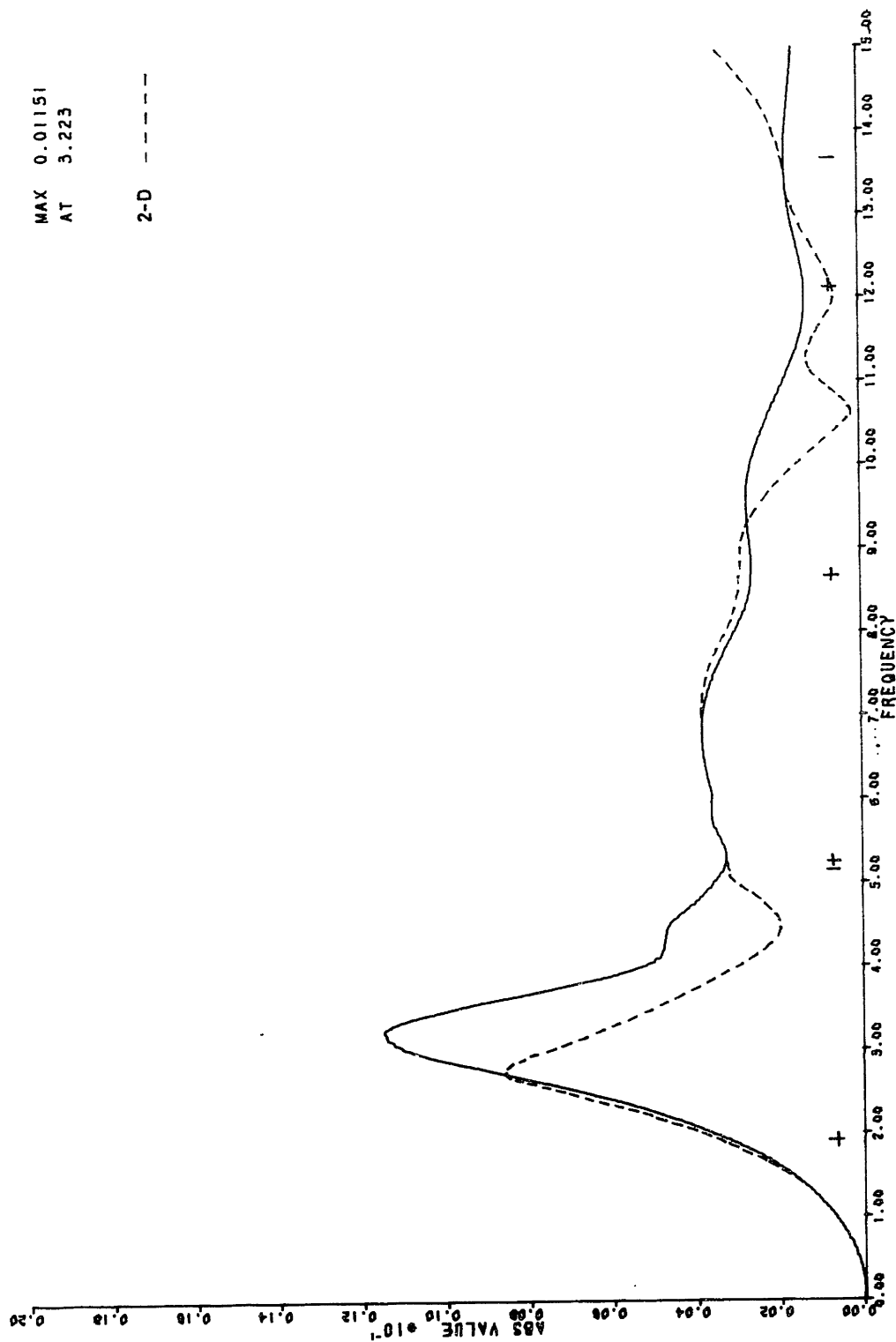






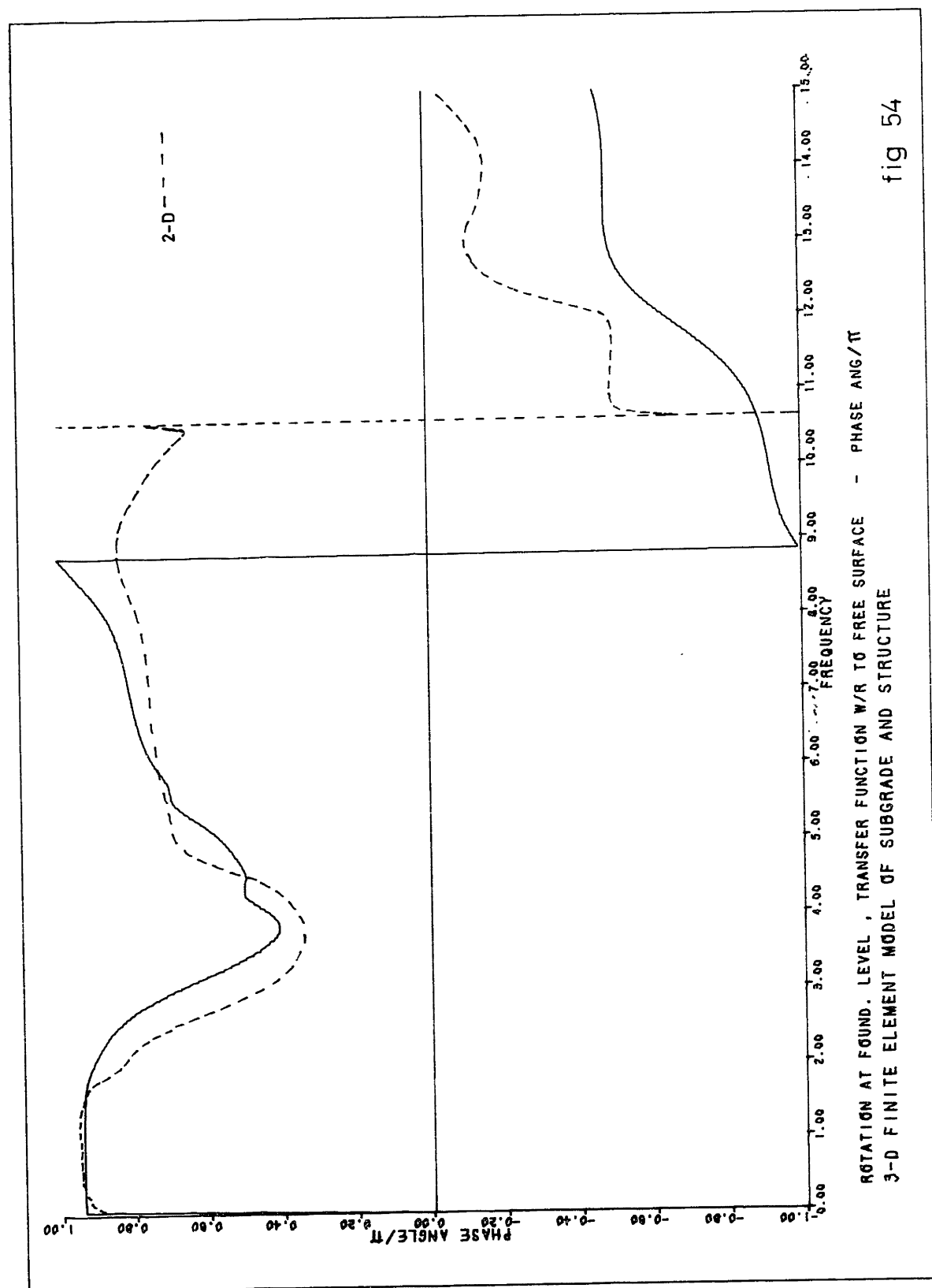
MAX 0.01151  
AT 3.223

2-D - - - -

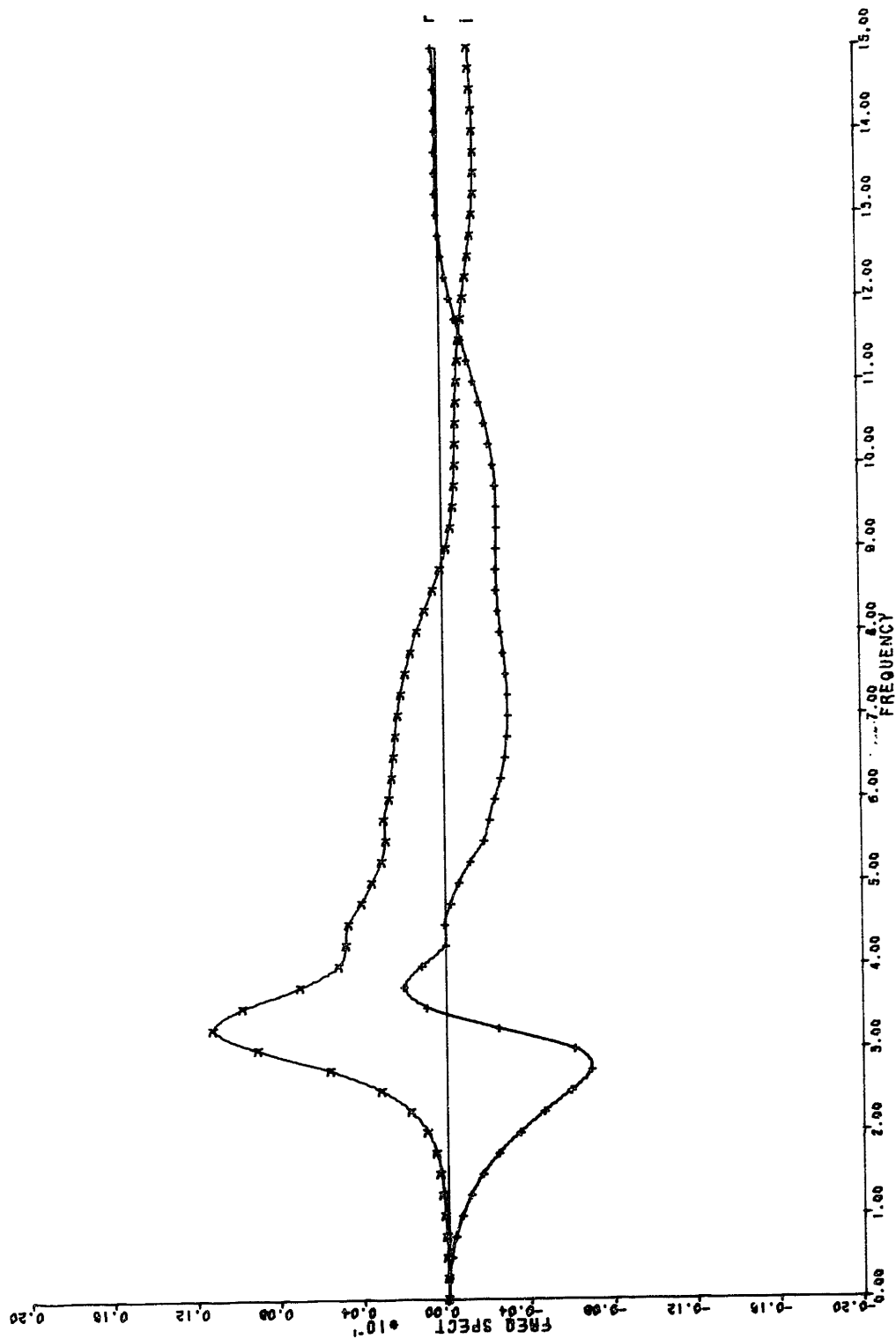


ROTATION AT FOUND. LEVEL, TRANSFER FUNCTION W/R TO FREE SURFACE - ABS VALUE  
3-D FINITE ELEMENT MODEL OF SUBGRADE AND STRUCTURE

fig 53

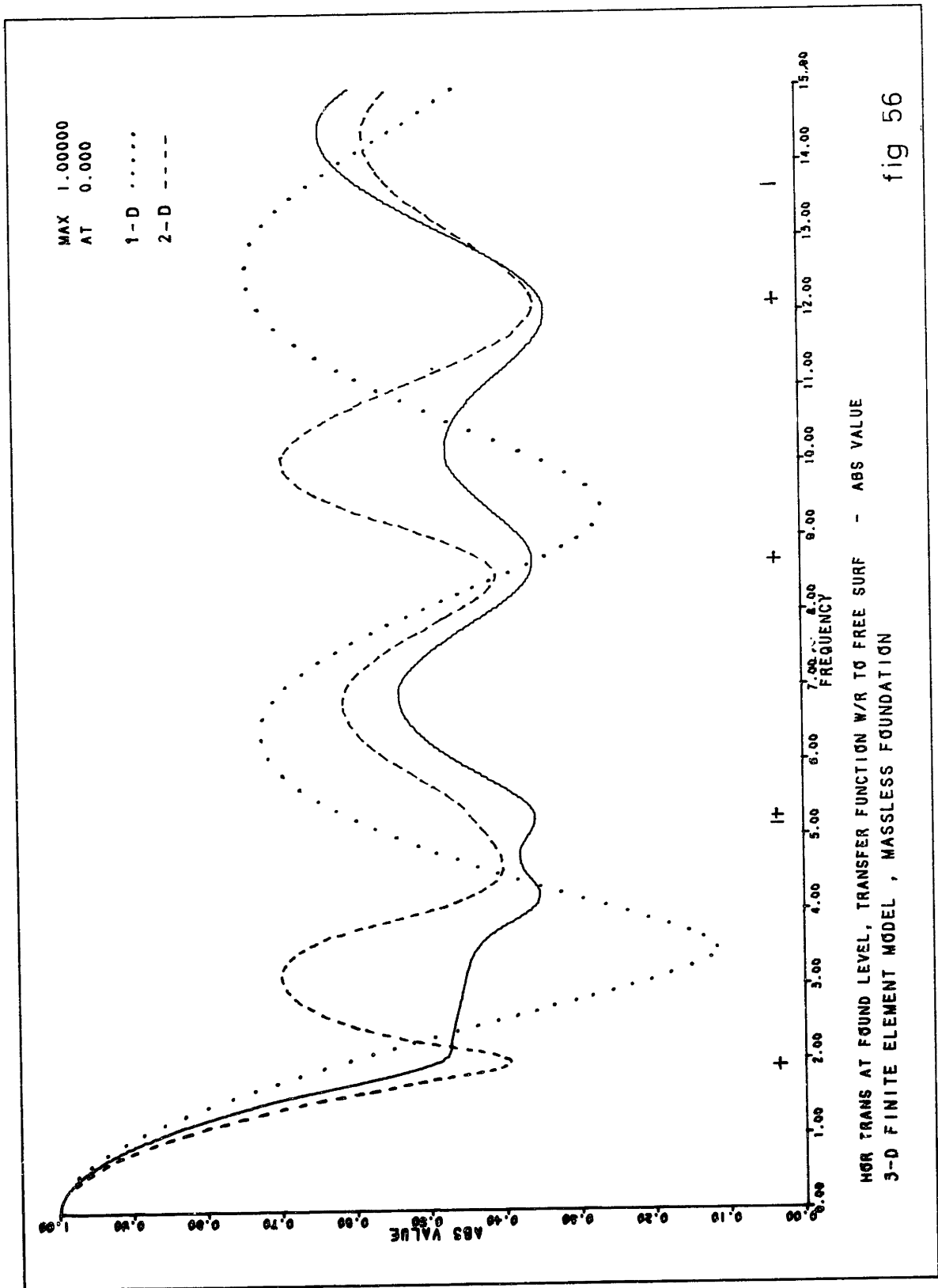


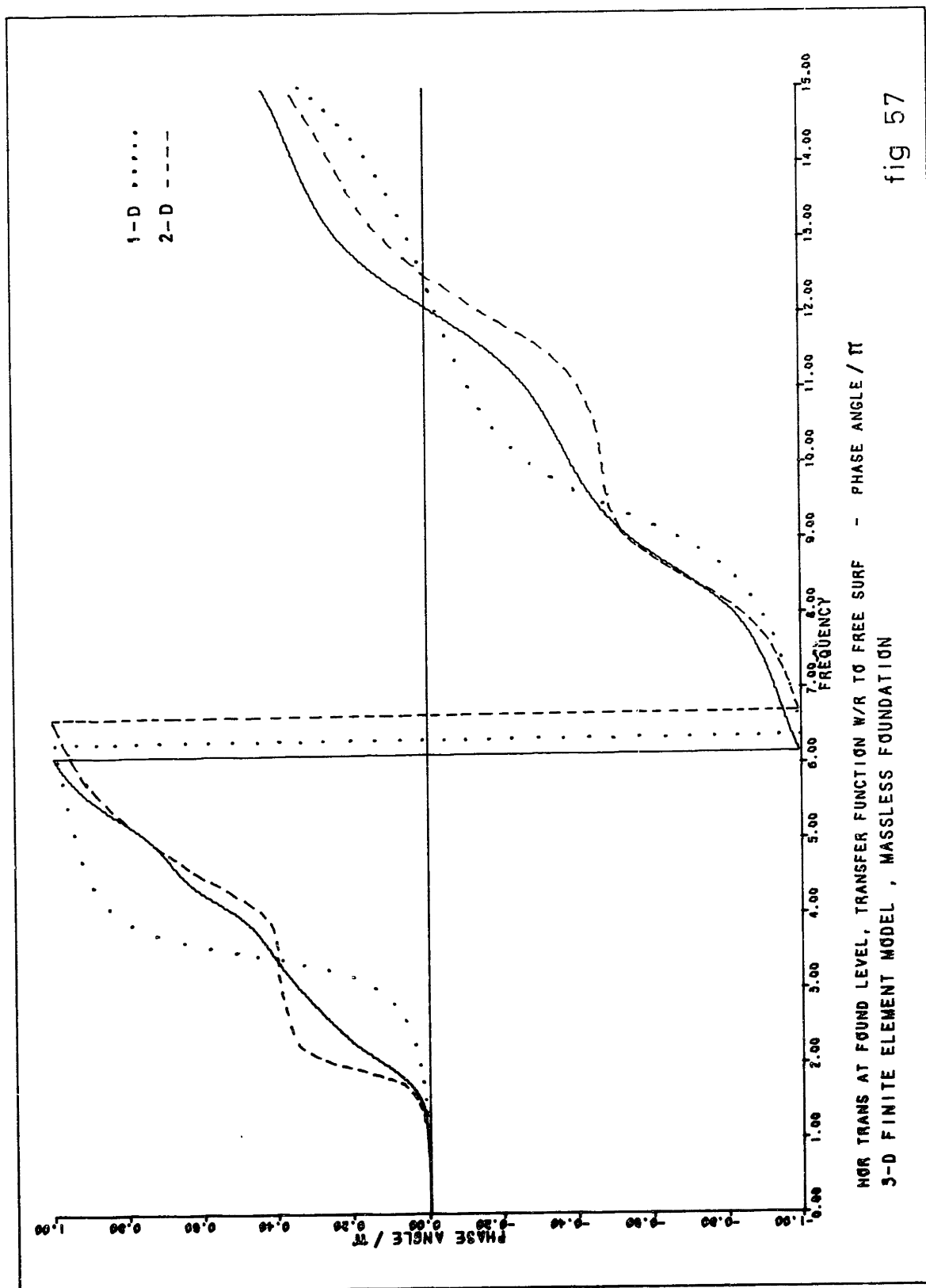


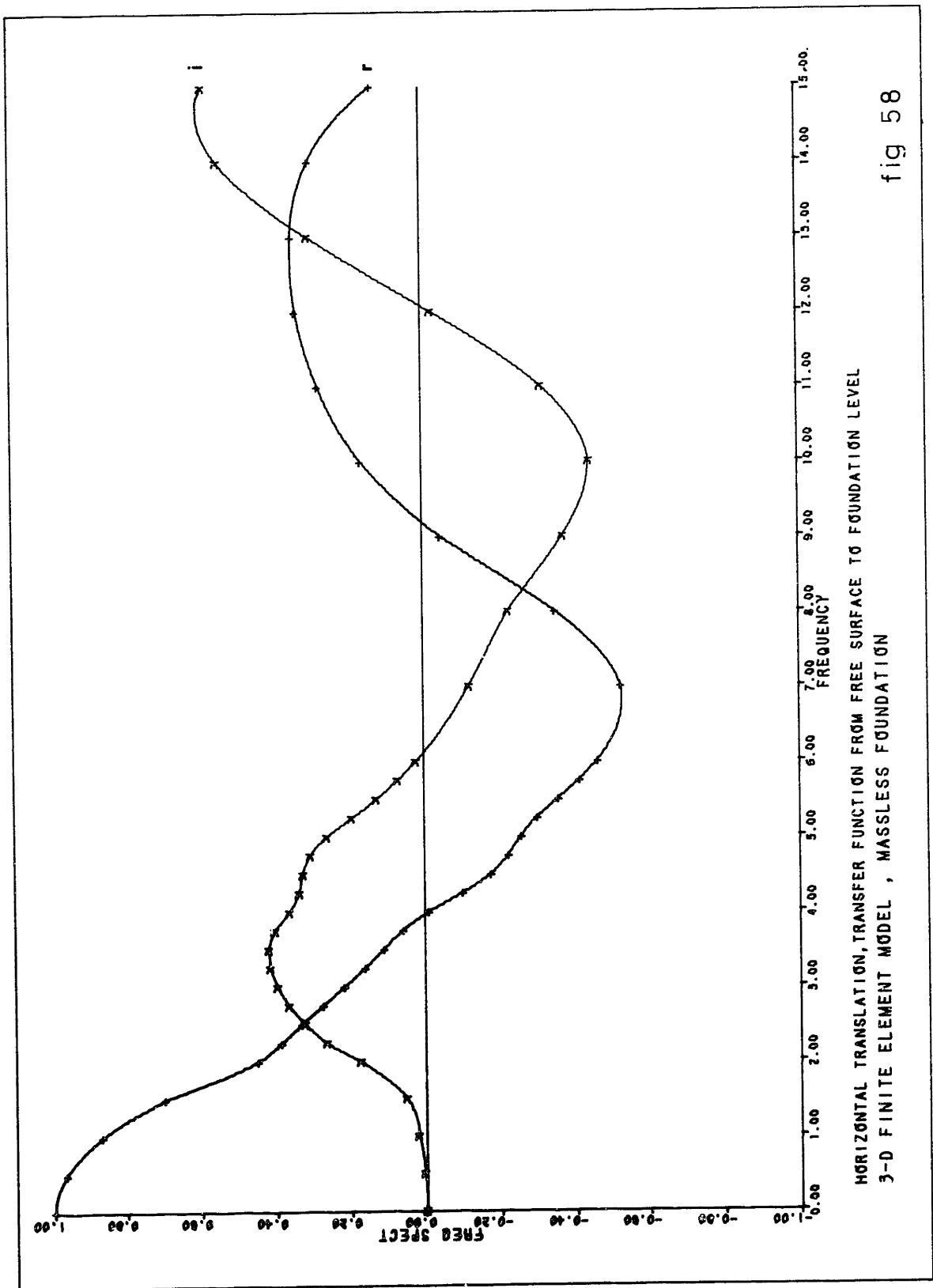


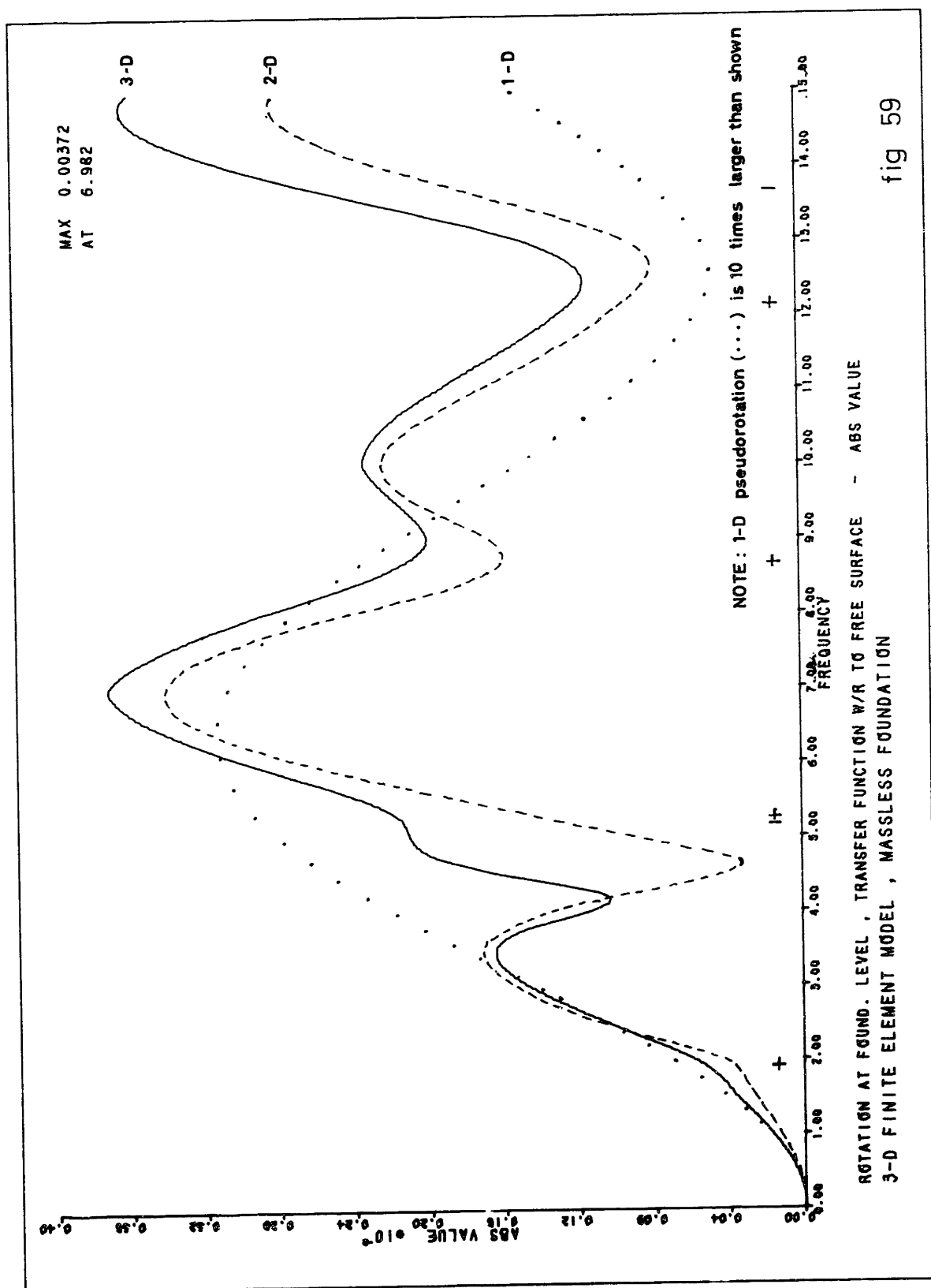
ROTATION AT FOUND. LEVEL, TRANSFER FUNCTION W/R TO FREE SURFACE  
3-D FINITE ELEMENT MODEL OF SUBGRADE AND STRUCTURE

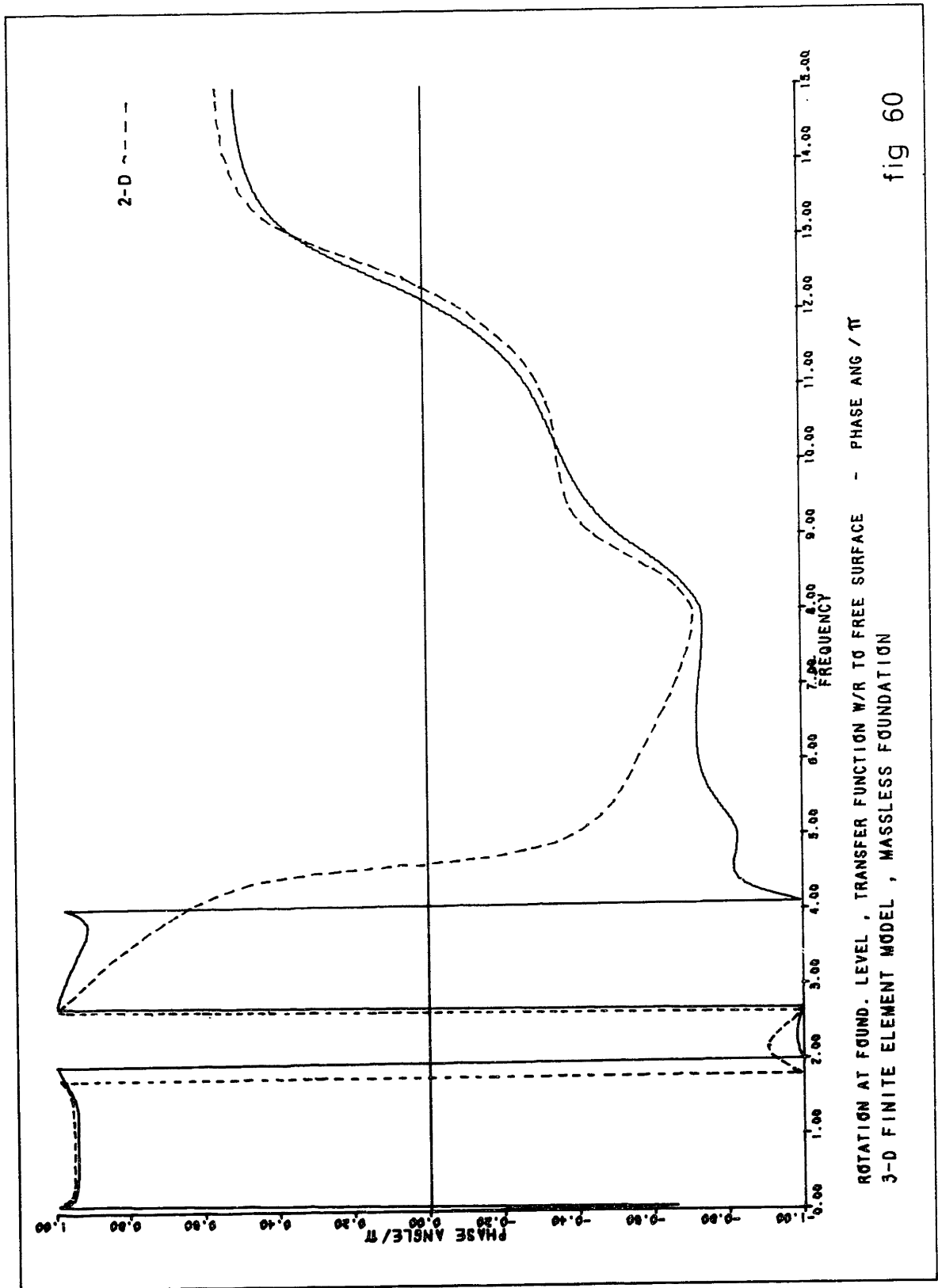
fig 55

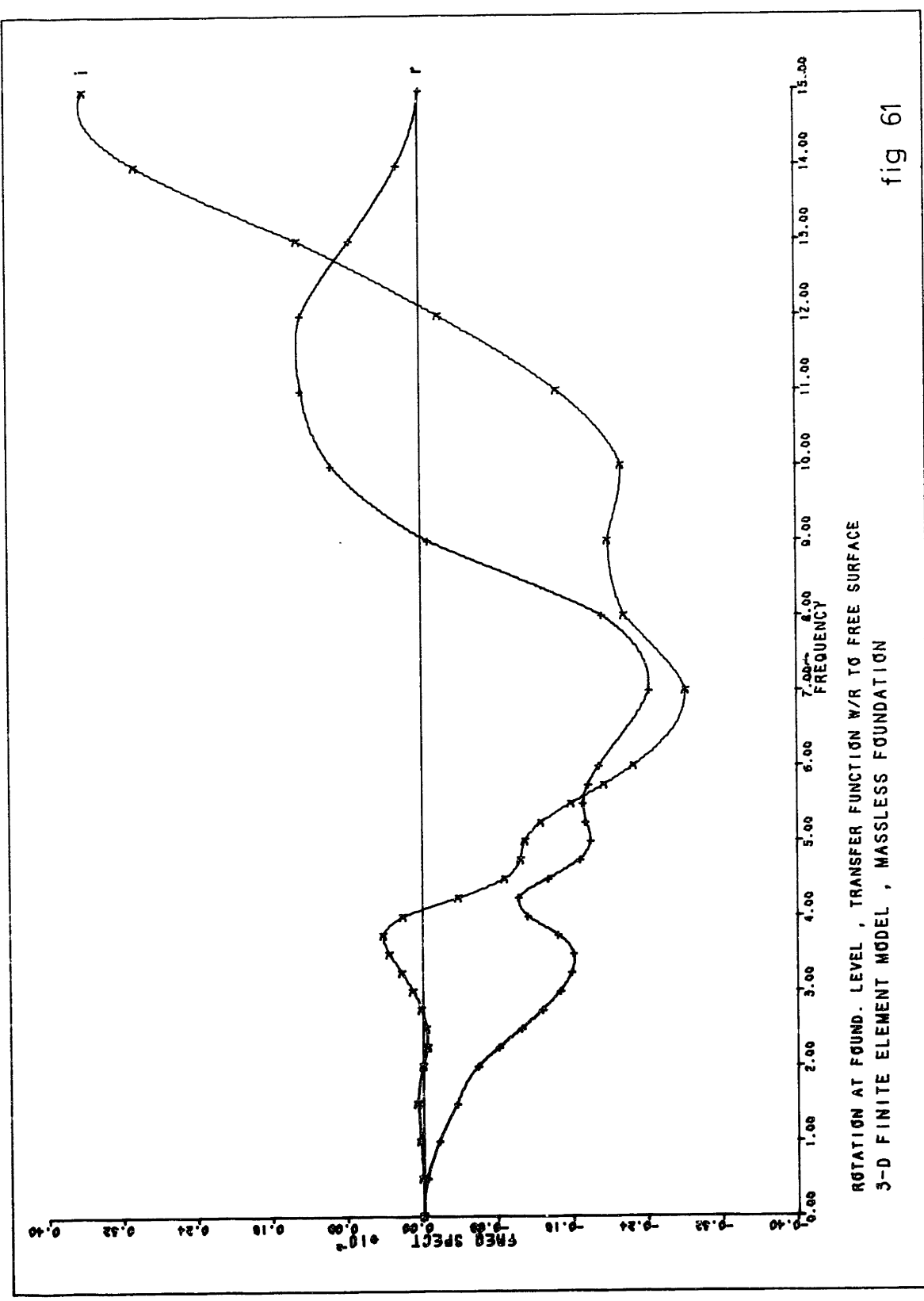


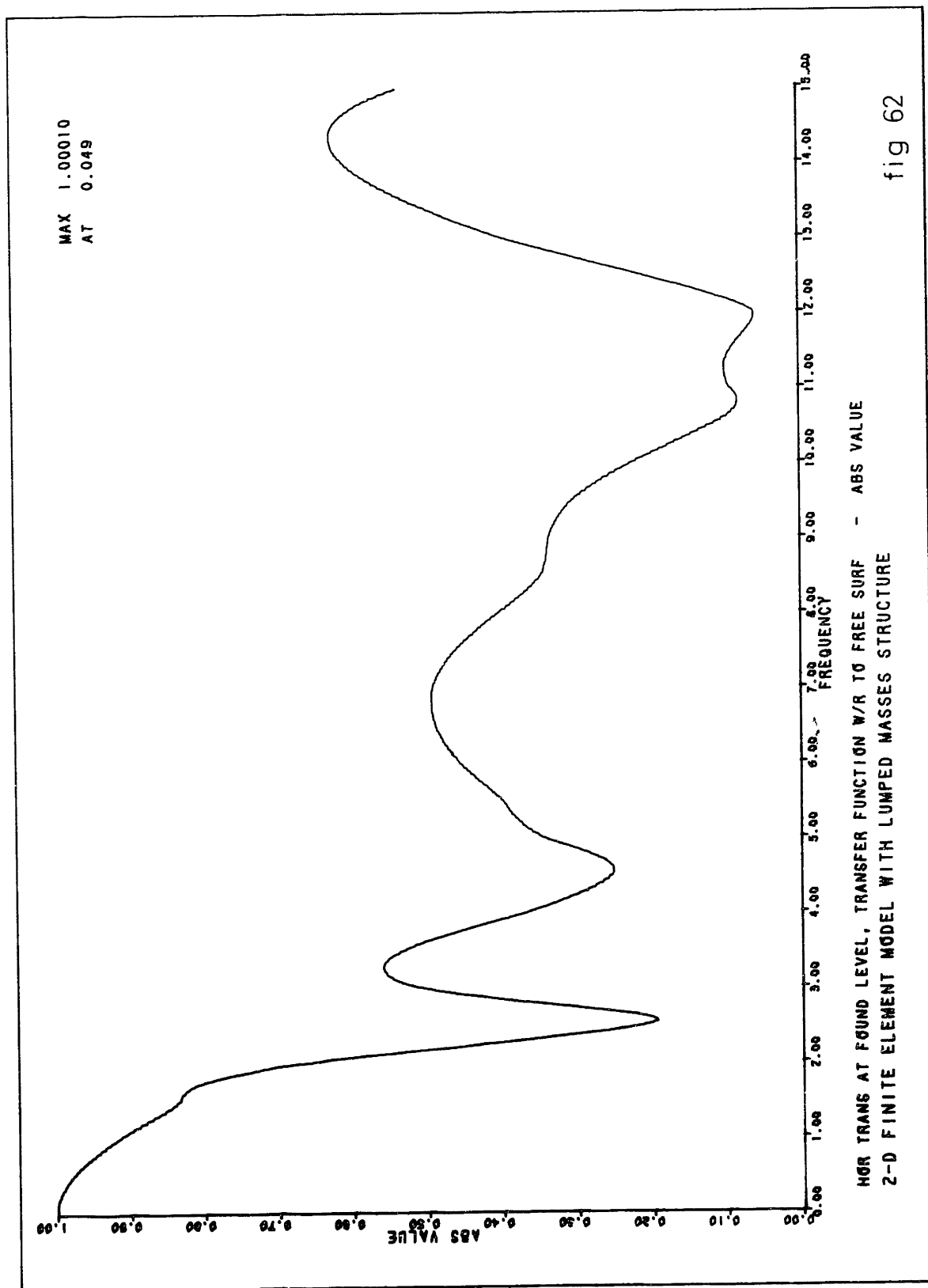




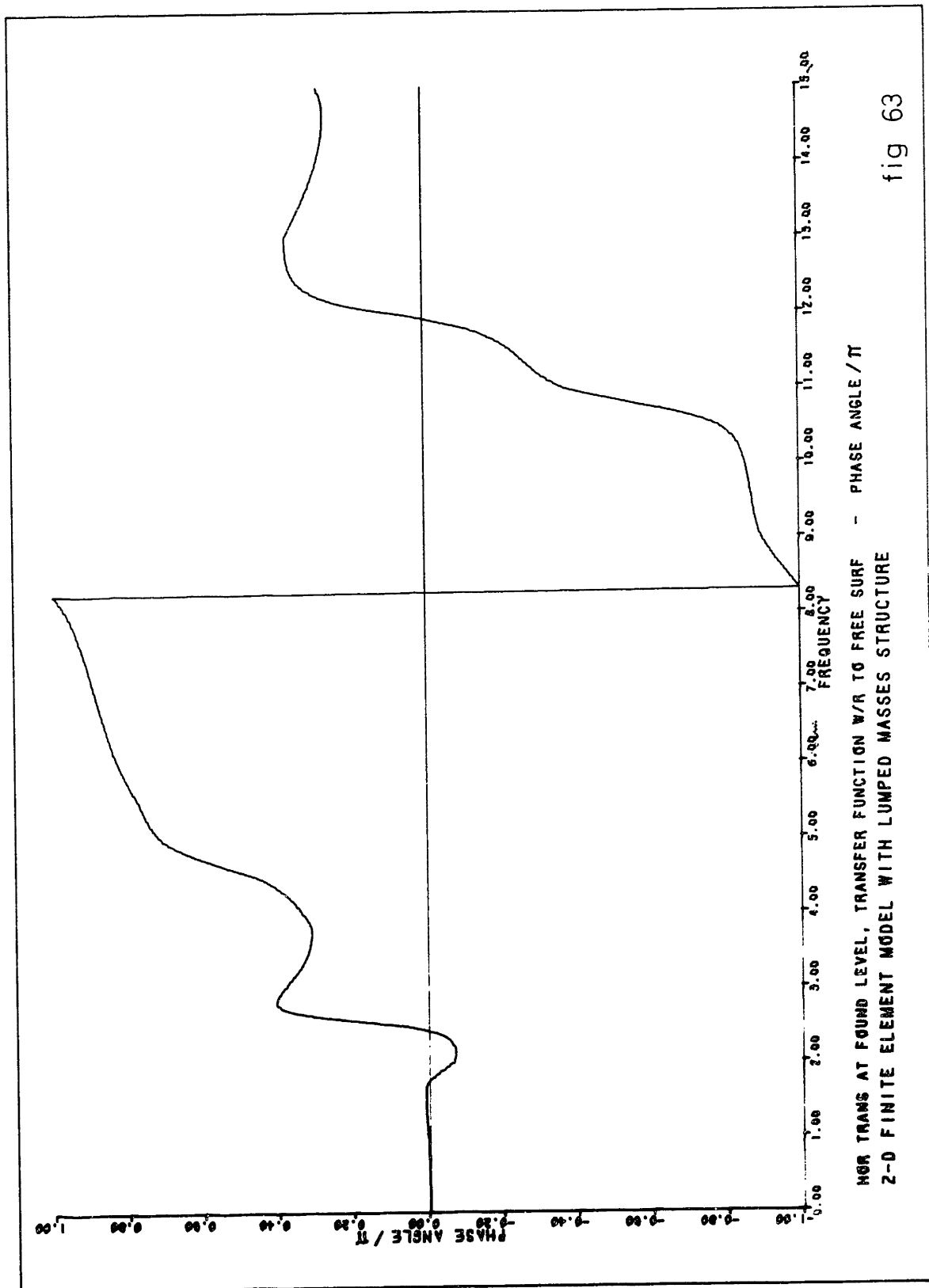


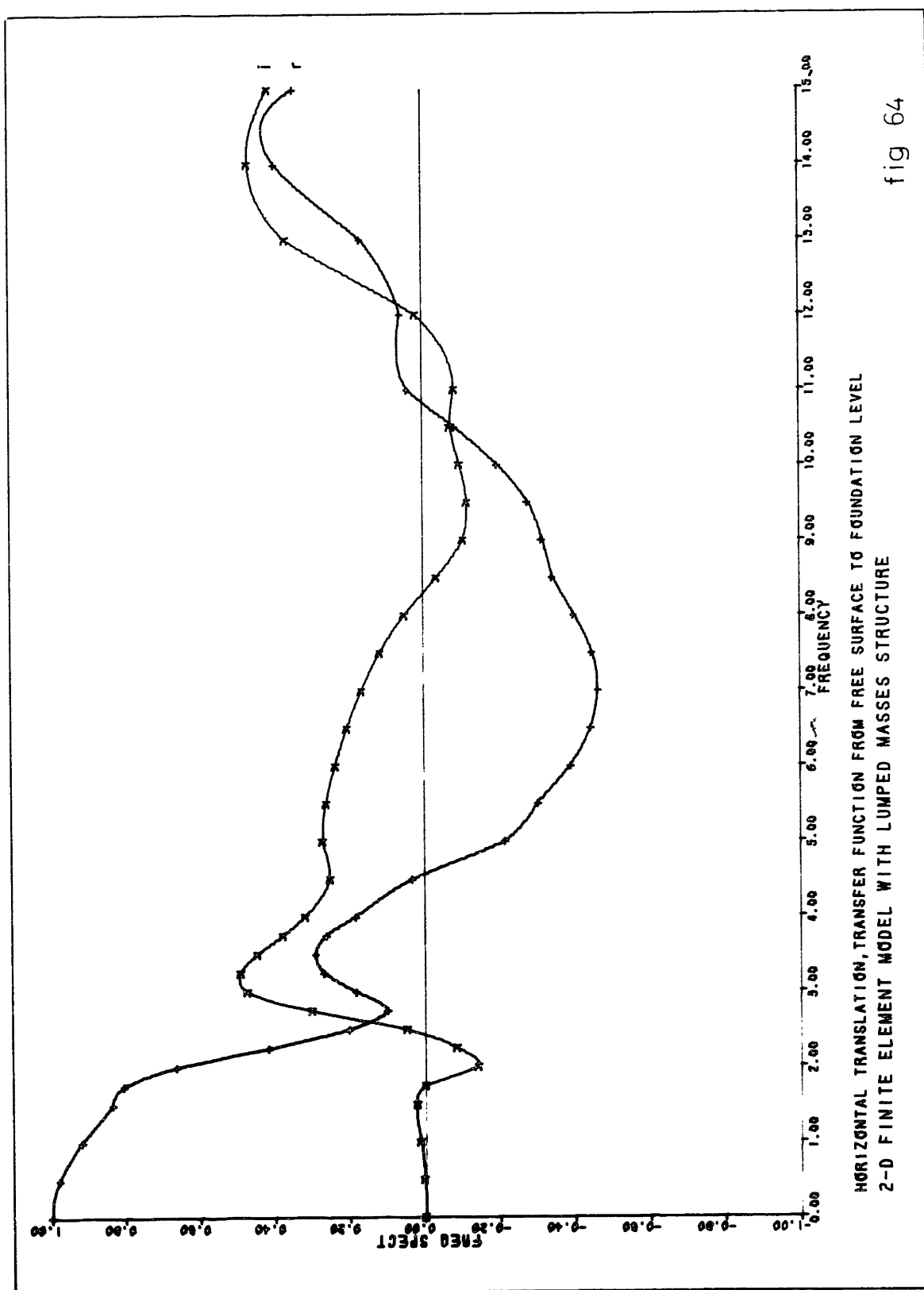












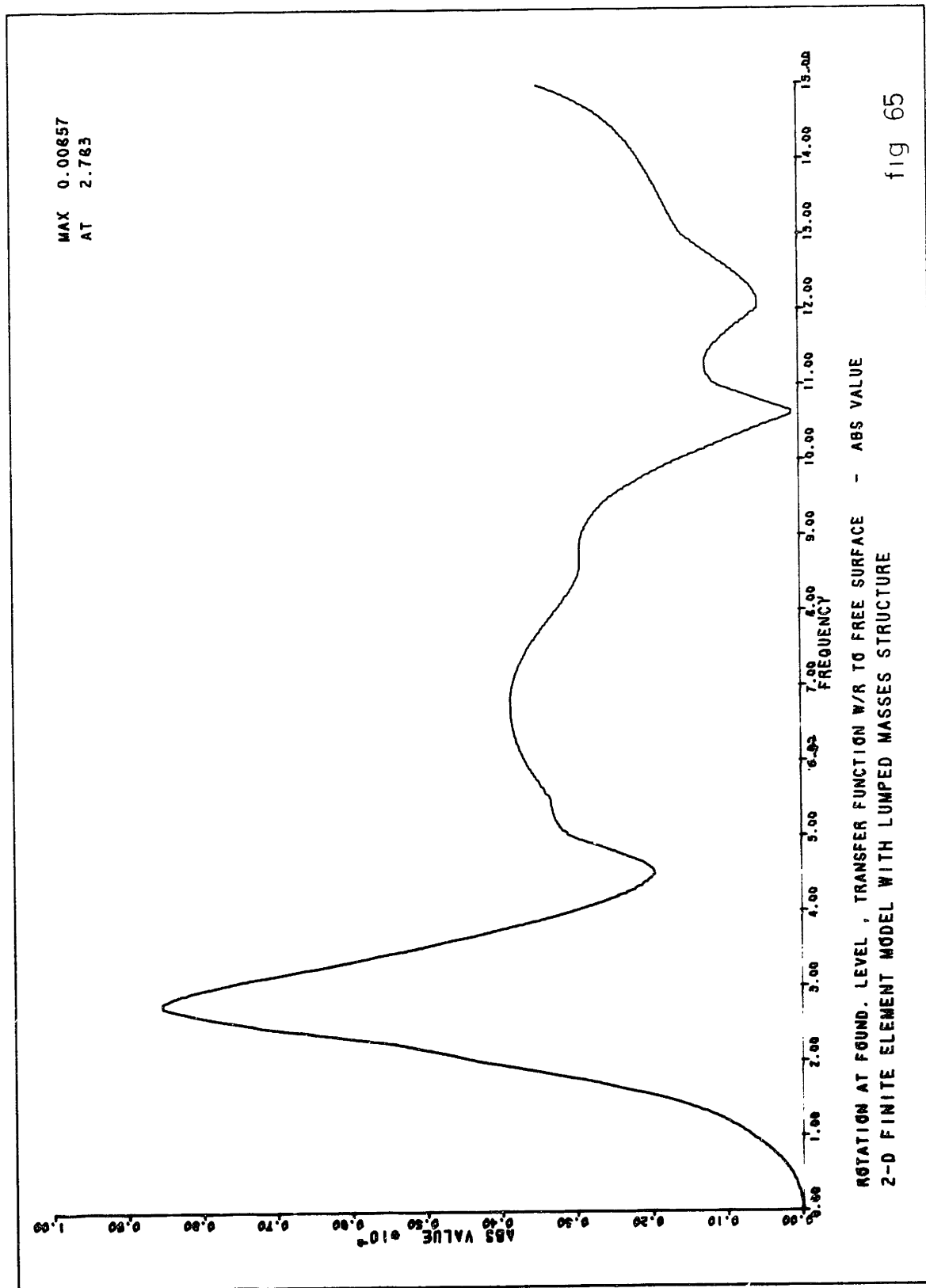
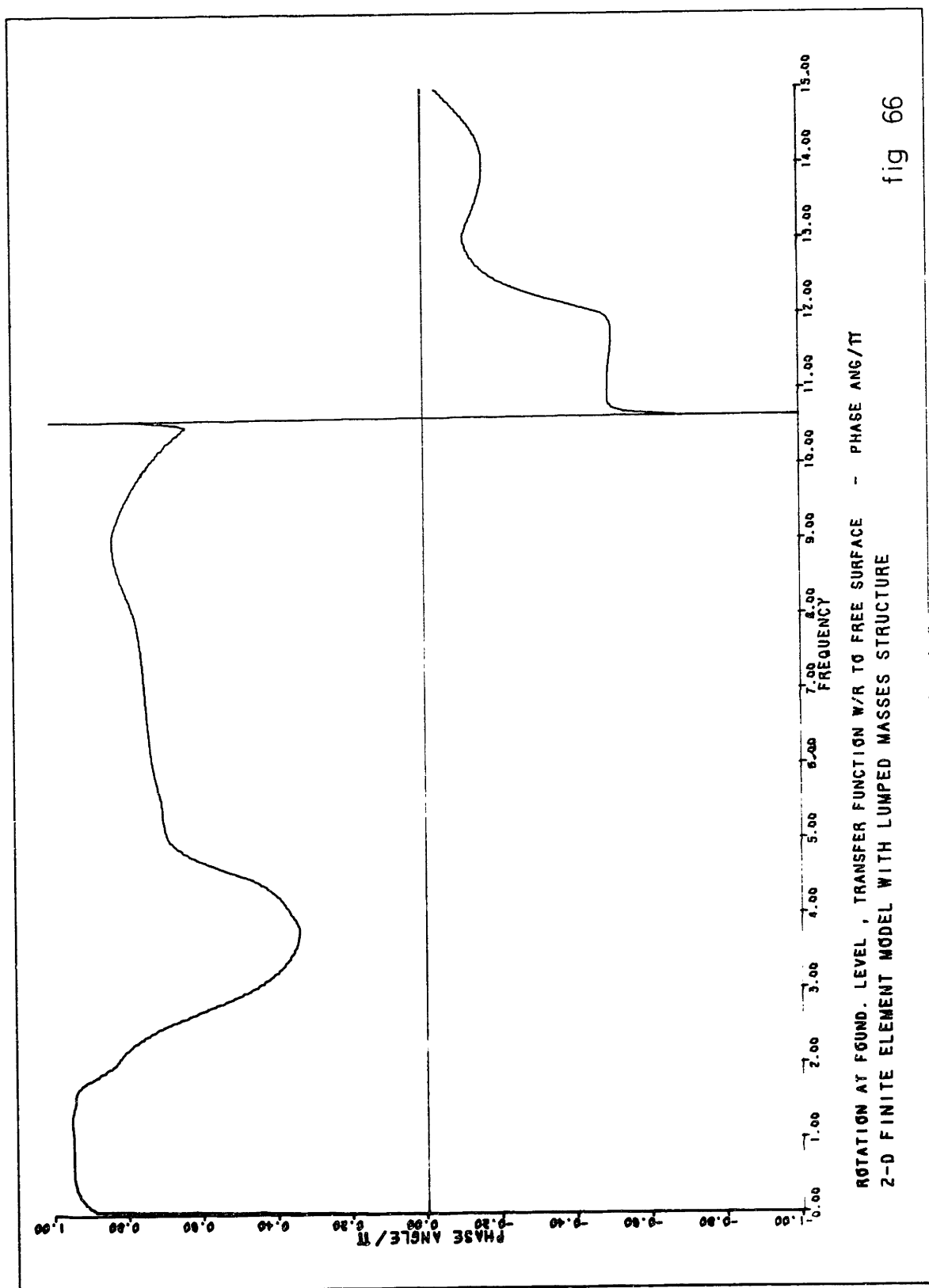
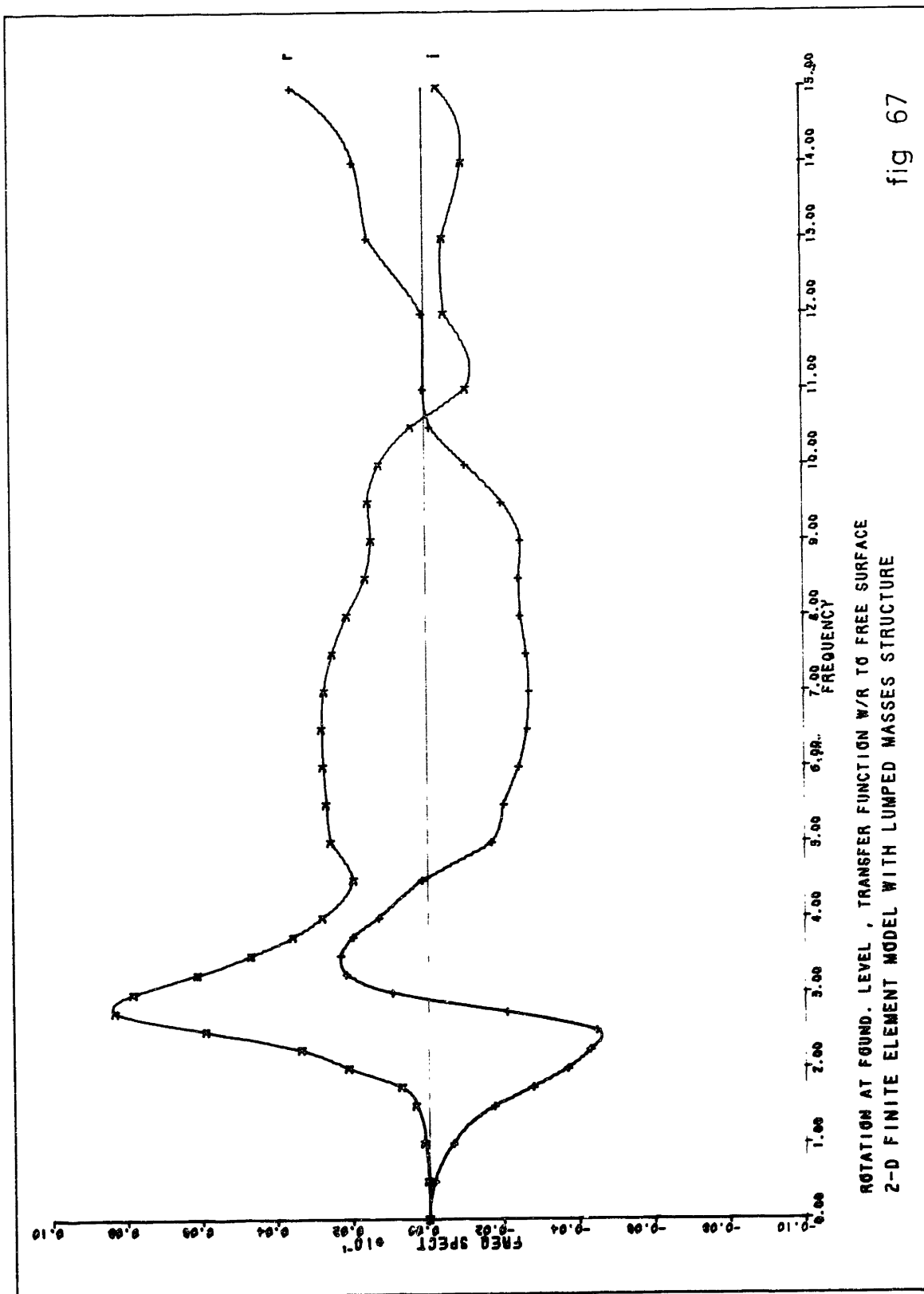
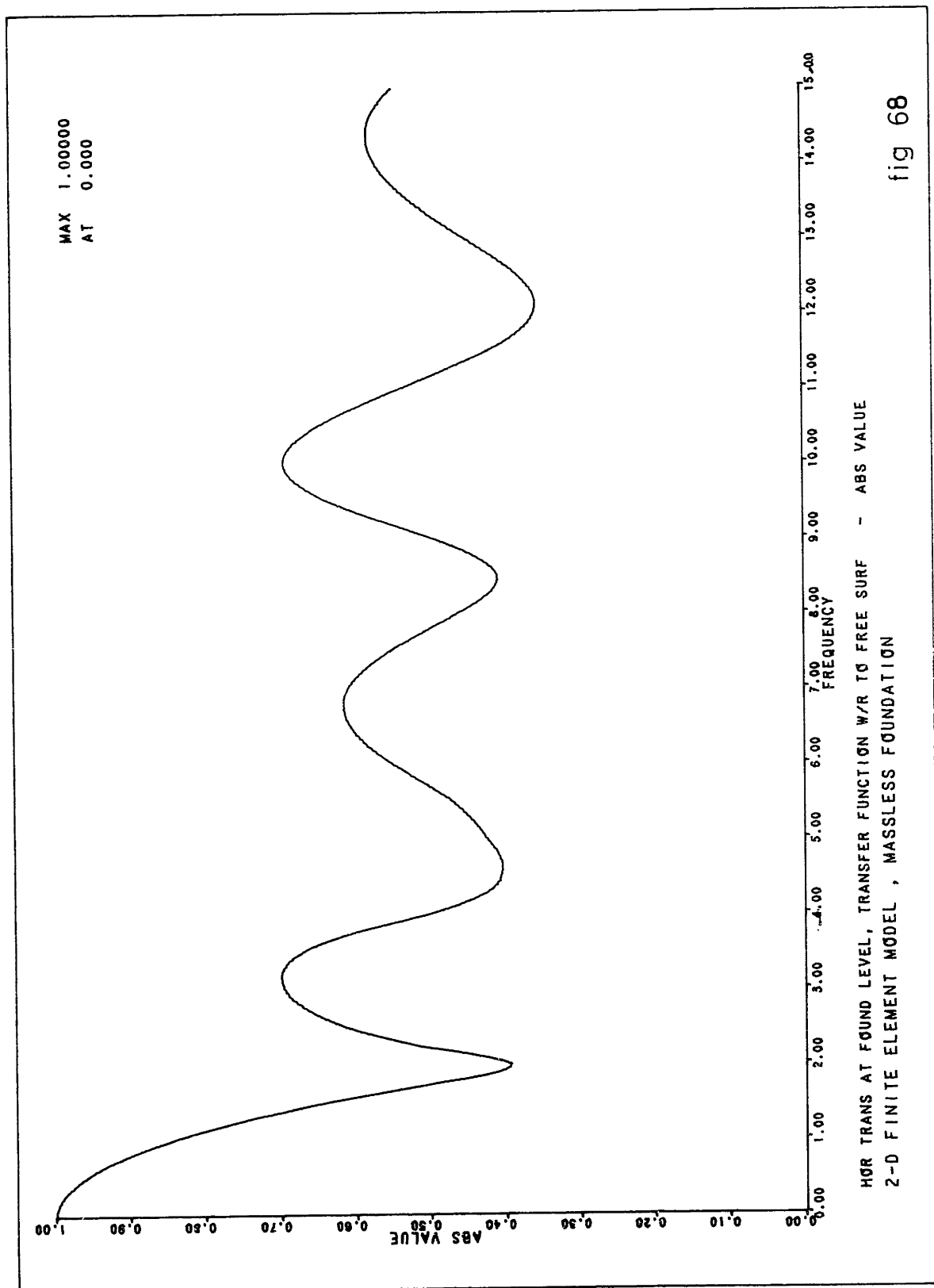
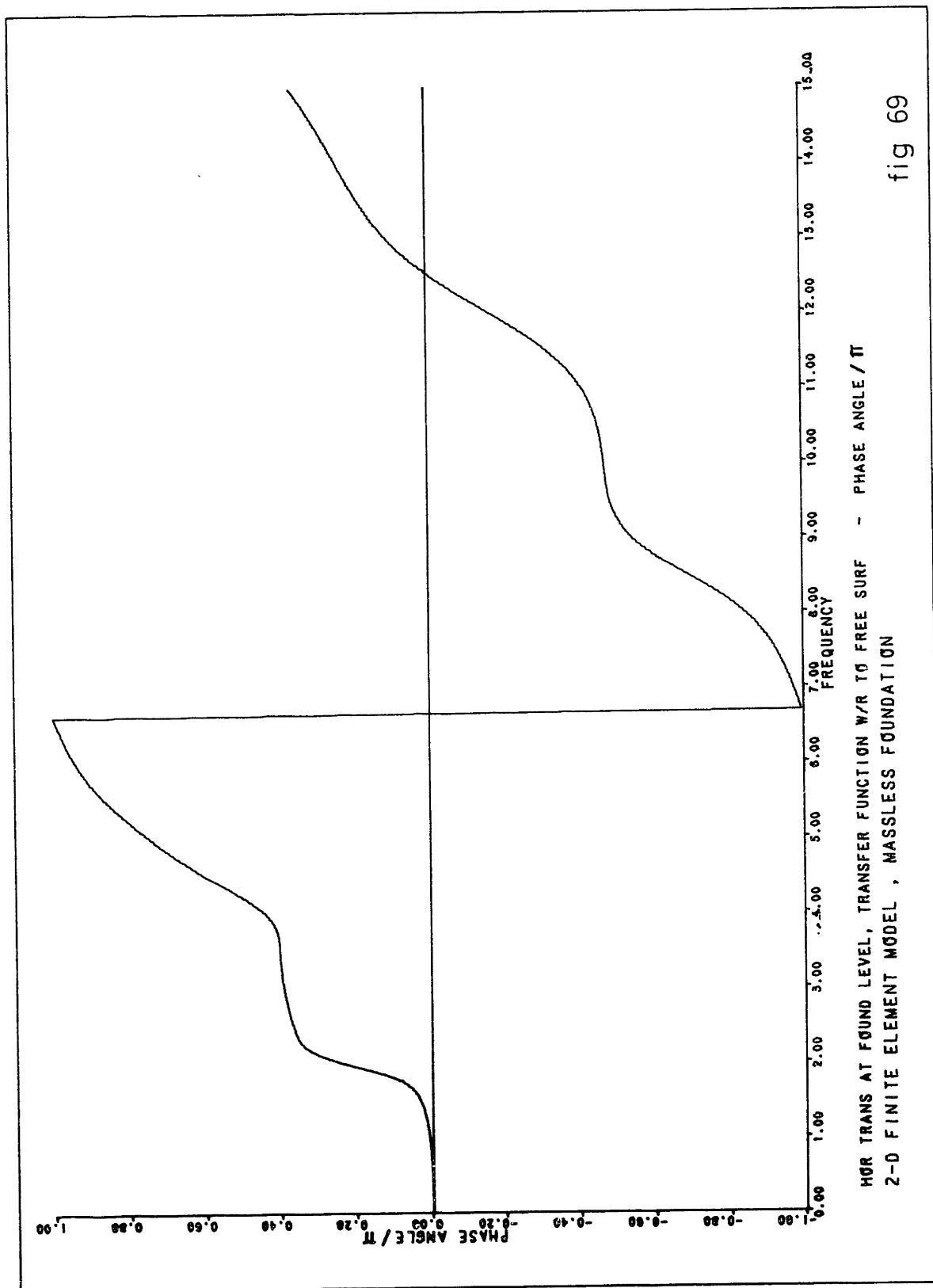


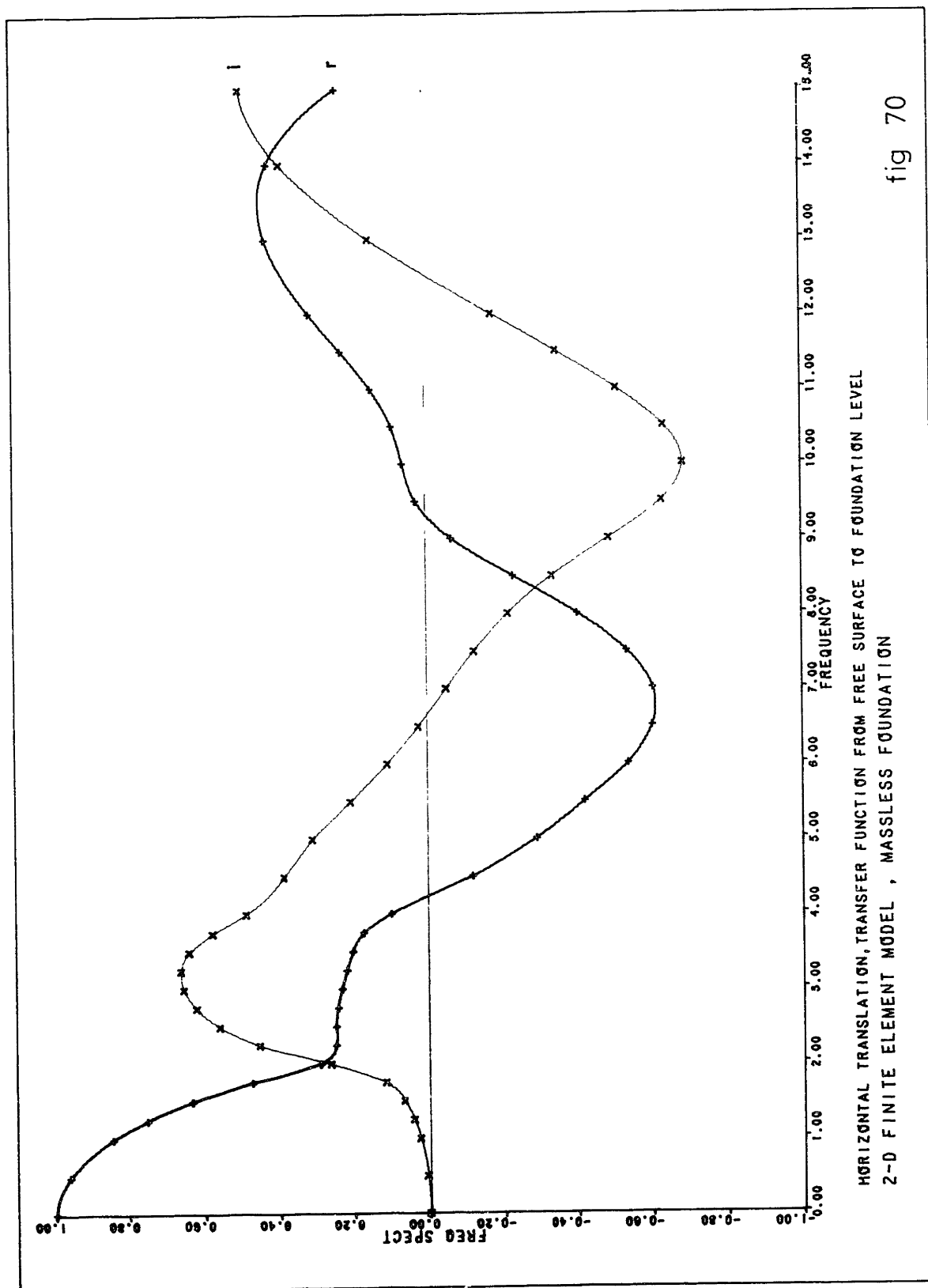
fig 65



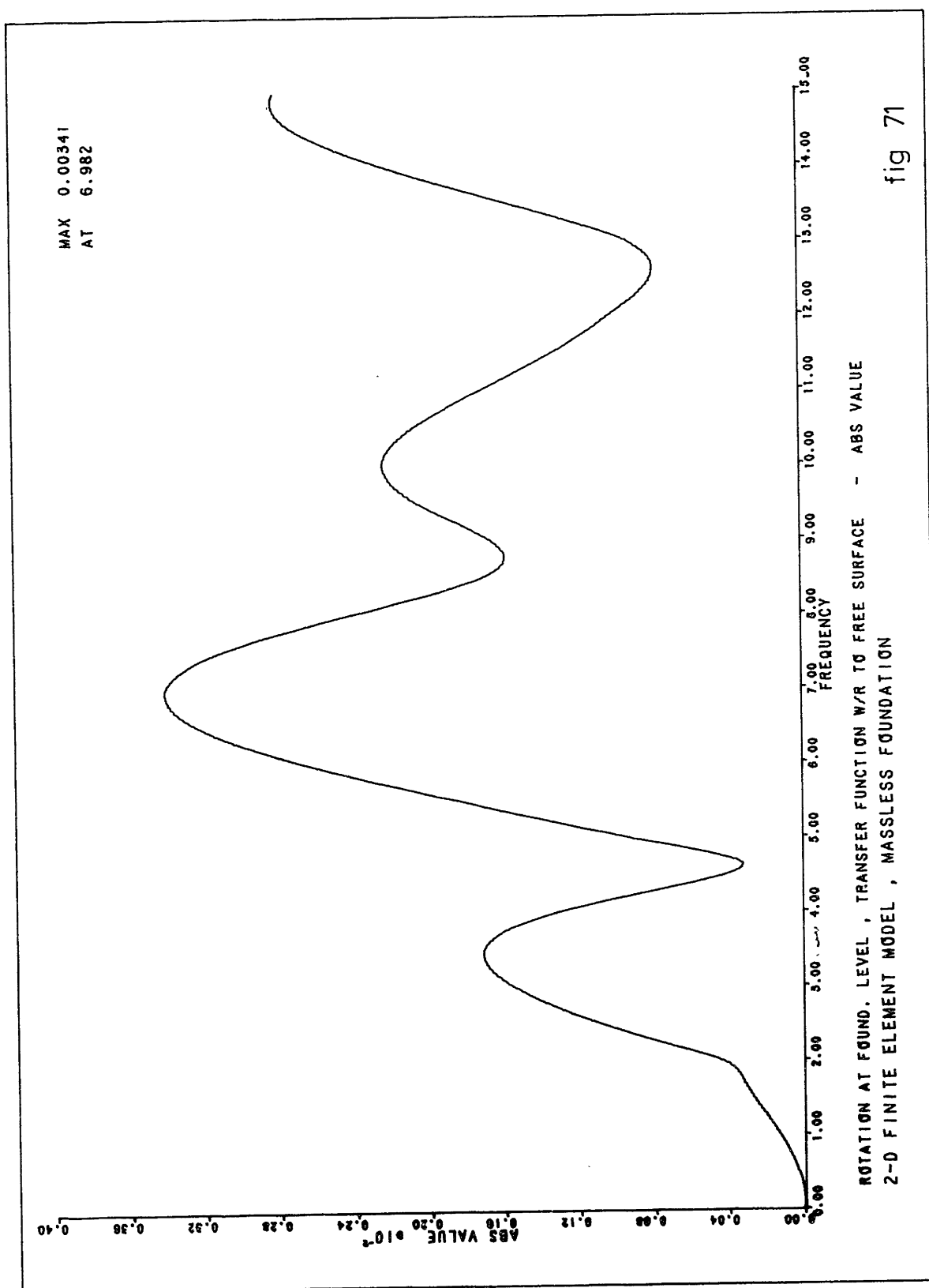


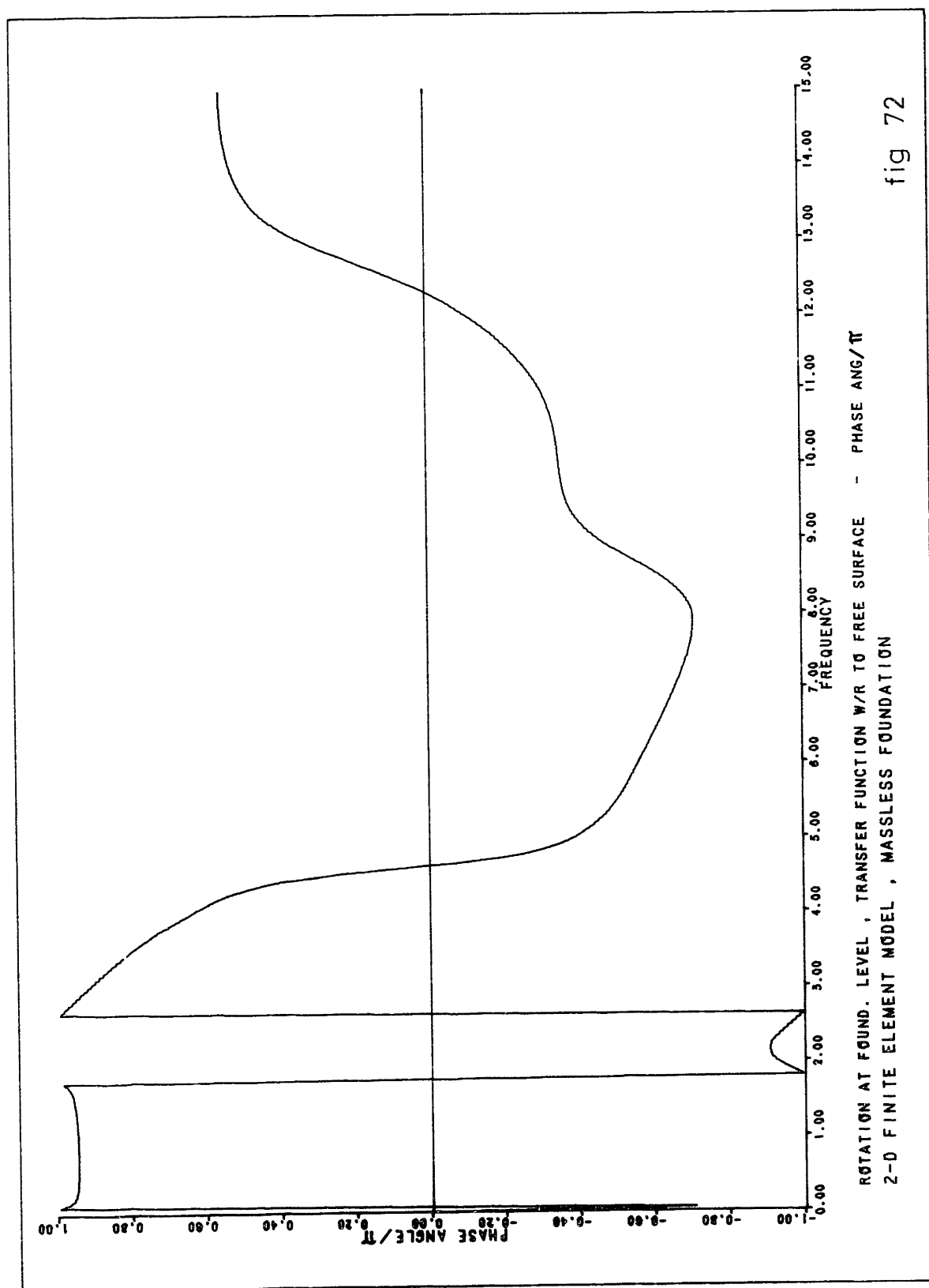


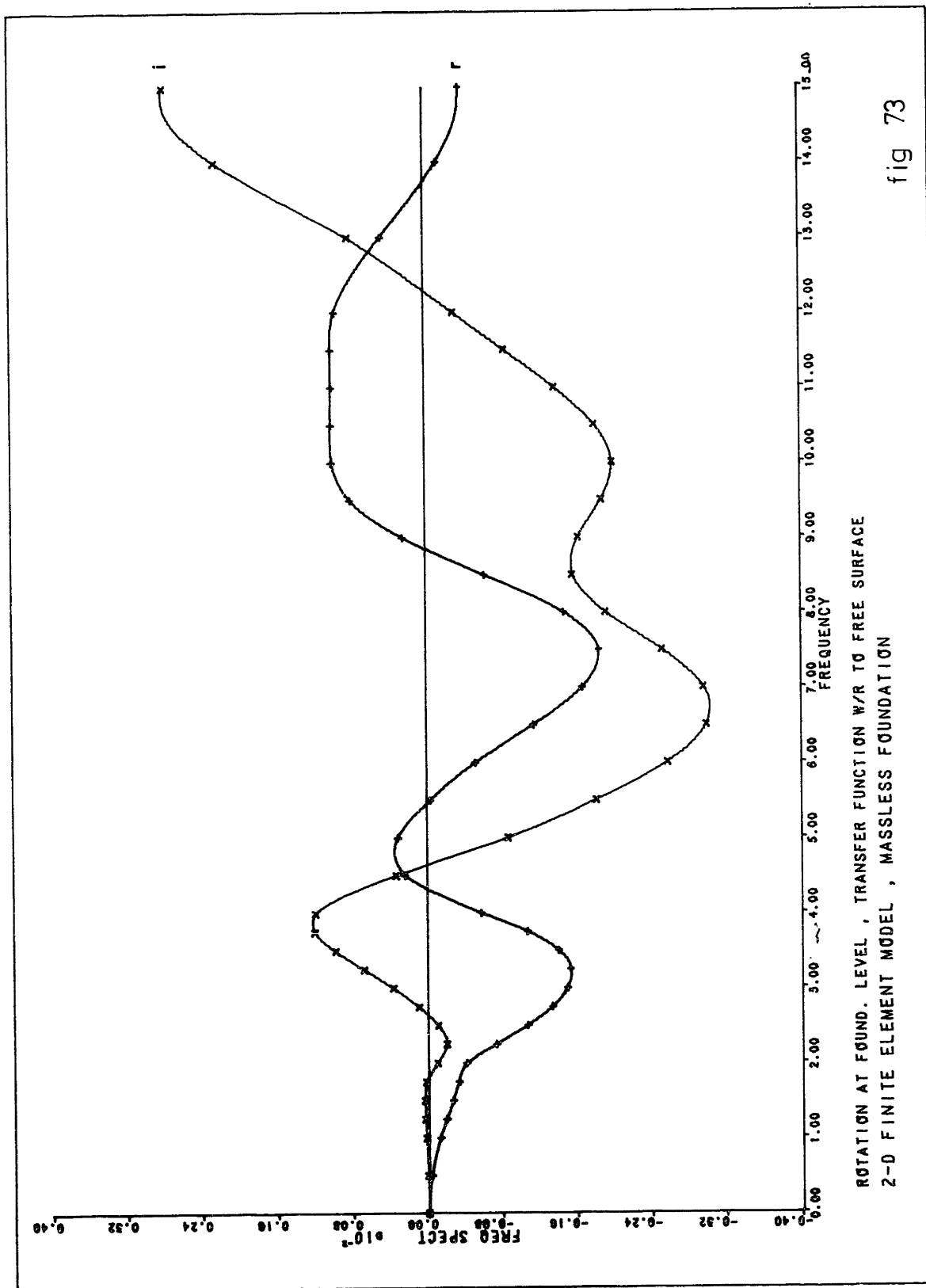










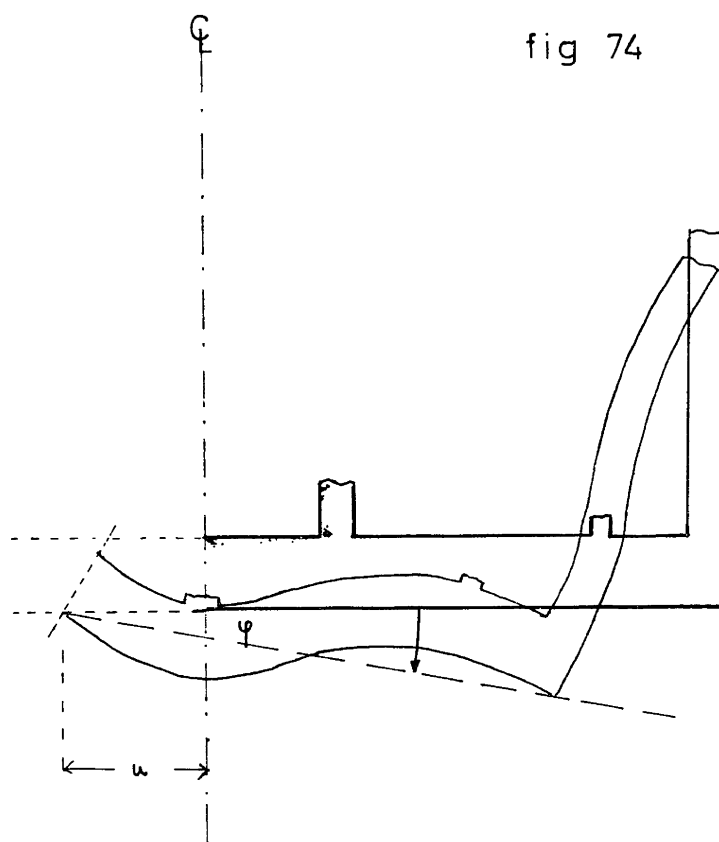


ROTATION AT FOUND. LEVEL , TRANSFER FUNCTION W/R TO FREE SURFACE  
2-D FINITE ELEMENT MODEL , MASSLESS FOUNDATION

fig 73

discrepancies between the two models are much larger for the massless case than for the case with structure. The differences in the models are erased in the case with mass probably because the response is controlled mainly by inertia rather than by stiffness. The rotation is about 1 order of magnitude smaller than the 1-dimensional pseudorotation (defined as the average shear distortion between grade and the foundation level (Fig. 59), although the overall variation pattern with frequency is strikingly similar.

The addition of the structure modifies to a certain degree the displacement transfer function, particularly close to the first coupled rocking-swaying frequency. For higher frequencies, the inertial effects introduced by the mass of the structure decrease the response w/r to the massless case. The rotation (Fig. 53), on the other hand, is completely modified by the presence of the structure, as could be expected, and reaches a peak at the 1st coupled rocking-swaying frequency. Some discrepancies between the two models occur at this frequency, which might be due to the flexibility of the mat in the 3-D model. The relative importance of this effect can be appreciated from the foundation displacement configuration, as shown below for a frequency of 5.75 cps (approximately, the 1st structural frequency) :



MAT DISTORTION .  
AT 5.75 cps

NOTE: SCHEME IS APPROXIMATE BECAUSE OF SLIGHT  
PHASE DIFFERENCES IN THE NODE DISPLACEMENTS

Possibly, the discrepancies introduced by the mat distortion could be reduced by an improvement in the 2-D model, working with a flexible foundation mat and attaching three coaxial structural columns as in the scheme below:

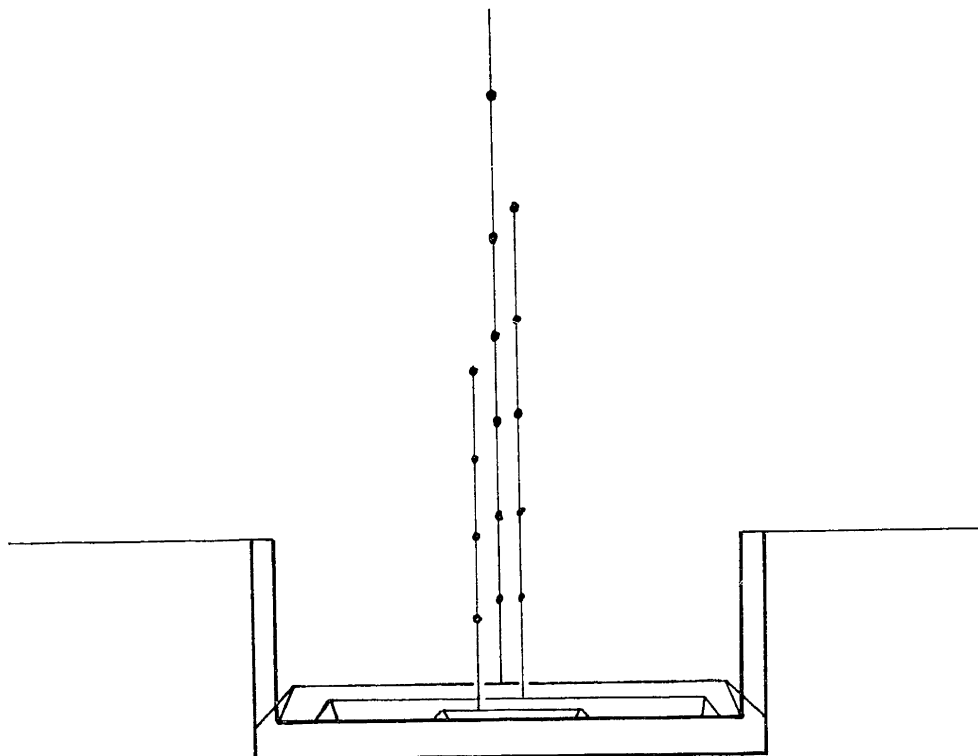


fig 75

Specification at grade of a spectrum compatible artificially generated earthquake (Figs. 76 through 78 ) with a maximum acceleration of 0.125 g yields the response curves shown in Figs. 79 through 94 . The differences in the transfer functions do not significantly affect the response at foundation level. However, the differences could affect

significantly the response at the top of the structure, because of the discrepancies in the rotation transfer function.

The results of the comparison between the two models are not conclusive. The transfer functions as well as the time histories for the effects studied show in both cases a similar variation pattern; nevertheless, seemingly minor differences in the transfer functions could lead in some instances to large differences in the responses. Further research, beyond the scope of this dissertation, is needed, in which a wider range of parameters is covered. Response spectra at the different floor levels may provide a better basis of comparison, and shed more light on the accuracy of some improved plane model. Also, in view of Fig. 74 showing the deformation of the mat, it appears desirable to study the effect of the mat flexibility on the response at the top of the structure for either of the two models.

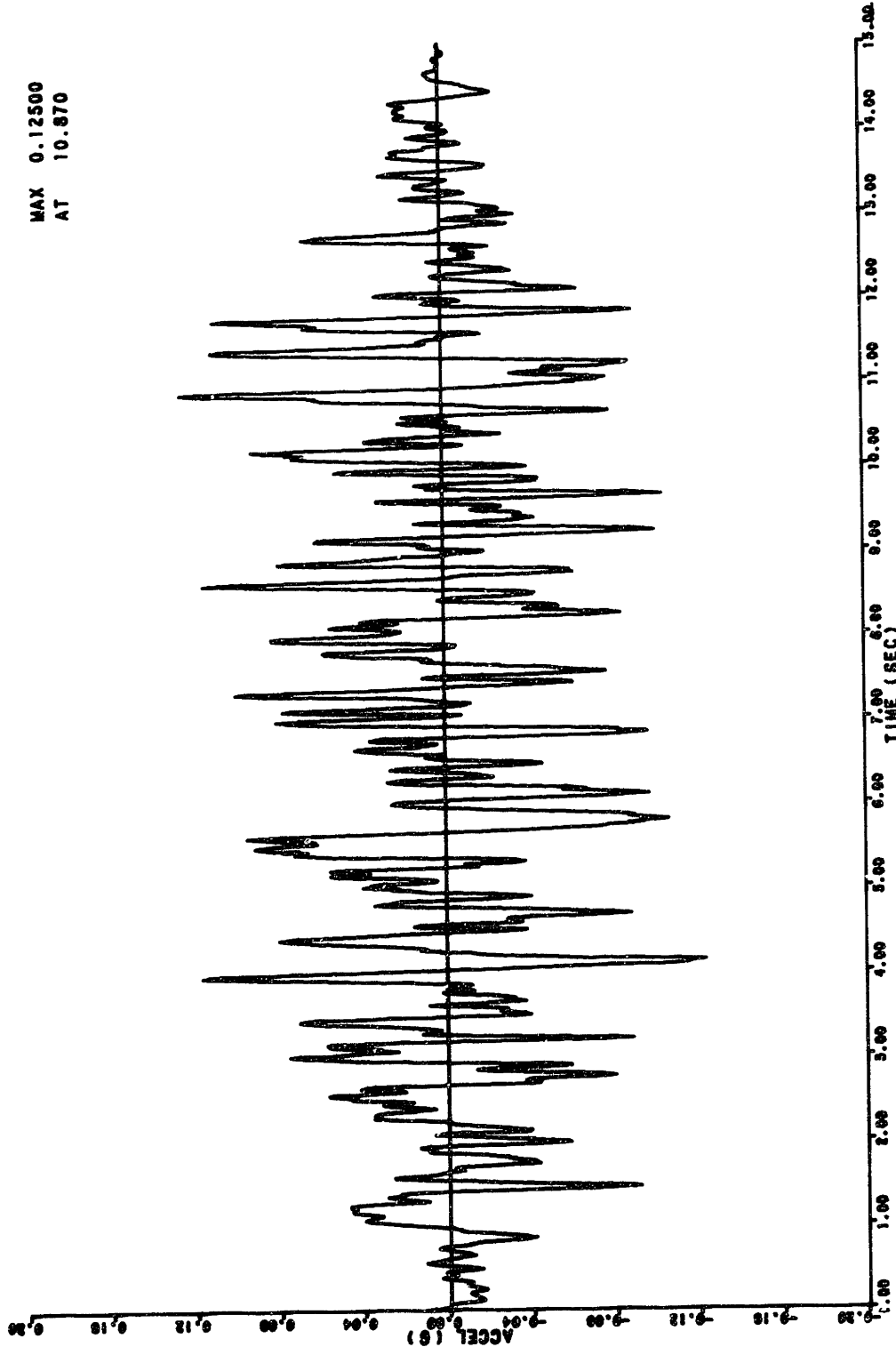
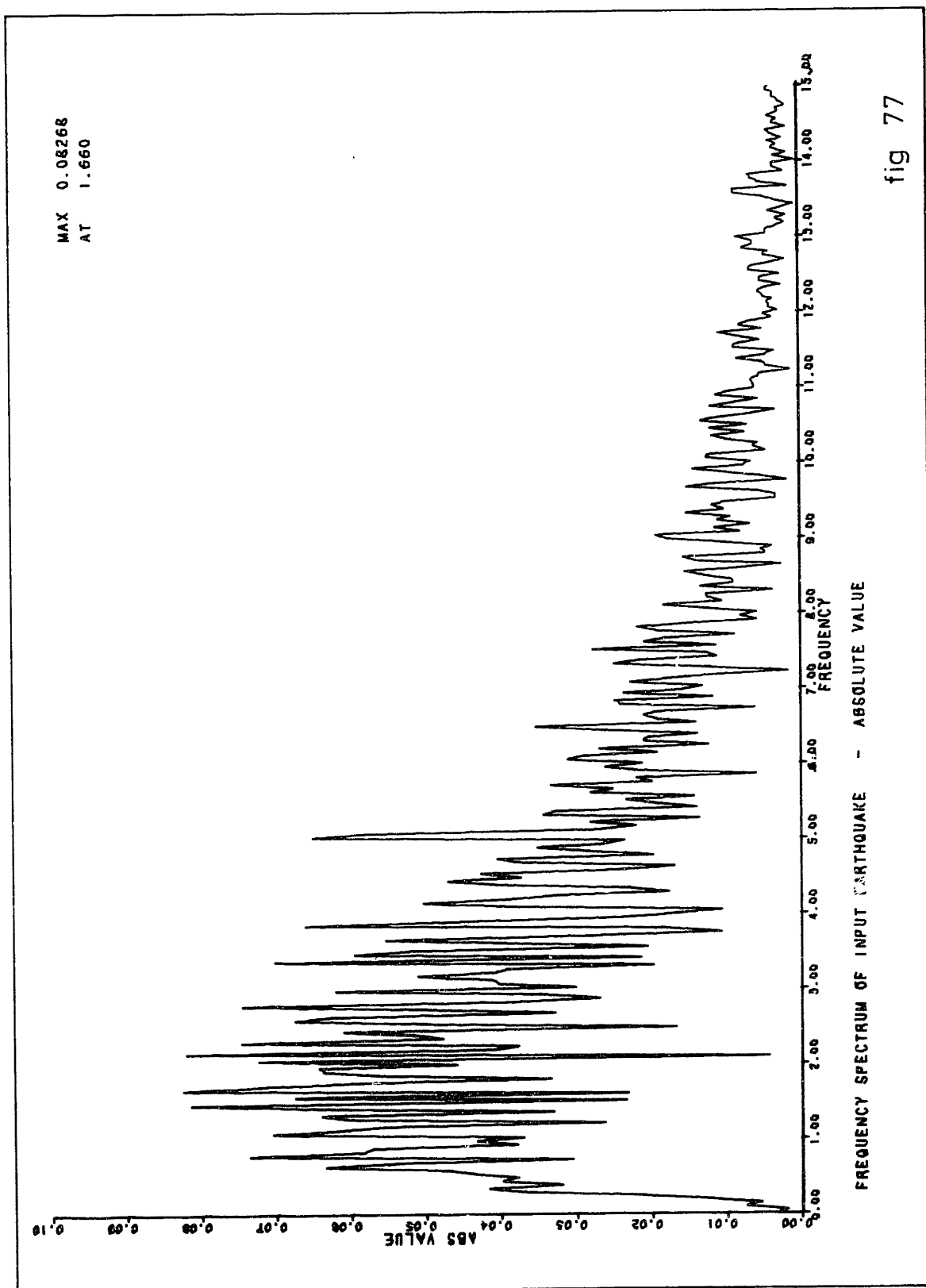
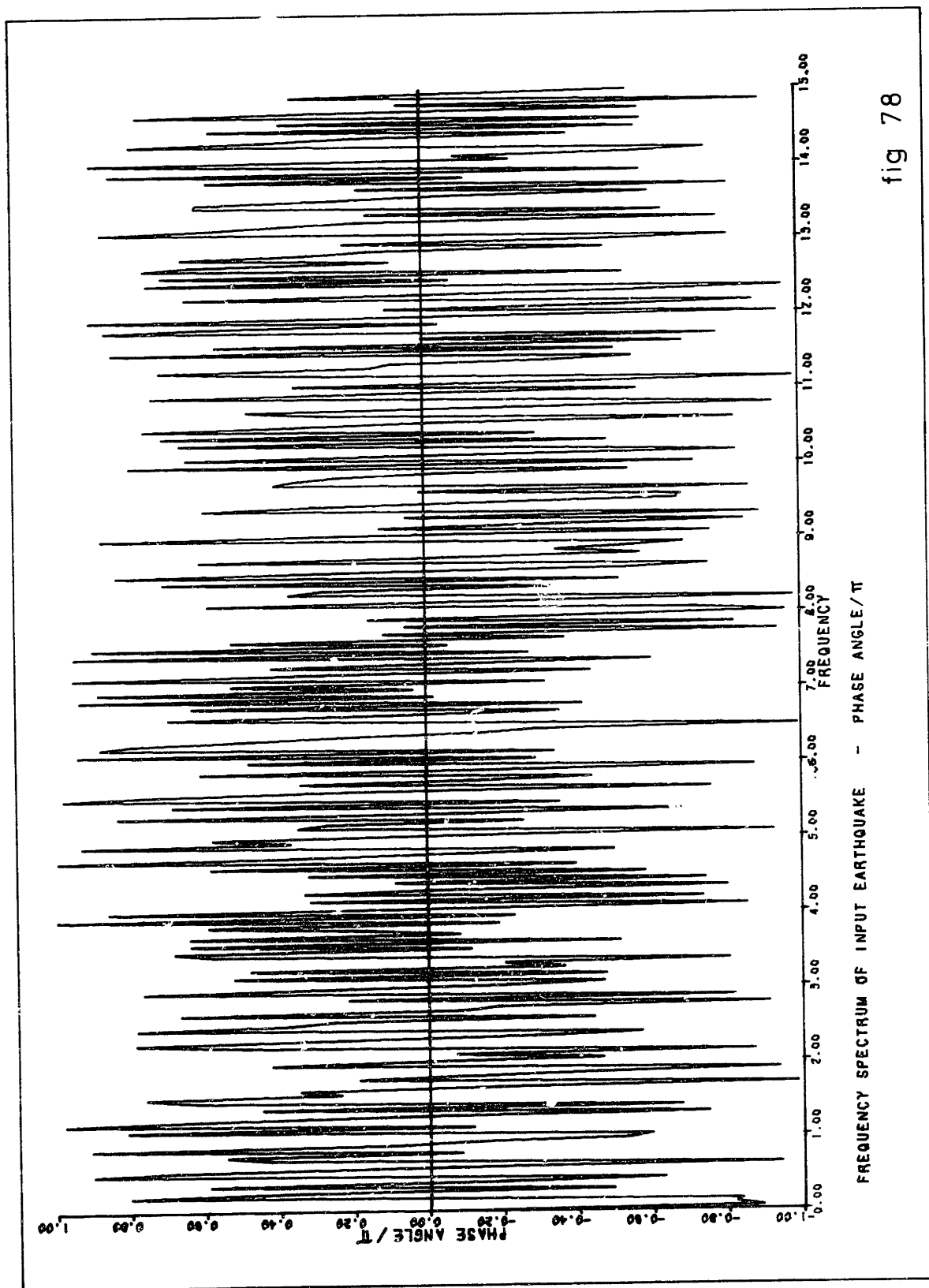


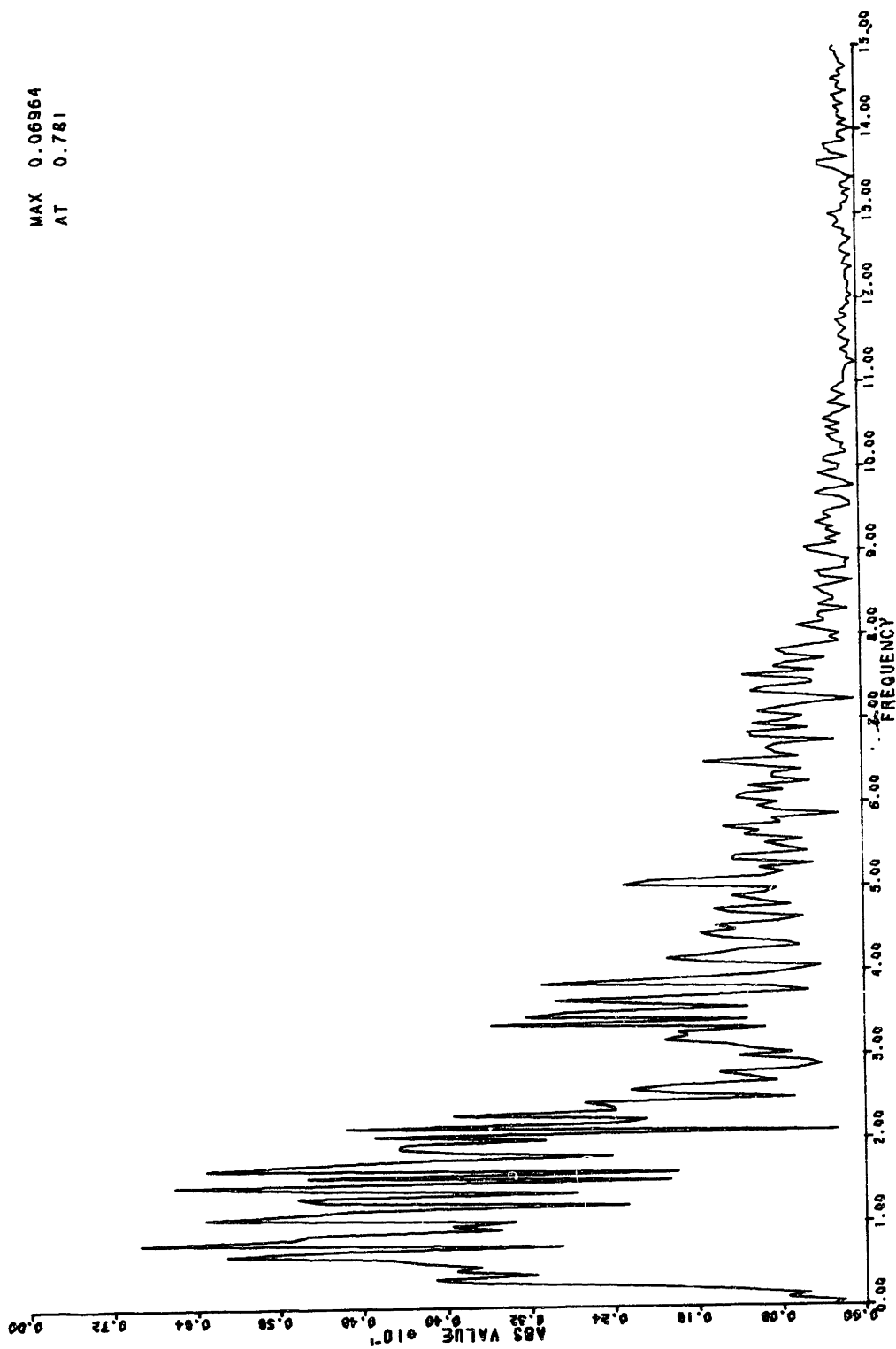
fig 76





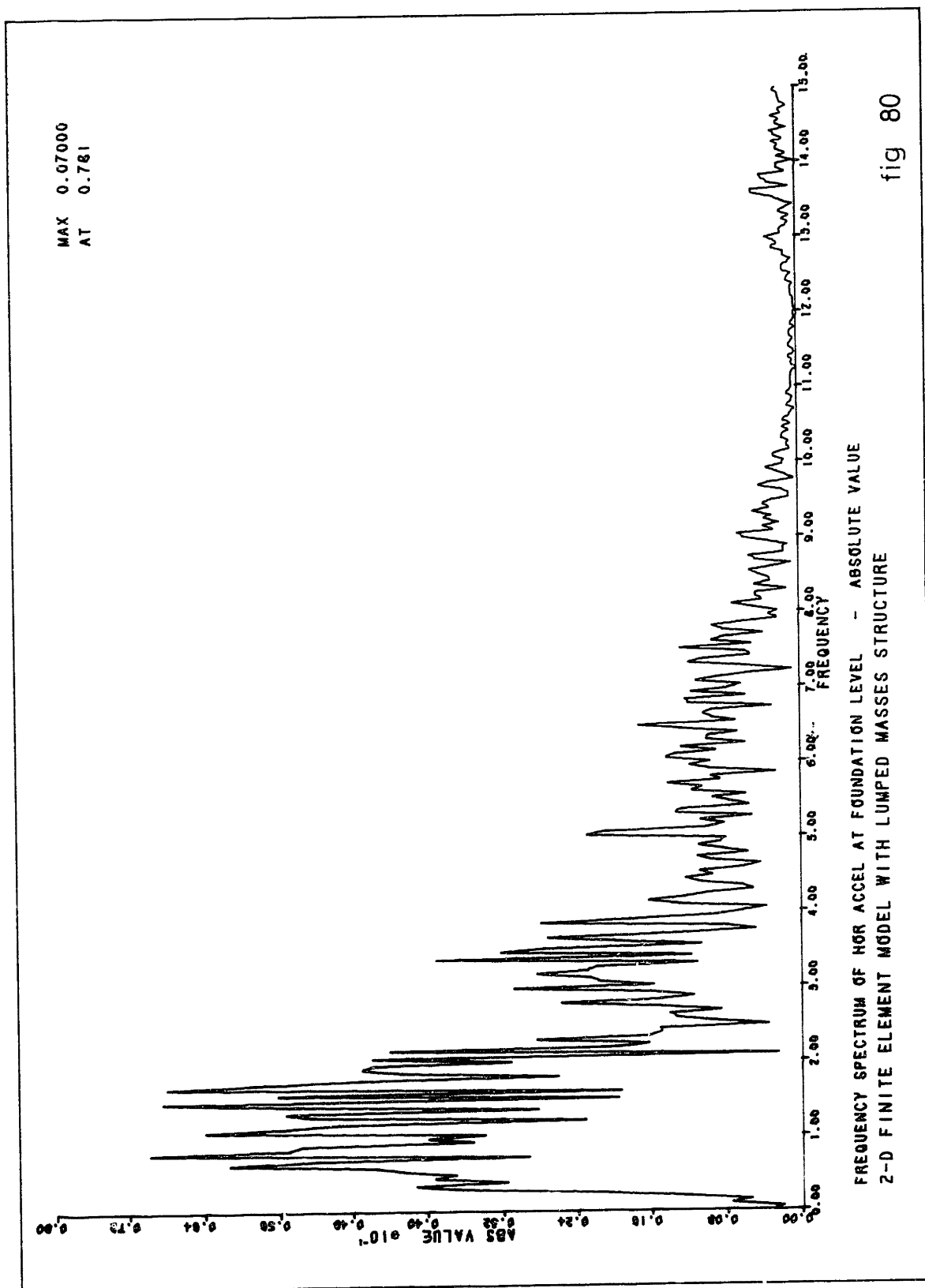


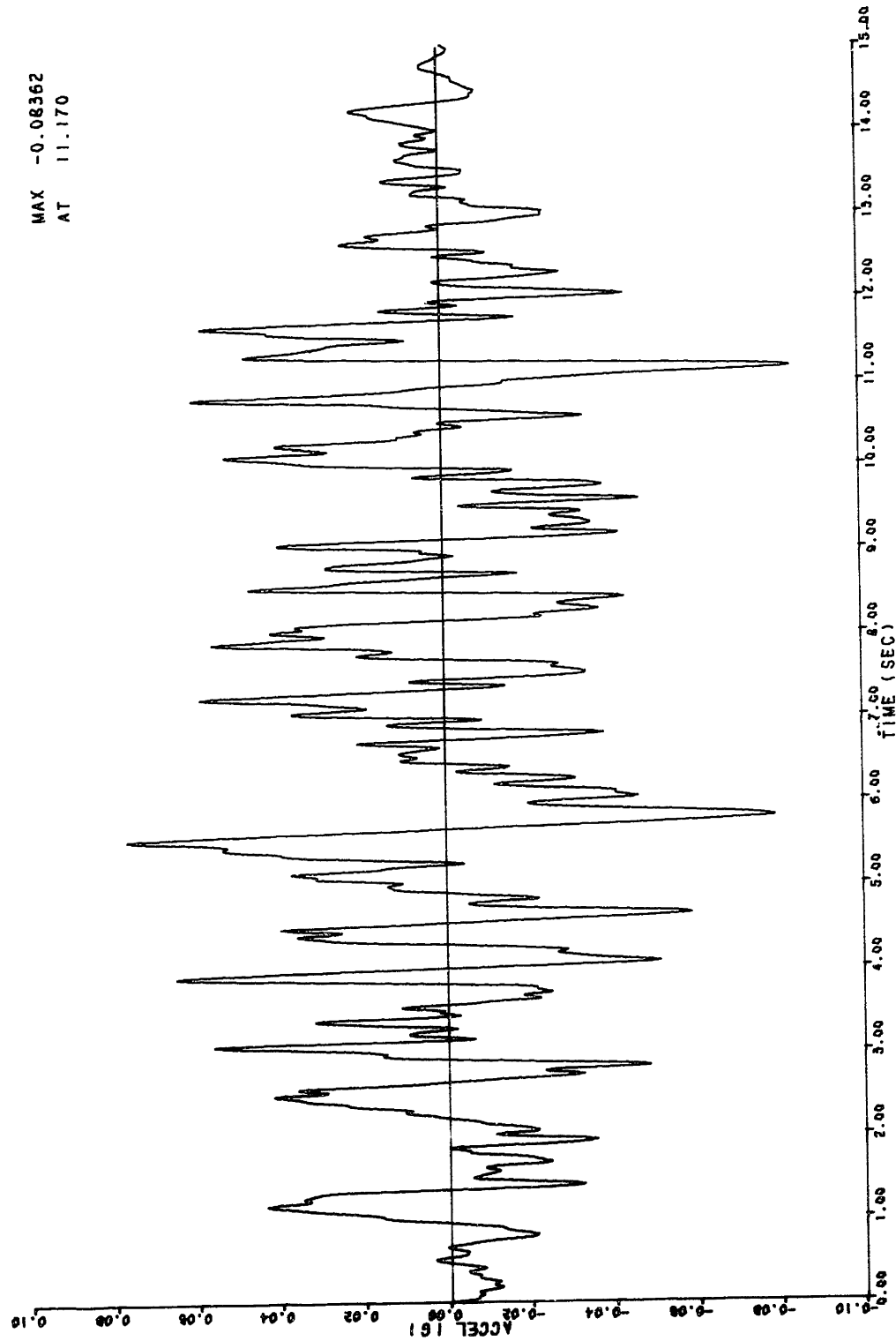
MAX 0.06964  
AT 0.781



FREQUENCY SPECTRUM OF HOR ACCEL AT FOUNDATION LEVEL - ABSOLUTE VALUE  
3-D FINITE ELEMENT MODEL OF SUBGRADE AND STRUCTURE

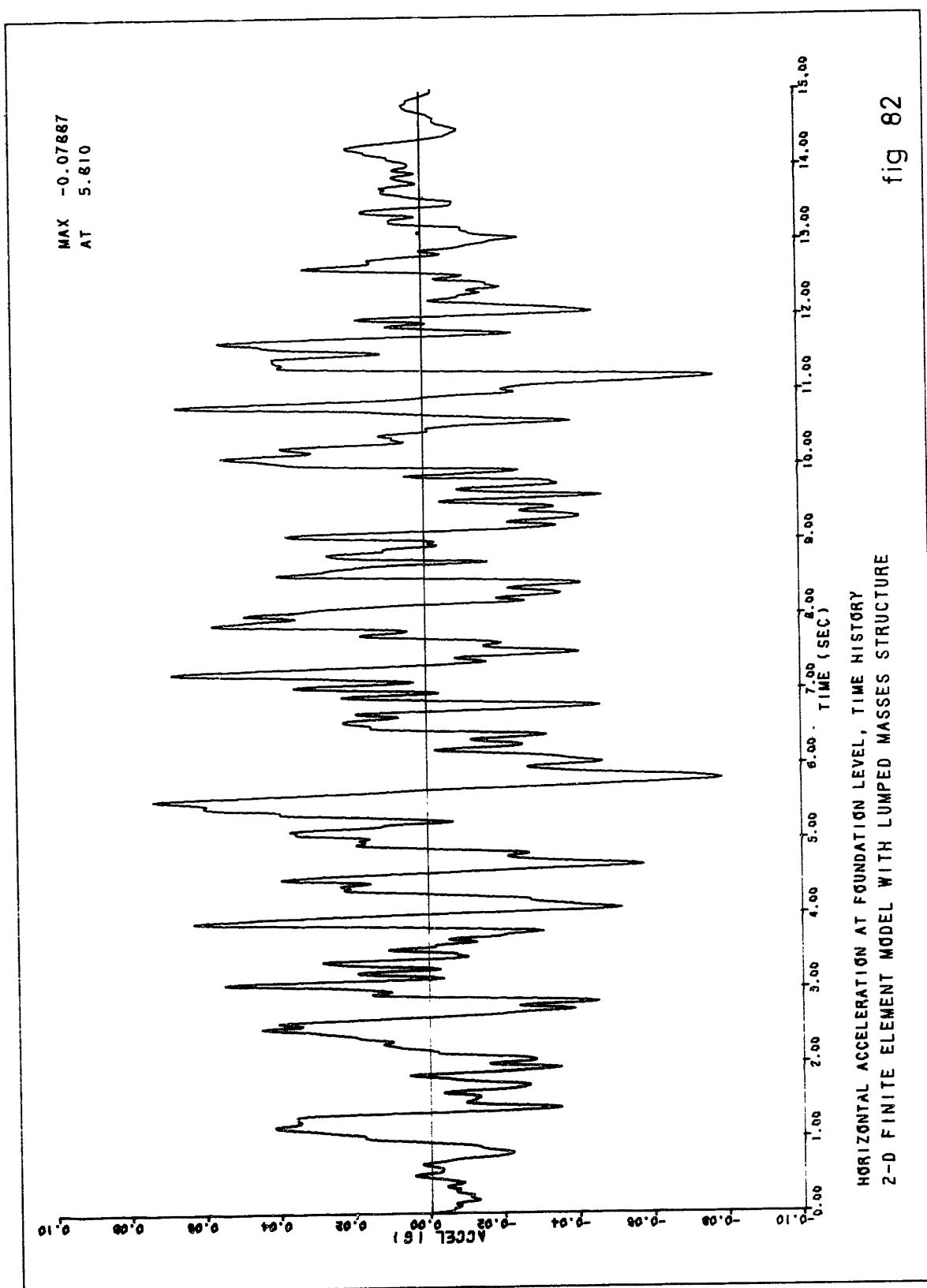
fig 79

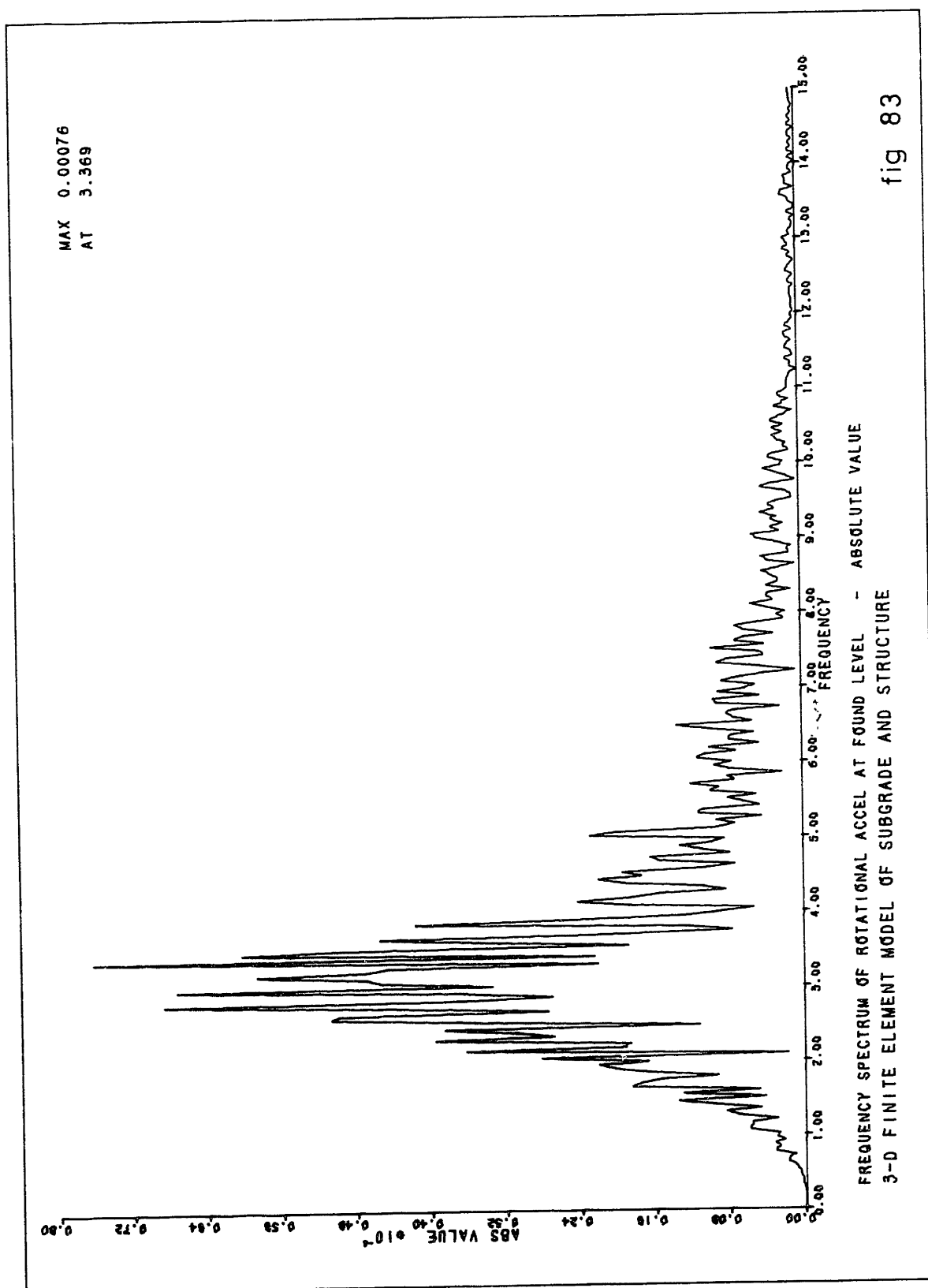




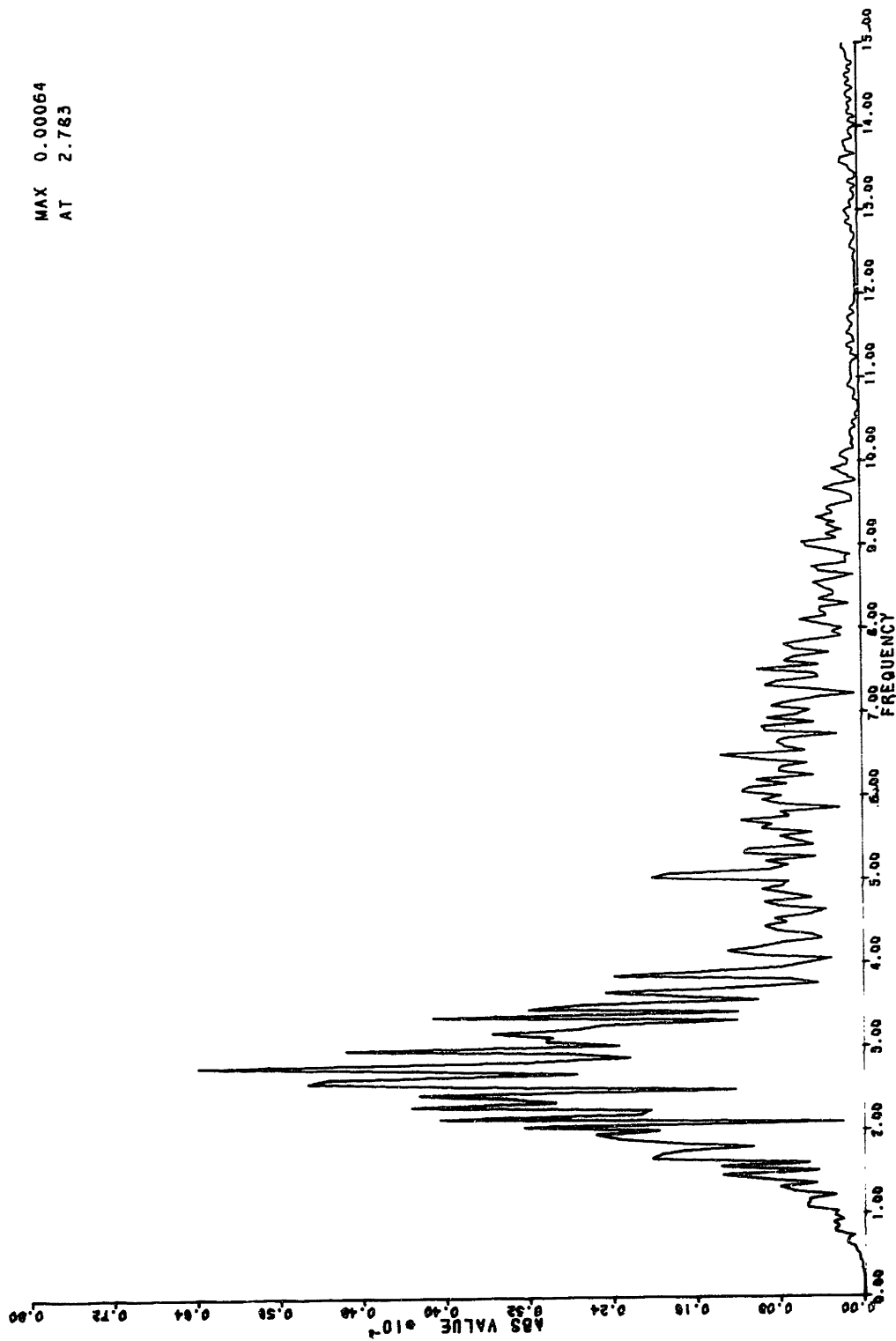
HORIZONTAL ACCELERATION AT FOUNDATION LEVEL, TIME HISTORY  
3-D FINITE ELEMENT MODEL OF SUBGRADE AND STRUCTURE

fig 81





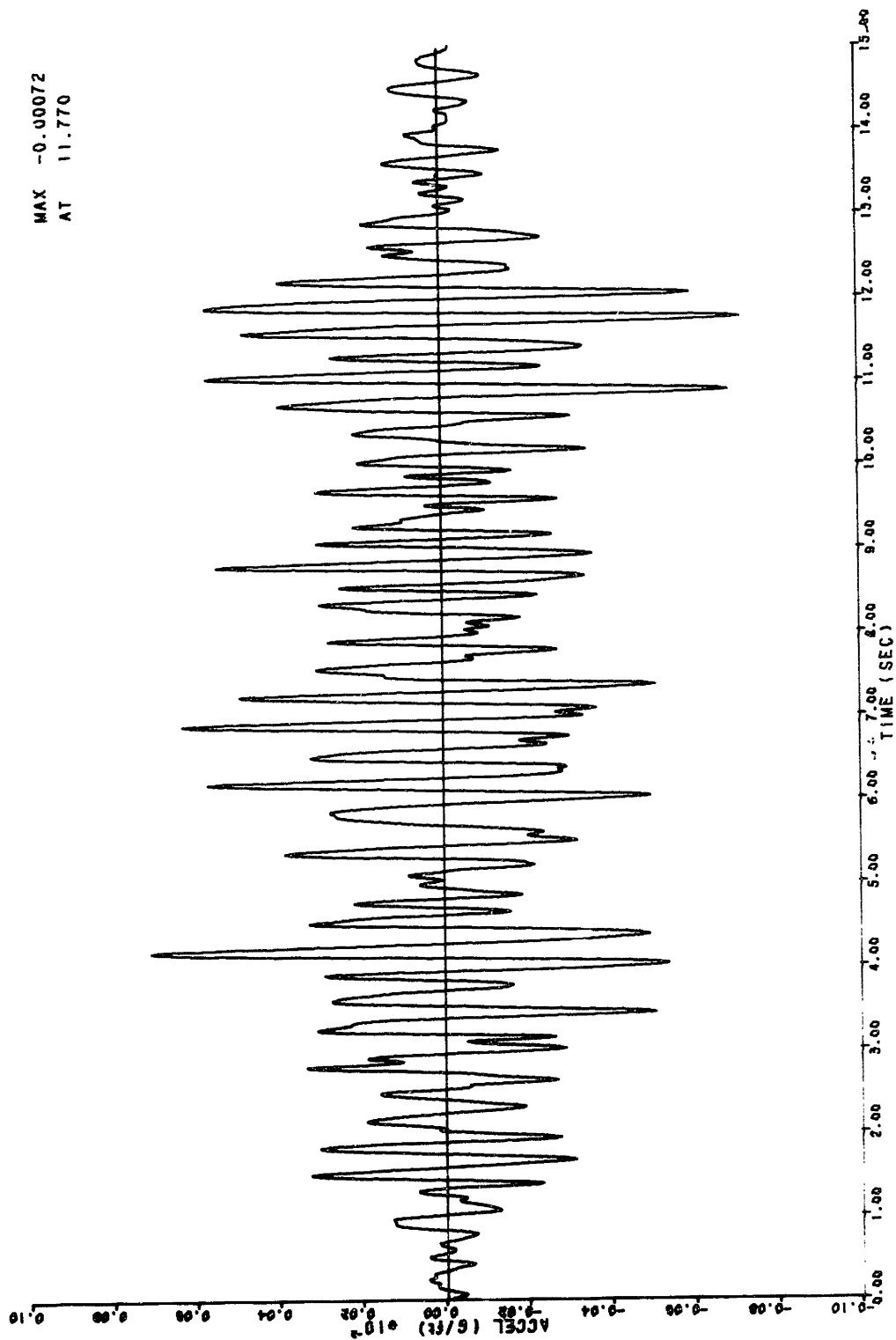
MAX 0.00064  
AT 2.783



FREQUENCY SPECTRUM OF ROTATIONAL ACCEL AT FOUND LEVEL - ABSOLUTE VALUE  
2-D FINITE ELEMENT MODEL WITH LUMPED MASSES STRUCTURE

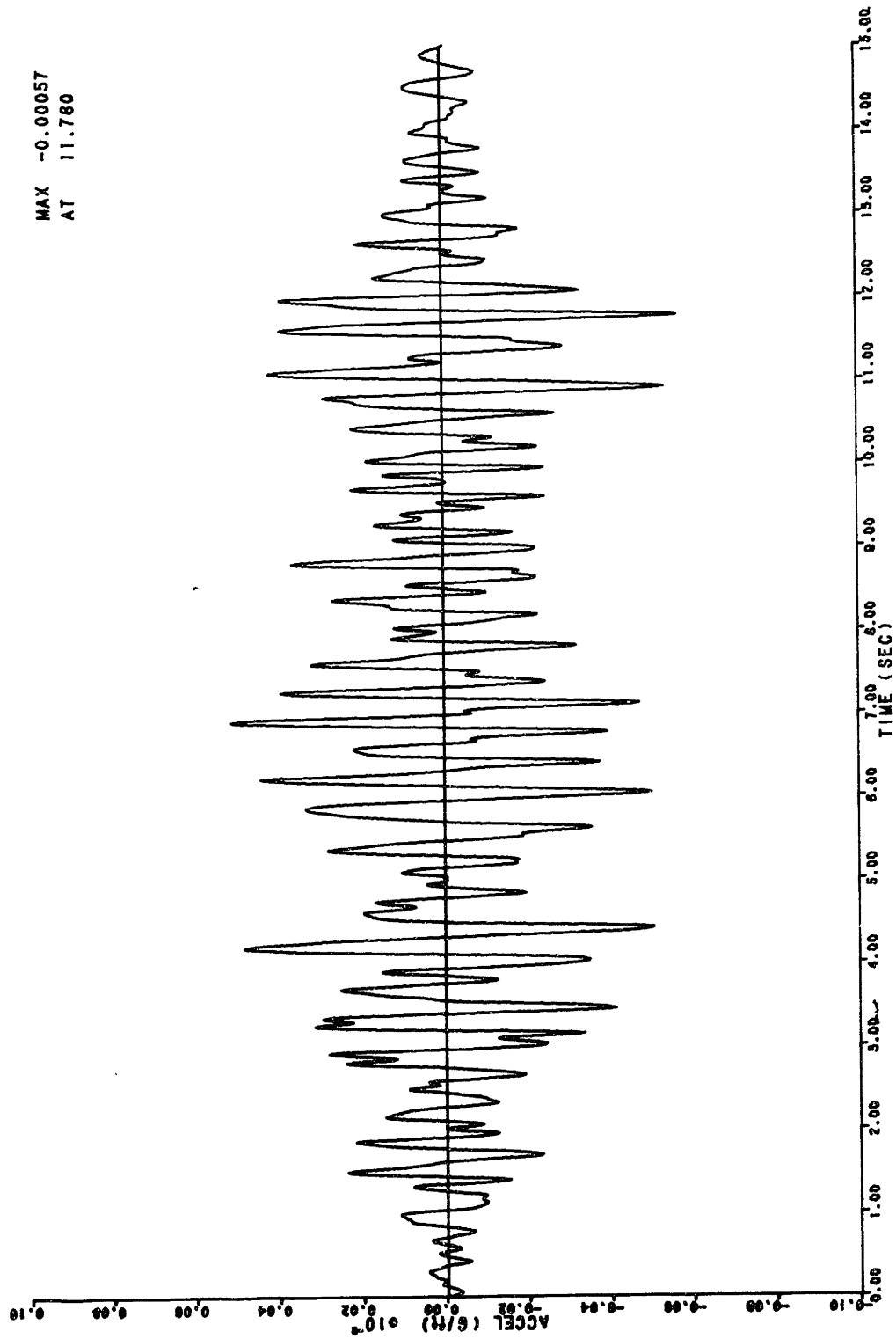
fig 84





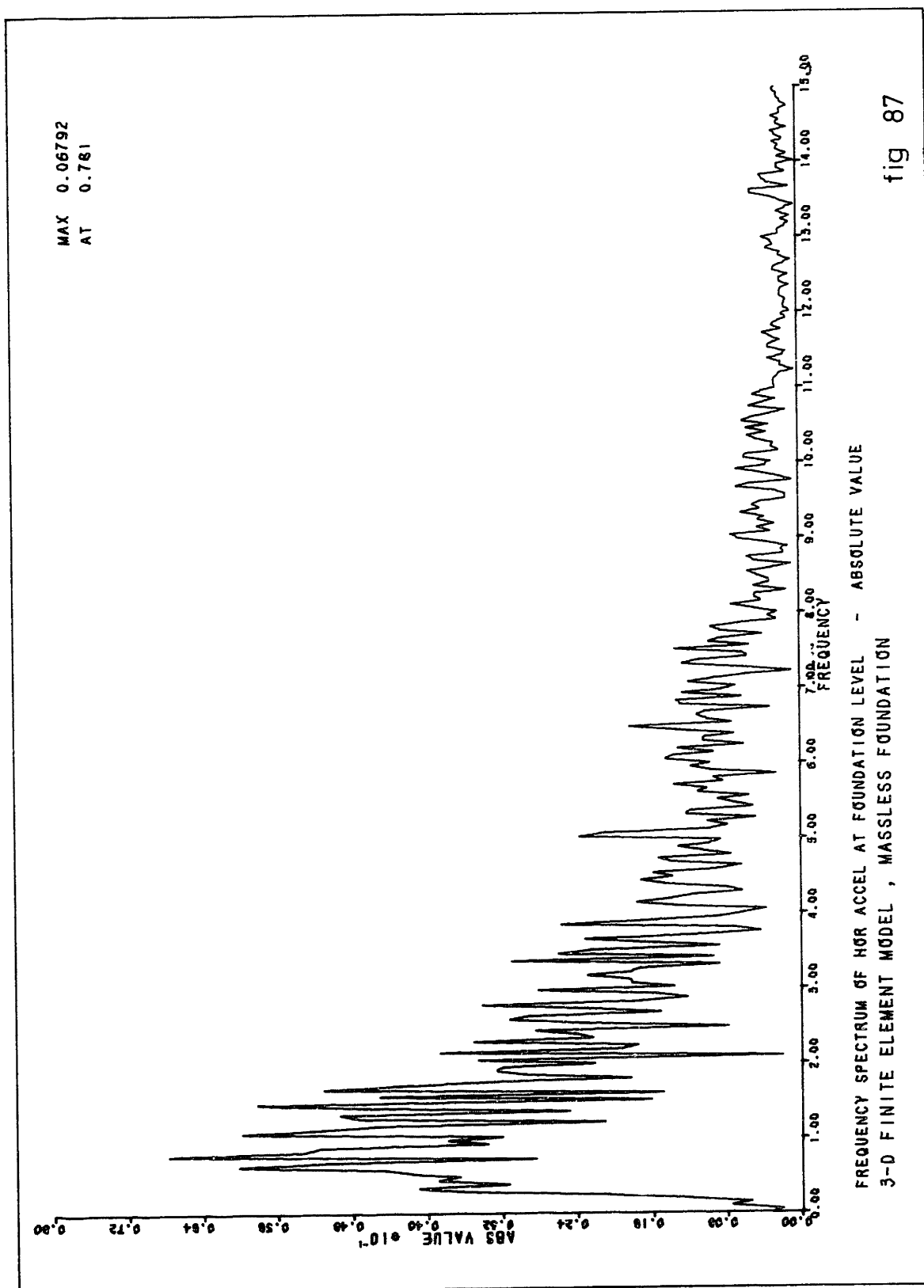
ROTATIONAL ACCELERATION AT FOUNDATION , TIME HISTORY  
3-D FINITE ELEMENT MODEL OF SUBGRADE AND STRUCTURE

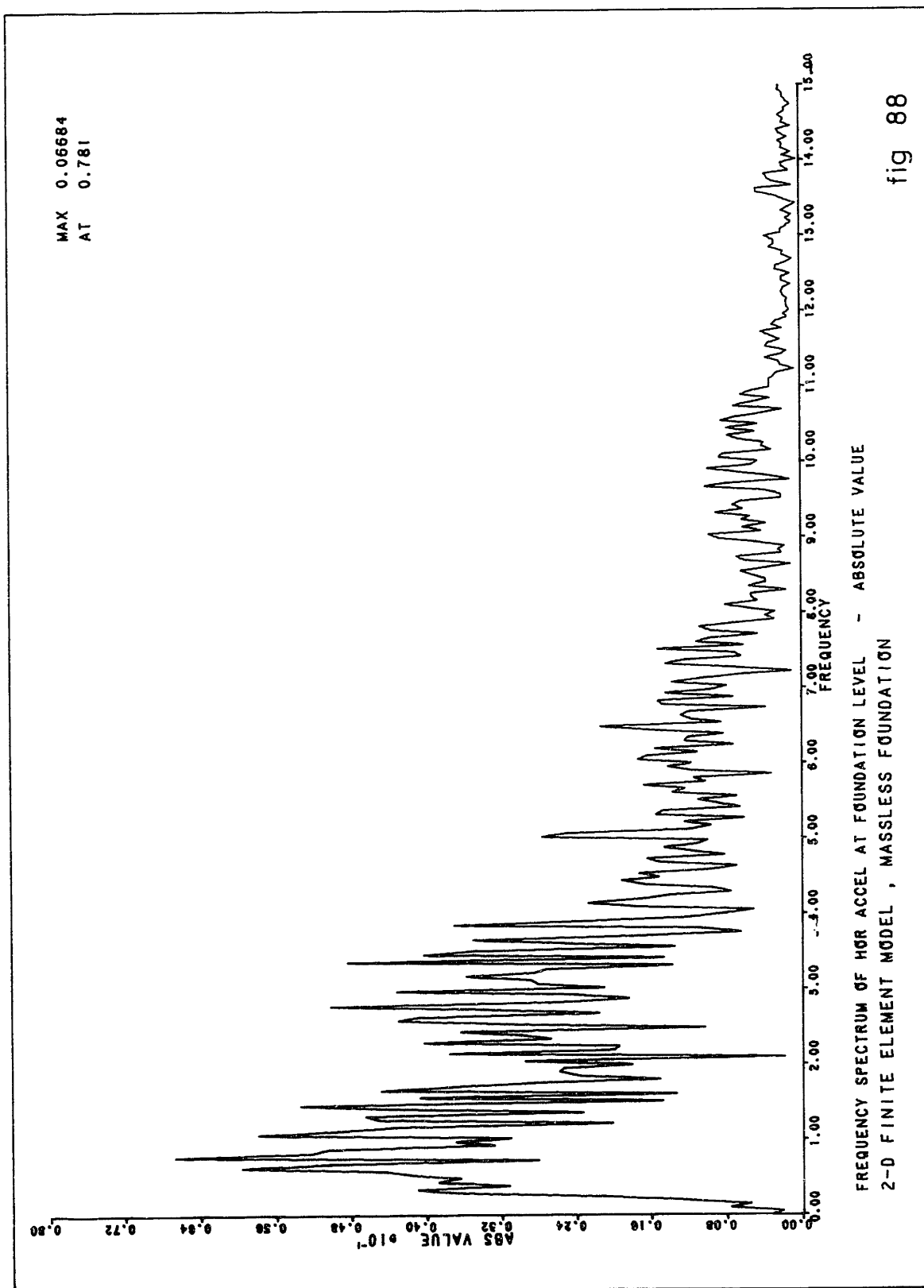
fig 85

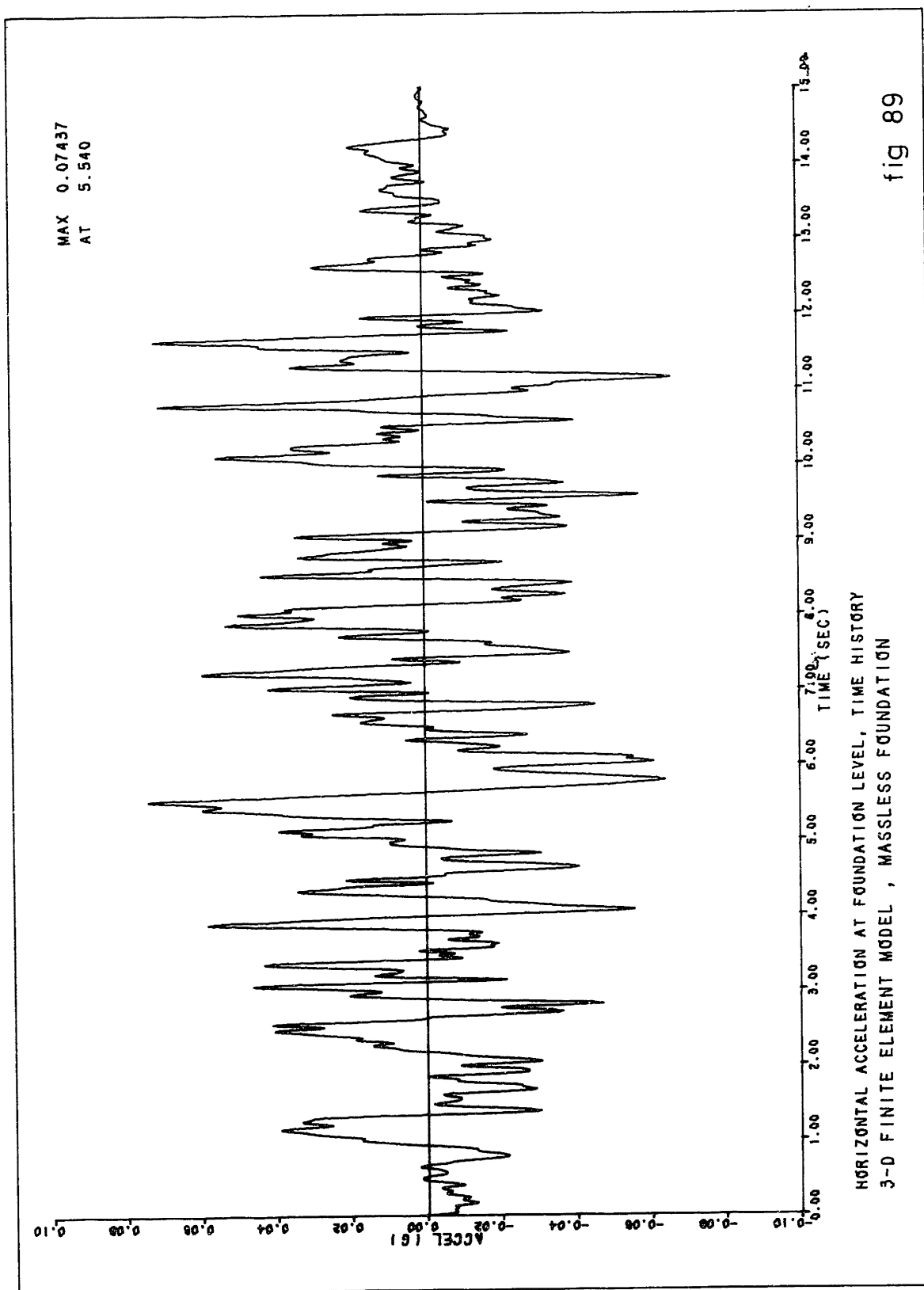


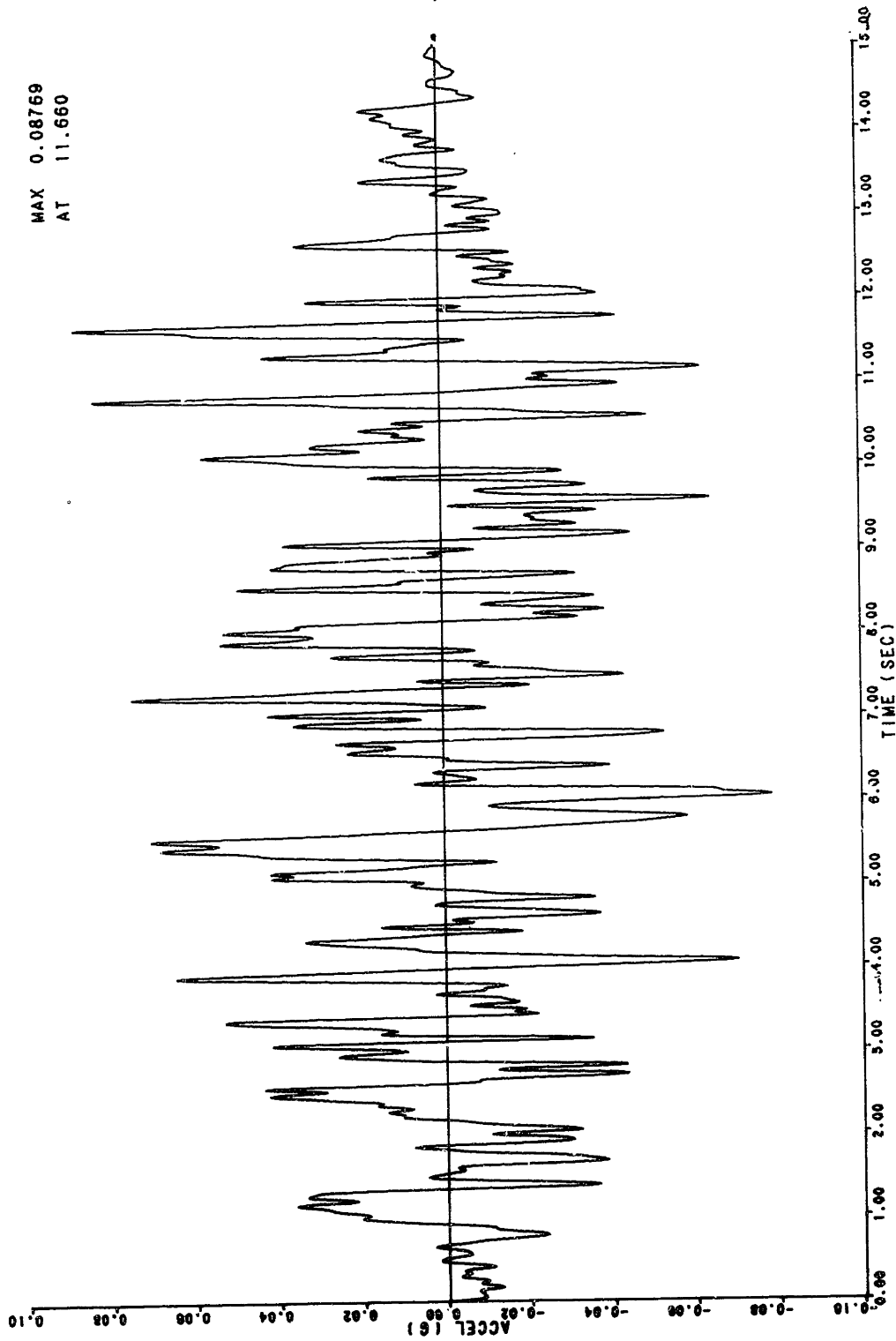
ROTATIONAL ACCELERATION AT FOUNDATION , TIME HISTORY  
2-D FINITE ELEMENT MODEL WITH LUMPED MASSES STRUCTURE

fig 86



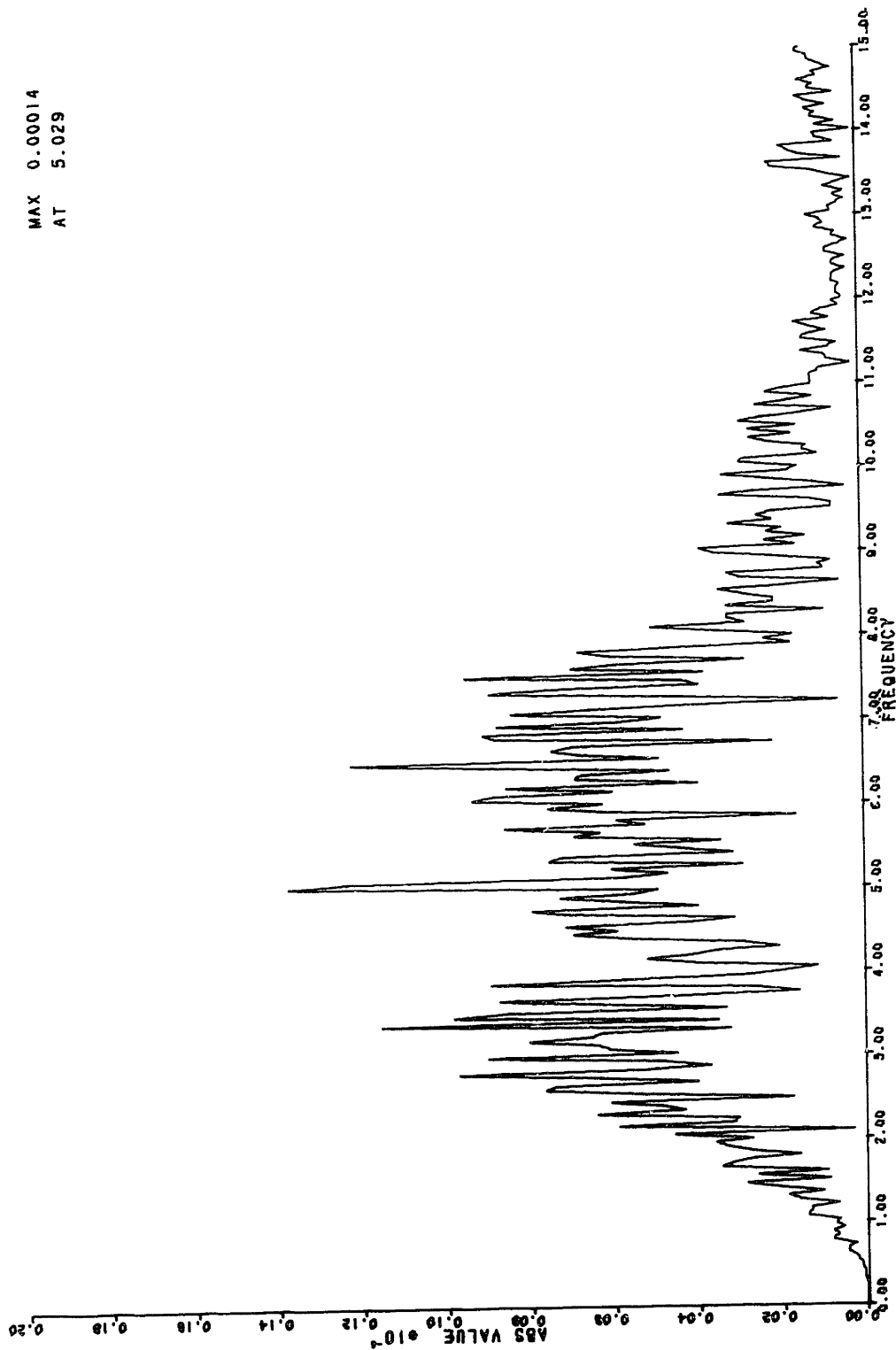






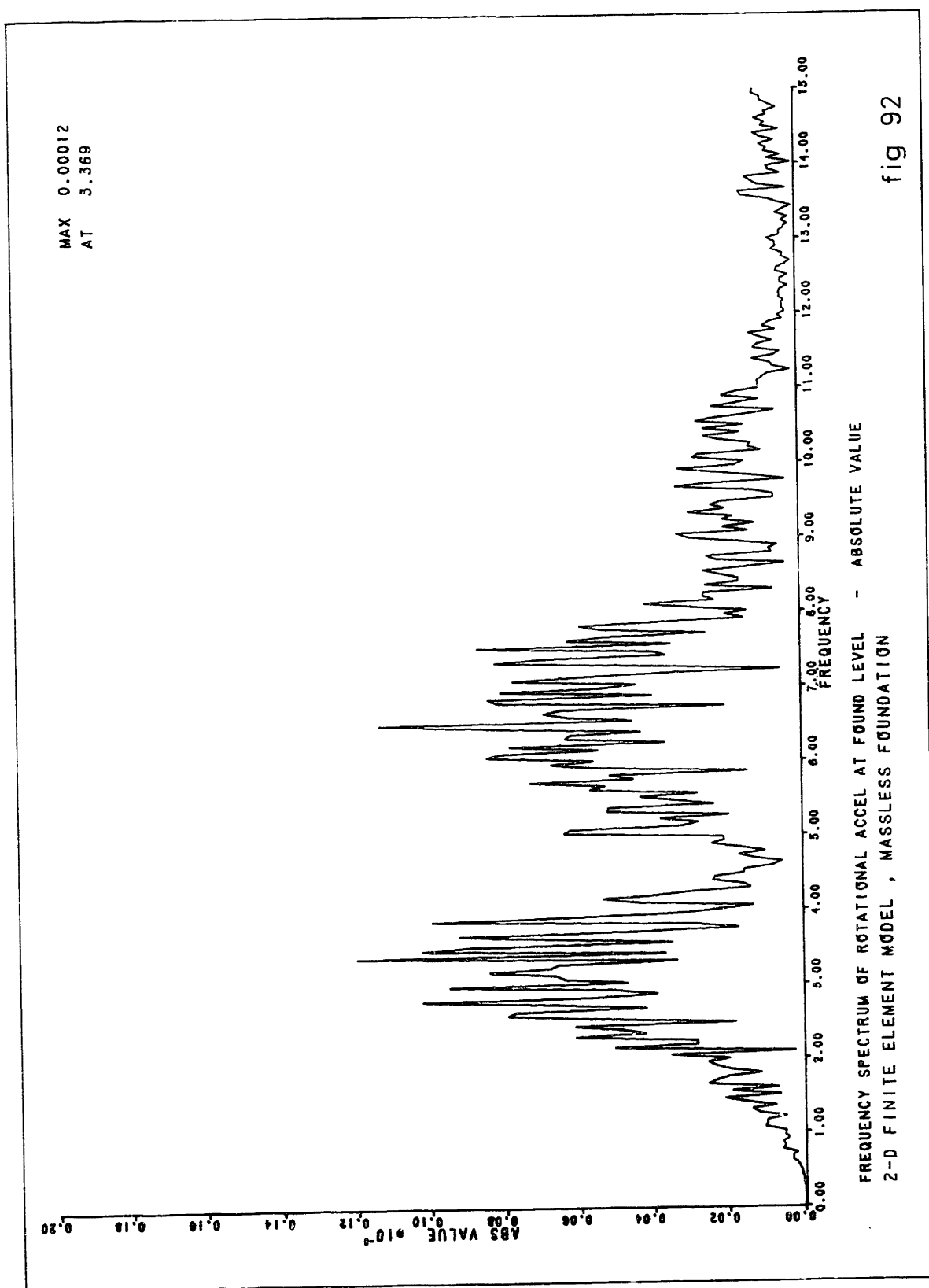
HORIZONTAL ACCELERATION AT FOUNDATION LEVEL, TIME HISTORY  
2-D FINITE ELEMENT MODEL , MASSLESS FOUNDATION

fig 90

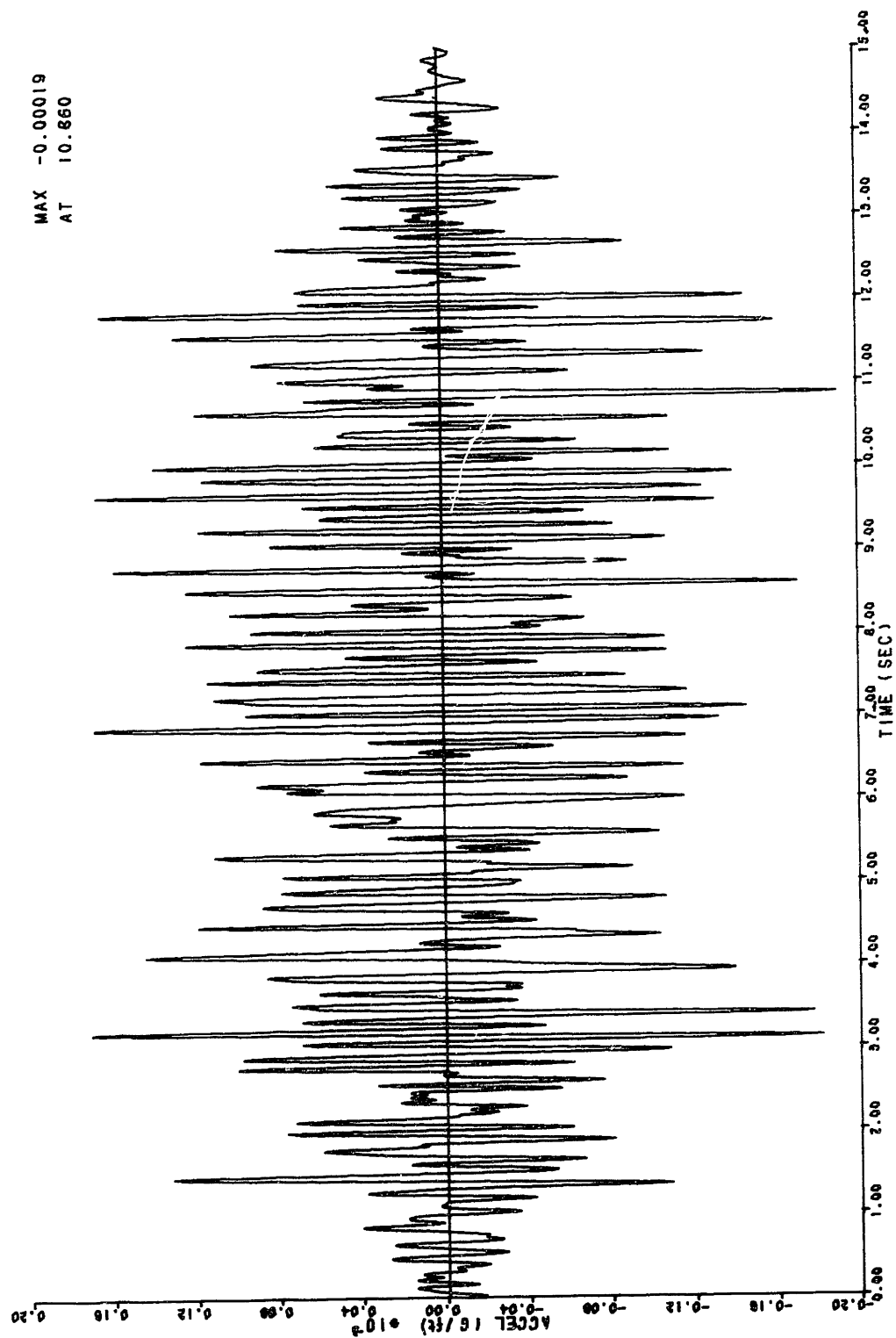


FREQUENCY SPECTRUM OF ROTATIONAL ACCEL AT FOUND LEVEL - ABSOLUTE VALUE  
3-D FINITE ELEMENT MODEL , MASSLESS FOUNDATION

fig 91

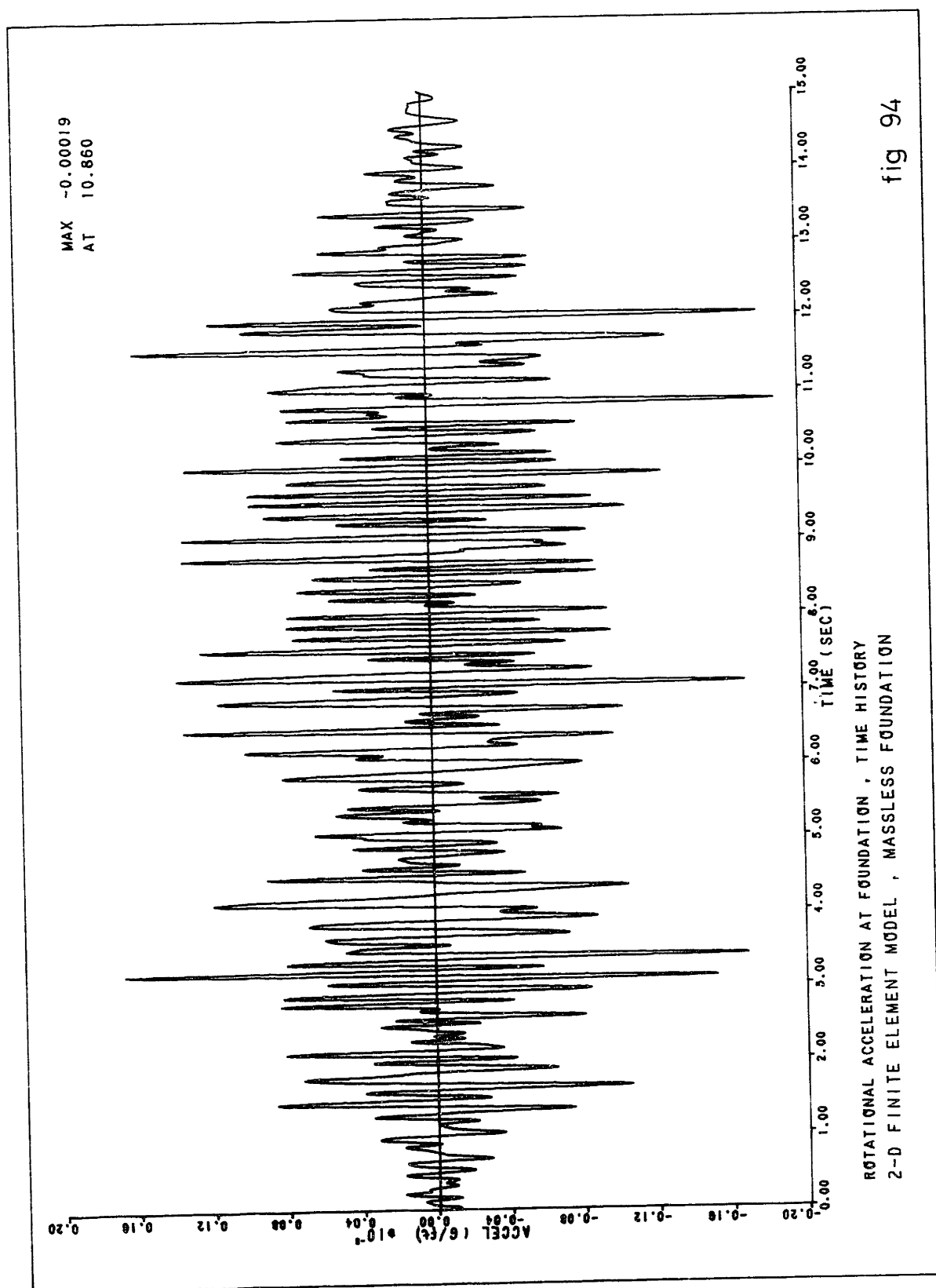






ROTATIONAL ACCELERATION AT FOUNDATION , TIME HISTORY  
3-D FINITE ELEMENT MODEL , MASSLESS FOUNDATION

fig 93



## 6. Summary and conclusions:

A numerical method to determine the response of axisymmetric foundations and soil-structure systems to arbitrary non-axisymmetric forced vibrations was developed and applied to some particular cases. The method is based on finite element analysis using the Fourier expansion technique reported by Wilson (51), and a generalization of an energy transmitting boundary developed by Waas and Lysmer (44), (21).

It was shown that the size of the finite element mesh is controlled throughout the geometry by the length of the shortest shearwave length of interest. The size of the dynamic pressure bulb is about one plate diameter for rocking, and larger than 3 plate diameters for swaying. The location of the Waas-Lysmer boundary affects the results only slightly, but economies in computation time dictate that it be placed as close as possible to the axis. Except for very shallow strata and for low internal damping ratios, it is believed that the results of the halfspace theory could be applied successfully to the case of a stratum, provided that the static stiffnesses are modified adequately, say, according to eqs. 4.6, 4.7. Similar conclusions apply to embedded foundation, for which an estimate of the location of the center of stiffness must be made (or eventually obtained

from a conventional finite element static analysis) to determine the cross-coupling terms in the subgrade stiffness matrix; the location of the center of stiffness can then be assumed independent of frequency. The results for the stratum are consistent with those of the halfspace for the three Poisson's ratios considered. Internal damping plays a significant role, and the sensitivity of the results to this parameter cautions against deriving solutions to the damped halfspace by merely multiplying the stiffness functions by the complex factor  $1+2i\beta$ .

A comparison was made between the responses predicted by a three dimensional model and an equivalent plane strain model of a nuclear power plant founded on a stratum, and subjected to an earthquake excitation. A reasonable agreement was found in the results, which might possibly be improved by modification to the equivalent plane model. Differences in the mat rotation amplitude warn against generalizing this conclusion to the responses at other points in the structure, particularly at the dome. Additional comparisons, possibly between amplified floor response spectra, should be performed to assess the accuracy of the plane strain model for a range of soil parameters. The significant mat distortion found for the 3-D model indicates the need for more research concerning

the effect of the foundation flexibility on the structural response.

References

- 1) Arnold, R. N., Bycroft, G.N., Warburton, G.B.: "Forced vibrations of a body on an infinite elastic solid," Journ. of appl. Mech., No. 77, pp. 391-401, 1955
- 2) Awojobi, A.O., and Grootenhuys, P.: "Vibration of rigid bodies on semiinfinite elastic media," Proc. Roy. Soc., Vol 287, Series A, 1965, pp 27-63
- 3) Barkan, D.D.: "Dynamics of bases and foundations," McGraw Hill, New York, 1962
- 4) Bullen, K.E.: "An introduction to the theory of seismology," Cambridge Press, 1963
- 5) Bycroft, G.N., "Forced vibrations of a rigid circular plate on a semiinfinite elastic space and on an elastic stratum," Phil. Trans. of the Roy. Soc of London, Vol 248, 1956, pp. 327
- 6) Capelli, A.P., Agrawal, G.L., Romero, V.E.: "A computer program for the elastic-plastic analysis of dome structures and arbitrary solids of revolution subjected to unsymmetrical loadings," Air Force Weapons Lab., Tech. rep No AFWL-TR-69-146
- 7) Collins, W.G.: "The forced torsional oscillations of an elastic half-space and an elastic stratum," Proc. London Math. Soc., Vol 12, No 46, 1962
- 8) Connor, T.: Class notes and personal communication,

- 9) Ewing, W.M., Jardetsky, W.S., and Press, F.: "Elastic waves in layered media," McGraw Hill, New York, 1957
- 10) Fung, Y.C." "Foundations of solid mechanics," Prentice Hall, 1965
- 11) Gladwell, G.M.L.: "Forced tangential and rotary vibration of a rigid circular disk on a semiinfinite solid," Intl. Journ. of Eng. Sc., Vol 6., pp 591-607, 1968
- 12) "Handbook of Mathematical Functions," U.S. Dept. of Commerce, Nat. Bureau of Standards, June 1964
- 13) Isenberg, J., Adham, S.: "Interaction of soil and power plants in earthquakes," Jour. of Pw. Div., ASCE, Vol 98, Oct. 1972
- 14) Karasudhi, P., Kier, L.M., Lee, S.L.,: "Vibratory motion of a body on an elastic halfplane," Jour. of Appl. Mech, Vol. 35, Series E No 4, Dec. 1968, pp 697-705
- 15) Krizek R., Gupta, D.C., Parmlee, R.A.: "Coupled sliding and rocking of embedded foundations," Jour. Soil Mech. and Found. Div., ASCE, Vol 98, Dec. 1972
- 16) Kuhlemeyer, R: "Vertical vibrations of footings embedded in layered media," Ph.D. diss., U of Cal., Berkeley 1969
- 17) Lamb, H.: "On the propagation of tremors over the surface of an elastic solid," Phil-Trans. of the Roy. Soc. of London, Series A, No 203, pp. 1-42, 1904
- 18) Langhaar, H.L.,: "Energy methods in applied mechanics," J. Wiley and Sons, 1962

- 19) Luco J.E., Westmann, R.: "Dynamic response of circular footings", Jour. of the Eng. Mech. Div., ASCE, Vol 97, Oct. 1971
- 20) Lysmer, T., Kuhlemeyer, R.L.: "Finite dynamic model for infinite media," Jour. Eng. Mech. Div., ASCE, Aug. 1969, pp. 859-877
- 21) Lysmer, T., Waas G.: "Shear waves in plane infinite structures", Jour. Eng. Mech. Div., ASCE, Vol. 98, Feb. 1972, pp. 85-105
- 22) Marguerre, K.: "Spannungsverteilung und Wellenausbreitung in der kontinuierlich gestutzten Platte," Ing. Archiv, Vol. 4, 1933, pp. 332-353
- 23) Novak, M.,: "Vibrations of embedded footings and structures," ASCE National Struct. Meeting Preprint 2029, April 1973
- 24) Novak, M., Beredugo, Y.O.: "Vertical vibration of embedded footings," Jour. of the Soil Mech. and Found. Div., ASCE, Vol 98, Dec. 1972
- 25) Parmlee, R. : "Designing for soil-structure interaction," ASCE National Struct. Eng. Meeting Preprint 1985, April 1973
- 26) Reissner, E.: "Stationare, axialsymmetrische, durch schuttelnde Masse erregte Schwingungen eines homogenen elastischen Halbraumes," Ing. Archiv, Vol 7, pp. 381-396, 1936



- 27) Reissner, E: "Freie u. erzwungene Torsionsschwingungen des elastischen Halbraumes," Ing. Archiv, Vol. 8, No. 4, pp. 229-245, 1937
- 28) Reissner, E., Sagoci, H.F.: "Forced Torsional Oscillations of an elastic halfspace," Journ. App. Phys., Vol 15, No. 9, pp 652-662,
- 29) Richart, F.E., Hall, J. R., Woods, R.D.: "Vibrations of soils and foundations," Prentice Hall, 1970
- 30) Robertson, I.A.: "On a proposed determination of the shear modulus of an isotopic elastic halfspace by the forced torsional oscillations of a circular disk," Appl. Sc. Research, The Hague, Netherlands, Vol. 17, 1967, pp. 305-312
- 31) Robertson, I.A.: "Forced vertical vibration of a rigid circular disk on a semiinfinite elastic solid," Proc. Camb. Phil. Soc., Camb. England, Vol 62, Series A, 1966 pp. 547-553
- 32) Roesset, J.M.: Personal communication,
- 33) Roesset, J.M., Whitman, R.V., Dobry, R.: "Modal analysis for structures with foundation interaction," ASCE Journ. of the Struct. Div., Vol. 99, March 1973, pp. 399-416
- 34) Sezawa, K.: "Further studies on Rayleigh waves having some azimuthal distribution," Bull. Earth. Res. Inst. Tokyo, 1929, Vol. 6, pp. 1-18
- 35) Shah, P.M.: "On the dynamic response of foundations

- systems," Ph.D thesis, Rice Univ., Houston, Texas, 1968
- 36) Snowdon, J.C.: "Vibration and shock in damped mechanical systems," J. Wiley and sons, 1968.
- 37) Stallybrass, M.P., "On the Reissner-Sagoci problem at high frequencies," Intl. Jour. Eng. Sc., Vol 5, 1967, pp. 689-703
- 38) Thomas, D.P.: "A note on the torsional oscillations of an elastic halfspace," Intl. Jour. of Eng. Sc., Vol 6, 1968. pp. 565-570
- 39) Thomas, D.P.: "Torsional oscillations of an elastic halfspace," Quart. Jour. of App. Mech. Vol 21, 1968, pp. 51-65
- 40) Tong, P., Pian, T.H.H., Bucciarelli, L.L.: "Mode shapes and frequencies by finite element method using consistent and lumped masses," Computers and Structures, Vol 1, pp. 623-638, Pergamon Press
- 41) Ufliand, I.S.: "On torsional vibrations of halfspace," App. Math. and Mech., Vol. 25, No 1, 1961
- 42) Veletsos, A., Wei, Y.: "Lateral and rocking vibration of footings," Jour. of the Soil Mech. and Found. Div. ASCE, Vol 97, Sept. 1971
- 43) Waas, G.: personal communication
- 44) Wass, G.: "Linear two-dimensional analysis of soil dynamics problems in semi-infinite layer media," Ph. D Thesis, U. of Cal., Berkeley, 1972

- 45) Warburton, G.B.: "Forced vibration of a body on an elastic stratum," Jour. of Appl. Mech., March 1957, pp 55-58
- 46) Weissmann, G.: "Torsional vibrations of circular foundations," Jour. Soil Mech. and Found. Div. ASCE, Vol 97, Sept. 1971
- 47) White, J.E.: "Seismic waves: radiation, transmission and attenuation," McGraw Hill, 1965
- 48) Whitman R. V., J. N. Protonotarios, M. F. Nelson,: Case study of soil structure interaction," ASCE National Environmental Eng. Meeting Preprint 1816, Oct. 1972
- 49) Whitman, R. V., Richart, F.E.: "Design procedures for dynamically loaded foundations," Jour. S. Mech. and F. Div., ASCE, Vol 93, pp. 169-193, 1967
- 50) Whitman, R.V.: "Vibration in Civil Engineering," Butterworths, London, 1966
- 51) Wilson, E.: "Structural analysis of axisymmetric solids," AIAA Jour., Vol. 3, No 12, Dec. 1965, pp. 2269
- 52) Zakorov, V.N., Rostovtsev, N.A.: "Dynamic contact problem of steady vibrations of an elastic halfspace," App. Math. and Mech., Vol 29, pp. 644-653, 1965
- 53) Zienkewics, O.C.: "The finite element method," McGraw Hill, 1970 (reprint)

## Biography

KAUSEL, EDUARDO, Born February 14, 1943

Married, 1 child

Education:

Escuela de Ingeniería, University of Chile (1961-1966)  
Ingeniero Civil (1967)

Technische Hochschule, Darmstadt, Germany, Postgraduate  
Studies (1969-1970)

Massachusetts Institute of Technology (1970-1973)  
Master of Science (1972)

Languages: English, Spanish, German

Registrations: Instituto de Ingenieros de Chile  
Colegio de Ingenieros de Chile

Honor Societies: Member of Sigma Xi

Experience Summary:

While a student in Chile, engineering aide to a private consulting engineer. After graduating with honors ("distinción unánime") Mr. Kausel worked for 2 years in the planning division at the Empresa Nacional de Electricidad, S.A. (ENDESA). Having been awarded a scholarship by the German government, he moved to Darmstadt to conduct postgraduate studies at the local Technical Institute under the supervision of Prof. Klöppel. From 1970 on he worked as Research Assistant in the Civil Engineering Department at the Massachusetts Institute of Technology, and received the Master of Science degree in June 1972. Since May 1973 Mr. Kausel has been an engineer in the Structural Division at Stone & Webster Engineering Company in Boston.

# List of Figures

241

Fig. No.		Page
1	Model . . . . .	9
2	Voigt spring-dashpot system . . . . .	17
3	Hysteresis loop . . . . .	18
4	Coordinate system . . . . .	22
5	Isoparametric finite element . . . . .	.45
6	Soil discretization . . . . .	.52
7	Discrete layer . . . . .	53
8	Discrete layer . . . . .	57
9	Discrete layer . . . . .	58
10	Boundary stresses . . . . .	71
11	2-D Wave propagation . . . . .	88
12	Boundary forces . . . . .	94
13	Plate foundation . . . . .	,107
14	Finite element meshes . . . . .	111
15	Extrapolation of static constants . . . . .	112
16	Influence of the mesh size . . . . .	.114
17	Finite element meshes . . . . .	117
18	Finite element meshes . . . . .	119
19	Test pressure bulb, rocking . . . . .	120
20	Test pressure bulb, rocking . . . . .	121
21	Test pressure bulb, swaying . . . . .	122

Fig. No.		Page
22	Location of boundary . . . . .	125
23	Effect of boundary location, swaying . . . . .	126
24	Finite element meshes . . . . .	128
25	Extrapolation swaying springs . . . . .	129
26	Extrapolation rocking springs . . . . .	130
27	Swaying static constant, effect of layer depth . . . . .	132
28	Rocking static constant, effect of layer depth . . . . .	132
29	Effect of layer depth, swaying . . . . .	134
30	Effect of layer depth, rocking . . . . .	135
31	Determination of natural frequencies . . . . .	143
32	Effect of internal damping, swaying . . . . .	148
33	Effect of internal damping, rocking . . . . .	149
34	Effect of internal damping, swaying . . . . .	150
35	Effect of internal damping, rocking . . . . .	151
36	Effect of Poisson's ratio, rocking . . . . .	154
37	Effect of Poisson's ratio, rocking . . . . .	155
38	Effect of Poisson's ratio, swaying . . . . .	157
39	Embedded foundation . . . . .	158
40	Rigid foundations . . . . .	160
41	Center of stiffness . . . . .	161
42	Effect of embedment, swaying . . . . .	166
43	Effect of embedment, rocking . . . . .	167
44	Effect of embedment, swaying . . . . .	168

Fig. No.		Page
45	Effect of embedment, rocking . . . . .	169
46	Frequency dependence of center of stiffness . . . . .	171
47	Structural idealization . . . . .	176
48	3-D Finite element model . . . . .	178
49	2-D Model . . . . .	179
50	Hor. trans. at found. level, transfer function W/R to free surface - abs. value . . . . .	184
51	Hor. trans. at found. level, transfer function W/R to free surface - phase angle $/\pi$ . . . . .	185
52	Hor. trans., transfer function from free surface to found. level . . . . .	186
53	Rotation at found. level, transfer function W/R to free surface - abs. value . . . . .	187
54	Rotation at found. level, transfer function W/R to free surface - phase angle $/\pi$ . . . . .	188
55	Rotation at found. level, transfer function W/R to free surface . . . . .	189
56	Hor. trans. at found. level, transfer function W/R to free surface - abs. value . . . . .	190
57	Hor. trans. at found. level, transfer function W/R to free surface - phase angle $/\pi$ . . . . .	191
58	Hor. trans., transfer function from free surface to foundation level . . . . .	192
59	Rotation at found. level, transfer function W/R to free surface - abs. value . . . . .	193
60	Rotation at found. level, transfer function W/R to free surface - phase angle $/\pi$ . . . . .	194
61	Rotation at found. level, transfer function W/R to free surface . . . . .	195

Fig. No.

Page

62	Hor. trans. at found. level, transfer function W/R to free surface - abs. value . . . . .	196
63	Hor. trans. at found. level, transfer function W/R to free surface - phase angle $/\pi$ . . . . .	197
64	Hor. trans., transfer function from free surface to foundation level . . . . .	198
65	Rotation at foundation level, transfer function W/R to free surface - abs. value . . . . .	199
66	Rotation at foundation level, transfer function W/R to free surface - phase angle $/\pi$ . . . . .	200
67	Rotation at foundation level, transfer function W/R to free surface . . . . .	201
68	Hor. trans. at found. level, transfer function W/R to free surface - abs. value . . . . .	202
69	Hor. trans. at found. level, transfer function W/R to free surface - phase angle $/\pi$ . . . . .	203
70	Hor. trans., transfer function from free surface to foundation level . . . . .	204
71	Rotation at found. level, transfer function W/R to free surface - abs. value . . . . .	205
72	Rotation at found. level, transfer function W/R to free surface - phase angle $/\pi$ . . . . .	206
73	Rotation at found. level, transfer function W/R to free surface . . . . .	207
74	Mat distortion at 5.75 cps . . . . .	209
75	2-D Model . . . . .	210
76	Input earthquake in horizontal direction . . . . .	212
77	Frequency spectrum of input earthquake - abs. value . .	213
78	Frequency spectrum of input earthquake - phase angle $/\pi$ . . . . .	214



Fig. No.

Page

79	Frequency spectrum of hor. accel. at foundation level - abs. value . . . . .	.215
80	Frequency spectrum of hor. accel. at foundation level - abs. value . . . . .	.216
81	Hor. accel. at foundation level, time history . . . . .	.217
82	Hor. accel. at foundation level, time history . . . . .	.218
83	Frequency spectrum of rotational accel. at found. level - abs. value . . . . .	.219
84	Frequency spectrum of rotational accel. at found. level - abs. value . . . . .	.220
85	Rotational accel. at found., time history . . . . .	.221
86	Rotational accel. at found., time history . . . . .	.222
87	Frequency spectrum of hor. accel. at foundation level - abs. value . . . . .	.223
88	Frequency spectrum of hor. accel. at foundation level - abs. value . . . . .	.224
89	Hor. accel. at foundation level, time history . . . . .	.225
90	Hor. accel. at foundation level, time history . . . . .	.226
91	Frequency spectrum of rotational accel. at found. level - abs. value . . . . .	.227
92	Frequency spectrum of rotational accel. at found. level - abs. value . . . . .	.228
93	Rotational accel. at foundation, time history . . . . .	.229
94	Rotational accel. at foundation, time history . . . . .	.230